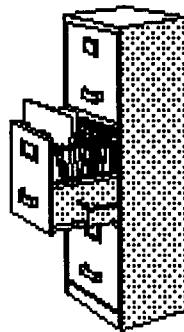


YUCCA MOUNTAIN SITE DESCRIPTION

BOOK 2 SECTION 4,5



RECIEVED WITH LETTER DATED 9/30/98
FILE CODE 102.8 ACCESSION # 9902040045

WBS: 1.2.3.9
QA: L

**Civilian Radioactive Waste Management System
Management & Operating Contractor**

BOOK 2 - SECTIONS 4, 5

YUCCA MOUNTAIN SITE DESCRIPTION

B00000000-01717-5700-00019 REV 00

September 1998

**INFORMATION COPY
LAS VEGAS DOCUMENT CONTROL**

Prepared for:

U.S. Department of Energy
Yucca Mountain Site Characterization Office
P.O. Box 30307
North Las Vegas, Nevada 89036-0307

Prepared by:

TRW Environmental Safety Systems Inc.
1261 Town Center Drive
Las Vegas, Nevada 89134-6352

Under Contract Number
DE-AC08-91RW00134

9902040045 - Part 4

Disclaimer

This report was prepared as an account of work sponsored by an agency of the United States Government. Neither the United States nor any agency thereof, nor any of their employees, makes any warranty, expressed or implied, or assumes any legal liability or responsibility for the accuracy, completeness, or usefulness of any information, apparatus, product, or process disclosed, or represents that its use would not infringe privately owned rights. Reference herein to any specific commercial product, process, or service by trade name, trademark, manufacturer, or otherwise, does not necessarily constitute or imply its endorsement, recommendation, or favoring by the United States Government or any agency thereof. The views and opinions of authors expressed herein do not necessarily state or reflect those of the United States Government or any agency thereof.

CONTENTS

	Page
PREFACE	xiii
ACRONYMS	xv
SYMBOLS/UNITS	xvii
4. CLIMATOLOGY AND METEOROLOGY	4.1-1
4.1 PRESENT CLIMATE AND METEOROLOGY	4.1-1
4.1.1 Planetary-Scale Atmospheric Features	4.1-2
4.1.2 Description of Synoptic-Scale Features and Processes	4.1-4
4.1.3 Regional and Site Climatology	4.1-5
4.1.3.1 Data Sources	4.1-5
4.1.3.2 Precipitation	4.1-6
4.1.3.3 Temperature, Humidity, and Evaporation	4.1-8
4.1.3.4 Wind	4.1-9
4.1.4 Meteorological Monitoring Network	4.1-12
4.1.4.1 Meteorological Sites	4.1-13
4.1.4.2 Measurements	4.1-14
4.1.4.3 Monitoring Program Database	4.1-15
4.1.4.4 Quality Assurance Activities	4.1-16
4.1.5 Climatological Summary	4.1-16
4.2 PALEOCLIMATOLOGY	4.2-1
4.2.1 Introduction	4.2-1
4.2.2 Causes and the Nature of Global Quaternary Climate Change	4.2-3
4.2.2.1 Relations of Climate Change to Factors Operating on Different Time Scales	4.2-3
4.2.2.1.1 Orbital Parameters	4.2-4
4.2.2.1.2 Climate Variability: Factors That Can Vary Climate at Short Time Scales	4.2-6
4.2.2.1.3 Long Records of Climate Change—Linkages between Millennial-Scale Climate Change and Orbital Parameters	4.2-9
4.2.2.1.3.1 Marine Records	4.2-9
4.2.2.1.3.2 Ice-Core Records	4.2-11
4.2.3 Long Regional Records of Quaternary Climate Change	4.2-12
4.2.3.1 Devils Hole	4.2-12
4.2.3.2 Death Valley	4.2-14
4.2.3.3 Owens Lake	4.2-16
4.2.3.3.1 Climate Setting	4.2-16
4.2.3.3.2 Limnologic and Climatic Setting	4.2-17
4.2.3.3.3 Climate Linkage to Owens Lake Chemistry	4.2-18
4.2.3.3.4 Microfossils as Proxy Records of Solute Composition and Total Dissolved Solids	4.2-19
4.2.3.3.5 Chronology of the Owens Lake Record	4.2-19
4.2.3.3.6 The Paleoclimate Record of Owens Lake	4.2-20

CONTENTS (Continued)

	Page
4.2.3.3.7 Glacial and Interglacial Variability Documented by the Owens Lake Record	4.2-22
4.2.3.3.8 Correlation of Owens Lake Paleolimnology and Oxygen Isotope Records of Global Climate	4.2-24
4.2.3.3.9 Owens Lake Conclusions	4.2-24
4.2.4 Local Records of Late Quaternary Climate Change	4.2-25
4.2.4.1 Pack-Rat Middens	4.2-25
4.2.4.2 Wetland and Spring Deposits	4.2-28
4.2.4.2.1 Corn Creek Flat Section OBI-11 Ostracode Data ...	4.2-28
4.2.4.2.2 Cactus Springs Section—Stable Isotope Data	4.2-31
4.2.4.2.3 Lathrop Wells Diatomite Microfossil and Isotope Data	4.2-32
4.2.4.2.4 Summary of Local Records	4.2-33
4.2.5.1 Secondary Mineral Deposits in the Yucca Mountain Tuffs ...	4.2-34
4.2.5.2 Stable Isotope Geochemistry of Secondary Calcite in the Unsaturated Zone	4.2-36
4.2.5.2.1 Controls on Infiltration $\delta^{13}\text{C}$ Values	4.2-36
4.2.5.2.2 Controls on Infiltration $\delta^{18}\text{O}$ Values	4.2-37
4.2.5.2.3 Formation and Distribution of Secondary Minerals ..	4.2-38
4.2.5.3 Secondary Mineral Evidence of Past Climates	4.2-39
4.3 FUTURE CLIMATE VARIATION	4.3-1
4.3.1 Modeling	4.3-1
4.3.2 Forecasting Using Paleoclimate Data	4.3-3
4.4 SUMMARY	4.4-1
4.5 REFERENCES	4.5-1
4.5.1 References Cited	4.5-1
4.5.2 Codes, Standards, Regulations	4.5-15
5. HYDROLOGIC SYSTEM	5.1-1
5.1 SURFACE WATER HYDROLOGY	5.1-1
5.1.1 Surface Water Bodies and Drainage Areas	5.1-1
5.1.1.1 Amargosa River System	5.1-1
5.1.1.2 Perennial Surface Water	5.1-4
5.1.2 Monitoring Network	5.1-5
5.1.3 Water-Control Structures and Diversions	5.1-7
5.1.4 Drainage Development, Paleohydrology, and Flood History	5.1-8
5.1.4.1 Drainage Development	5.1-8
5.1.4.2 Paleohydrology	5.1-8
5.1.4.2.1 Site and Subregional Paleohydrologic Studies	5.1-8
5.1.4.2.2 Regional Paleohydrologic Studies	5.1-10

CONTENTS (Continued)

	Page
5.1.4.3 Streamgauge Flood Record	5.1-10
5.1.4.3.1 Site and Subregional Paleohydrologic Floodstream Studies	5.1-10
5.1.4.3.2 Regional Streamgauge Flood Studies	5.1-13
5.1.4.4 Streamgauge Volume Record	5.1-13
5.1.4.4.1 Site and Subregional Streamgauge Volume Studies ..	5.1-13
5.1.4.4.2 Regional Streamgauge Volume Studies	5.1-14
5.1.5 Flood Potential	5.1-15
5.1.5.1 Site and Subregional Flood Potential Studies	5.1-15
5.1.5.2 Regional Flood Potential Studies	5.1-25
5.1.6 Chemistry of Surface Water	5.1-26
5.1.7 Location, Quantity, and Quality of Surface Water Extracted	5.1-30
5.1.8 Projected Surface Water Use	5.1-30
5.2 REGIONAL HYDROGEOLOGY	5.2-1
5.2.1 Flow System Boundaries and Hydrogeologic Units	5.2-1
5.2.1.1 Boundaries of Regional Flow System	5.2-3
5.2.1.2 Boundaries of Subregional Flow System	5.2-4
5.2.1.3 Hydrogeologic Units	5.2-4
5.2.1.4 Hydraulic Properties of Hydrogeologic Units	5.2-9
5.2.1.5 Summary of Flow System Boundaries and Hydrogeologic Units	5.2-15
5.2.2 Potentiometric Levels and Hydraulic Gradients	5.2-17
5.2.2.1 Previous Potentiometric-Surface Maps	5.2-17
5.2.2.2 Current Potentiometric Surface	5.2-22
5.2.2.3 Gradients and Potentiometric Features	5.2-26
5.2.2.4 Summary of Potentiometric Levels and Hydraulic Gradients ...	5.2-27
5.2.3 Recharge and Discharge	5.2-28
5.2.3.1 Characterizing the Recharge Component	5.2-28
5.2.3.1.1 Previous Methods of Characterizing Recharge from Precipitation	5.2-29
5.2.3.1.2 Limitations of the Empirical Maxey-Eakin Method ..	5.2-34
5.2.3.1.3 Modifying the Maxey-Eakin Method	5.2-35
5.2.3.1.4 Accuracy of the Modified Maxey-Eakin Method	5.2-38
5.2.3.1.5 Evaluation of Current Recharge Estimate	5.2-38
5.2.3.1.6 Summary Characterizing the Recharge Component ..	5.2-39
5.2.3.2 Characterizing the Discharge Component	5.2-40
5.2.3.2.1 Evapotranspiration by Phreatophytes and Wet Playas	5.2-40
5.2.3.2.2 Spring Discharge Accounting	5.2-44
5.2.3.2.3 Groundwater Pumpage	5.2-45
5.2.3.2.4 Summary Discharge in the Death Valley Region	5.2-45
5.2.4 Chemistry of Regional Groundwater	5.2-45
5.2.4.1 Major Ion Composition of Regional Groundwater	5.2-45
5.2.4.2 Isotopic Composition of Regional Groundwater	5.2-47

CONTENTS (Continued)

	Page
5.2.4.3 Age of Regional Groundwater	5.2-50
5.2.5 Groundwater Flowpaths	5.2-51
5.2.5.1 Source and Movement of Groundwater	5.2-51
5.2.5.1.1 Northern Death Valley Subregion	5.2-51
5.2.5.1.2 Central Death Valley Subregion	5.2-52
5.2.5.1.3 Southern Death Valley Subregion	5.2-54
5.2.5.2 Regional Flow System Water Budget	5.2-55
5.2.5.3 Summary of Groundwater Flowpaths	5.2-56
5.2.6 Regional Paleohydrology	5.2-57
5.2.6.1 Paleo Groundwater Levels	5.2-57
5.2.6.2 Groundwater Flowpaths During the Quaternary Period	5.2-62
5.2.7 Regional-Scale Flow Modeling	5.2-62
5.2.7.1 Model Construction	5.2-62
5.2.7.2 Model Geometry	5.2-63
5.2.7.3 Boundary Conditions	5.2-63
5.2.7.4 Model Calibration	5.2-64
5.2.7.5 Alternate-Climate Simulations	5.2-65
5.3 SITE HYDROGEOLOGY	5.3-1
5.3.1 Hydrogeologic Framework of the Flow System	5.3-1
5.3.2 Testing and Baseline Monitoring	5.3-7
5.3.2.1 Unsaturated-Zone Data Collection	5.3-9
5.3.2.1.1 Infiltration Data	5.3-10
5.3.2.1.1.1 Neutron Logging of Boreholes	5.3-10
5.3.2.1.1.2 Matrix Properties and Geochemical Analysis of Core Samples	5.3-12
5.3.2.1.1.3 Meteorological and Climatic Data Collection ...	5.3-12
5.3.2.1.1.4 Measurement of Pan Evaporation	5.3-13
5.3.2.1.1.5 Measurement of Soil Hydrologic Properties	5.3-14
5.3.2.1.1.6 Monitoring Soil Water Potential Using Heat Dissipation Probes	5.3-14
5.3.2.1.2 Matrix Hydrologic Properties Data	5.3-14
5.3.2.1.2.1 Sample Collection Methods	5.3-15
5.3.2.1.2.2 Core Processing in the Laboratory	5.3-16
5.3.2.1.2.3 Moisture Retention Characterization	5.3-17
5.3.2.1.3 Air-Injection Testing in Surface Based Boreholes	5.3-17
5.3.2.1.3.1 Field Test Method	5.3-18
5.3.2.1.3.2 Air-Injection Test Analysis	5.3-19
5.3.2.1.4 Instrumentation and Monitoring of Surface Based Boreholes	5.3-20
5.3.2.1.4.1 In Situ Pneumatic Pressure Measurements	5.3-20
5.3.2.1.4.2 In Situ Water Potential Measurements	5.3-22

CONTENTS (Continued)

	Page
5.3.2.1.4.3	In Situ Temperature Measurements 5.3-23
5.3.2.1.5	Collection of Water and Gas Samples From Surface Based Boreholes for Chemical and Isotopic Analysis 5.3-24
5.3.2.1.6	Testing and Monitoring in the Exploratory Studies Facility 5.3-25
5.3.2.1.6.1	Pneumatic Monitoring and Air-Injection and Gaseous Tracer Tests 5.3-25
5.3.2.1.6.2	Hydrochemical Data Collection 5.3-27
5.3.2.2	Saturated-Zone Data Collection 5.3-28
5.3.2.2.1	Water Level Monitoring Program 5.3-28
5.3.2.2.2	Saturated-Zone Hydraulic Tests and Analytical Procedures 5.3-29
5.3.2.3	Geophysical Logging 5.3-33
5.3.3	Properties of Hydrogeologic Units 5.3-35
5.3.3.1	Unsaturated Zone 5.3-36
5.3.3.1.1	Characterization of Hydrogeologic Units Using Core-Scale Matrix Properties 5.3-36
5.3.3.1.1.1	Porosity and Saturation 5.3-38
5.3.3.1.1.2	Effects of Mineral Alteration and Estimation of Saturated-Hydraulic Conductivity 5.3-44
5.3.3.1.1.3	Mean Matrix-Property Values for Hydrogeologic Units 5.3-46
5.3.3.1.1.4	Moisture-Retention Characteristics and Unsaturated-Hydraulic Conductivity 5.3-47
5.3.3.1.1.5	Lithologic Stratification: Transitions and Capillary and Permeability Barriers 5.3-48
5.3.3.1.1.6	Properties of Fault Zones 5.3-50
5.3.3.1.1.7	Spatial Variability of Matrix Properties 5.3-51
5.3.3.1.1.8	Three-Dimensional Modeling of Rock-Property Heterogeneity 5.3-53
5.3.3.1.2	Field-Scale Characterization of Hydrogeologic Units Using Air-Injection Testing 5.3-60
5.3.3.1.2.1	Surface-Based Air-Injection Testing 5.3-60
5.3.3.1.2.2	Exploratory Studies Facility Air-Injection Testing 5.3-65
5.3.3.1.2.3	Comparison of Laboratory Permeability Values with Surface-Based and Exploratory Studies Facility Air-Injection Permeability Values 5.3-72
5.3.3.1.2.4	Comparison of the Surface-Based, Exploratory Studies Facility, and Pneumatic-Monitoring Air-Permeability Values and Estimation of Anisotropy 5.3-72
5.3.3.2	Saturated Zone 5.3-76
5.3.3.2.1	Core Scale Hydrologic Properties 5.3-77

CONTENTS (Continued)

	Page
5.3.3.2.2	Rock-Mass Hydraulic Properties 5.3-88
5.3.3.2.2.1	Single-Borehole Tests 5.3-88
5.3.3.2.2.2	Multiple-Well Tests 5.3-92
5.3.3.2.2.3	Uncertainty of Hydraulic Properties 5.3-97
5.3.4	Unsaturated-Zone System 5.3-99
5.3.4.1	Site Infiltration 5.3-100
5.3.4.1.1	Overview of Studies and Methods for Determining Net Infiltration and Recharge in the Vicinity of the Site 5.3-101
5.3.4.1.1.1	Flux Calculations Using Measured Hydraulic Properties 5.3-101
5.3.4.1.1.2	Water Balance Models for Estimating Net Infiltration and Recharge 5.3-102
5.3.4.1.1.3	Statistical Models for Estimating Net Infiltration at the Site 5.3-105
5.3.4.1.1.4	Geochemical Methods 5.3-105
5.3.4.1.1.5	Temperature Models 5.3-106
5.3.4.1.1.6	Deterministic Water-Balance Modeling of Net Infiltration and Recharge 5.3-106
5.3.4.1.2	Conceptual Model of Net Infiltration 5.3-107
5.3.4.1.2.1	Field Water Balance 5.3-108
5.3.4.1.2.2	Climatic Factors 5.3-109
5.3.4.1.2.3	Physiographic and Topographic Factors 5.3-112
5.3.4.1.2.4	Soils 5.3-113
5.3.4.1.2.5	Bedrock Hydrologic Properties 5.3-113
5.3.4.1.2.6	Vegetation 5.3-114
5.3.4.1.2.7	Summary of the Conceptual Model of Infiltration and the Episodic Occurrence of Fracture Flow .. 5.3-116
5.3.4.1.3	Results of Infiltration Monitoring and Water Balance Studies 5.3-116
5.3.4.1.3.1	Measurement of Water-Content Profiles in Neutron-Access Boreholes 5.3-117
5.3.4.1.3.2	Continuous Monitoring of Water Potential Using Heat-Dissipation Probes 5.3-119
5.3.4.1.3.3	Precipitation and Runoff Monitoring 5.3-120
5.3.4.1.4	Development of the Numerical Net-Infiltration Model 5.3-121
5.3.4.1.4.1	Daily Precipitation Input 5.3-122
5.3.4.1.4.2	Field Moisture Capacity 5.3-123
5.3.4.1.4.3	Evapotranspiration 5.3-123
5.3.4.1.4.4	Surface Water Runoff 5.3-124
5.3.4.1.4.5	Model Calibration 5.3-125
5.3.4.1.5	Application of the Numerical Infiltration Model 5.3-126

CONTENTS (Continued)

	Page	
5.3.4.1.5.1	Estimates of Present-Day Net Infiltration Rates for Yucca Mountain	5.3-126
5.3.4.1.5.2	Comparison of Numerical-Model-Derived Net Infiltration Rates With Flux Estimates From a Chloride Mass-Balance Method	5.3-128
5.3.4.1.5.3	Estimates of Net Infiltration Rates for Potential Future Climates	5.3-129
5.3.4.1.5.4	Estimates of Net Infiltration Rates Using a Coupled Infiltration-Surface Flow-Routing Model	5.3-131
5.3.4.1.6	Summary of Net Infiltration Modeling Results	5.3-133
5.3.4.2	Characterization of the Deep Unsaturated Zone	5.3-137
5.3.4.2.1	Pneumatic Pressure and Gaseous-Phase Movement	5.3-138
5.3.4.2.1.1	Synthesis of Subsurface Pneumatic Pressure Prior to the Influence of Exploratory Studies Facility Excavation	5.3-139
5.3.4.2.1.2	Determination of Pneumatic Diffusivity and Vertical Permeability Using Borehole Pneumatic-Pressure Data	5.3-142
5.3.4.2.1.3	Effects of Excavation of the Exploratory Studies Facility Tunnel on In Situ Pneumatic-Pressure Measurements in Boreholes	5.3-144
5.3.4.2.1.4	Determination of Horizontal Permeability and the Vertical Anisotropy of the Topopah Spring Tuff by Numerical Simulation of Pressure Responses to Exploratory Studies Facility Excavation	5.3-148
5.3.4.2.1.5	Parameter Estimation for Boreholes UZ#4 and UZ#5	5.3-152
5.3.4.2.2	Distribution of In Situ Water-Potential and Occurrences of Perched Water in the Deep Unsaturated Zone	5.3-153
5.3.4.2.2.1	In Situ Water Potentials	5.3-154
5.3.4.2.2.2	Perched-Water Occurrences in the Site Area	5.3-161

CONTENTS (Continued)

	Page	
5.3.4.2.3	Estimation of Heat Flux Using Borehole Temperature Data	5.3-167
5.3.4.2.4	Geochemistry and Isotopes	5.3-172
5.3.4.2.4.1	Major-Ion Chemistry	5.3-172
5.3.4.2.4.2	Tritium and Chlorine-36	5.3-173
5.3.4.2.4.3	Carbon Isotopes ($\delta^{13}\text{C}$ and ^{14}C)	5.3-178
5.3.4.2.4.4	Stable Isotopes (δD and $\delta^{18}\text{O}$)	5.3-179
5.3.4.2.4.5	Interactions of Old Matrix Water with Younger Percolating Water	5.3-180
5.3.4.2.4.6	Gas-Phase Chemistry and Gas-Water Interactions	5.3-181
5.3.4.3	Movement of Water in the Unsaturated Zone	5.3-183
5.3.4.3.1	Percolation Flux	5.3-183
5.3.4.3.1.1	Infiltration Modeling	5.3-184
5.3.4.3.1.2	Temperature and Heat Flow	5.3-185
5.3.4.3.1.3	Isotopic Evidence of Fluid Flow and Percolation	5.3-193
5.3.4.3.1.4	Chloride Mass Balance	5.3-196
5.3.4.3.1.5	Effective Hydraulic Conductivity/Potential Gradient Methods	5.3-203
5.3.4.3.1.6	Calcite Accumulation Rates	5.3-206
5.3.4.3.1.7	Perched-Water Volumes/Residence Times	5.3-208
5.3.4.3.2	Flowpaths in the Unsaturated Zone	5.3-212
5.3.4.3.2.1	Distribution of Percolation Flux	5.3-212
5.3.4.3.2.2	Role of Discrete Pathways	5.3-216
5.3.4.3.2.3	Inferences From Perched Water	5.3-222
5.3.4.3.2.4	Fracture-Matrix Interaction	5.3-222
5.3.4.4	Three-Dimensional Unsaturated-Zone Modeling	5.3-224
5.3.4.4.1	Introduction	5.3-224
5.3.4.4.2	Previous Work on Unsaturated-Zone Modeling of Yucca Mountain	5.3-227
5.3.4.4.3	Conceptual Model of the Unsaturated Zone	5.3-228
5.3.4.4.3.1	Geological Framework	5.3-230
5.3.4.4.3.2	Infiltration	5.3-231
5.3.4.4.3.3	Percolation Flux	5.3-232
5.3.4.4.3.4	Capillary Barriers and Lateral Flow Diversion . .	5.3-234
5.3.4.4.3.5	Characterization of Major Faults and Their Effect on Flow	5.3-234
5.3.4.4.3.6	Perched Water	5.3-236
5.3.4.4.3.7	Fracture Flow and Fracture-Matrix Interactions .	5.3-237
5.3.4.4.3.8	Fluid (Water and Gas) Flowpaths and Ages	5.3-240
5.3.4.4.3.9	Geothermal Gradient	5.3-241
5.3.4.4.4	Summary of Unsaturated-Zone Modeling Studies and Results	5.3-242
5.3.4.4.4.1	Input Data	5.3-243

CONTENTS (Continued)

	Page
5.3.4.4.4.1.1 Geological Framework and Rock Properties . . .	5.3-243
5.3.4.4.4.1.2 Infiltration Rates	5.3-243
5.3.4.4.4.1.3 Pneumatic Data	5.3-244
5.3.4.4.4.2 Calibration of the Model	5.3-245
5.3.4.4.4.3 Output Data	5.3-248
5.3.4.4.4.3.1 Flow Above the Potential Repository	5.3-248
5.3.4.4.4.3.2 Percolation Flux at the Potential Repository Horizon	5.3-249
5.3.4.4.4.3.3 Fracture Flow	5.3-250
5.3.4.4.4.3.4 Seepage into Drifts	5.3-251
5.3.4.4.4.3.5 Flow Below the Potential Repository	5.3-251
5.3.4.4.4.3.6 Impact of Future Climate-Change Scenarios . . .	5.3-253
5.3.4.4.5 Summary and Conclusions	5.3-255
5.3.5 Saturated-Zone System	5.3-256
5.3.5.1 Potentiometric Levels and Gradients	5.3-256
5.3.5.1.1 Potentiometric Levels	5.3-256
5.3.5.1.2 Earthquake Effects	5.3-258
5.3.5.1.3 Potentiometric Surface	5.3-262
5.3.5.1.4 Potentiometric Gradients	5.3-264
5.3.5.2 Temperature, Thermal Gradients, and Heat Flow	5.3-270
5.3.5.3 Hydrochemical and Isotopic Evidence of Flowpaths and Groundwater Age	5.3-277
5.3.5.4 Conceptual Model of the Saturated Zone at Yucca Mountain .	5.3-277
5.3.5.4.1 Site Saturated-Zone Groundwater Flow	5.3-278
5.3.5.4.2 Large Hydraulic Gradient Area	5.3-280
5.3.5.4.3 Influence of Faults	5.3-280
5.3.5.4.4 Recharge	5.3-281
5.3.5.4.5 Discharge	5.3-282
5.3.5.4.6 Conceptual Uncertainties	5.3-283
5.3.5.5 Site Saturated-Zone Flow Modeling	5.3-283
5.3.5.5.1 Previous Flow Modeling	5.3-284
5.3.5.5.2 Quality Assurance Considerations	5.3-286
5.3.5.5.3 Preliminary 3-D Groundwater Flow Model of the Site Saturated Zone	5.3-286
5.3.5.5.3.1 Hydrogeologic Framework Model	5.3-286
5.3.5.5.3.2 FEHMN	5.3-289
5.3.5.5.3.3 PEST	5.3-290
5.3.5.5.3.4 Model Assumptions	5.3-291
5.3.5.5.3.5 Boundary Conditions	5.3-292
5.3.5.5.3.6 Model Calibration	5.3-292
5.3.5.5.3.7 Sources of Error	5.3-293

CONTENTS (Continued)

	Page
5.3.6 Site Paleohydrology	5.3-294
5.3.6.1 Record of Unsaturated-Zone History	5.3-294
5.3.6.2 Past Water Table Elevations at Yucca Mountain	5.3-298
5.4 REFERENCES	5.4-1
5.4.1 References Cited	5.4-1
5.4.2 Codes, Standards, and Regulations	5.4-50

PREFACE

The *Yucca Mountain Site Description* (Site Description) presents our current understanding of the natural system at Yucca Mountain. The natural system is being characterized because of its key role in establishing the ability of the proposed repository at Yucca Mountain to demonstrate a safety case for the preclosure and postclosure periods. The natural system forms the environment for which engineered barriers must be designed. Working in concert, the natural and engineered systems must provide reasonable assurance that the health and safety of the public will be protected.

The safety strategy for the proposed repository relies on a number of key attributes of the natural and engineered systems at Yucca Mountain. These attributes are:

- The combined systems will limit water contacting the waste packages.
- The lifetime of the waste packages will be long.
- The rate of release of radionuclides from the waste form will be slow.
- The concentration of radionuclides will be reduced as they are transported through the engineered and natural barriers.

Site characterization activities have, in large part, addressed the scientific underpinnings of these attributes. They have focused on producing an adequate understanding of the natural system such that the performance of the proposed repository can be assessed. In addition, they also provide the framework for design of the proposed repository and the information needed to address requirements described in Part 60 of Title 10 of the Code of Federal Regulations.

The description of the site and surrounding region represents a snapshot in time. Results of characterization activities completed by the end of September 1997 are included. In some exceptional cases, additional work carried out during the early part of fiscal year 1998 is also discussed (e.g., results of a seismic hazard assessment). Because it represents a snapshot in time, and because it summarizes work carried out at different times, there are some inconsistencies within the document. As work to characterize the site reaches its completion and more complete integration of results is accomplished these inconsistencies will be resolved, and the technical information will be better integrated both between and within chapters.

The Site Description summarizes and synthesizes both work carried out in accordance with the *Quality Assurance Requirements and Description* (DOE/RW-0333P) and also work performed outside that quality assurance program. Because the Site Description is a summary and synthesis document, no data were generated in preparing it. In general, information on the quality status of data discussed in the Site Description is, therefore, found in the reports forming the basis for the summarized material and cited in the text. In some cases, however, information on the quality status of data is specifically addressed in the Site Description. For Section 3, the Q status of some references is indicated by a [Q] or [NON-Q] notation in the reference list. For references without a notation, the source document should be consulted. In Section 5.3, the Q status of many data sets is addressed in the subsections in which the data are discussed. Q status of data in Sections 6.1 and

6.4 is described at the end of Section 6.4. For data in Section 6.3, the Q status of data is listed in the introduction to the section. For all other sections, readers interested in the Q status of data should consult the source references cited in the text.

For some of the data discussed in the Site Description, a Data Tracking Number (DTN) is provided. These numbers indicate that the data are available in the Technical Data Management System. In other cases, the location of data is addressed in the cited references. Although for future revisions a data verification process will be implemented to ensure data are available in the Technical Data Management System and that the DTNs cited are correct, this version has not benefited from such a quality check. At the present time, therefore, cited data should be considered "to be verified (TBV)."

The Site Description will evolve over the next several years to support the Site Recommendation and, if the recommendation is favorable and approved, a license application. New results will be incorporated and integration of the various sections will be enhanced. Thus, while the findings presented in this document represent our understanding today, ongoing and future work may modify some of the conclusions.

The Site Description begins with a brief discussion of the geography and demography of the site. It then describes relevant facilities that are located at the site or in its vicinity. This is followed by a presentation of the current state of knowledge for the site's geology, climatology and meteorology, hydrology, and geochemistry. Finally, the effects of repository construction, including especially heat, are addressed as they affect the geomechanical, geohydrological, and geochemical aspects of the natural environment in the near-field and altered zone.

ACRONYMS

ADEM	Automated Digital Electron Microscope
AZ	Altered Zone
BLM	Bureau of Land Management
BREN	Bare Reactor Experiment Nevada
CHn	Calico Hills nonwelded
CNWRA	Center for Nuclear Waste Regulatory Analyses
CRWMS	Civilian Radioactive Waste Management System
DOE	U.S. Department of Energy
DOPA	Dihydroxyphenylalanine
DTN	Data Tracking Number
ESF	Exploratory Studies Facility
IARC	International Agency for Research on Cancer
INAA	Instrumental Neutron-activation Analysis
IRSR	Issue Resolution Status Report
LA	License Application
MAP	Mean Average Precipitation
MAT	Mean Average Temperature
M&O	Management and Operating Contractor
MSL	Mean Sea Level
NAFA	Nordic Aquatic Fulvic Acid
NFE	Near-Field Environment
NRC	U.S. Nuclear Regulatory Commission
OIS	Oxygen Isotope Stage
PET	Pentaerythritol
PTn	Paintbrush Tuff Nonwelded
R/EFPD	Radiological/Environmental Field Programs Department
RMR	Rock Mass Rating
RQD	Rock Quality Designation

ACRONYMS (Continued)

SMOW	Standard Mean Ocean Water
SNL	Sandia National Laboratories
SZ	Saturated Zone
TCw	Tiva Canyon Welded
TDIF	Technical Data Information Form
TSPA	Total System Performance Assessment
TSw	Topopah Spring welded
USAF	U.S. Air Force
USGS	U.S. Geological Survey
UZ	Unsaturated Zone
VA	Viability Assessment
YMP	Yucca Mountain Site Characterization Project

SYMBOLS/UNITS

Ag	silver
Al	aluminum
Am	americium
Ar	argon
As	arsenic
Au	gold
Ar	argon
B	boron
b.y.	billions of years
Ba	barium
Be	beryllium
C	carbon
°C	degree celsius
Ca	calcium
Ce	cerium
Cl	chlorine
Co	colbalt
Cr	chromium
Cs	cesium
DC	direct current
Eu	europium
F	fluorine
Fe	iron
Ga	giga-annum
Gd	gadolinium
H	hydrogen
Hf	hafnium
K	potassium
k.y.	thousands of years
ka	kilo-annum
La	lanthanum
Li	lithium
Lu	lutetium
m.y.	millions of years
Ma	mega-annum
md	millidarcy
Mg	magnesium
mL/g	milliliters per gram
Mn	manganese
MPa	megapascals
N	nitrogen
Na	sodium

SYMBOLS/UNITS (Continued)

Nb	niobium
Np	neptunium
O	oxygen
P	phosphorus
Pb	lead
pCi	picocurie
pmc	percent modern carbon
ppm	parts per million
ppmv	parts per million by volume
Pr	praseodymium
Pu	Plutonium
Rb	rubidium
S	sulfur
Sc	scandium
Si	silicon
Sm	samarium
Sr	strontium
Ta	tantalum
Tb	terbium
Tc	technetium
Th	thorium
Ti	titanium
U	Uranium
Y	yttrium
Yb	ytterbium
Zr	zirconium
‰	parts per mil

4. CLIMATOLOGY AND METEOROLOGY

4.1 PRESENT CLIMATE AND METEOROLOGY

The purpose of this subsection is to provide a description of the present-day climatic and meteorological conditions in the Yucca Mountain area, and to show the importance of the broad range of atmospheric mechanisms that influence the past, present, and future Yucca Mountain climate. The distinction between climate and meteorology in this section is based on time scales. The present climate is a summary of weather conditions representative of a few tens of years; meteorology refers to weather conditions lasting from a few minutes (atmospheric dispersion or extreme values of wind speed and temperature) to a few years in duration. Climatic and meteorologic data representative of the Yucca Mountain area are applied in environmental, geohydrology, engineering design studies, and long term performance studies (Total System Performance Assessment (TSPA)-Viability Assessment (VA) and License Application (LA)).

The climate descriptions are intended to satisfy the U.S. Nuclear Regulatory Commission (NRC) guidance provided in the *Standard Review Plan for the Review of Safety Analyses Reports for Nuclear Power Plants* (NUREG 0800) (NRC 1987) to include:

- Types of weather patterns that influence the site.
- Data summaries using a period of record long enough (in time) to adequately describe current conditions, with qualifications for the extent to which the data are representative of the site area.
- Descriptions of the local meteorology of the site, including topographic influences. Thirty years is the time period used in standard climatic analyses and publications for the climatological "normal" conditions.

Central and Southern Nevada currently have an arid/semi-arid climate due to the present-day dominant large-scale weather features as well as the distance and many mountain ranges between the local area and the Pacific Ocean and Gulf of Mexico moisture sources. Very large (planetary) scale atmospheric features control the occurrence and motion of smaller (synoptic) scale weather features, which in turn cause significant inter-annual and seasonal variations in air temperature, cloud cover, and precipitation occurrence in a given area. Local terrain features modify the weather and airflow patterns, causing considerable variations of meteorological conditions over short distances (Mock 1996). Thus, descriptions are provided in Subsections 4.1.1 through 4.1.3 of atmospheric features on these scales: global (planetary), synoptic (Western United States), and regional and site (Southern Nevada down to the immediate vicinity of Yucca Mountain). The global and synoptic features are most relevant when relating present climatic conditions to the paleoclimate and future climate studies. Details on the Yucca Mountain Site Characterization Project (YMP) local network of meteorological monitoring stations is provided in Subsection 4.1.4.

4.1.1 Planetary-Scale Atmospheric Features

Planetary-scale features range in size from a few to tens of thousands of kilometers horizontally (continent size), to about 10 km vertically (within the troposphere), and have durations up to a month or more (Miller and Thompson 1970). These features are driven by solar radiation, the rotational motion of the earth, and the tilt of the earth's axis.

The spherical shape of the earth creates an imbalance in energy received at the surface, the equatorial band heating more than the temperate zones and much more than the polar regions causing the air to rise near the equator. As the relative rate of atmospheric pressure decrease with height is less in the tropics than at higher latitudes, a horizontal pressure gradient exists in the upper troposphere from the equator to the poles. Air at high altitudes moves poleward and air at low altitudes moves toward the equator to maintain mass conservation. Because of the rotation of the Earth, this one-cell circulation generally breaks down into an idealized three-cell circulation (see Figure 4.1-1).

The first cell is between about 5 and 30° latitude is known as a Hadley, or trade wind, cell (Randerson 1984). As the respective latitudinal air movements occur, the Coriolis effect force turns the airflow toward the right in the Northern Hemisphere causing generally westerly winds aloft and easterly winds near the surface. In addition, friction of the moving air with the underlying surface causes the surface winds to be angled toward the lower pressure near the equator. The surface winds in this cell are then from the northeast (NE Trade Winds) in the Northern Hemisphere and from the southeast (SE Trade Winds) in the Southern Hemisphere. The resultant convergence of the surface winds near the equator is termed the Inter Tropical Convergence zone (Figure 4.1-2).

Vertically, this means air rises in the tropics and sinks at the poleward edge of the Hadley cell. Because precipitation tends to be associated with the areas of rising air motions, the equatorial band experiences frequent rainfall. The poleward edge of the Hadley cell experiences downward moving air, causing clearing skies and reduced relative humidity. This action results in areas of high pressure (subtropical high) that predominate around the 30° latitude band where there is little precipitation and deserts over some of the land areas.

Poleward of the Hadley cell to about 60° latitude is an area of large, slow moving waves in the upper atmosphere that have smaller-scale waves and eddies transiting west to east through the larger waves. These waves and eddies are reflected at the surface as high and low pressure systems (Randerson 1984) and provide the mechanism for heat and momentum exchange between the tropics and polar regions. Within these waves, a narrow band of high-speed, high-altitude winds called the jet stream, shown in Figure 4.1-3, steer these circulations. The jet stream position varies and tends to be discontinuous. Because upward vertical motions occur beneath the jet stream, areas crossed by the jet stream have enhanced precipitation.

Poleward of about 60° latitude, the surface wind flow is generally easterly. This results from the spreading of the descending air over the poles. This air converges with the westerly flowing air from lower latitudes forming the subpolar low pressure area and is termed the Polar Front. The jet stream discussed in the previous paragraph is generally associated with the Polar Front and is termed the Polar Front Jet.

The tilt of the spin axis of the earth causes the change of seasons. The locations and strength of each of the circulation cells vary with the seasons. In the Northern Hemispheric winter, the earth's spin axis is sloped away from the sun. The Northern Hemispheric belt of high-pressure centers are closer to the equator, near 35° latitude, and weaker than in the summer. The Polar Front Jet is stronger and also closer to the equator, extending to near 30° latitude (see Figure 4.1-3). In the Northern Hemispheric summer, the earth's spin axis is sloped towards the sun. Both the Polar Front and the Northern Hemispheric belt of high pressure centers are more poleward (normally 45° latitude and 40°, respectively). The Polar Front Jet is weak and the high pressure centers are stronger in the hemispheric summer.

Interaction of the atmosphere with the oceans influences the planetary circulations of both mediums. About half of the northward transport of heat from the tropics is produced through atmospheric flux, but ocean circulation carries the remaining heat that balances the excesses at low latitudes with deficits at high latitudes. A significant amount of the heat transport is produced by the Kuroshio Current system, which brings relatively warm water across the Northern Pacific to the Gulf of Alaska and the coastal regions of the northwestern United States (Gill 1982). The origin of the Kuroshio Current is the mass of water piled up in the Western Pacific by the Equatorial Current, which is driven by the trade winds. In turn, rising air induced by the warmer waters of the Western Equatorial Pacific tends to be compensated by sinking motions in the Eastern Equatorial Pacific. The overall longitudinal and vertical air motion produces a circulation known as the Walker cell.

For reasons not yet fully understood, the planetary circulation previously described can become altered for periods of several months or years. A significant alteration has been given the name El Niño Southern Oscillation. El Niño Southern Oscillation is a part of the natural oscillation in the ocean/atmosphere system and has no defined beginning and end, but seems to recur on a 2 to 6 year cycle. However, the identifications and descriptions of the changes associated with El Niño Southern Oscillation are well known (Glantz 1996). These changes impact atmospheric circulation patterns and can modify climate conditions across the globe.

Essentially, El Niño Southern Oscillation results from breakdown of the Walker cell. The trade winds relax in the Central and Western Pacific and the warm surface waters that normally predominate in the Western Pacific then move toward the Eastern Pacific. This leads to an increase of convective activity in the Central and Eastern Pacific equatorial regions. At the same time, the jet stream becomes stronger in the Eastern Pacific. During the initial phases of El Niño Southern Oscillation development, the southward wind components along the West Coast of the United States decrease, causing reduced coastal up welling and near shore warming. As an El Niño Southern Oscillation event dissipates, the trade winds strengthen and the warm surface waters recede from the Eastern Pacific, reestablishing the Walker cell.

The effects of the El Niño Southern Oscillation cycle on the Western United States vary, depending on the phase, intensity, and duration of the event. The impact is most noticeable during the months of November through March. Figures 4.1-4 and 4.1-5 show the precipitation and temperature anomalies, respectively, for the years within the period 1950 through 1991 characterized by intense El Niño Southern Oscillation events. The Southern Nevada area is in the 0 to 1 inch (0 to 25 mm) precipitation anomaly range from November through February and the > 1-inch range in March. For

temperature, the same area is in the $<-1^{\circ}\text{C}$ range for December and March and in the -1 to $+1^{\circ}\text{C}$ range during November, January, and February.

4.1.2 Description of Synoptic-Scale Features and Processes

Synoptic-scale features are smaller than the planetary-scale features, generally with horizontal dimensions between 500 and 3,000 km, and tend to last a few days to a few weeks. These systems appear in upper-level charts as ridges and troughs; in surface weather maps as high pressure centers, low pressure centers, and fronts; and in satellite imagery as bands and vortices of clouds.

The origin of most synoptic systems is the air mass source regions established by the planetary flow pattern, in conjunction with the distribution of land and ocean. Generally, high pressure becomes established near the centers of air masses, while fronts and low pressure areas form where differing air masses meet. On charts of mean sea-level pressure, certain regions tend to have a predominance of either high or low pressure areas (Figure 4.1-6). These centers of action have acquired characteristic names (Huschke 1980). There are three centers of action that primarily affect the southwestern United States: the Bermuda High in the western part of the North Atlantic Ocean, the Aleutian Low in the Gulf of Alaska, and the Pacific High in the North Pacific between 30 and 40° N latitude and 140 to 150° W longitude. Great Basin precipitation characteristics have been related to three air trajectories: Pacific, Gulf, and Continental (Benson and Klieforth 1989). The most important to the Yucca Mountain area by far is the Pacific trajectory, followed to lesser extent by the Continental and Gulf trajectories.

In the winter, the eastward extension of the North Pacific High steers most cyclonic storms away from the southwestern United States. Thus, the desert southwest region experiences relatively few storm passages and tends to have mild, dry weather. As the centers of action shift position and change strength, the associated synoptic patterns also undergo changes. When the North Pacific High occasionally weakens and moves south or west, the Polar Front Jet drives storms, precipitation, and cooler air into the southwest. Cyclones movement is associated with jet stream positions. Figure 4.1-7 shows specific examples of upper-air patterns and the general orientation of jet stream positions associated with the passage of cyclones across Southern Nevada during winter and spring.

The situation depicted in Figure 4.1-7a produces the least precipitation of the examples. Evaporation from the cool moisture source region, the Gulf of Alaska, is lower than that over warmer water regions, therefore there is less available precipitable water in these systems. The long trajectory over land forces the airflow over several mountain ranges, causing much of the moisture to fall as precipitation before reaching the Southern Nevada region.

The condition shown in Figure 4.1-7b produces more precipitation in Southern Nevada because the trajectory is over warmer water longer, allowing more available precipitable water. The trajectory is still over mountain ranges which depletes a great deal of the precipitable water before reaching Southern Nevada.

The greatest potential for precipitation in the winter and spring occurs with the position shown in Figure 4.1-7c due to the warm water source area, the relatively short land trajectory and fewer mountainous obstacles. Cyclones on this path tend to stall, as so-called "cut-off lows," over the

desert southwest, creating a "circulation pump" that can produce precipitation as long as the cyclone remains in place.

In the summer, the North Pacific and North Atlantic (Bermuda) Highs control the southwestern United States weather. Much of the time the North Pacific High prevails over the area, producing dry, hot weather and a surface thermal low in the interior (Figure 4.1-6). By late summer, the Bermuda High extends more to the west, enhancing what is popularly termed the Southwest Monsoon to bring irregular surges of moisture inland from the Gulf of California and the Gulf of Mexico. On rare occasions, remnants of tropical cyclones also cross into the desert southwest. Both situations produce short-lived, intense precipitation episodes over widely-scattered areas.

The synoptic patterns influencing western North America precipitation anomalies have been examined using two circulation indices (Mock 1996). They are the Pacific-North American teleconnection index and the subtropical ridge index. Each describes air-pressure and air-mass relations that result in above-or below-average seasonal levels of precipitation.

4.1.3 Regional and Site Climatology

The Yucca Mountain region is arid/semi-arid and warm. Total rainfall is typically less than 10 inches (254 mm) per year. The air temperatures range between over 40°C during summer days to below 0°C during winter nights. Occasional stormy periods can have strong winds and/or significant rainfall. Snowfall occasionally occurs at elevations over about 3,500 feet above mean sea level on Yucca Mountain and elsewhere on the region. Lightning can accompany summer thunderstorms, but very few tornadoes have been reported in the region. Other potentially severe weather events, such as blizzards and hurricanes, do not occur in the region. Regional and local topography, and large-scale atmospheric circulation patterns, strongly influence both the typical and extreme precipitation events, air temperature, and airflow patterns under present-day climate.

4.1.3.1 Data Sources

In order to characterize the regional, long-term meteorological characteristics, data were analyzed from both the Radiological/Environmental Field Programs Department (R/EFPD) meteorological monitoring network (which is described in detail in Subsection 4.1.4) and selected regional National Oceanic and Atmospheric Administration meteorological stations. The sparsely populated region in the vicinity of Yucca Mountain has produced very few stations with sources of long-term (tens of years) historical climatic data. The stations are typically near populated areas such as Amargosa Valley and Beatty. Most of the stations are operated by cooperative observers coordinated by the National Weather Service; these stations have only daily measurements of precipitation total and the maximum and minimum air temperature. Some data useful to the regional climate analysis were also obtained from a network of meteorological stations operated by the National Oceanic and Atmospheric Administration, Air Resources Laboratory, Special Operations and Research Division in support of Nevada Test Site activities. The stations used in the regional analysis are identified in the map shown in Figure 4.1-8, and by geographic information listed in Table 4.1-1. The R/EFPD meteorological monitoring network stations are shown in Figure 4.1-9; the geographic information and detail on the monitoring program are provided in Subsection 4.1.4.

A recent report (CRWMS M&O 1997a) provides detailed descriptions of the spatial and temporal variations in meteorological conditions and summaries of meteorological data from both National Oceanic and Atmospheric Administration sources and the R/EFPD meteorological monitoring network. Relevant climatic summary tables from that report are included with this document. Further information on regional and local airflow patterns near Yucca Mountain is given in another recent report (CRWMS M&O 1997b). Discussions of the precipitation, air temperature and atmospheric humidity, and wind results follow in the next subsections.

4.1.3.2 Precipitation

Regional precipitation characteristics are described in this subsection, focusing on spatial and temporal variations. Data from surrounding stations are compared with data taken in the R/EFPD meteorological monitoring network in the immediate vicinity of Yucca Mountain to identify which regional stations might be the most representative of the immediate Yucca Mountain area (CRWMS M&O 1997a). Data from representative stations were analyzed to provide better understanding of long-term conditions near Yucca Mountain. The long-term data are described for three different time periods.

Annual average precipitation data for four nearby regional stations were compared with data from the nine-station R/EFPD meteorological monitoring network. The period of record for the comparison was from 1993 through 1996, which optimized the data available when the total network was operational. The 4-year average annual precipitation totals from the Beatty 8N and Desert Rock sites were 5.80 and 5.85 inches (147 and 149 mm), respectively. These results were similar to data from R/EFPD Sites 1 and 5, which were 5.79 and 5.37 inches (147 and 136 mm), respectively. Site 1 is in west-central Midway Valley on the east side of Yucca Mountain near the proposed repository surface facility area, and Site 5 is in lower Jackass Flats, midway between the Fortymile Canyon and Amargosa Valley areas.

The 4-year average precipitation total for Amargosa Valley was 4.01 inches (102 mm), which is similar to the 4.20-inch (107 mm) average from nearby R/EFPD Site 9. The average from the National Oceanic and Atmospheric Administration, Air Resources Laboratory, Special Operations and Research Division station JA in upper Jackass Flats was 7.18 inches (182 mm), which is similar to Sites 2, 3, 4, 7, and 8 on Yucca Mountain and in Midway Valley. These results show similarities between certain portions of the R/EFPD meteorological monitoring network and nearby stations, though the spatial differences on both the immediate local (few kilometers) and regional (tens of kilometers) scales are evident in the results.

Data were available from R/EFPD Site 1 and nearby National Oceanic and Atmospheric Administration sites from the 11 year period 1986 to 1996 (CRWMS M&O 1997a). Thus, data from the Beatty 8N, Amargosa Valley, and R/EFPD Site 1 sites were analyzed to show current inter-annual variations of annual precipitation totals. The annual data plotted in Figure 4.1-10 show differences approaching a factor of 2 for some years. The precipitation total in Amargosa Valley is consistently less than that at Site 1 or at the Beatty sites, but the relative amounts from year to year are similar. Table 4.1-2 is a listing of the means, extremes, and standard deviations of annual precipitation totals from these three sites during the period. These results demonstrate the similarities in annual precipitation totals for multi-year periods at these three sites. Therefore, an

examination of data from longer periods of record at the Amargosa Valley and Beatty sites could provide indications of precipitation characteristics near Yucca Mountain relevant to longer periods than are otherwise available through measurements in the local network.

Data from the Amargosa Farms and Beatty stations for a 30-year period were analyzed for longer term summary statistics, because these sites showed similarity to the R/EFPD Site 1 data. Thirty-year periods are used to calculate climatological "normal" values; this is the time period mentioned in some regulatory guidance (NRC 1987) as an acceptable period to characterize current climatic conditions. The 30-year period from 1966 through 1995 was selected to optimize the data available from the Yucca Mountain network and the nearby Amargosa Farms station, even though Amargosa Farms data were missing from 1971 through 1977. Data from two formal locations of the Beatty station were combined for this analysis, because of the reasonable compatibility between the two data sets. The station was moved about 9 km north of the previous location in 1972. Selected annual precipitation statistics for these two stations are shown in Table 4.1-3. The annual totals range between < 1 inch to >11 inches (25 to 279 mm); the averages for Amargosa Farms and Beatty are 4.21 and 5.53 inches (107 and 140 mm), respectively. The annual totals are plotted in Figure 4.1-11 to show the variations in annual totals.

By comparison, the northern portion of the higher terrain of Rainier Mesa north of the Yucca Mountain area typically has more precipitation than that near Yucca Mountain. The National Oceanic and Atmospheric Administration, Air Resources Laboratory, Special Operations and Research Division station A-12 is about 27 miles (44 km) north of Yucca Mountain, at an elevation of 7,490 feet (2,283 m) above mean sea level. The mean annual precipitation during the period from 1959 through 1993 was 12.76 inches (324 mm). The annual values ranged from 5.55 to 27.00 inches (141 to 686 mm). The maximum 24-hour precipitation total was 2.99 inches (76 mm).

Even longer term precipitation records and topical publications were studied to estimate the magnitude of extreme value precipitation events suitable for the Yucca Mountain area. The analyses of these extreme values are complicated by the infrequent occurrences of precipitation and the sparse coverage of measurement stations in Southern and Central Nevada, which increases the overall uncertainty in the results. The highest 24-hour precipitation values were estimated by statistical methods using data taken during 1957 to 1996 at the National Oceanic and Atmospheric Administration, Special Operations and Research Division station 4JA, which is located in the Nevada Test Site Area 25 in upper Jackass Flats. The 50-year, 100-year, and 200-year return periods for 4JA were estimated to be 2.78, 3.23, and 3.71 inches (71, 82, and 94 mm), respectively. Estimates of the same return period values based on 11 years of data from R/EFPD Site 1 were 2.68, 3.03, and 3.40 inches (68, 77, and 86 mm) (CRWMS M&O 1997a). The similarity in results enables the use of the long-term 4JA results for estimates of conditions in the Yucca Mountain area.

Observed daily rainfall totals have exceeded 3 inches (76 mm) at nearby sites within the last 15 years. The maximum daily precipitation event within 50 km of Yucca Mountain is not expected to exceed 5 inches (127 mm) (CRWMS M&O 1997a). This estimate is based on statistical analyses of observations, and considerations of atmospheric mechanisms. One guidance document produced by the National Weather Service (NWS 1977) developed estimates of maximum daily precipitation events that could occur (Probable Maximum Precipitation) in the Great Basin and Colorado River drainage. The value for the Yucca Mountain area is approximately 10 inches (254 mm) of rainfall.

This estimate is perceived as extremely conservative. A National Oceanic and Atmospheric Administration guidance document, NOAA Atlas 2 (NOAA 1973), shows the expected 100-year return period 24-hour rainfall for Yucca Mountain to be 2.60 inches (66 mm). A recent study by National Oceanic and Atmospheric Administration staff supporting Nevada Test Site activities (NOAA 1997) concluded that the 100-year return period value of a 24-hour precipitation event is 3.50 inches (89 mm). This estimate was based on more recent data than were used for the NOAA Atlas 2 document, which included some larger precipitation events than had been observed previously.

4.1.3.3 Temperature, Humidity, and Evaporation

The climatic summary tables in this report include monthly and annual summaries of mean, extreme, and mean of the extreme temperatures for the R/EFPD and select regional sites. The tables also include monthly averages of relative humidity data for four select hourly periods of the day. The periods are 0400, 1000, 1600, and 2200 Pacific Standard Time; 0400 and 1600 are the approximate times of minimum and maximum temperatures, respectively, which are near the maximum and minimum daily relative humidity values during the typical diurnal cycle. Atmospheric humidity is not recorded at the National Oceanic and Atmospheric Administration Cooperative Observer sites.

The annual mean temperatures reported (CRWMS M&O 1997a) at the R/EFPD sites ranged between 15.1°C at Site 6 and 18.2°C at Site 9, with the temperatures generally decreasing with increasing site elevation. Monthly mean temperatures span a larger range. For example, the highest and lowest monthly mean temperatures at Site 1 were 28.6°C in July and 6.0°C in December. The diurnal temperatures near Yucca Mountain tend to span a large range, particularly for valley floor site locations that are influenced by nighttime cold air drainage winds. An indication of the diurnal range is the difference between mean minimum and mean maximum temperatures at Site 1, which ranged from 8.5°C during December and January to 12.1°C in July.

The temperature data from the National Oceanic and Atmospheric Administration stations Desert Rock, Amargosa Valley, and Beatty were similar to the data taken at the R/EFPD sites. Temperature data from R/EFPD Site 1 in Midway Valley, R/EFPD Site 5 in Jackass Flats, Desert Rock, Austin and Caliente are summarized in Table 4.1-4. The mean extremes for the typical extreme months, January and July, are shown in the table. The data from Desert Rock are similar to those taken at the R/EFPD sites, while the data from Austin to the north and Caliente to the east show cooler conditions with lower temperatures.

The atmospheric humidity data taken at the R/EFPD sites also support the general climatic description of the area as "arid." Two humidity parameters were summarized, dew-point temperature and relative humidity. Dew-point temperature is the better indication of actual moisture content in the atmosphere, because it is not affected by ambient temperature as is the case with relative humidity. However, relative humidity is a measure of the ratio of actual moisture to the saturation value, which is a better indicator of drying potential of the air.

The monthly average dew-point temperatures at R/EFPD Site 1 during 1986 through 1996 ranged from -7.9°C in December to 1.1°C in August; the annual average is -4.2°C. The corresponding monthly and annual average temperatures are 6.2°C, 27.9°C, and 16.8°C, respectively. Thus, the

average annual difference between air temperature and the dew-point temperature (known as dew-point depression) is 21.0°C.

The annual average relative humidity at Site 1 (period 1986 to 1996, CRWMS M&O 1997a) ranged from 11.5 percent at 1600 Pacific Standard Time to 22.0 percent at 0400 Pacific Standard Time. These two time periods tend to represent the minimum and maximum values, respectively, of the diurnal cycle related to the air temperature cycle. The winter months tend to have higher average relative humidity levels, while the summer values are lower. The averages for January range from 33.1 percent at 1600 Pacific Standard Time to 44.6 percent at 0400 Pacific Standard Time. The averages for July range from 13.4 percent at 1600 Pacific Standard Time to 23.5 percent at 0400 Pacific Standard Time.

An important feature of the arid/semi-arid, warm climate of Yucca Mountain is the very high potential evaporation rate that occurs. The typically abundant sunshine, low atmospheric relative humidity, and moderate wind speeds contribute to the great evaporation potential in the area. Actual evaporation from the desert surface is limited by availability of water in the surface layers, though evapotranspiration rates from irrigated crop areas can be large because of water availability to the crops. A limited amount of evaporation data exists for Southern Nevada that would be representative of the Yucca Mountain area. One estimate of annual evaporation from a hypothetical lake is approximately 66 inches (Houghton et al. 1975), which is about a factor of ten greater than the average annual precipitation. Thus, the average annual precipitation is approximately 10 percent of the annual potential evapotranspiration. By contrast, large precipitation events result in significant runoff rather than evaporation of the precipitation.

Engineering design calculations frequently use routine summaries made from the American Society of Refrigeration, Heating, and Air Conditioning Engineers. The results for R/EFPD Site 1, which is located near the proposed location of some surface facilities, include a winter 99 percent dry-bulb design value of -5°C, and a summer 1 percent dry-bulb with coincident wet-bulb of 37°C and 16°C, respectively (CRWMS M&O 1997a). Wet-bulb temperatures are temperature depressions caused by water evaporating from the bulb of a thermometer. The greater the depression of the wet-bulb temperature relative to the dry-bulb, the drier the air and the lower the relative humidity.

4.1.3.4 Wind

The wind characteristics near Yucca Mountain reflect the high-desert, complex terrain environment of Southern Nevada, with topographic wind channeling, complicated nighttime atmospheric structure, and diurnal slope wind reversals. The resulting local and regional wind patterns are a product of topographic constraints, the diurnal ground heating cycle, and seasonal mesoscale weather systems.

Airflow resulting from mesoscale weather patterns in valley areas within the first few hundred meters above ground level is frequently channeled by valley topography to a narrow range of directions that follow along the axes of valley topographic features. Similar channeling occurs, though in shallower layers, in smaller canyons that are tributaries to larger valleys. Channeling is stronger during periods of stable atmospheric structure (reduced mixing conditions) which are typically associated with the nighttime hours.

Valleys and canyons also tend to cause airflow in an upslope direction during periods of heating of the ground surface, and in a downslope direction during periods of ground cooling. Competing slope winds in valley areas during the very stable (little vertical mixing) nighttime hours cause multiple airflow layers aloft with markedly different wind speed and direction characteristics.

The persistence of the local slope winds and regional-scale winds tends to make average wind speeds in the Yucca Mountain area about 2 to 4 m/s. Extreme wind speeds have exceeded 25 m/s at most of the monitoring sites in the area. Detail on average and extreme wind speed data at sites in the R/EFPD meteorological monitoring network are included in the climatological summary tables in Subsection 4.1.5 and a report on regional meteorological conditions (CRWMS M&O 1997a). Atmospheric dispersion and other airflow characteristics were the subject of another report (CRWMS M&O 1997b).

Wind rose figures are used in this report as graphical summaries of joint-frequency distributions of wind speed and wind direction. The figures resemble irregular spokes of a wheel; each spoke corresponds to wind directions from one of sixteen cardinal direction categories, such as north, east-southeast, etc. The length of the spoke is proportional to the frequency of occurrence of winds from the directions included in that category, with a scale shown in the figure. Each spoke also is structured with different pattern bars. These correspond to the occurrences of winds within six speed categories from the given direction, hence, the joint-frequency distribution.

Wind rose figures from all hours of the period 1993 through 1996 from five of the nine R/EFPD sites are shown in Figures 4.1-12 through 4.1-14. The pairs of wind rose figures were selected to show comparisons and contrasts between various wind characteristics.

The wind roses from the 10 and 60-m levels at Site 1 shown in Figure 4.1-12 both indicate the occurrence of two dominant directions, each occurring approximately one-half of the total hours. The southerly winds occurring at both levels have been shown (CRWMS M&O 1997b) to correspond to the daytime hours. The northerly winds at the 60-m level and the northwest through north-northwesterly winds at the 10-m level correspond to the nighttime hours. The directions at the 10-m level correspond to local drainage winds from surface topographic features on the east side of Yucca Mountain, while the northerly winds at the 60-m level correspond to airflow parallel to Yucca Mountain flowing through Midway Valley at this location.

Data from the hilltop Site 4 and nearby wash floor Site 7 were analyzed both for comparison with Site 1, since these sites are across Midway Valley northeast of Site 1, and for vertical structure, because their elevations differ by 153 m. The wind roses from Sites 4 and 7 shown in Figure 4.1-13 also show two dominant directions which also indicate (CRWMS M&O 1997b) a distinctive diurnal pattern. As with Site 1 data, both Sites 4 and 7 show southerly winds during the daytime hours. The Site 7 winds are shifted slightly toward the east due to topographic channeling through the gap between Fran Ridge and Alice Hill. The other dominant directions in the Site 4 data were north through northeast. These directions correspond to the higher terrain elevations in those directions, including Fortymile Canyon and the Calico Hills areas, and resemble the conditions of winds through Midway Valley seen in the 60-m level data at Site 1. The second dominant direction at Site 7 includes the west-northwest through north directions, particularly the northwest. These directions

correspond to downslope winds from Midway Valley flowing along the surface through Sever Wash and the gap between Alice Hill and Fran Ridge.

Data from Site 3 were analyzed as an example of exposure in a narrow canyon as a comparison to exposure in a broad valley, at Site 9. The wind roses from Sites 3 and 9 shown in Figure 4.1-14 are similar to the preceding figures with two basically dominant directions. The southeasterly winds at Site 3 in Coyote Wash correspond to flow in the upslope direction on the east side of Yucca Mountain. The very focused downslope wind direction is west-northwest; about one-fourth of the total hours at Site 3 had winds from the west-northwest at speeds less than 3.3 m/s, which was shown (CRWMS M&O 1997b) to be associated with nighttime drainage winds. The daytime winds at Site 9 indicate airflow toward the north, or up-valley, direction from Amargosa Valley into Jackass Flats. The nighttime winds at this site are mostly from the north-northeast and northeast directions. Although the valley is broad at this site, the nighttime winds remain consistent from a narrow range of directions.

Wind data taken from the twice daily upper-air rawinsonde ascents at the Desert Rock Airport by the National Weather Service were summarized as wind rose figures to compare the airflow conditions aloft in the area. The wind speed categories were modified from those used with the surface winds to distinguish between the higher wind speeds that occur aloft. The lowest speed category used with the surface-level winds was omitted from the upper-air plots, and the highest level was changed to the speeds that exceed 22 m/s, rather than 11 m/s.

The levels aloft used for the summaries are some of the pressure levels that are reported with all rawinsonde ascents. The pressure levels and their corresponding height above mean sea level in a standard atmosphere are: 850 mb at 1,457 m, 700 mb at 3,011 m, 500 mb at 5,572 m, and 300 mb at 9,159 m. The elevation of the Desert Rock Airport is 1,009 m above mean sea level. The 850 mb level is approximately the same elevation as the top of the Yucca Mountain ridge.

The wind roses for the 850 and 700 mb levels are shown in Figure 4.1-15, and the wind roses for the 500 and 300 mb levels are shown in Figure 4.1-16. The outer frequency ring is 20 percent for all the figures. The 850 mb level shows the regular occurrences of southwesterly winds, followed by nearly one-fourth of the time with winds from the north-northeast through east directions. Southwesterly winds are still the dominant direction at the 700 mb level, but the northeasterly winds seen at 850 mb are replaced by northwesterly winds. Both the 500 and 300 mb levels show the dominance of westerly wind directions.

Maximum observed wind gust speeds can exceed 40 m/s, particularly in exposed terrain locations. Observed 1-minute average wind speeds (frequently associated with previous "fastest-mile" data, that is, the outdated method of reporting the speed associated with the shortest time interval during which wind passing a totalizing anemometer would travel 1 mile) are approximately 30 m/s (67 mph). Statistical estimates of the 100-year return period of the gust and 1-minute speeds are about 50 m/s (112 mph) and about 45 m/s (101 mph), respectively. The fastest winds tend to be from either the northerly or southerly directions, with topographic channeling steering the winds along valley axes.

4.1.4 Meteorological Monitoring Network

The U.S. Department of Energy (DOE) YMP has been collecting and reporting results of measurements from a meteorological network in an environmental monitoring program since December 1985. The network site locations and measurements were chosen to: characterize local airflow and atmospheric dispersion, support engineering design of surface facilities, and comply with the State of Nevada air quality permit conditions related to site characterization field activities. Seventeen precipitation recording sites previously operated by the U.S. Geological Survey (USGS) as part of the Yucca Mountain studies were added to the network late in 1996. Previously collected data from these sites were used in the infiltration studies discussed in Subsection 5.3. The precipitation-only site locations were chosen to provide additional precipitation measurement coverage to YMP in current geohydrology studies.

The airflow and dispersion studies were focused in two primary locations: near potential emission sources in Midway Valley and the east side of Yucca Mountain; and along potential airflow pathways toward the nearest populated area, Amargosa Valley. The meteorological monitoring network expanded from five to nine sites during 1992 to improve understanding of local airflow in the area around the Exploratory Studies Facility and at the southern boundary of the Nevada Test Site near Amargosa Valley. Since topographic features such as hills and valleys have significant influence on local airflow and related dispersion characteristics, the sites were located in a variety of topography and over a wide area. Airflow studies (Blumen 1990) in areas with similar topography to that of Yucca Mountain have demonstrated complicated airflow and dispersion patterns.

The nine meteorological site locations cover a distance of 25 km (15.5 miles) on Yucca Mountain and the immediate vicinity, from Gate-510 on the southern boundary of the Nevada Test Site near Amargosa Valley to well pad WT-6 along the western Nevada Test Site boundary in Yucca Wash on the north side of Yucca Mountain. Site elevations range from 838 m (2,750 feet) MSL at Gate-510 to 1,478-m (4,850 feet) MSL on top of the Yucca Mountain ridge. Thirteen of the seventeen precipitation-only sites are focused in the east side of Yucca Mountain area; three sites are west of Yucca Mountain in Solitario Canyon and Crater Flat, and one site is a short distance north of Midway Valley in Fortymile Canyon. Site elevations of the precipitation-only sites range from 998 m (3,275 feet) MSL in Jackass Flats, northeast of Busted Butte, to 1,562 m (5,125 feet) MSL on the northern portion of Yucca Mountain. Figure 4.1-9 is a map showing the 26 site locations, with topographic contours at 100 m increments and primary elevations highlighted to show topographic features of the area. Topography is shown since it is relevant in the airflow, precipitation, and other meteorological characteristics of the area. Tables 4.1-5 and 4.1-6 are lists of the geographic coordinates and elevations of the full meteorological and precipitation-only sites, respectively.

Eight of the nine meteorological sites have towers with wind and temperature sensors mounted 10-m above ground level, and one site has a tower with these sensors also mounted at 60-m above ground level. The nine sites have temperature, atmospheric humidity, and solar radiation sensors mounted at the 2-m level, with barometric pressure and precipitation measurements made near the surface. All of the sites have tipping-bucket precipitation gauges. Detail on the measurements is given in Subsection 4.1.4.2.

4.1.4.1 Meteorological Sites

Detail on the nine meteorological sites is provided in this subsection, including the topographic exposure of the sites and any special purposes intended for the information collected at the site. The primary identifier of the sites is the site number; names for the sites are included to facilitate recalling the location, and to identify the site relative to site descriptions in older reports.

Site 1 (Nevada Test Site-60)—Site 1 is at an elevation of 1,143 m (3,750 feet) MSL. It is located in western Midway Valley, an area bounded on the west by Yucca Mountain, a north-south narrow ridge with a maximum elevation of 1,523 m (4,997 ft) MSL; on the east by Fran Ridge; and on the south by a saddle between Fran Ridge and Yucca Mountain, with elevations up to approximately 1,220 m (4,000 ft) MSL. This site has a multi-level meteorological tower that makes continuous wind and temperature measurements at 60 m and 10 m heights typically required by the NRC for dispersion analyses. The atmospheric profile information helps define both the vertical temperature and wind layer structures. Of the network sites, this site is the most representative of the Exploratory Studies Facility and proposed surface facilities area. Thus, data from this site are likely to be the focal point of atmospheric dispersion modeling activities. Because of its primary location, the remaining site locations are given relative to this site.

Site 2 (Yucca Mountain)—Site 2 is on top of the Yucca Mountain ridge, near the northern end. It is approximately 3.4 km (2.1 miles) west-northwest of Site 1 at an elevation of 1,478 m (4,850 feet) MSL. Data from this ridge top site were used to characterize airflow and other meteorological conditions along this portion of the Yucca Mountain ridge. This information can be useful in studying airflow above Midway Valley.

Site 3 (Coyote Wash)—Site 3 is midway up Coyote Wash, 2.3 km (1.4 miles) west-northwest of Site 1 at an elevation of 1,279 m (4,195 feet) MSL. This site is in one of the many canyon drainage areas that dominate the eastern slope of Yucca Mountain. Data from this site can be used to assess atmospheric conditions typical of these canyons, which are important to characterizing the frequent nocturnal drainage winds that affect airflow through Midway Valley.

Site 4 (Alice Hill)—Site 4 is on Alice Hill, in the northeastern portion of Midway Valley near the junction of Yucca Wash and Fortymile Canyon. It is 3.4 km (2.1 miles) northeast of Site 1 at an elevation of 1,234 m (4,050 feet) MSL. Data from this exposed hilltop location can be compared with that from Site 1, in Midway Valley, and Site 7, in Sever Wash, to study the vertical structure of the airflow along this likely pathway from the proposed repository in Midway Valley toward the nearest populated area in Amargosa Valley.

Site 5 (Fortymile Wash)—Site 5 is in the broad valley of lower Jackass Flats, on the eastern edge of Fortymile Wash, about midway between Yucca Wash to the north and Amargosa Valley to the south. The site is 9.4 km (5.8 miles) southeast of Site 1 at an elevation of 953 m (3,125 feet) MSL. Data from this site provides information on airflow between Midway Valley and Amargosa Valley through this portion of Jackass Flats.

Site 6 (WT-6)—Site 6 is the northernmost tower in the network; it is at well pad WT-6 on the western border of the Nevada Test Site, adjacent to the Nellis Air Force Gunnery Range, in the northern

portion of Yucca Wash. It is 6.1 km (3.8 miles) northwest of Site 1 at an elevation of 1,315 m (4,315 feet) MSL. This site monitors the southerly daytime airflow exiting the northern end of Midway Valley. It also monitors the nighttime drainage winds entering Midway Valley through Yucca Wash.

Site 7 (Sever Wash)—Site 7 is in the gap between Fran Ridge and Alice Hill on the east side of Midway Valley, 2.1 km (1.3 miles) east-northeast of Site 1 at an elevation of 1,081 m (3,545 feet) MSL. The site is near the lowest elevation in Midway Valley and is on a surface pathway of nocturnal drainage airflow that exits Midway Valley through this gap. Comparisons between conditions at this site and Site 4 on Alice Hill, which is 2 km north-northeast of Site 7 and 153 m (approximately 505 feet) higher in elevation, provides information on the vertical structure of airflow in this area.

Site 8 (Knothead Gap)—Site 8 is in the southern portion of Midway Valley in the saddle between the Yucca Mountain ridge and Fran Ridge, just northeast of Bow Ridge. It is 1.7 km (1.1 miles) south of Site 1 at an elevation of 1,131 m (3,710 feet) MSL. The site is east of the Exploratory Studies Facility South Portal. This location was chosen primarily to determine the pathway of nocturnal airflow in this portion of Midway Valley.

Site 9 (Gate-510)—Site 9 is near the southwest corner of the Nevada Test Site. It is 19.2 km (11.9 miles) south of Site 1 at an elevation of 838 m (2,750 feet) MSL, between Jackass Flats and Amargosa Valley. The site monitors near-surface airflow between the Nevada Test Site portion of the site characterization area and the community of Amargosa Valley, the populated area nearest the proposed repository location.

4.1.4.2 Measurements

The choices of meteorological monitoring equipment and methods were based on NRC regulations (AEC 1972; NRC 1977), the U.S. Environmental Protection Agency (EPA) guidance on monitoring for Prevention of Significant Deterioration (EPA 1987a) and regulatory modeling applications (EPA 1987b), and wind characterization guidance from the American Society for Testing and Materials (ASTM D5741-96). Although Prevention of Significant Deterioration regulations do not apply to the site characterization activities, meeting these requirements significantly increases the probability that the data collected can meet future dispersion modeling requirements. In addition, the State of Nevada air quality operating permit stipulates that equipment and methods must comply with the Prevention of Significant Deterioration guidance. The monitoring program also complies with YMP requirements, including the *Quality Assurance Requirements and Description* (DOE 1997).

The monitoring station equipment was purchased as systems and was installed and operated by the R/EFPD. The sensors were calibrated by either vendors or R/EFPD technical staff using equipment traceable to the National Institute of Standards and Technology, or other approved standards organizations. The sensors are described in Table 4.1-7; a summary of the measurement methods follows.

- All nine sites have horizontal wind speed and direction and vertical speed measured at 10-m above ground level. This is a standard height for wind measurements in dispersion studies.

The tower at Site 1 is instrumented with additional horizontal wind sensors at 60 m-above ground level to monitor conditions aloft near the proposed surface facilities. This is particularly relevant if there are emissions from elevated sources, such as stacks.

- Air temperature, incoming solar radiation, and relative humidity (Sites 2 through 9) or dew-point temperature (Site 1) are measured at 2 m-above ground level. Air temperature is also measured at 10 m-above ground level, providing a delta-temperature (an indicator of atmospheric stability) difference between 10 and 2 m-above ground level. Temperature is also measured at 60-m above ground level at Site 1 for the temperature difference between 60 and 10-m above ground level. The air temperature measurements have been made with mechanically aspirated shields since September 1993 at all sites, and since installation during 1992 at Sites 6 through 9. Prior temperature measurements were made in naturally-ventilated shields.
- Barometric pressure is measured near the surface. It is used in airflow analyses, and with ambient radon measurements in YMP radiological studies.
- Precipitation is measured near the surface by tipping bucket gauges to record the times of precipitation events. The gauges at Sites 1 through 4 and 6 through 8 were heated to measure frozen precipitation as it occurred. Sites 5 and 9 rarely receive measurable frozen precipitation, so those gauges were not heated. The 17 precipitation-only sites are unheated, due to equipment availability. Equipment temperature is measured with the precipitation events to assist interpreting the time and type of actual precipitation occurrences. Another type of gauge capable of measuring frozen precipitation as it occurs is being considered for some higher-elevation sites. Storage gauges were added at the nine meteorological sites during 1995 to measure precipitation totals by this method as well.

4.1.4.3 Monitoring Program Database

The onsite data loggers at the nine meteorological sites sample each measurement channel once per second. The measurement interval is 10 seconds at the precipitation-only sites. The measurements are processed into combinations of means, totals, and extremes and are recorded at 10-minute, 1-hour, and daily intervals. Precipitation events are also recorded as they occur.

Onsite data processing is used to calculate some special-purpose parameters, which are also recorded. The fastest 1-minute average wind speed (with corresponding direction) and the fastest running 3-second horizontal wind speed are relevant to engineering design. The daily extreme 1-minute average temperatures are relevant to climatic studies. The standard deviations of horizontal wind direction (σ -theta, also known as σ -A), vertical wind speed (σ -w), and horizontal wind speed (σ -u) are indicators of atmospheric stability and other airflow characteristics.

In addition to site identifier and time information, the onsite data records include system and temperature shield aspirator battery voltages, an event-marker used during onsite actions by site technicians, and a unique data logger and on-site calculation routine identifier.

The monitoring program produces a database of valid, qualified data for each site. Tables 4.1-8 through 4.1-10 contain descriptions of the parameters in this database.

4.1.4.4 Quality Assurance Activities

The meteorological monitoring program includes quality assurance and quality control activities that ensure the program collects documented, valid data. Work instructions control the quality assurance and quality control activities based on a combination of NRC and Prevention of Significant Deterioration monitoring guidelines and the DOE Office of Civilian Radioactive Waste Management Quality Assurance program presented in the *Quality Assurance Requirements and Description* (DOE 1997).

The onsite activities include system checks at the sites by the R/EFPD operations staff. Technical and scientific staff track equipment usage and identify and resolve out-of-tolerance operating conditions. Data were downloaded from electronic storage media from the sites at least monthly, and sent to the R/EFPD data processing staff to begin the validation process. Data files were imported into a database, during which unusual values were listed for examination by data staff. Objective data processing routines, supplemented by professional judgement and multiple reviews, are used to validate the database. The data were given technical reviews by field meteorologists and technical staff as part of the routine validation process controlled by procedures.

The active monitoring systems were given periodic performance audits by independent contractors, following U.S. Environmental Protection Agency Prevention of Significant Deterioration monitoring guidance. Other project conformance audits were performed by Management and Operating Contractors (M&O), YMP, and other DOE organizations.

4.1.5 Climatological Summary

Summary tables of present climatological data obtained from recent historical records from the YMP and other sources are presented in this subsection. Data from these tables were discussed in previous portions of this subsection. These data summaries were created to provide the reader with more comprehensive listings of summary data. The summary tables are grouped into four topics. The first group is typical climatological summaries of data from the YMP's R/EFPD meteorological monitoring stations, followed by similar data from nearby National Weather Service stations in Central and Southern Nevada. The third group is two sets of annual precipitation totals from the few National Weather Service stations in Central and Southern Nevada with long periods of record. Finally, specific R/EFPD data are summarized for certain engineering design tasks.

The statistical terms used in this subsection are identified below. Further information is also provided for the application of these terms to specific measurements.

Statistical Terms:

Extreme Maximum - The absolute highest daily value

Mean Maximum - The average of the highest values

Mean - The average of all values taken over a given period of time

Mean Minimum - The average of the lowest values

Extreme Minimum - The absolute lowest daily value

Fastest 1-Minute - The highest wind speed measured over any 1-minute period, with the associated wind direction

Peak 3-second wind speed - The highest 3-second running average wind speed

Mean Diurnal Range - The average of the differences between the highest and lowest one-hour average temperature values

Summaries Specific to Measurements:

Temperature - The mean values, and the daily extreme values prior to 1994 (1996 at Site 1) are based on hourly averages of one second samples. As of 1994 (1996 at Site 1), the daily extreme values are based on one second data averaged over one minute.

Number of Days - The number of days summaries are based on the number of calendar days for the period meeting the precipitation or temperature occurrence criteria. The averages were taken of the occurrences during the years of the summary.

Barometric Pressure - Barometric pressure averages are based on hourly averages of one second data.

Mean Relative Humidity - Averages are based on hourly averages of one second data calculated for four specific hours during the day spaced at six-hour intervals: 0400, 1000, 1600, and 2200 Pacific Standard Time.

Precipitation - The maximum for the 6 and 24 hour periods are based on a continuous running period which may encompass more than one calendar day. The total is based on the average of the entire period for each month. Entries with a "T" indicate that a trace of precipitation (or snowfall) was observed.

Wind - Average wind speed is based on hourly averages of one second data. The fastest one-minute wind speed and peak three-second gust are based on extremes of one second data averages.

Tables 4.1-11 through 4.1-19 are monthly and annual climatological summaries from R/EFPD Sites 1 through 9, respectively. Table 4.1-20 is the annual summaries for all nine R/EFPD Sites. The sites locations are described in Subsection 4.1.4. The data periods for the summaries of the R/EFPD Sites are shown below:

Site 1: All measurements are based on an 11 year period running from 1986-1996.

Sites 2 - 5: Temperature, relative humidity, and average wind speed are based on a 11 year period running from 1986-1996. Barometric pressure and precipitation are based on an eight year period running from 1989-1996. Fastest one minute wind speed is based on a four year period running from 1993-1996 and peak three second gust on a 3.5 year period running from mid 1993-1996.

Sites 6 - 9: All measurements except for peak three second gust are based on a four year period running from 1993-1996. Peak three second gust is based on a 3.5 year period running from mid 1993-1996.

Tables 4.1-21 through 4.1-24 are monthly and annual climatological summaries of temperature, precipitation, and snowfall data from National Weather Service sites in central and southern Nevada.

Tables 4.1-25 and 4.1-26 are annual precipitation totals for some central and southern Nevada National Weather Service sites during two respective time periods: 1921 through 1947, and 1948 through 1995.

Table 4.1-27 is a summary of the American Society of Heating, Refrigerating, and Air Conditioning Engineers data for the R/EFPD Sites. The contents of Table 4.1-27 is identified below by the columns in the table (see ASHRAE 1993).

Column 1, Station: Site number and (name) for the Environmental Field Programs Division meteorological monitoring station.

Column 2, Latitude: Site latitude in degrees, minutes, and seconds.

Column 3, Longitude: Site longitude in degrees, minutes, and seconds.

Column 4, Elevation: Site elevation in meters.

Column 5, Design Dry-Bulb: The dry-bulb temperatures in degrees Celsius that have been equaled or exceeded by 99 percent and 97.5 percent of the total hours in December, January, and February.

Column 6, Design Dry-Bulb and Mean Coincident Wet-Bulb: The dry-bulb temperatures in degrees Celsius that have been equaled or exceeded by 1 percent, 2.5 percent, and 5 percent of the total hours in June, July, August, and September. The listed wet-bulb temperature is the mean of all wet-bulb temperatures coincident with those dry-bulb temperatures exceeding the given levels.

Column 7, Mean Daily Range: The difference between the average daily maximum and average daily minimum temperatures in degrees Celsius for the warmest month.

Column 8, Design Wet-Bulb: The wet-bulb temperatures in degrees Celsius that have been equaled or exceeded by 1 percent, 2.5 percent, and 5 percent of the total hours in June, July, August, and September.

Column 9, Prevailing Wind: (Winter) The wind direction occurring coincidentally with the 97.5 percent dry-bulb temperature in December, January, and February. (Summer) The wind direction occurring coincidentally with the 2.5 percent dry-bulb temperature in June, July, August, and September. (M/S) The mean wind speed in meters per second occurring coincidentally with the 97.5 percent dry-bulb temperature in December, January, and February.

Column 10, Median of Annual Extremes: The median of the annual extreme maximum and minimum temperature in degrees Celsius.

INTENTIONALLY LEFT BLANK

4.2 PALEOCLIMATOLOGY

4.2.1 Introduction

Climate change, along with the resulting hydrological change has the potential to affect the long-term performance of a repository system within Yucca Mountain. In contrast to volcanism and tectonism, climate states typical of the past are certain to re-occur in the future on time scales short enough to be of great significance to the interaction between the repository and the hydrologic system at Yucca Mountain and for long-term assessments of exposure pathways. This subsection documents the timing, magnitude, and character of past climate change in the Yucca Mountain area and establishes the rationale for projecting such changes into the future.

Estimating and bounding future hydrologic conditions within the Yucca Mountain unsaturated zone, saturated zone, and groundwater discharge zone requires an understanding of potential future climate-change scenarios, including their timing. Climate change on the century through millennium to tens of millennia time scales are of most interest to this project, because a repository must isolate or impede radionuclide transport during the postclosure period. Wetter and or cooler climates that persist for centuries or millennia are of the greatest interest, because such climates produce more infiltration, percolation, higher water tables, and groundwater discharge relative to present hydrologic conditions. See also Subsections 5.1.4, 5.2, but especially, 5.2.6, and Subsections 5.3.3, 5.3.4, 5.3.5, and 5.3.7 in Subsection 5.3 in the Hydrology Chapter for aspects of the hydrological system that are directly linked to climate change.

Paleoclimatology offers insights into long-term climate history and factors thought to cause climate change. Interpretation of paleoclimate records provides a rationale to link unsaturated zone percolation, saturated zone hydrology (*sensu* a higher regional water table), past groundwater discharge, and climate history. The linkage of past climate, especially parameters such as mean annual temperature and mean annual precipitation, and past Yucca Mountain hydrology offers a basis for bounding the relation between climate and hydrology in the future. The general characteristics of future climate change are discussed below in Subsection 4.3.

The paleoclimate subsection provides an analysis of the Quaternary climate by describing the astronomic, atmospheric, hydrospheric, cryospheric, and biospheric aspects of the successive past climatic regimes, and the magnitude and rates at which the climate change has occurred. Changes in precipitation and air-temperature regimes are discussed and changes in wind flow patterns are inferred. The primary records of past climate change largely come from stratigraphic successions of plant and animal fossils and both stable oxygen ($\delta^{18}\text{O}$) and carbon ($\delta^{13}\text{C}$) isotopes as well as from radiogenic strontium isotopes ($\delta^{87}\text{Sr}$). The equally important age relations of the climate records are derived from uranium-series disequilibria, $^{230}\text{Th}/\text{U}$, uranium/lead (U/Pb), radiocarbon (^{14}C), tephrochronology, paleomagnetic polarity stratigraphy, and stratigraphic position.

Climate change drivers and history are discussed in the context of global, regional, local, and site records of climate change. The term "region" includes records from outside of the Yucca Mountain precipitation area, but within approximately 100 miles in any direction from Yucca Mountain. As such, the regional records will identify the rate and timing of climate change as well as the duration of climate states, but the magnitude of that change may or may not apply to the Yucca Mountain

precipitation area. "Local," by contrast, involves records from within the Yucca Mountain precipitation area and would include, for example, precipitation falling on the Spring and Sheep Mountains as well as on the Yucca Mountain catchment itself. "Site" records are those on and within Yucca Mountain. Climate records, whether at regional, local, or site scales may be long and continuous, such as those from Owens Lake or Devils Hole, or short and discontinuous, such as those obtained from pack-rat middens and marsh deposits.

Quality Assurance Controls The work described in Section 4.2 is based on both Q and non-Q data. The non-Q data are derived from the literature. The Q data were collected in accordance with the *Quality Assurance Requirements and Description* (DOE 1997) for the Yucca Mountain Site Characterization Project. Data quality status for each subsection is indicated below:

Section	Data Quality Status
4.2.2	Causes and the Nature of Global Quaternary Climate Change–Non-Q.
4.2.3.1	Long Regional Records of Quaternary Climate Change: Devils Hole–Non-Q.
4.2.3.2	Long Regional Records of Quaternary Climate Change: Death Valley–Non-Q.
4.2.3.3	Long Regional Records of Quaternary Climate Change: Owens Lake–Q and non-Q. Microfossil data sets (ostracodes and diatoms) are Q. Cores, age models, radiocarbon ages, volcanic ash determinations, stratigraphy, and sedimentology are all non-Q.
4.2.4.1	Local Records of Late Quaternary Climate Change: Pack-Rat Middens–Q and non-Q. Radiocarbon ages and plant macrofossil data collected from the middens are Q. Interpretations of the midden data and interpretations referenced from the literature are non-Q.
4.2.4.1	Local Records of Late Quaternary Climate Change: Wetland and Spring Deposits–Q and non-Q. Interpretations and data from references with Quade as the senior author are non-Q. Data in Brennan and Quade (1997) and other data in this subsection are all Q.
4.2.5	Site Records of Climate Change–Q and non-Q. Data specifically collected for the Yucca Mountain Project are Q. Data from other studies, such as those by Quade and Cerling (1990) and Cerling and Quade (1993), are non-Q.
4.3.1	Future Climate Variation: Modeling–Q and non-Q. Data from Schelling and Thompson (1997) are Q; other material is non-Q.
4.3.2	Future Climate Variation: Forecasting Using Paleoclimate Data–Q and non-Q. Data used to reconstruct climate from Owens Lake is Q; other material is non-Q.

4.2.2 Causes and the Nature of Global Quaternary Climate Change

Climate change operates on a wide range of time scales. The Phanerozoic, the last 570 m.y. of earth history when life flourished on the planet, contains many climates, some like the Quaternary (about the last 1.6 m.y.) and many very unlike the Quaternary and unlike any that will occur in the next million years. Unusual past climates include long-term global aridity during the Lower to Middle Triassic period or humid tropical conditions common to the Cretaceous (Dickens 1993; Donn 1987).

All of the drivers of modern-day climate and of climate for about the past 500 k.y. operate in a world with a particular land, mountain, ocean, and atmospheric-circulation configuration. Geological scale climate drivers, such as continental drift, which result in different land and ocean configurations, and the location and heights of mountain ranges, change slowly over thousands of millennia, so operate on time scales outside the interest of the YMP. As those longer-term drivers of climate change, then so does the general nature of climate even though factors such as variation in solar insolation remain about the same. The global aridity during the Triassic or the tropical humidity of the Cretaceous were subject to essentially the same orbital parameters and similar variability in solar output as the world is today. If the land and ocean configuration of the Quaternary had been different, then climate during the past 2 m.y. would have been quite different. The climate for the next 500 k.y., like that of the past 500 k.y., will be determined by changes in climate drivers that operate on the hundred to ten millennia and even shorter time scales.

4.2.2.1 Relations of Climate Change to Factors Operating on Different Time Scales

Climatic changes on time scales of hundreds to tens of millennia correlate with, and may be driven by changes in insolation received by the earth in the upper atmosphere. Changes in insolation may, for example, result from multi-millennial earth orbital cycles or from decade to century solar output cycles. The way in which the earth's lower atmosphere (troposphere) transfers that insolation into climate is further influenced by nonperiodic phenomena such as volcanic eruptions, cloud cover, CO₂ and water-vapor levels, and snow or ice cover that affect the refractive and reflective characteristics of the atmosphere.

Refractive and reflective characteristics of the atmosphere affect the amount of incoming short-wave and outbound, long-wave radiation and hence the atmosphere's energy (heat) budget. Global warming, for example, is based on the capacity of elevated levels of atmospheric CO₂ and water-vapor to reduce outbound, long-wave radiation resulting in a gain in atmospheric energy (heat). Conversely, snow cover increases the reflective characteristics of the earth surface and increases outbound radiation resulting in an energy (heat) loss. Cloud cover may both reflect and capture inbound, short-wave radiation creating an energy (heat) loss. Sulfate derived from volcanic eruptions also reflects and absorbs inbound radiation resulting in heat loss. Atmospheric dust, especially if it resides in the stratosphere where it cannot rain out, also plays a significant role in the atmospheric energy budget.

The tropospheric heat budget has a variety of often complex checks and balances or feedback mechanisms that maintain it within certain energy bounds. For example, if global warming persists, the level of water vapor in the atmosphere (specific humidity) will increase potentially resulting in an increase in cloud formation that, over time, could counter the heat gains due to global warming.

Gain or loss of heat between the oceans and the atmosphere represent another important and complex set of atmospheric heat budget feedback phenomena. All of these tropospheric processes operate within present day insolation levels that are determined by orbital parameters and the amount of solar output. Because the earth orbital parameters and solar output change with time, then so too must the gross insolation levels received in the earth's upper atmosphere. Thus the tropospheric processes are ongoing but they must ultimately deal with the changing amounts of insolation. Those orbital and solar-induced changes in insolation are small, but based on long climate records, are correlated with the advance and retreat of the glacial periods.

4.2.2.1.1 Orbital Parameters

The shape of the earth's orbit, angle of its spin axis relative to the ecliptic, and the seasonal tilt toward or away from the sun change on a cyclical basis (Berger and Loutre 1991). Changes in the distance from the sun or the angle of incidence of incoming sunlight are important factors determining the amount of insolation the earth receives at a particular moment in time. Of course, the seasonal differences in insolation, when the earth's hemispheres face toward or away from the sun, are the largest.

The shape of the earth's orbit changes from almost circular to slightly elliptical on roughly a 100 k.y. time scale due to the gravitational pull of the sun and the other planets, but especially Jupiter. The tilt of the earth's spin axis relative to the ecliptic changes by about 2.5° about every 44 k.y. Finally, the earth slowly wobbles over about a 24 k.y. cycle during its orbit resulting in a change in the seasonal tilt of the spin axis with respect to the sun about every 12 k.y. These orbital parameters are called eccentricity, the shape of earth's orbit; obliquity, the angle of the earth's spin axis; and precession, the wobble of the earth's spin axis (Figure 4.2-1). Berger and Loutre (1991) describe the behavior and timing of earth orbital parameters and the criteria to calculate these parameters past and future.

The cyclical and systematic changes in the distance and aspect of the earth relative to the sun and the resulting changes in insolation on a millennial time scale are correlated with the waxing and waning of the glacial periods. Because the glacial periods dominate Quaternary climate history and are periods of sustained higher effective moisture, understanding the past and possible future relation between climate and insolation is key to understanding the Yucca Mountain site hydrology.

Global climate may be thought of as processes operating within the atmosphere to balance a perpetually out-of-balance heat budget resulting from the fact that the earth receives more insolation (heat) at the equator than at the poles. As a consequence of the insolation imbalance, heat is transported toward the poles from the equator by both the atmosphere and the ocean. Heat transport within the atmosphere interacts in complex ways with the oceans and the land resulting in the large and small-scale features of synoptic and global circulation described in Subsections 4.1.1.1 and 4.1.1.2.

Changes in the earth's insolation over millennia results in a change in the heat budget between the equatorial regions and the poles; as the heat budget changes so does climate. Change from one millennium to the next is small, but over many millennia the changes are significant and correlative with the major features of climate change, the glacial and interglacial periods.

Eccentricity plays a key role in the nature of earth's insolation. When the earth's orbit is nearly circular, the tropics receive the same amount of heat in all months. Also, heat input to the Northern and Southern Hemispheres is seasonally symmetrical, that is, the Northern Hemisphere receives the same amount of heat in its seasons (for example, winter, December) as does the Southern Hemisphere in its equivalent season (for example, winter, June). When the orbit is elliptical heat input to the tropics varies seasonally and the heat input to the Northern and Southern Hemispheres is asymmetrical, i.e., not seasonally equal. The change from circular to elliptical orbits occurs over an approximately 100 k.y. cycle, but successive cycles differ in magnitude of the change from a circular to an elliptical orbit. Commonly, four 100 k.y. cycles "cluster" to form a 400 k.y. cycle (Berger and Loutre 1991). Figure 4.2-2 shows two such cycles during the last 1 m.y.

Obliquity determines the angle of incident rays from the sun and hence the magnitude of insolation change at high latitudes. The tilt of the earth's spin axis changes from about 22 to 24.5° over approximately a 44 k.y. cycle. A change in the earth's axial tilt results in a change in the areal extent of the polar circle and hence the relative amount of heat received by the polar region during the year. Obliquity serves to increase or decrease the polar heat deficit relative to the tropics and in this way increases or decreases the strength of the polar cell. The obliquity effect will be expanded or contracted as its periodicity moves in and out of phase with eccentricity.

Precession amplifies or dampens the changes in insolation that occur with eccentricity. Today the earth's orbit is slightly elliptical and the earth is at its minimum distance from the sun during the Northern Hemisphere winter, but is tilted away from the sun. Necessarily, the Southern Hemisphere is tilted towards the sun today when the earth is at its minimum distance from the sun. Thus the Southern Hemisphere receives more insolation during its summer than does the Northern Hemisphere during its summer and the opposite is true for the winters. However, because the earth wobbles on its axis over a 12 k.y. period, the seasonal minimum and maximum distances to the sun reverse for the Northern and Southern Hemispheres every 12 k.y. So, a full precession cycle is 24 k.y. and is of major importance to the global heat budget. Eccentricity exercises a major influence over precession (Figure 4.2-3).

The orbital parameters eccentricity, obliquity, and precession operate on a millennial scale and either add or subtract to insolation. Seasonal changes in insolation at the Equator and in the Northern and Southern Hemispheres drives the climate system as described in the subsection above on modern climate. Change in insolation has the potential to change climate on a global scale in a major way, not just perturb it as happens with, for example, volcanic eruptions. Because insolation is calculated from known principles of celestial mechanics, future values of insolation may be determined (Figure 4.2-4). The next 100 k.y. subcycle will describe a relatively circular rather than elliptical orbit. The last time that occurred was 400 k.y. ago and as shown in Figure 4.2-5, insolation for the next 100 k.y. will be quite similar to that between 400 ka and 300 ka. Clearly because the eccentricity, obliquity, and precession cycles have different frequencies, they collectively will act to reinforce or dampen their affect on insolation as can be seen by inspection of long-term insolation curves for different latitudes of earth (Figure 4.2-6a and b).

4.2.2.1.2 Climate Variability: Factors That Can Vary Climate at Short Time Scales

A number of phenomena affect the energy budget of the atmosphere on short time scales ranging from decades to several centuries. These phenomena occur across all climate modes and therefore act variably on the sensible climate at the surface of the earth. Sometimes the effects of the phenomena will be small, sometimes self-canceling, but at other times additive, thereby creating major changes in precipitation and temperature. These changes can be important in the future climate of Yucca Mountain and, to the extent they are predictable, need to be incorporated into future scenarios for climate-mediated, hydrologic change at the repository site.

Solar Variability—The energy delivered to the earth from the sun is not constant, but changes a fraction of a percent in relation to solar activity or the number and distribution of turbulent and calm areas on the sun surface. By itself, the small change in irradiation is not considered to be sufficient for climate change. Nevertheless, climate changes have coincided with changes in solar activity, possibly for reasons related to cosmic radiation and its role in cloud formation and enhancement of precipitation (Karlen and Kuylenstierna 1996).

Variability in solar activity occurs in short-term cycles ranging from the familiar “sun-spot cycles” of 11 years duration to longer periods of greater and lesser activity. The total solar irradiance, which is a measure of the climate-driving radiative energy received by the earth from the sun, has a direct association to solar magnetic activity (sun spots) and also to climate change as measured by historical records of climate and sun spots (Eddy 1976; Willson 1997).

Changes in the variability of solar irradiance may impact climate globally. For example, Willson and Hudson (1988) suggested that the decrease in total solar irradiance during the Maunder Minimum (a period of very low sun spot activity between A.D. 1650 and 1715) may have been a contributing factor to the Little Ice Age climate anomaly that coincided with expansion of glaciers throughout much of Northwestern Europe (Bradley and Jones 1992; Grove 1988) and a general lowering of temperature of about 1°C. Similarly, colder and moister climates indicated by tree ring chronologies of the White Mountains in Eastern California (La Marche 1974) also correlate to the time of Little Ice Age environments in Europe. In addition, interpretation of pollen records from the Pahranaagat Marshes, about 110 km northeast of Yucca Mountain (Wigand 1997), show persistent sub-millennial-scale gains in precipitation and reductions in temperature that correlate in time with Little Ice Age-style climate changes seen in tree ring records. The Pahranaagat Marsh core for the past 2.0 k.y. also records century-scale fluctuations of pollen types indicative of episodes of wetter and drier climates that indicate a regional effect of short-term climate change on desert vegetation.

Total solar irradiance may affect important climate drivers such as insolation. At present the earth experiences an increasing trend in solar irradiance, which may be part of a 250- to 350-year cycle (Wigley and Kelly 1990). If this continues, it can significantly add to the predicted effects of global warming caused by greenhouse gases (Willson 1997).

Volcanism—Volcanic eruptions indirectly affect climate by particulate and aerosol emissions, particularly of sulfur. The idea that dust from volcanoes causes earth cooling by blocking solar radiation has been shown to be of limited importance when the dust is in the troposphere because it is readily rained-out. In contrast, volcanic sulfur emissions react to produce sulfuric acid aerosols,

which have much longer residence times and can efficiently back scatter and absorb incident solar radiation causing atmospheric cooling (Carroll 1997). Such emissions can cause cooling of global temperatures on the order of a few tenths of a degree Celsius (Bryson 1989; Self et al. 1981). Typically such effects last about 1 to 5 years, but when they occur in combination with other short-term climate variables, such as El Niño events, large changes in precipitation can occur. For example, the recent (June 1991) Mt. Pinatubo eruption, in combination with El Niño, may have contributed to the above normal precipitation in the southwest.

Although there have been periodicities in the number and size of volcanic eruptions (Bryson 1989), they appear related to crustal movements caused by tectonics and possibly by ice loading or unloading that may or may not follow regular cycles of variation. Consequently, although the climatic effects of volcanic eruptions can be considered in future climate scenarios, they cannot be accurately predicted.

Carbon Dioxide—Human-caused increases in CO₂ have generated much public concern about their role in changing climate, because higher levels of atmospheric CO₂ act as a trap for outbound long-wave radiation, thus warming the earth (Broecker 1997). The consequences of a warmer earth will almost certainly result in greater amounts of water vapor entering the atmosphere which should appear as increased precipitation at least in some areas. There is less agreement at present whether climate variability observed today, or in the last few years, actually results from increased CO₂ levels whose rise arguably began in the industrial revolution with the widespread use of coal and then petroleum products for energy or from the variable impacts of other factors such as the current solar radiation cycle and volcanic dust (Crowley 1996).

Natural levels of CO₂ varied significantly in the past, particularly between glacial and interglacial periods, as a function of ocean circulation, ocean chemistry, ocean productivity, ocean temperatures, terrestrial vegetation cover, and other factors including volcanism. Low CO₂ levels during glacial periods changed to pre-industrial modern levels over the course of millennia in some ice cores (Neftel et al. 1988) but rapid (50 years or less) changes of smaller magnitude occurred both within glacial and interglacial periods (Stauffer et al. 1984). The basic individual mechanisms underlying CO₂ variations are known, but neither the details nor the dynamics of the overall changes (Siegenthaler 1989). Nor is it known whether climate changes affected CO₂ levels or visa versa. Climate changes at Yucca Mountain were and will certainly be affected by changes in the global carbon budget. Because CO₂ is so intimately linked with climate change, their separation at this time is not possible.

El Niño—The eastward migration of warm surface ocean water from the tropical Western Pacific Ocean occurs as a result of relaxed trade winds linked to barometric pressure differences between the Western and Central Pacific. This reversal of “normal” atmospheric circulation in which surface airflows from east to west towards low-pressure areas in the Western Pacific Ocean occurs when surface atmospheric pressures are higher in the west (over Indonesia and Australia) and lower to the east. The relaxation of trade wind flow is a complex relation between ocean and atmosphere whose cause is not fully understood. From a global atmospheric perspective the relaxation of the trades, in part, represents a reduction or fragmentation of Hadley circulation. Further, circulation along the equatorial Pacific called Walker flow (see discussion under Subsection 4.1.1), collapses and a similar, but unnamed circulation, originates in the Eastern Pacific, as winds blow from west to east

carrying warm water to the west coasts of North and South America. This results in drought in Australia and increased precipitation over Western South America. The warm ocean water increases atmospheric convection, and in combination with a strengthened flow of the polar jet stream can dramatically increase precipitation in the Southwestern United States over periods of 2 to 8 years (Cayan and Webb 1992).

Analyses of high-resolution, proxy records of climate, tree rings, corals, ice cores, and valved sediments, have made it possible to extend the history of El Niño Southern Oscillation farther back in time. Of relevance to Yucca Mountain are data that suggest variability in the intensity and frequencies of El Niño Southern Oscillation events in the past. For example, Anderson (1992) statistically examined historical El Niño Southern Oscillation records to show that the warm, El Niño, phase of El Niño Southern Oscillation occurred more frequently in cycles of 90, 50, and 22 years and that during the Medieval Warm Period, El Niño events were less common. Farther back in time, paleoenvironmental records from Australia and South America suggest that in the early Holocene El Niño Southern Oscillation events were either of much reduced amplitude or were of different expression due to changed boundary conditions (McGlone et al. 1992).

Documentation of El Niño Southern Oscillation related climate events in the Yucca Mountain region requires proxy paleoclimate records from annual tree ring chronologies taken from conifer stands in the White and Spring Mountains of California and Nevada, respectively. Tree ring studies on Southern California forests, including the White Mountains, have been integrated with other tree ring records in the Western United States to track potential El Niño Southern Oscillation periodicities (Meko 1992). The results show that southwest tree rings are highly inter-correlated in the El Niño Southern Oscillation wavelength band (2.8 to 10.2 years). However, the tree ring width series are also well correlated at longer and shorter periodicities indicating that not only El Niño Southern Oscillation affects tree growth regionally. In fact, even correlations within the El Niño Southern Oscillation wavelength band cannot be unambiguously related to El Niño Southern Oscillation, as many other climate-controlled factors also operate within the El Niño Southern Oscillation Band (Meko 1992).

The variable role El Niño Southern Oscillation has played in past climate will certainly continue into the future, especially as boundary conditions change due to changing insolation and ocean circulation. Yucca Mountain will experience these changes and consequently any prediction of future climate in Southern Nevada must at least recognize the natural variability of climate in response to processes like El Niño Southern Oscillation. For example, abundant winter precipitation in the local, Yucca Mountain area in response to the 1969 and 1993 El Niño Southern Oscillation events caused sufficient flow in the Amargosa River to form shallow lakes in Death Valley (Grasso 1996). During the 1983 El Niño Southern Oscillation event, both winter and summer precipitation events were so large that the Amargosa flow gauge at Tecopa, California (35° 53' N, 116° 14' W) 100 km south of Yucca Mountain, was destroyed in the ensuing flood.

4.2.2.1.3 Long Records of Climate Change—Linkages between Millennial-Scale Climate Change and Orbital Parameters

Long paleoenvironmental records of climate change are critical for understanding the nature of climate change within the Yucca Mountain region:

- Long records provide the linkages between orbital parameters (discussed in Subsection 4.2.2.1.1), which force or, at least time, climate change, and the interpretable climate records. For example, during the late Pleistocene, about 22 ka during a Northern Hemisphere insolation minimum, continental glaciers flowed into the United States. As a consequence, polar air masses, now largely confined in the winter to latitudes above 55°N latitude (see Section 4.1) moved to and remained at latitudes approximately 20 to 25°N farther south (Kutzbach and Guetter 1986). This change brought storm tracks regularly to the latitude of Yucca Mountain (36.75°N) and in a sense transported the modern-day northern climate processes of North-Central British Columbia, Canada to the Yucca Mountain area.

Because climate change is global, such records may come from anywhere on the earth and still be relevant for establishing this linkage. Marine basins from the world oceans are the prime source of long, continuous records that are used to link climate change to planetary orbital dynamics.

- Long records also provide data on the cyclicity of climate change that has occurred in Yucca Mountain region and that will impact the hydrologic cycle in the future. Such records, close to Yucca Mountain, have the advantage of identifying global climate cyclicity with specific patterns of past regional climate changes relevant to the repository site that can be expected to occur in the future.

4.2.2.1.3.1 Marine Records

The world's oceans contain long (millions of years) records of global climate change preserved in marine sediments. These sediment sequences have been and are being studied for several proxies of climate change (for example, microfossils, stable isotopes, geochemistry, mineralogy, and sedimentology).

One such proxy, stable isotope values from calcareous organisms, commonly Foraminifera (single-celled animals) and coccoliths (single-celled algae), provides a climate-related history of the growth and decline of continental glaciers. When a marine organism makes a calcite or aragonite shell, the isotopic value of the shell is directly related to the isotopic value of ocean water by way of a temperature-dependent fractionation factor. As continental glaciers grow, the volume of the world oceans declines, resulting in a change in the oxygen isotope values of ocean water. The lighter isotope (^{16}O) preferentially, by way of a temperature-dependent fractionation, goes to the vapor phase and is stored in continental and mountain glaciers. The heavier isotope (^{18}O) preferentially, due to temperature-dependent fractionation, is both retained in the oceans and is lost from the vapor by way of precipitation. Consequently, during glacial periods, the oceans become enriched in $\delta^{18}\text{O}$ and so the ocean water is said to become heavier. Similarly, when continental glaciers melt the oceans

increase in volume and the isotope value of ocean water shifts back toward lighter values. Thus the stable isotope analyses from marine cores provide a long-term record of the growth and decline of continental glaciers. Stable isotope records from marine cores are common and they show that the earth's climate has shifted cyclically from glacial to interglacial climates throughout the Quaternary (the past 1.6 Ma).

Emiliani (1955) noticed that his $\delta^{18}\text{O}$ stratigraphic profiles, which he attributed more to past ocean temperatures than to ice-volume, from marine cores resembled changes in solar insolation. This observation reawakened interest in the astronomical theory of climate change based on periodic differences in the distance between the earth and the sun developed by Milankovitch (1938). The cyclic changes in insolation predicted by the Milankovitch theory also appeared to match evidence for lower sea levels, consistent with the concept that the ocean water tied up in continental ice sheets during glacial periods appreciably lowered sea level (Fairbridge 1961). Later, other marine isotope records were statistically compared with the insolation record and found to exhibit a high degree of correlation (Imbrie and Imbrie 1986). Isotope records from a number of cores were averaged to form a continuous record that minimized local variations such as variable sediment accumulation rates, missing sedimentary sequences, and local oceanic effects specific to different depositional environments. That averaged record (Figure 4.2-7) became known as the Spectral Mapping Project record, which documents the growth and retreat of continental ice sheets for the last 750 k.y. of earth's ocean/climate history.

Emiliani (1955) identified the successive and alternating cold and warm periods from his oxygen isotope studies on Foraminifera by numbers, beginning with #1 at the top of his core. His numbering system continued to be used and later became formalized (Shackleton and Opdyke 1973) into the numbered oxygen isotope stage sequence in use today. The even-numbered Spectral Mapping Project oxygen isotope stages (OIS) indicate periods of increased buildup of continental ice whereas the odd-numbered oxygen isotope stages indicate interglacial or interstadial periods of reduced continental ice and relatively higher sea levels.

Because the Spectral Mapping Project and other marine isotope records were only dated at the top (modern or 0 ka) and at the bottom (783 ka at the paleomagnetic, Brunhes/Matuyama boundary), a chronology for the intermediate record was provided by correlating or "tuning" the oxygen isotope fluctuations in the sediments with the orbital time scale developed first by Milankovitch and refined by Berger (Imbrie, Hays et al. 1984). This was possible because the deep marine basins receive a continual, slow rain of sediment over millennia and thereby form a continuous depositional record capable of recording all significant (global) climate-produced changes throughout the Quaternary. The chronological scheme followed the statistically-determined match between marine oxygen isotope fluctuations of the Spectral Mapping Project and the orbital dynamical clock. This chronology has since been used to date marine sediments throughout the world oceans because other chronological tools are rarely practical for this purpose.

As the separate lines of evidence came together with a consistent chronology, it became clear that the orbital parameters that describe the relation between the earth and the sun, and hence the amount of insolation the earth receives, was tightly linked to global climate changes, including the waxing and waning of ice sheets, the rise and fall of lakes in desert basins, changes in sea level, and many other profound environmental changes around the earth. It is still not known whether insolation

directly causes these changes, whether it serves as a trigger, or whether it simply operates as an important interactive component of ocean/atmosphere dynamics that combine to change climate over the earth. Whatever the role of insolation in climate change, it does appear to serve as an accurate clock for climate change on the millennial time scale.

4.2.2.1.3.2 Ice-Core Records

Just as the isotope values of the world oceans change as water is stored in or lost from ice sheets, so do the oxygen isotope values of precipitation forming the ice. During a glacial period, isotope values from ice are depleted in $\delta^{18}\text{O}$, because of the fractionation processes described above. The $\delta^{18}\text{O}$ records from ice cores on Greenland and Antarctica provide a detailed record of glacial to interglacial climate change because that record reflects the temperature of precipitation at the site, or more specifically, the nature of the temperature gradient along the path from source water to precipitation.

Most atmospheric water vapor originates from the tropical oceans. If those oceans are warm, the overlying vapor contains more ^{18}O than if those oceans are cold. Similarly, vapor from more northerly sources contains less ^{18}O than the tropical source areas. As vapor moves from tropical source areas towards the pole, or from northern sources towards the pole or continents, vapor cools and condenses to precipitation. The condensation and precipitation preferentially removes ^{18}O from the remaining vapor, which becomes depleted in ^{18}O . The degree of depletion depends on how much vapor is lost to precipitation along the vapor path trajectory and on the ambient temperature of condensation. More ^{18}O is lost from vapor condensed at cold than at warm temperature. During glacials, the thermal gradient between the ice caps and the tropics is steep and long, and condensation temperatures are probably cold, so the precipitation reaching the ice cap is very depleted in ^{18}O . During the interglacials, the thermal gradient is shallow. Specific humidity of northern air is higher, precipitation along the path is less, condensation temperatures are warmer, so snow falling on the ice caps becomes relatively ^{18}O enriched (Cuffey et al. 1995).

Ice cores taken from the ice caps of Greenland and Antarctica provide high-resolution records of changes in the isotope values of precipitation. Each year the accumulation of snow on an ice cap gradually turns to ice and the boundaries between successive annual deposits of ice show as lines of air bubbles or textural changes in the ice mass. Counting the layers provides an annual chronology that extends thousands of years into the past. Chronologies from earlier levels are estimated with models. In addition to isotopic precipitation records, dust, methane, calcium, bases, and acids trapped in the ice provide important paleoclimatic records directly linked to atmospheric changes (GRIP members 1993; Taylor et al. 1993).

Ice-core records (Figure 4.2-8) from the Greenland and Antarctic ice caps extend back to the penultimate glacial period (OIS-6), about 180 to 130 ka (GRIP members 1993). However, ice flow near the base of the ice sheets, especially during warm climates of the last interglacial, make the chronologies and correlations of the lower parts of the ice cores uncertain (Alley et al. 1995). Ice core paleoclimate records are not easily dated or interpreted beyond 100 ka, but they do provide another indication of the change in the global climate system on millennial (insolation) time scales.

Annually banded upper parts of ice cores spanning the past 15 k.y. illustrate decadal and even sub-decadal rates of change between major climate modes. A good example is the Younger Dryas climate oscillation between 12.9 and 11.7 ka (calendar years). This sudden shift to cold climates (Figure 4.2-9) identified by the interplay of wind-borne dust (stadial or cold conditions) and deposition of acidic aerosols (interstadial or warm conditions) occurred in 1 to 3 years and ended about as rapidly (Taylor et al. 1993). The Benson et al. (1997) correlation of rapid fluctuations of Owens Lake, California climate proxies with these ice core events (Figure 4.2-10) underscores the relevance of such dramatic, short-term climate changes to Yucca Mountain.

Ice-core chronologies, developed by counting of annual ice layers and by ice dynamic flow models, are independent of the orbitally tuned Spectral Mapping Project chronology. It becomes important, therefore, that climate changes registered by ice cores are closely synchronous with changes seen in marine oxygen isotope and paleontologic records. This synchrony supports the concept that the dynamics between the atmosphere, oceans and cryosphere do operate at global scales and that the orbitally-forced changes in insolation may be the root of global climate variations. The specific nature of climate change at any locality will depend on its location within this global dynamic and within the context of its geographic placement relative to latitude, longitude, elevation, mountains, and oceans. In this sense, long regional records of climate change help determine the character of past climates near Yucca Mountain.

4.2.3 Long Regional Records of Quaternary Climate Change

Three long climate records occur within about 100 miles of Yucca Mountain. The first, Devils Hole, is a well-dated stable isotope record from calcite precipitated on the submerged walls of an extensional fracture within the regional carbonate aquifer. Devils Hole also contains the Browns Room paleo water table elevation record (Szabo et al. 1994). Devils Hole lies within the Yucca Mountain precipitation basin and because of its well constrained chronology serves to link the timing of global climate change to the Yucca Mountain local area. The isotope record from Devils Hole does not, however, provide a clear sense of the past changes in air temperature and precipitation. The second, Owens Lake, occupies a structural graben immediately east of the Sierra Nevada Mountains and contains an 800 k.y. proxy record of precipitation and runoff from the Sierra Nevada. The Owens Lake record does provide a sense of past changes in temperature and precipitation, but the timing of those changes is less reliable than the Devils Hole record. The third long paleoclimate record comes from Death Valley, California. This fault-controlled basin that today lies 86 m below sea level contained deep fresh water and saline lakes during past glacial periods that identify a runoff history from the Amargosa River and other drainages near Yucca Mountain.

4.2.3.1 Devils Hole

Devils Hole, about 60 km southeast of Yucca Mountain (Figure 4.2-11), is a large, open, extensional fracture within the carbonate aquifer and located in the Ash Meadows discharge area. Over the past 600 k.y., the fracture has maintained the opening and calcite has slowly precipitated on the fracture walls, leaving a stable isotope record of the water in the aquifer. The isotopic chemistry of the water in the regional carbonate aquifer, like that from the oceans or in the precipitation forming the ice caps, reflects the response of the hydrological cycle to global climate change. Coring and dating the calcite on the walls of Devils Hole and then measuring the stable isotope values from the calcite

provides a detailed history of the isotope values of precipitation falling in the recharge area of the regional carbonate aquifer. The timing of change in the Devils Hole isotope record, when correlated with other regional and local climate records provides a way to link those records to global climate records and to orbital insolation dynamics.

The Devils Hole oxygen isotope curve (Figure 4.2-12) shows cyclic fluctuations of isotopically lighter and heavier values that respectively track a progression of colder and warmer periods (Winograd, Szabo et al. 1988). The published records of those cores (DH-11 and DH-2), end at about 60 ka (DH-11) or 51 ka (DH-2) leaving the last glacial episode (30 to 12 ka) as yet undocumented.

Uncertainties exist in the magnitude of all the operative fractionation processes in this system from the moisture sources to Devils Hole recharge. Consequently, specific paleoclimatic interpretations have not been made of past climate scenarios from this record. However, the generalized conditions that lead to particular isotope events within the Devils Hole record can be understood and described. As continental glaciers expand, the polar front and the latitudinal position of the storm tracks associated with it moves southward. The southerly position of polar air, whether seasonally or annually, steepens the thermal gradient between the Devils Hole recharge areas, and the largely tropical and subtropical oceanic moisture source areas, thousands of kilometers west and south of Yucca Mountain. The steep thermal gradient and the cold precipitation condensation temperatures along the moisture-flow path between source areas and recharge areas increase the ^{18}O -depletion of recharge precipitation due to the enhanced rain-out effect. During interglacial periods, the thermal gradient between moisture source area and the recharge area is shallower and precipitation condensation temperatures warmer resulting in less isotopic depletion due to a lesser rain-out effect and hence a recharge precipitation that is enriched in ^{18}O . The characteristics of the thermal gradient and condensation temperatures between source and recharge area determines the isotopic values of the recharge precipitation. As those characteristics can be related to glacial and interglacial periods, the resulting Devils Hole $\delta^{18}\text{O}$ record also identifies climate change.

Other factors than the steepness of thermal gradient can affect the $\delta^{18}\text{O}$ values of recharge precipitation. Some of these factors include: ocean temperature, windiness, other moisture source areas, and groundwater temperatures. The influence of the latter factors on the Devils Hole record are not known, but their effects would tend to accentuate or reduce the peaks and troughs of that record (Winograd, Coplen et al. 1992).

The isotopically lighter precipitation arriving at Devils Hole during glacial periods is not unlike precipitation arriving farther north, falling as snow and ultimately making ice caps. The oxygen isotope records of Devils Hole and Greenland show changes in the same sense—both becoming lighter during glacial periods and heavier during interglacial periods. On the other hand, the Devils Hole oxygen isotope record will vary inversely with the marine isotope record; the former gets lighter during glacial periods whereas the later gets heavier as ^{18}O is enriched in the ocean water. During interglacial periods, Devils Hole will receive precipitation enriched in ^{18}O , but the ^{18}O content of the oceans becomes progressively depleted by the influx of glacial melt waters that raise sea level.

The principal research at Devils Hole (Winograd, Coplen et al. 1992; Winograd, Szabo et al. 1988) has focused on the excellent chronology of the recorded isotopic changes. The chronology is now well established with three different uranium clocks. As a consequence of the chronology, Winograd, Coplen et al. (1992) and Winograd, Szabo et al. (1988) have been able to clearly define discrepancies between the timing of climate change at Devils Hole versus that implied by the orbitally-tuned Spectral Mapping Project chronology. The major discrepancy between the timing at Devils Hole and the Milankovitch timing of climate change occurs at the end of oxygen-isotope Stage 6 (OIS-6), at what is called Termination II. Age discrepancies exist with earlier glacial terminations, but not to the degree seen at Termination II, which occurs at about 140 ka at Devils Hole versus the orbital forcing date of about 128 ka.

Significantly for Yucca Mountain studies, while debate has centered over the early termination of glacial periods at Devils Hole, the timing of the onset of glacial periods and the shape of the isotopic curve through the glacial periods from Devils Hole and from the Spectral Mapping Project are essentially identical (Imbrie, Mix et al. 1993). Indeed, in that the YMP is interested in the origin and duration of glacial periods in the Yucca Mountain region, the Devils Hole record provides the critical evidence that the orbital dynamics, described above, at a minimum represent a clock that signals the beginning of glacial periods.

The specific causes of both the origins and terminations of glacial periods remain unknown. They probably involve multiple orbital, marine and terrestrial forcing functions that work in different ways. The importance of a particular forcing function will vary according to its distance and relation to the proxy studied. Changes in insolation related to change in orbital parameters is the common factor cited as a primary cause. However, because orbitally determined insolation is opposite in opposite hemispheres, it cannot alone explain the approximately simultaneous appearance and disappearance of glacial and interglacial periods in both hemispheres. To the extent that the glacial period terminations at Devils Hole are not coincident with the orbital clock, lags and leads in the effects of insolation relative to the source areas of precipitation and local temperature changes have been invoked to explain the timing of ^{18}O changes in this record (Shaffer et al. 1996). Whatever the detailed relation between orbital mechanics, insolation, and local isotope records, there is a correlation between the onset, and to a lesser extent the end, of major glacial periods and orbital/insolation values.

The Browns Room paleohydrograph record, like the Devils Hole isotope record, is well dated and shows that the water table was remarkably high during the last interglacial and remained high until the present interglacial. Szabo et al. (1994) note that the height of the table could be explained by tectonic or other phenomena that would affect the regional or local hydrology, however, they favor climate as the primary driver of this record. Those findings are consistent with the discussion below on the regional climate record from Owens Lake and with interpretations of various local records.

4.2.3.2 Death Valley

A 186 m core from lake deposits in the Badwater Basin of Death Valley (36° 14'N, 116° 48'W, Figure 4.2-11) consists of interbedded silty-muds and evaporites deposited during the past 200 k.y. Sedimentary structures of muds and evaporites, evaporite mineralogy, and analysis of fluid inclusions (Li et al. 1996; Roberts and Spencer 1995) provide a paleolimnologic and temperature

history for the Death Valley basin that compares to the upper parts of the Owens Lake core and to the Devils Hole oxygen isotope record.

Death Valley is potentially fed by three major sources of water:

- Drainage from the Sierra Nevada via the Owens River and through Owens Lake, Searles Lake, Panamint Valley, and ultimately, to Death Valley
- The Mojave River flowing from the Transverse Ranges directly into the southern side of Death Valley
- The Amargosa River draining the highlands north of Yucca Mountain via Fortymile Wash and flowing into Death Valley on the southeast margin of the basin

Debate continues on the timing and relative influence of each of the potential influx sources (e.g., Roberts 1996), but the Amargosa River provides the only significant water to Death Valley today, and is likely to have been a major contributor to the basin in the past. Because Death Valley is the primary sump of the Amargosa River, its record closely relates to the hydroclimatic history of Yucca Mountain (Li et al. 1996).

Sedimentologic studies of the salts and muds indicate four distinct playa/lake environments: dry mud flats, playa salt pans, layered halite of permanent saline lakes, and black mud with sedimented halite that represents large saline lakes receiving allochthonous detrital materials from the drainage basin. These four sediment types track progressively deeper and more persistent saline lacustrine environments that occupied the Death Valley Basin in the past (Roberts et al. 1994).

The chronology of these depositional environments (Figure 4.2-13) has been established by uranium-series (U-series) dates of bedded salts. Dry mud flats represent Holocene and last interglacial arid environments, whereas shallow to deep, permanent saline lakes characterize the last and penultimate glacial periods. In Death Valley, the initial transition between the penultimate glacial period and the last interglacial period began about 128 ka according to a U-series date on halite precipitated from lake-water when the climate shifted to more arid conditions. A saline water episode occurred at about 146 ka within the black muds, which are thought to have been deposited in a large probably freshwater lake during the penultimate glacial period, appears to correlate with a similar oscillation to slightly drier conditions at Owens Lake reflecting some combination of less runoff and more evaporation. The U-series dates for the Death Valley core partly confirm the sediment mass accumulation rate chronology of the Owens Lake core.

Fluid inclusions in halite crystals precipitated from lake-water from the Death Valley core offer a way to measure paleo water temperature. The inclusions were studied using the methodology described by Roberts and Spencer (1995). The resulting temperature reflects the maximum water temperature at which the halite precipitated (Lowenstein 1997; Roberts and Spencer 1995). Modern-day halite homogenization temperature maxima were collected from halite that precipitated from a shallow lake during the late spring of 1993 and those data compared with air temperature values (Roberts and Spencer 1995). Fluid inclusions in halite, which precipitated from the Death Valley lake, provide maximum paleowater temperature values that can be compared with halite fluid

inclusion temperature data collected from the shallow modern-day lake. Such fluid inclusion data provides actual, not proxy, paleo temperature information of great value to modeling past and future climates in the Yucca Mountain region (Figure 4.2-14).

The fluid inclusion paleowater temperatures from the last glacial period are typically 4 to 15°C below the modern values. During the penultimate glacial period (OIS-6) temperatures are 7 to 20°C below the modern values. Maximum brine temperatures for the Holocene and for much of the past interglacial period are near modern values although cold periods also exist in the record. The range of these brine temperature values are consistent with and supportive of the temperature reconstructions based on pack-rat midden and ostracode data sets discussed below for the last glacial period (see Subsection 4.2.4)

The overall size of a lake in Death Valley, in part, reflects the size of its catchment area. The size of the catchment area may reflect purely geomorphic phenomena that are nonclimatic or it may reflect the magnitude of climate change in the region. The lake that formed during the penultimate glacial period (OIS-6) was very large and is estimated to have been about 125 m deep. Roberts (1996) suggests that the lake may have received flow from the Owens as well as the Mojave and Amargosa Rivers. Such drainage combination, supports the argument for a long and persistent wet climate as the Owens Lake record suggests (see discussion below). The Death Valley lake appears to have only reached a maximum depth of about 90 m (Lowenstein 1997) during the last glacial period (OIS-2) and is thought to have received flow primarily from the Amargosa River at that time, although the Mojave may have also contributed water. Because the Amargosa does not have high mountain ranges, like the Sierra Nevada in its drainage area, the last glacial period lake in Death Valley supports the reconstructions of cold and somewhat wet climates derived from climate proxy data in the region.

4.2.3.3 Owens Lake

Owens Lake, a present-day playa in Inyo County, California, about 160 km west of Yucca Mountain (Figure 4.2-11), contains a thick sequence of lacustrine deposits, which contains diatoms, ostracodes, pollen, and geochemical proxies for paleohydrology and climate. The USGS Global Change and Climate History Program took three cores to a total depth of 324 m from the south-central part of the playa in 1992 with a rotary, truck-mounted coring rig (Smith and Bischoff 1997). The composite core represents 80 percent of the section. Three other cores taken by S.P. Lund of the University of Southern California (Benson, L.V. et al. 1996, 1997) provide additional sediment for a high-resolution study of the upper part of the Owens Lake section. The cored record of Owens Lake spans the past 850 k.y. In accordance with project interests in climate of the last long orbital cycle, the following discussion will focus on the past 400 k.y.

4.2.3.3.1 Climate Setting

The Owens Lake region lies in a winter-wet climate regime. During the winter, as westerly flow intensifies due to the southward migration of the polar front, numerous storms move into the Southern California area. As those storms, pushed by the energized westerlies, rise over the Sierra Nevada mountains, they commonly deliver large quantities of snow and rain to the higher elevations. Some storms are strong enough to deliver moisture to the Owens Lake Basin, but more commonly,

the prominent rain shadow effect of the Sierra Nevada isolates the Owens Lake Basin from westerly storms.

The crest of the Sierra Nevada often receives 150 cm or more of precipitation, typically as snow, whereas Owens Lake proper only averages about 14 cm and most of that comes in the winter (Smith and Bischoff 1997). Because strong westerly flow and consequent high California winter precipitation relates to the southward migration of the polar front, exceptionally wet winters relate to the seasonal dominance of a southward positioned polar front. Conversely, winter dry conditions occur when the polar front is situated in a more northerly or possibly a still more southerly position. Eighty percent of the year-to-year variation in precipitation at Owens Lake is a function of the strength of the westerly (winter) flow (Bell and Basist 1994).

Summer precipitation is typically limited. It is usually related to extended tropical cyclone activity (Pyke 1972; Hansen et al. 1981; Kay 1982) that brings moisture in from the Gulf of California and the Pacific Ocean which moves into the Owens Basin. Higher levels of summer precipitation often occur in years when winter precipitation is low.

4.2.3.3.2 Limnologic and Climatic Setting

During the mid- to late- 19th century, natural flow from the Owens River maintained a saline and alkaline lake that was about 15 m deep. Between 1872 and 1905, flow was reduced to about 25 percent of its natural level due to irrigation in the Owens Valley (Gale 1914). Even so, the inflow was sufficient to maintain a perennial, if very saline, lake about 6 m deep. The construction of the Los Angeles Aqueduct in 1913 diverted the Owens River, the principal source of water to the lake, and it soon desiccated under the local semiarid climate.

Surface flow in the Owens River system is sustained principally by snow melt and rain at high elevation. Base-flow is derived from local alluvial aquifers and from a volcanic aquifer, which also supports alkaline spring discharge along the Owens River and on the margins of Owens Lake. Modern-day levels of surface and base flow are sufficient to support a shallow, saline, lake, even under current low effective moisture levels: evaporation ca. 150 cm/year, precipitation ca. 14 cm/year (Smith 1976). During the winter of 1968 to 1969 (Figure 4.2-15) surface flow was so great that Los Angeles diverted unneeded water to the basin, making a lake with a depth of 240 cm (Friedman et al. 1976). Within two years and no further diversion of water to the basin, the lake evaporated depositing salts on the basin floor.

The overwhelming importance of winter snow and rain to Owens Lake limnology is illustrated by meteorological data from the 20th century for years with weak winter and strong tropical circulation. Strong tropical circulation occurs when the Hawaiian high-pressure cell on the northern edge of the Hadley cell expands northward during the summer. However, during years with high summer precipitation, such as 1963, 1976, and 1977, winter precipitation was only moderate or low and flow in the Owens River, and thus support for the lake, was below normal (Figure 4.2-15). Much of the summer precipitation is lost by evaporation and uptake by vegetation. These data indicate the importance of winter precipitation, specifically snow pack in the Sierra Nevada, to flow in the Owens River. Snow pack in the Sierra Nevada, as discussed above, relates to the persistence and position of the polar front. When tropical climate activity, related to El Niño, and hence a weak

Hadley flow, combines with a strong polar front, conditions also exist for excessive snowpack in the Sierra Nevada and hence flow in the Owens River.

4.2.3.3 Climate Linkage to Owens Lake Chemistry

Owens Lake records climate through its hydrological response to relative position of the storm tracks and the relation the storm track position has to the level of surface flow in the Owens River. The total dissolved solids of waters throughout the drainage range from dilute rainwater and snow melt to saline groundwater discharge and saline lake water brines. Although the waters in the basin are chemically diverse, they may be divided into two groups based on the total alkalinity to dissolved calcium ratio (alk/Ca). Surface water flow from high elevations typically has a low alk/Ca ratio, whereas base-flow, at low elevations, typically has a high alk/Ca ratio.

The solute content (total dissolved solids, alk/Ca ratio) in Owens Lake at any moment in time will depend on the volume of flow from high elevations. If flow is very high and persistent from year to year, then the solute composition in Owens Lake will move to the high-elevation chemical signature and that signature will be further maintained by the lake rising to its outlet and draining. If, at the other end of the spectrum, flow from high elevations is very low then the solute composition in Owens Lake will move to the low-elevation chemical signature. Low flow and high evaporation will prevent the lake from rising to its outlet further concentrating the solutes. Very little is known about hydrological characteristics of the aquifer that supports the high alk/Ca ratio base-flow (Hollett et al. 1991), but its water is ultimately dependent on high-elevation recharge and would be limited during extended dry periods. The combination of high evaporation and little or no base flow in the Owens River results in a dry, saline mineral-rich Owens Lake bed.

The Owens Lake solute budget, therefore, offers a way of identifying the climate characteristics of the basin. When the polar front moves south seasonally or more permanently during glacial periods, westerly flow is energized. Energized westerly flow brings numerous storms into Southern California and those storms produce a large snow pack at higher elevations in the Sierra Nevada mountains. Upon melting, that snow pack provides sufficient flow to the Owens River, so high-elevation solute chemistry retains its signature on the valley floor and within Owens Lake. Conversely, a weak polar front results in less snow pack and flow in the Owens River will be reduced, so Owens Lake solute composition moves toward the valley bottom chemical signature.

The variability of solute composition, particularly the alk/Ca ratio, and of total dissolved solids in Owens Lake water then becomes a measure of the variability of the climate system within the region. If, for example, the alk/Ca ratio and total dissolved solids fluctuate in tandem over wide ranges from decade to decade, it indicates a similar variability in the climate system. Such variability might occur if a few years with strong polar fronts in combination with strong El Niño years, alternate with correspondingly dry periods owing to opposite atmospheric conditions. A low variation in solute chemistry and total dissolved solids, for example, a continuously high ratio and high total dissolved solids, imply dominance by weak westerly flow and a consistent retreat of the average location of the polar front to the north. On the other hand, little variation in low-ratio solute chemistry and low total dissolved solids implies persistent dominance of the polar front and westerly storm tracks.

4.2.3.3.4 Microfossils as Proxy Records of Solute Composition and Total Dissolved Solids

In broad terms, the fossil diatoms and ostracodes in the Owens Lake cores reflect the spectrum of water chemistry found in the Owens River drainage. The fresh and low alk/Ca waters are characterized by freshwater planktic diatoms such as *Stephanodiscus* that indicate large, deep, freshwater lakes (Fritz et al. 1993), or ostracodes such as *Cytherissa lacustris*, which today live in dilute cold lakes situated in the boreal forest (Delorme 1970). The saline and high alk/Ca waters also have specific, high conductivity, shallow-water diatoms, such as *Campylodiscus clypeus* (Fritz et al. 1993) and ostracode taxa, such as *Limnocythere sappausensis* (Forester 1983, 1986). Other diatom and ostracode species are sensitive to the spectrum of alk/Ca ratios and total dissolved solids conditions that could occur under all other possible flow conditions between these extremes.

The microfossil record can be translated into a chronological progression of climate-induced hydrochemical environments. The translation involves the standard assumption common to all paleoenvironmental reconstructions from fossils; the abundances of the fossil species reflect their habitat ecology and are proportional to the type of environment that existed at a site when those species were alive. For example, the abundance of taxa that today live in cold, low alk/Ca, freshwater would imply a polar front was situated in a southerly position on a persistent basis. As a consequence of this paleoclimatic scenario, regional Yucca Mountain mean annual temperature would be lowered and mean annual precipitation elevated. As some or all species composing a particular assemblage become rare or disappear, others appear and become common in a stratigraphic series of samples. The change in species abundance with stratigraphy signals and characterizes change in the paleoenvironmental characteristics of the paleolake. Thus, the paleoenvironmental characteristics of the paleolake identify the nature of the climate system. A change in fossil abundance suggests a proportional climate change.

The rate of climate change can be estimated from the stratigraphy and chronology within which key environmental indicator species' abundances change. Similarly, the persistence of key environmental indicator species provides an estimate of the duration of a climate state. Thus the stratigraphic profiles of microfossil abundances from the Owens Lake sedimentary record provide a proxy for the nature, rate of change, and duration of climates in this region in the past.

4.2.3.3.5 Chronology of the Owens Lake Record

The Brunhes/Matuyama magneto-stratigraphic boundary (783 ka) and the Bishop ash (760 ka) lie near the base of Owens Lake core OL-92 at 312 m and 309 m, respectively (Sarna-Wojcicki et al. 1997). Radiocarbon dates in the upper 23 m of core OL-92 (Bischoff, Stafford et al. 1997) and from the University of Southern California cores (Benson et al. 1996, 1997) provide the ages for the deposits. The base of the core is estimated to be about 850 ka. Based on these data, the composite core has a dry bulk sedimentation rate of approximately 40 cm/k.y. Ages for all horizons between the upper, radiocarbon-dated part and the bottom of the core come by extrapolation from this age model describing sediment mass accumulation rates (Bischoff, Stafford et al. 1997). As with any age model based on sediment mass accumulation rates one expects to find some events being assigned ages that are too young or too old simply because natural sediment accumulation is not constant. However, in a long record, such as this one, the relative fast and slow rates seem to yield a mean that results in the ages of many, but not all, climate events being approximately correct.

The derived, extrapolated chronology appears to explain the major paleolimnologic fluctuations of the Owens Lake record in a manner generally consistent with well-dated changes in the Devils Hole and Death Valley records. When the climate proxy record (discussed below) is examined in stratigraphic order, one finds long intervals that can be attributed to glacial periods and shorter intervals that can be attributed to interglacial periods. When the age estimates from the Owens Lake age model for the glacial and interglacial periods are compared to the Devils Hole chronology, the agreement varies in the timing of those events from good to poor. Both records, however, appear to have the same sequence of glacial and interglacial events. Consequently, just as the undated marine record was tuned to an orbital time scale, the Owens record could be tuned to the Devils Hole or the Spectral Mapping Project records.

4.2.3.3.6 The Paleoclimate Record of Owens Lake

The paleoclimate record of Owens Lake is based primarily on the stratigraphic distribution and abundances of diatoms and ostracodes in cores taken from the basin (Figures 4.2-16 and 4.2-17). These microfossils track climate-induced water chemistry and temperature of the lacustrine habitats in which they have lived for the past 400 k.y. There are five principal climatic scenarios whose limnological impact on the Owens Lake Basin can be readily identified by abundances of fossil diatoms and ostracodes. These climate/limnologic relations of the microfossils are summarized below. The following scenarios are ordered from the coldest, wettest, and most stable conditions to the warmest, driest, and most variable conditions:

- A. *A permanent (year-long) residence of the Polar Front at or south of the latitude of Owens Lake.* This cold frontal boundary directs westerly storm tracks to the Sierra Nevada and into the Owens Valley, would provide abundant moisture and cold, seasonally-stable temperatures, relative to today. The resulting cold, wet climate would support extensive valley glaciers in the Sierra Nevada and possibly in the Spring Mountains, NV. Continental glaciers would have been both large and extensive, thus maintaining polar air and possibly arctic air at Yucca Mountain latitudes throughout the year. In response to this climate type, Owens Lake would overflow and contain cold, and fresh water with a low alk/Ca solute content. Glacial flour derived from mountain glaciers characterize sediment loads in the Owens River. This climate is identified particularly by the modern-day boreal ostracode *Cytherissa lacustris*. Diatoms in Owens Lake under such climates are low-light, freshwater species of *Stephanodiscus* and *Cyclostephanos* that bloom during the short open-water season.

- B. *A persistent residence of the Polar Front during each winter year after year, but a retreat of this frontal boundary during most summers.* The seasonal cold and wet conditions may promote the growth of regional valley glaciers during the waxing phase of continental ice-sheet, or the retreat or loss of valley glaciers during the waning phase of a continental ice-sheet. Continental ice-sheets would have been less extensive. Owens Lake would be large, fresh, with a low alk/Ca solute type, and draining, but shows seasonality in temperature and perhaps limited seasonality in chemistry. *Candona caudata*, an ostracode species that lives in the Owens Lake drainages at higher elevations, and to the north, dominates the ostracode assemblage under this climate scenario, but *Cytherissa lacustris* is rare or absent. The diatom assemblage probably changes to include planktic species that

bloom in the late summer or fall as well as species prospering in the early open-water season.

- C. *An intermediate climate state between the glacial states described above (B) and the interglacial state described below (D).* This climate scenario is characterized by a relatively common movement of the Polar Front to Owens Lake latitudes during most but not all winters. Continental ice-sheets are either in the early stages of growth or nearing the final stages of retreat. Mountain glaciers probably exist in the high cirques and may expand or contract on decadal or century scales. Although the Polar Front is present in most years in this scenario, it probably isn't as persistent or consistently resident for the entire winter as in scenario B. During some winters the Polar Front resides to the north of Owens Lake, but still is close enough to ensure ample precipitation to provide the lake with regular seasonal discharge that results in either seasonal overflow or a large relatively freshwater lake, which seasonally may shift to a slightly saline (a few grams per liter) and in which the alk/Ca ratio is elevated. Summer seasons are warm to hot and Owens Lake becomes smaller due to evaporation and reduced flow in the Owens River. Total dissolved solids would increase during the summer. *Limnocythere ceriotuberosa* characterizes this climatic environment, but depending on whether the system is at a wet or dry end of its range, other taxa are also present such as *Candona caudata* (wet) or *Limnocythere sappaensis* (dry). The diatom flora of Owens Lake under this climate regime exhibit similar variability. Dry decadal-scale intervals would support saline planktic diatoms or summer-blooming freshwater planktic species depending on the net hydrologic balance in the lake.
- D. *Holocene-like climate conditions in which the average position of the Polar Front varies from year to year.* Westerly atmospheric flow brings snow to the Sierra Nevada, but in most years snow pack is not especially deep. Very deep snow pack occurs infrequently (a few times in a decade or only a few times in a century). Deep snow pack results from a strong El Niño conditions or from several centuries of enhanced polar air activity similar to the Little Ice Age. Conversely, weak polar activity such as the several centuries known as the Medieval Warm Period, result in less snow pack. Continental ice sheets would have been small like those of today. Flow in the Owens River is proportional to available snow pack and in some years, such as 1968 to 1969 (see discussion above), flow is very high and freshens the saline lake. In most years, however, flow is modest to low and may only seasonally expand the lake above that size supported by base-flow. Evaporative water loss in summer serves to sustain a saline, high alk/Ca water. Overflow of the lake is unusual. *Limnocythere sappaensis*, an ostracode of moderately to highly alkaline and saline lakes, dominates. Saline benthic diatoms document the shallowness of the lake and the variably high salinity. Diatom preservation is often poor due to corrosion and breakage in shallow, alkaline water.
- E. *The average position of the Polar Front is typically north of the Owens Lake latitudes, westerly flow is weak, and so snow pack is typically negligible.* Any summer precipitation would be mostly used locally by valley bottom plant communities. These conditions may be common for centuries or even a few millennia with only infrequent reversals to wetter conditions. The middle Holocene from about 4 to 8 ka was a recent period when the latter

conditions were common. Because snow pack is limited, recharge is also limited, and consequently base flow in the Owens River eventually falls to a very low level or the river goes dry. Due to limited surface flow and eventually base flow Owens Lake becomes a dry and perhaps deflating playa at least seasonally and probably for decades at a time. Neither diatoms nor ostracodes live in this limnological setting long enough to leave a significant record. During rare flood events redeposition of fossils from high-stand lake deposits is possible, but generally the sediments are barren.

4.2.3.3.7 Glacial and Interglacial Variability Documented by the Owens Lake Record

The response of the Owens Lake to the major past climates, as described above, offers a way to examine the characteristics, i.e., magnitude, duration, and rate of change, of climate change during the long, 400 ky, orbital cycle with its four roughly 100 k.y. glacial-interglacial couplets, that are identified and dated from the stable-oxygen isotope record at Devils Hole.

The microfossil record (Figures 4.2-16 and 4.2-17) overall indicate a longer and more persistent history of a fresh and overflowing lake system than of a shallow, saline system. Over the past 400 k.y. Owens Lake has been fresh (implying climates wetter than today) for about 80 percent of the time and saline (implying climates like today's) about 20 percent of the time. Although there is some variation, intervals of wet climate (freshwater conditions) average about 32 k.y. in length whereas dry climates (saline conditions) average about 13 k.y.

The microfossil records suggest rapid changes from interglacial to glacial periods. Those transitions occur on a scale of one or two millennia to as little as a few centuries. For example, change from modern-like dry climates indicated by *Limnocythere sappaensis* to wetter periods typically occurs in hundreds not thousands of years. Such rapid changes from warm/dry to cold/wet climates suggest a southerly shift in the average position and strengthening of the westerly/Polar Front associated with the Polar jet stream. Analog interpretation of regional pack-rat midden data and paleoecological proxies from Owens Lake during glacial periods suggest a mean climate change sufficient to allow juniper woodlands to descend 1000 m to the valley floor (Bradbury 1997). A 1,000-m lowering in life zones is consistent with pack-rat midden analyses near Yucca Mountain (Spaulding 1990). The apparent rapidity and severity of climate changes at Owens Lake therefore implies that the small changes in the Devils Hole isotopic record from groundwater interglacial to glacial conditions (see discussion in Subsection 4.3, Future Climate Variation) reflect substantial changes in ambient temperature and moisture characteristics within the region.

The microfossil record also shows that the various glacial periods were not alike, nor were the interglacial periods. For example, the ostracode record of *Cytherissa lacustris*, indicates that the last and penultimate glacial periods were characterized by climate scenario A, whereas the first two glacial periods in 400 k.y. orbital cycle were more like scenario B. The persistence and commonness of *C. lacustris* during the penultimate glacial relative to the last glacial, suggests a colder, wetter, longer-lived glacial, the so called super pluvial within the long (400, k.y.) orbital cycle. The abundance of juniper pollen between 170 and 120 ka (Litwin et al. 1997) indicates that the penultimate glaciation had much higher effective moisture than any of the others, supporting the inferences from the lacustrine microfossils.

The first glacial period in the orbital cycle (OIS-10, about 400 to 360 ka) was cool and wet as implied by the fresh water planktic diatoms that live in lakes without ice cover today. This suggests that Owens Lake did not regularly freeze, and hence winters probably were not significantly colder than today, but, because the lake was large and overflowing, mean annual precipitation was much higher than today, especially winter precipitation.

Similarly, the interglacial and interstadial periods were not identical to each other. The climate of OIS-3, for example, suggests more glacial than interglacial conditions with wet environments under a warm summer temperature regime that maintained a stable, stratified lake. The present interglacial period, the Holocene (also called OIS-1), may be the most arid of the past 800 k.y. (Smith et al. 1997), in part, because of the presence of oolites (which form in shallow, agitated, highly saline water) are unique to the uppermost levels of lake deposits. Furthermore, the Holocene interval is often barren of microfossils suggesting climate scenario E. By contrast, OIS-5 (the last interglacial period) is well represented by saline diatoms that indicate open water of generally low salinity. This indicates greater precipitation, probably both in summer and winter, than characterized the lake when it was first studied in the late 19th century. Indeed, the beginning of OIS-5, a substage called 5e, assuming the age estimates are correct, witnessed a full and overflowing Owens Lake and a deep saline lake in Death Valley (Lowenstein 1997). A full and overflowing lake during a period of time when it is well established from oceanographic studies that less continental ice existed during 5e than exists today, does not fall in any one of the above climate scenarios, but might represent some mix of scenarios C and D. The record from Browns Room (Szabo et al. 1994) also implies that the last interglacial period was wet.

The Owens Lake microfossil record, when interpreted in the terms of the five climate scenarios, shows that the region has undergone significant climate change on the millennial time scale. The past climates differed from those of today because the predominate circulation pattern of the atmosphere was different from that which typifies the modern world. The present atmospheric circulation pattern along with a significant rain shadow effect are the reasons for today's semiarid climate (see Subsection 4.1). The Devils Hole stable isotope record also shows the climate system has changed and provides the timing of those changes. The Owens Lake microfossil record shows that those changes were regional.

The YMP is in the process of determining probable levels of change in both mean annual temperature and mean annual precipitation for much of the past record. Studies within the local Yucca Mountain area (Subsection 4.3.2) suggest that during the past glacial period, mean annual temperature was depressed from modern values by about 7 to 10°C, mean annual precipitation was roughly similar to today at high elevations and as much as three times modern amounts at low elevations (see discussion Subsection 4.2.4.1). Considering that the last glacial period based on the Owens Lake record looks cold and dry relative to past glacial periods, then the OIS-10 and -8 glacial periods should have been cooler than today, but not as cold as OIS-6 and -2. Hence they may be thought of as relatively "warm" wet glacial periods.

4.2.3.3.8 Correlation of Owens Lake Paleolimnology and Oxygen Isotope Records of Global Climate

Unlike the Devils Hole stable isotope record, which has a chronology derived from direct radiometric dating, or the Spectral Mapping Project, which has a chronology derived from celestial mechanical calculation, the chronology for the Owens Lake record is largely derived from an age model (Bischoff, Stafford et al. 1997). During the past 400 k.y., microfossils from the Owens Lake core document five major cool and wet periods: 400 to 330 ka, 250 to 220 ka, 170 to 120 ka, 70 to 64 ka, and 50 to 10 ka (Figures 4.2-16 and 4.2-17). In all cases, the expected sequencing of glacial to interglacial and back to glacial climate is observed. These glacial and interglacial intervals can be correlated with the oxygen isotope stages of glacial periods (even-numbered stages) and interglacial periods (odd numbered stages), respectively (Table 4.2-1) in sequential patterns. The age estimates derived from the age model are in general agreement with this correlation. The correlation of the Owens Lake climate/hydrological record to either the Spectral Mapping Project or to Devils Hole, however, is not perfect (see Figures 4.2-18 and 4.2-19). Some of the larger discrepancies between the Owens Lake record and the global isotope records, such as OIS-8, probably originate from inaccuracies in the Owens Lake age model. Other, smaller differences may identify a complex climate system, where regional lags or leads may exist relative to the global system.

The presence of a glacial and interglacial biostratigraphy within the Owens Lake microfossil record implies that, like the Devils Hole record, the Owens Lake record is both complete and can be interpreted in terms of global climate changes that are correlated with orbital parameters. This chain of linked evidence allows the Owens Lake record to serve as a guide to future climate changes there and at nearby Yucca Mountain. The similar sequence of events recorded at Death Valley strengthens this argument and documents the regional character of climate change in Western North America.

4.2.3.3.9 Owens Lake Conclusions

- The Owens Lake record is coupled to climate by the relative quantities of water and solutes delivered to the lake during different climate modes. The microfossil record from Owens serves as a proxy for the climate controlled hydrology and shows that during the past 400 k.y. climate was wetter than modern about 80 percent of the time.
- The wet periods coincide with long, complex glacial climates. Most of those glacial climate periods correlate with the Spectral Mapping Project and Devils Hole records of global climate change, and thereby, suggest future climate change should occur on a schedule that is related to the changes in the earth astronomically-based insolation cycle.
- The Owens Lake record suggests that climate during the various glacial periods was not the same and further suggests the wettest and coldest occurred during OIS-6. OIS-2 was cold and relatively dry compared with OIS-6, but due to cold temperatures its effective moisture (Precip-evap) was high. Presuming this relation can be verified by all proxies and by showing that climate is recorded in the same way throughout the 400 k.y. cycle, the next glacial will probably have a climate that is milder, but probably wetter than the last two.

4.2.4 Local Records of Late Quaternary Climate Change

Local records of climate change are common throughout the region and include pack-rat middens, paleo wetland and paleo spring deposits, groundwater carbonate fracture fillings, and tree-rings. The groundwater carbonates, principally at Devils Hole, were discussed above. Local and regional tree ring records remain to be synthesized for the Yucca Mountain area. The remaining records are by their nature discontinuous, but provide important insights to the timing and magnitude of local climate change in the Yucca Mountain region.

Paleo wetland and spring deposits are discontinuous records because most basins within the Yucca Mountain precipitation area are topographically open or are situated well above the regional groundwater table. The lack of topographic closure means that during wet periods the basins behave more as streams than as lakes and have only limited and often local deposition of sediments in a series of interconnected wetlands. Erosion of these deposits may occur either during ensuing wet or dry climate episodes or both.

Topographically closed basins, such as Yucca Flats or Frenchman Flats, are situated well above the water table. Dilute runoff from large storms creates an ephemeral, perched lake. Sediment accumulation is often episodic and accumulated sediments are usually eroded by deflation. These dilute, nutrient-poor, lakes generally contain a depauperate biological community, which leaves little or no fossil record. As perched lakes, water loss occurs by leakage or evaporation. Evaporative concentration of solutes results in calcite or other minerals being precipitated and then those minerals are often lost to deflation, leaving an incomplete limnologic and climatic record.

Pack-rat midden records are temporally discontinuous. A sample from a pack-rat midden typically represents the plant material collected during the life of one or a few pack rats and hence the data from a sample only captures short moments in time (Finley 1990).

4.2.4.1 Pack-Rat Middens

The plant communities living in the region today vary from different Mojave Desert plant communities at low elevations to pigmy conifer forests (juniper, pinyon) at higher elevations (about 1800 m) to a montane conifer forests (white fir, ponderosa and limber pine) at still higher elevation (about 2200 m) and subalpine (bristlecone pine and shrubs) above about 2700 m (Spaulding 1990). The plant communities on valley floors and up to about 1800 m on the alluvial fans contain many frost sensitive or frost intolerant plants in addition to drought hardy species. Creosote, for example, would not survive in the area if the cold months had many days with temperatures below freezing. The plant communities found at progressively higher elevations are ever more tolerant of cold and require ever more water to survive. The interaction of both winter frontal storms and summer convective storms with the mountain ranges throughout the region provide the moisture levels needed to support the plant communities. The plant communities thus reflect the modern levels of effective moisture resulting from air temperature and precipitation.

To understand how past climate was different from today a large comprehensive data-set composed of the plant macrofossils from 200 pack-rat midden samples was compiled from YMP data and outside literature. Each pack-rat midden sample contains a record of the common plants that grew

within a few tens of meters of the midden. As the plant material can be accurately radiocarbon dated, a large midden collection from throughout the area and from a wide range of elevations provides a good picture of past plant-elevational relations. From present plant-elevational relations, in comparison with those of the past, one can reconstruct change in past temperature and precipitation.

The general features of the pack-rat midden dataset for the period from about 35 to 12 ka reveals important information about the late Pleistocene climate in the Yucca Mountain region. The common tree species in the middens from this area are Utah juniper, limber pine, and white fir. Bristlecone pine was found in midden samples from a number of high-elevation localities, but below its modern lower elevational range. Pinyon pine, common throughout the region today, is very rare in the samples, occurring infrequently in a few middens from the Sheep Range (Spaulding 1990), but it becomes common about 12 to 10 ka (Spaulding 1990; Thompson 1990). Shrubs and bushes include taxa such as sagebrush (*Artemisia* spp.) and others (see Spaulding 1990; Thompson 1990) that imply cold and relatively dry conditions. Creosote is absent during the last glacial period and does not become common until the late Holocene (last 4 k.y., Spaulding 1990).

Southwest and south of the Yucca Mountain region in Eastern California, Arizona, and Mexico, pinyon pines occur in Pleistocene middens (Spaulding 1990; van Devender 1990a, 1990b). The Southern Mojave Desert and Northern Sonora Desert, which today contain heat-loving drought-hardy plants such as creosote and many cactus species as well as ocotillo, supported a pigmy conifer woodland during the late Pleistocene about 20 to 12 ka (Spaulding 1990; van Devender 1990a). North and northeast of the Yucca Mountain region Thompson (1990) reports a variety of plant communities, with bristlecone and various junipers being the common trees, that are indicative of generally cold and dry conditions. However, a plant assemblage from a midden located in the Snake Range (north northeast of Yucca Mountain) dated at about 17 ka contained Engelmann spruce, which implies wetter conditions.

The distribution of common plant species during the late Pleistocene within and outside the Yucca Mountain region show that climate was very different from today. Indeed, the plant communities seen on the higher mountains in the region, e.g., the Spring Range, were redistributed spatially during the Pleistocene. Montane conifers had migrated downwards to elevations around 1700 m. The valley margins that supported Utah juniper and pinyon pine had largely moved south and out of the Yucca Mountain region as had the warm desert plant community and ponderosa pine (Spaulding 1990; Forester, R.M., Bradbury et al. 1996). The valley floors contained wetlands and flowing springs (see discussion below). Subalpine bristlecone pine communities that live on top of the highest mountains in the Yucca Mountain area today had also migrated down slope. For example, Spaulding (1990) reports bristlecone pine at about 2000 m during the full glacial period and at 1800 m before 23 ka on the Sheep Range. Similarly, at localities farther north, the bristlecone pine community migrated down towards the valley floors (Thompson 1990).

The movement of plant communities down slope during the late Pleistocene indicates colder and wetter conditions at all elevations relative to modern, just as those plant communities imply colder and wetter conditions up slope today. The past climate conditions can not, however, be a simple translation of climate parameters from higher elevations within the region today to lower elevations because some taxa from the higher elevation plant communities are rare or absent (e.g., pinyon pine,

creosote) from the Yucca Mountain region during the late Pleistocene. For example, the loss of pinyon pine from the region implies that mean annual temperatures during the late Pleistocene were at least as cold as that above about 2,200 m today where montane conifers thrive in the absence of pygmy conifers such as pinyon pine. Similarly, the absence of ponderosa pine likely implies the existence of relatively dry and cool summers. Climate during the late Pleistocene must have involved cold winters and cool probably dry summers. The modern, hot summers with convective storms did not exist during glacials, nor did the relatively mild winters with average temperatures above freezing. Instead, the presence of montane conifers at lower elevations would suggest cold, perhaps snowy winters with cool dry summers. This interpretation is consistent with the interpretation of past climate from the Owens Lake record (see discussion above).

Estimates of past temperatures and levels of precipitation can be made by comparing fossil plant assemblages with modern plant communities in order to acquire climate parameters related to those modern communities that best match the fossil community. This method is called the analog method and assumes that past climate conditions at one locality exist today at other localities and that a climate proxy (e.g., terrestrial plant assemblage) can be used to link the past and present localities. R.S. Thompson, USGS, and K.H. Anderson, INSTAAR (written communication to R.M. Forester, USGS, August 1997), used the analog method to reconstruct past climate parameters for four time periods (35 to 30 ka, 27 to 23 ka, 20.5 to 18 ka, and 14 to 11.5 ka, all dates in radiocarbon years) within the late Pleistocene of the Yucca Mountain region. The time periods were selected by paleo botanical participants at a workshop held in December 1996 and were based on a qualitative inspection of the plant species in the entire pack-rat midden database. Taxa found during these periods were thought (on visual inspection by K.H. Anderson (INSTAAR), W.G. Spaulding (Dames and Moore), S.E. Sharpe (Desert Research Institute), R.S. Thompson (USGS), and P.E. Wigand (Desert Research Institute), verbal communication, 1996) to potentially represent different temperatures and precipitation levels. Reconstructing past temperature and precipitation from these four episodes provides a range of climate variability within the late Pleistocene.

R.S. Thompson, K.H. Anderson, and P. J. Bartlein established a modern climate-plant database for North America that provides a basis for comparison with the fossil plant assemblages. Based on an analysis of the pack-rat midden database by R.S. Thompson, USGS, and K.H. Anderson, INSTAAR (written communication to R.M. Forester, USGS, August 1997), the modern-analogs were located in areas north of Yucca Mountain, often in Northern Nevada, and the four periods (35 to 30 ka, 27 to 23 ka, 20.5 to 18 ka and 14 to 11.5 ka) show more climatic similarity between the periods than expected. When the results were regressed against elevation, both the mean annual temperature and mean annual precipitation anomalies were found to be greater at low than at high elevations. The merged values suggest that the past mean annual temperature anomaly was about -9°C (below modern mean annual temperature) at 800 m, but only about -3°C at 1,800 m, whereas the precipitation was about 3 times modern values at 800 m and 1.5 times modern values at 1,800 m. Mean annual precipitation was too variable in the period 14 to 11.5 ka to be regressed; the variability may express a change in climate state within that period. The past climate-parameter anomaly pattern is consistent with the existence of a resident polar air-mass in the region that would have had a greater impact at low elevations than at high elevations. These climate values will be tested against the modern temperature and moisture requirements of taxa that live in the region today, but were rare or absent in the past. Presumably if the reconstructions are reasonable, they will not only account

for the taxa that were present, but should also account for common modern taxa that were absent from the Pleistocene midden assemblages.

4.2.4.2 Wetland and Spring Deposits

Wetlands and spring-discharge are rare in Southern Nevada today because of the low level of effective moisture. Hot, relatively dry summers result in the loss of precipitation to evaporation or uptake by plants. Winters are generally mild and persistent inter-annual frontal storms are rare. Winter storms and snowpack on the higher mountains support local spring discharge typically above about 2,000 m (Winograd and Riggs 1984) and limited seasonal stream flow. Spring discharge at low elevation typically comes from water in the regional carbonate or the volcanic aquifers recharged at high elevation and over large areas (Winograd and Thordarson 1975).

Sedimentary deposits on the valley floors throughout the Southern Nevada region show that during the glacial periods and transitions to and from glacial periods there were wetlands, flowing springs, and streams at low elevation (Quade, Mifflin et al. 1995). High-elevation recharge of the valley-fan alluvial aquifers resulted in discharge from about the lower third of the alluvial fans (based on field observations east of the Corn Creek Spring Wildlife Station, Figure 4.2-11). Regional water tables rose above land surface in many areas and, together with discharge from shallow valley-fan aquifers, supported valley bottom flowing springs, streams, and wetlands. Emergent aquatic vegetation, such as bullrush (*Scirpus* spp.), was common on the fans and in the wetlands. The springs and wetlands supported abundant aquatic organisms such as ostracodes, diatoms, and molluscs; and a diverse vertebrate community composed of everything from large mammals, such as mammoths and timber wolves, to small mammals such as pikas, northern pocket gophers, and northern meadow mice. Water birds such as ducks and wading birds also lived in the area during the late Pleistocene.

The existence and year-to-year persistence of groundwater discharge and permanent wetlands at low elevation requires that the past levels of effective moisture were much higher than today (Quade, Mifflin et al. 1995). The existence in the Northern Las Vegas Valley of small mammal fossils, found in the sediments and in nearby caves, that today either live at upper tree line or in the Northern United States supports the temperature reconstructions from the plant macrofossils discussed above. Similarly the existence of a variety of duck and wading bird fossils supports the interpretation of permanent wetlands on the valley floors.

Three discharge records that provide insights into the nature of past climate are discussed below. Those records include an ostracode record from a well-dated section in the Las Vegas Valley, an isotope record from a well dated section near Cactus Springs north of the Las Vegas Valley, and the diatomaceous deposits north of Highway 95 and south of Crater Flats down the regional flow gradient from Yucca Mountain. Other records are under study.

4.2.4.2.1 Corn Creek Flat Section OBI-11 Ostracode Data

Section OCI-11 (Figure 4.2-11) lies near the center of the Las Vegas Valley. The section is about 5 m thick and was sampled continuously by taking 5 cm thick samples from the bottom to the top of the section. The section can be subdivided into three informal stratigraphic units denoted B, D, and E, which were described by Quade (1986). These units are distinguished from each other by a

variety of sedimentary features such as bed forms, grain size, color, rhizolith content, and fossils (Quade 1986; Quade and Pratt 1989; Quade, Mifflin et al. 1995) and were identified in the field by Jay Quade. Sediments comprising units B and D occur throughout the Las Vegas Valley indicating they were deposited in extensive wetlands (Quade 1986; Quade and Pratt 1989).

Twenty-two radiocarbon dates constrain the age of the sediments comprising section OCI-11. The dates from unit B at the base of the section (Figure 4.2-20) are finite but many of them have large standard deviations, are near the limit of the radiocarbon age method, and some do not have a consistent relationship between terrestrial and aquatic molluscs (see Brennan and Quade 1997 for discussion of terrestrial and aquatic molluscs radiocarbon dates). The unit B dates, based on the latter criteria, are thought to be derived from molluscs whose age is much older than the limit of radiocarbon, but that have been contaminated by small quantities of radiocarbon, in this case less than 1 percent. By contrast, the dates from unit D₁ are also near the limits of radiocarbon, but have smaller standard deviations and maintain the expected relation between terrestrial and aquatic molluscs (Brennan and Quade 1997). Those radiocarbon dates therefore may be valid. The remaining radiocarbon dates from units D₂ and E are well within the range of radiocarbon, have small standard deviations and fit the terrestrial and aquatic mollusc criteria for acceptance. One radiocarbon date at the unit E/D₂ boundary comes from organic material rather than molluscs and is consistent with other dates accepted from the section.

The sedimentary section contains a diverse assemblage of ostracodes and aquatic and terrestrial molluscs. The ostracodes (Figure 4.2-20) suggest that a shallow, relatively freshwater, and typically permanent wetland supported by the regional water table and flowing springs existed on the valley floor. The ostracode species abundance profiles can be grouped together in terms of the component species preferred environment (Figure 4.2-21). In the case of these taxa, there are several possible choices including streams, flowing springs, seeps, wetlands, and aquifer. Aquifer taxa, which indicate the regional water table was higher in the past, are not considered further. Because these species live in the aquifer, their fossils could be contemporaneous or younger than the associated surface water species. For simplicities sake, the surface water categories are further reduced to just wetland and spring/stream taxa that is standing and flowing water. Some species will fall into both categories.

The wetlands and supporting springs must vary in their distribution at a particular site on a temporal basis due in part to hydrological variability unrelated to climate. Quade, Mifflin et al. (1995) use the Steptoe Valley (39° 33' N., 114° 50' W.) in Northern Nevada as an analog for the environments that existed in Southern Nevada in the past. Those modern wetlands and springs on the eastern side of the Ruby Mountains (40° 23' N., 115° 31' W.) have a variable ratio of spring to wetland ostracodes depending on where the collections are made. By analogy to the modern analog sites, section selection in the Las Vegas Valley will, in part, determine the ratio of wetland to spring taxa found, because the paleo wetland sediments represent deposition in an interconnected series of springs, wetlands, and streams aligned along the valley floor. As a consequence of this non-climate spatial variability the relative proportions of spring versus wetland taxa through time may or may not be important. However, these aquatic microfossil assemblages from wetland and spring deposits can be interpreted in general hydrologic and climatic terms. The presence, relative abundance, or absence of taxa from one unit to another does define the environment in which the species were living, whether that be due to hydrology or climate or both.

Ostracode taxa assigned to either a spring (including seeps, spring-pools, flowing-springs, and streams) or wetland (a standing or low flow surface water body supported largely by groundwater discharge) provide a means of understanding changing environmental settings on the valley floor. The distribution of those two general groups of taxa show that at this site wetlands and spring activity co-varied as might be expected. The stratigraphic profiles (Figure 4.2-21) suggest that unit B and unit D wetlands contain about the same numbers of wetland taxa suggesting that wetlands were equally important at this site during this time. By contrast, the spring-stream element was more common in the upper part of unit B than subsequently in unit D or E indicating active flow during that time. In unit E both the wetland and spring taxa are of less importance than they were lower in the section implying the wetland spring discharge activity was declining.

The unit B ostracode assemblages have rare occurrences of *Physocypria globula*, a species that today has a biogeographic distribution extending from the Southern United States into some parts of Southern Canada (Forester, Delorme et al. 1987). In the northern part of its biogeographic distribution, it is typically found in lakes that have water temperatures rising above 18 to 20°C during the day for at least 2 to 4 months.

The presence of common *Physocypria globula* in the unit D assemblages, but not in the unit B assemblages suggests that summer water temperatures in the unit B environments were colder than those in the unit D assemblages. The low temperature could be due to overall colder air temperatures or it could be due to spring flow sustained by recharge originating from snow-pack. Similarly, during the deposition of unit D, summers could have been warmer or there was less snow-pack-supported recharge.

The present biogeographic distribution of many of the ostracodes found in these deposits is on the northern prairies of North and South Dakota and Eastern Washington. Some of the northern species also occur south to places such as the Ruby Marsh wetlands in northeastern Nevada. The occurrence of these species implies a climate setting that is cold and relatively dry like that of Northern United States prairies. Taxa limited to lakes situated in the Southern United States are absent from the ostracode assemblages as are spring taxa limited to warm water springs having discharge temperatures above 20°C.

The unit E ostracode assemblage (Figure 4.2-20) contains only a few species relative to the large number of species found in the older units. The reduction in the number of species implies the wetland spring complex is becoming smaller and as a consequence effective moisture was lower than during unit D or B times.

Forester and Smith (1994) estimated mean annual precipitation based on ostracodes from a nearby section (LPM 34, Figure 2.d, see Figure 4.2-22). They suggested mean annual precipitation was 4 to 5 times higher than today. However, they did not recognize the importance of flow through the wetlands. The existence of flow creates an illusion of higher mean annual precipitation, because flowing water is usually less thermally and evaporatively coupled to the atmosphere than is standing water. The rate and probably the volume of flow are likely to be key factors that determine the degree of thermal and evaporative coupling between the water and the atmosphere (Forester 1987). Flow through the Corn Creek Flats wetlands was low, but none the less sufficient to keep the waters fresher and cooler than they would otherwise be. The mean annual precipitation levels of 400 to

600 mm reported by Forester and Smith (1994) probably did exist in this area, but at higher elevation, where present mean annual precipitation is also higher. Modern-day mean annual precipitation is 112 mm at this site (Corn Creek Wildlife Refuge). Applying the mean annual precipitation multiplier derived from the pack-rat midden studies, described above, for low elevation to this site would result in a mean annual precipitation of 336 mm (3 times modern value).

The ostracode assemblages found in unit D commonly live in eastern Washington and western Minnesota today, where mean annual temperature is 5 to 7°C, and effective moisture deficits are about 200 mm or roughly 5 times lower than the modern-day Las Vegas Valley (Winter and Woo 1990). A mean annual temperature of 5 to 7°C would be about 11 to 13°C colder than modern day (18°C, Corn Creek Wildlife Refuge). That anomaly is greater than estimated from the midden studies of about 9 to 10°C for this area (see subsection above), but does not conflict with the extremes of the plant dataset nor of the small mammal data.

The wetlands existed around 36 ka and they persisted until 12.1 ka, at section OCI-11 (Figure 4.2-22) and to somewhat younger times in nearby sections. The growth and persistence of wetlands in Southern Nevada is correlated to Northern Hemisphere summer insolation minimum, associated with the last glacial cycle. This insolation minimum is further associated with the expansion of the polar cell into this region resulting in increased effective moisture, increased recharge, and higher regional water tables that, in turn, gave rise to the wetlands. Similarly, the eventual loss of wetlands is associated with a rise in Northern Hemisphere insolation to its maximal value at 12 ka and the consequent retreat of the polar cell from the region. Such changes show there is a linkage between millennial scale climate forcing functions and regional scale hydrology in Southern Nevada.

4.2.4.2.2 Cactus Springs Section—Stable Isotope Data

Winograd and Riggs (1984) reported deuterium to hydrogen isotope ratio from water and $\delta^{18}\text{O}$ values for winter and summer precipitation collected from the Spring Range Mountains. The $\delta^{18}\text{O}$ values for summer precipitation averaged -8.8 per-mil ($(\delta^{18}\text{O} \text{ sample} - \delta^{18}\text{O} \text{ standard}) / \delta^{18}\text{O} \text{ standard} \times 1000$) relative to SMOW (standard mean ocean water arbitrarily considered to have a $\delta^{18}\text{O}$ value of 0) with a standard deviation of 4.2. Winter precipitation and snow pack both averaged -14.3 per-mil relative to SMOW with standard deviations of 5.0 and 1.5, respectively. Snow melt averaged -12.5 per-mil relative to SMOW with a standard deviation of 1.5. The study concluded that high elevation groundwaters and spring discharge were derived from cool season precipitation as such waters averaged -13.7 per mil relative to SMOW with a standard deviation of 0.4 (Winograd and Riggs 1984). Low $\delta^{18}\text{O}$ values change to higher $\delta^{18}\text{O}$ values by evaporative loss of water vapor, but higher $\delta^{18}\text{O}$ values can not by themselves become lower, because to become lower they must have mixed with a water having lower $\delta^{18}\text{O}$ values. The $\delta^{18}\text{O}$ value of -13.7 per mil could only come from a -8.8 per mil value if it were mixed, for example, in equal proportions with a water having a value of -18.6 per mil.

Sharpe et al. (1994) collected stable isotope data from aquatic and terrestrial molluscs living on the forest floor and in two springs on the east side of the Spring Range Mountains. Stable oxygen isotope data from the bivalve *Pisidium* spp. living in Cold Creek Spring at 1940 m and found as a fossil in the Cactus Spring (930 m) section (Figure 4.2-23) offers a way to compare modern data

from high elevation to fossil data at low elevation without concern for different vital effects. The $\delta^{18}\text{O}$ values for living *Pisidium* spp. from the Cold Creek Spring locality averaged about 18.7 per mil and the values from the fossil site sample averaged 19.6 per mil relative to SMOW. The $\delta^{18}\text{O}$ values of water collected from a small pond receiving flow from the Cold Creek Spring locality averaged about -14 per mil relative to SMOW and so the modern bivalve data is about 32.7 per mil heavier than the water. As the $\delta^{18}\text{O}$ value of the bivalve shell is determined by both the value of the water in which it lived and by the temperature of the water at the time it made its shell, the fossil data therefore can not be accurately converted into a value for the $\delta^{18}\text{O}$ for the paleowater. The temperature effect, however, is relatively small compared with the "water effect." The $\delta^{18}\text{O}$ values for the high- and the low-elevation bivalves are similar, suggesting that the low-elevation wetlands and springs were supported by waters having a low $\delta^{18}\text{O}$ value and hence by winter precipitation.

The similarity in the $\delta^{18}\text{O}$ values from *Pisidium* spp. living at higher elevation with fossil material from low elevation, supports the interpretations of the other climate proxy data from the region. Plant communities also move downslope and some species within that community move south out of the region. Fossil mammals that are extant today typically live at either higher elevations or farther north as do many of the ostracode species found in the wetland sediments. All of the climate proxy data suggests that climate was colder and wetter during the last glacial period than today.

4.2.4.2.3 Lathrop Wells Diatomite Microfossil and Isotope Data

Paces, Taylor et al. (1993) and Quade, Mifflin et al. (1995) show that the Lathrop Wells diatomite surface deposits are situated about 100 m above the regional water table. Paces, Taylor et al. (1993), Paces, Neymark et al. (1996), and Paces, Whelan et al. (1997) reconstruct the paleohydrology of this site based on the fossil and isotope data. Brennan and Quade (1997) discuss the importance of radiocarbon data collected at this site for understanding changes in travel time within the Yucca Mountain flow system as a function of climate change. Paleohydrology at this site and from other past discharge sites in the Amargosa Desert are treated in Section 5 and are not repeated here. Evidence for the age of these deposits is discussed in detail in Paces, Taylor et al. (1993), Quade, Mifflin et al. (1995), and Brennan and Quade (1997). The basis for the interpretation of paleohydrology and age of these deposits is summarized below.

Although Swadley and Carr (1987), based on field relations, believed these deposits are Pliocene to lower Quaternary, Paces, Taylor et al. (1993) provide U-series ages suggesting the deposits are late Quaternary ranging from the penultimate glacial (OIS-6) to the last glacial (OIS-2). Paces, Whelan et al. (1997) provide additional age determinations noting that the materials dated may exhibit some open system behavior with consequent loss of uranium. The best values among the latter determinations cluster in OIS-3 or about 30 to 60 ka. Brennan and Quade (1997) report radiocarbon ages centered on about 13 ka from a capping carbonate that lies above the diatomite. Vertebrate fossils found in these deposits, commonly the diatomite, are not particularly diagnostic and only imply a Quaternary age for the deposits. Other vertebrates, especially microtine rodents, often have limited age ranges and if found could provide age information independent from the isotopic determinations.

Isotopic evidence (Paces, Taylor et al. 1993) suggests the Lathrop Wells diatomite deposits were derived from a regional groundwater source. Strontium and uranium isotopic ratios for authigenic

materials in these deposits are similar to those from regional groundwaters sampled nearby, although groundwater from beneath this site remains unsampled. These data exclude a surface water source, and $^{234}\text{U}/^{238}\text{U}$, $\delta^{87}\text{Sr}$, and $\delta^{13}\text{C}$ data from authigenic materials in the deposit are inconsistent with perched-water compositions expected from interactions with local rock sources.

The diatomite itself also suggests a connection with water from a regional rather than a perched aquifer. Diatomite is a sediment that composed primarily of the opaline valves of diatoms (single-celled algae). Diatoms live in all kinds of surface water environments as well as in wet-terrestrial environments. Abundant diatom growth occurs in water rich in dissolved silica and other nutrients. Diatomite forms in depositional systems where clastic and chemical sediments do not dilute the accumulating flux of diatom valves. Discharge from perched aquifers in the region, such as Cane Springs, Nevada (36.8°N., 116.09°W.) or Pahroc Spring, Nevada (37.66°N., 114.98° W.), does not form diatomite, possibly because discharge is not sufficient to allow build-up of diatomite even though dissolved silica levels are relatively high, about 60 mg/L. Further, the Lathrop Wells diatomite contains species that today live in warm waters, commonly over 20°C. Assuming the diatomite formed during a glacial period, discharge at elevated water temperatures would be inconsistent with a perched aquifer, which would have a discharge temperature approximating mean annual temperature. Considering the silica and water temperature requirements the diatomite at this locality likely was a consequence of regional aquifer discharge.

The reconstruction of climate from aquatic microfossils and from stable isotope data in the Las Vegas and Indian Springs Valley, as discussed above, are consistent with the pack-rat midden plant macrofossil climate reconstruction. However, because the Las Vegas and Indian Springs Valley are bounded by some of the highest mountains in the region, the hydrological response to Pleistocene climate change there may be accentuated by local upland recharge relative to that in the immediate Yucca Mountain flow system. The Lathrop Wells diatomite, by contrast, represents the response of the Yucca Mountain paleohydrological system to climate change without significant effects of local high mountain recharge. Upland areas north of Timber Mountain (more than 50 km distant) most likely represent the recharge area for the Yucca Mountain systems. Today the regional water table at Lathrop Wells diatomite is thought to be about 100 m below ground surface. The water table may or may not have been that deep in the past when glacial climates caused it to rise to the surface. For example, the low elevation of the water table in Browns Room is a Holocene phenomena (see Szabo et al. 1994 for discussion). The fact the regional water table fluctuated up to about 100 m relative to today implies that past climates were sufficient to affect the regional flow system in significant ways. Greater recharge and flow in the Amargosa system was sufficient to support or significantly contribute to large lakes in Death Valley during the last glacial period (see Subsection 4.2.3.3).

4.2.4.2.4 Summary of Local Records

The climate interpretations based on the pack-rat midden data (terrestrial records) and on the diatom, ostracode, and isotope data (aquatic records), discussed above, collectively show that during the last glacial period mean annual precipitation was higher, probably about 2 to 3 times modern and mean annual temperature was much lower from about 5 to 10°C. The hydrologic consequence of wetter and colder climate was generally higher regional water tables with the Yucca Mountain regional water table being about 100 m above its present elevation. Further cold discharge from shallow alluvial aquifers was common and along with higher regional tables supported shallow wetlands

throughout the region. Water on the valley floors, based on the $\delta^{18}\text{O}$ values from bivalves, probably resembled modern-day high-elevation spring discharge, which is derived from winter precipitation recharge. The modern-day, hot summers with convective storms did not exist during the glacials; glacial period summers were probably cool and dry, so effective moisture would remain high throughout the year in part because the low air temperatures greatly reduced evaporation.

4.2.5 Site Records of Climate Change

Site records of past climate, those within or on Yucca Mountain, are common and comprise two isotopic data sets collected from calcite precipitated in fractures within Yucca Mountain (Whelan, Vaniman et al. 1994) and calcite precipitated in the soils on or near Yucca Mountain (Quade and Cerling 1990; Vaniman and Whelan 1994). In low-temperature calcite, CaCO_3 , the carbon isotopes are derived from a mixture of CO_2 originating from soil respiration, the atmosphere, and dissolution of existing carbonates. The soil respired carbon carries an isotopic signature of the general photosynthetic pathways used by the plant community from which it was derived and that information provides insights into climate. The calcite $\delta^{18}\text{O}$ values reflect equilibration with meteoric water and may (if the water is not greatly evaporated) register the $\delta^{18}\text{O}$ signature of the air mass from which the water precipitated and the probable season of the precipitation. Further, calcite incorporates strontium and other metals in its lattice and so records strontium isotope or geochemical information about the waters from which it precipitated. These relations offer insights into the nature of the climate, i.e., plant communities, air mass synoptics, percolation sources (from $\delta^{87}\text{Sr}$ and $\delta^{13}\text{C}$) prevalent in the region when the calcite precipitated. When the calcite can be dated (Whelan, Vaniman et al. 1994; Paces, Neymark et al. 1996; Paces, Whelan et al. 1997) the isotopic information can be placed in a past regional climate context, thus linking percolation and climate state into the orbital dynamics that provides the timing and estimated magnitude of future climate change (see discussion in Subsection 4.3).

Infiltration modeling suggests that these fluxes vary across the mountain as functions of the amount, timing, and duration of precipitation; soil thickness and moisture conditions; outcropping lithologies; and solar radiation (or evapotranspiration) (Flint et al. 1996). The results of numerical infiltration modeling are described in Site Description Subsection 5.3.4.1.5. For current climate, net infiltration ranges from 0.0 to 63.2 mm/year and averages 3.2 mm/year for the "site area" (228 km^2). For the area of the potential repository (11.6 km^2), net infiltration ranges from 0.0 to 29.7 mm/year and averages 6.0 mm/year. These data are from Site Description Table 5.3-38. Stable isotope studies of unsaturated zone waters (Yang et al. 1998) and saturated zone groundwaters (Benson and Klieforth 1989), coupled with studies of local meteoric waters (Benson and McKinley 1985) indicate that recent infiltration is dominated by winter precipitation (for example, see Cactus Springs discussion Subsection 4.2.4.2).

4.2.5.1 Secondary Mineral Deposits in the Yucca Mountain Tuffs

Secondary minerals have formed in both the unsaturated zone and the saturated zone. Within the saturated zone, these minerals appear to have resulted from an early, moderate temperature, hydrothermal alteration event. Broxton et al. (1987) related this calcite to a hydrothermal event that altered the tuff matrix and deposited alteration minerals (quartz, calcite, feldspars, etc.) in the tuffs, and Bish and Aronson (1993) reported K-Ar age determinations which they suggested may relate the

event to the formation of the Timber Mountain caldera, about 10 Ma. Because saturated zone secondary minerals are unrelated to either Quaternary processes or to regional groundwater, they are not related to climate processes and will not be discussed further in this section.

Secondary calcite and silica (quartz, chalcedony, and opal) also occur as drusy coatings on fractures and in lithophysal cavities¹ within the unsaturated zone. Deposition in unsaturated zone (i.e., vadose) settings is demonstrated by restriction of these coatings to the footwalls of fractures and the floors of lithophysae.

Unsaturated zone secondary mineralization can be broken down into three stages: an early stage that consists of quartz and chalcedony with minor calcite; a main stage that consists largely of blocky to bladed calcite and minor opal; and a late stage that consists of clear calcite as blades and overgrowths, also with minor opal. Recent geochronologic studies (e.g., Paces, Whelan et al. 1997; Neymark et al. 1998) have indicated that the early secondary mineralization in the tuffs may have closely followed their eruption. In addition, this early calcite has unusually large $\delta^{13}\text{C}$ values and lower $\delta^{18}\text{O}$ values (Whelan, J.F. and Moscati, R.J., *Origins and Paleoclimatic Implications of Secondary Calcite and Opal Within the Tuffs of Yucca Mountain, Nye County, Nevada*, USGS-OFR, in press; Whelan, J.F. et al., *Applications of Isotope Geochemistry to the Reconstruction of Yucca Mountain Paleohydrology*, USGS-OFR, in press), and fluid inclusion evidence (Roedder et al. 1994; Dublyansky et al. 1996) indicates the presence of reduced carbon species such as CH_4 and deposition at somewhat warmer temperatures than are found in the unsaturated zone today. As such, the early calcite probably does not reflect past climate and is therefore excluded from succeeding discussions.

Main and late-stage secondary mineralization (as defined above), which consists of multiple generations of calcite spatially and temporally interspersed with opal, appears to have formed directly from percolating waters at ambient temperatures. Percolation water, discussed in more detail below, carries the dissolved inorganic carbon $\delta^{13}\text{C}$ values derived predominately from the resident plant community and from that a carbon isotopic signature of climate. Similarly, rain or snow infiltrating through the soils and becoming percolation will have a $\delta^{18}\text{O}$ value reflecting the moisture source and pathway of the air-mass causing the precipitation. Because these change as a function of global climate circulation patterns, percolation $\delta^{18}\text{O}$ values will also vary with climate. Therefore, to the extent that secondary calcite in the unsaturated zone can be dated and thus integrated with regional climate history, it provides a record of past climate states.

Placing the unsaturated zone secondary minerals in a time framework is the subject of an isotopic dating effort. These chronological studies focus on occurrences exposed in the Exploratory Studies Facility and applied ^{14}C and $^{230}\text{Th}/\text{U}$ geochronometers, with useful ranges of ~45 ka and ~400 ka, respectively, to dating of the most recent mineralization events (Paces, Neymark et al. 1996; Paces, Whelan et al. 1997). However, due to extremely slow rates of mineral deposition in the unsaturated zone (1 to 10 mm/m.y.) and low uranium concentrations in calcite (often <1 ppb), sampling techniques were physically unable to resolve individual depositional episodes. The age determinations shown in Figure 4.2-24 range from 16 to 400 k.y., but all probably represent physical mixtures, and average ages, of depositional periods spanning the present to more than 10^6 years in

¹ Lithophysae are bubble-like cavities formed by gases devolving from erupted tuffs during their cooling (Jackson 1997).

the past (Paces, Neymark et al. 1996; Paces, Whelan et al. 1997). Nonetheless, the majority of ^{14}C ages determined from sampling outermost calcite crystal surfaces yielded finite ages ($< \sim 45$ k.y.) indicating the presence of ^{14}C and deposition of the youngest calcite probably within the last 10 to 20 k.y., the last glacial period (Paces, Neymark et al. 1996). Unfortunately, these records do not lend themselves to more refined chronologies.

The U/Pb geochronometer extends much farther into the past and has been applied to several dozen opal or chalcedony occurrences from deeper in the paragenetic sequence (Neymark et al. 1998). Although opal and chalcedony are neither sufficiently abundant nor prevalent within the paragenesis to provide systematic constraints on mineralization history, these data do provide coarse constraints on the long-term variability of past climates.

4.2.5.2 Stable Isotope Geochemistry of Secondary Calcite in the Unsaturated Zone

4.2.5.2.1 Controls on Infiltration $\delta^{13}\text{C}$ Values

Soil carbonate dissolution is expressed by the general reaction



wherein Ca^{2+} (or other cations) come from pedogenic carbonate and much of the CO_2 comes from plant matter, either directly through oxidation and decay or from plant respiration. The carbon in the HCO_3^- then comes either from plant CO_2 or via dissolution of carbonate that, in arid to semi-arid climates is often pedogenic carbonate previously formed per the reverse reaction in equation 1. Very fine-grained pedogenic calcite has formed extensively in the soils, as well as in bedrock fractures in the near-surface, on and around Yucca Mountain. During times of higher infiltration, the resulting percolation will potentially dissolve pedogenic carbonate or, if infiltration is excessive may carry largely a plant matter and soil gas carbon isotope signature. Pedogenic carbonate on and around Yucca Mountain has $\delta^{13}\text{C}$ values ranging from -8 to -4‰ (Quade and Cerling 1990; Vaniman and Whelan 1994), reflecting plant assemblage responses to past changes in climate.

The style of photosynthesis used by various kinds of plants is preserved in the $\delta^{13}\text{C}$ values of the organic matter as well as the respired CO_2 . More specifically, biochemical controls and isotopic effects during diffusion of CO_2 into leaves and photosynthesis result in ^{13}C depletion of plant matter with respect to atmospheric CO_2 . Plants have evolved three different photosynthetic pathways, designated as C3, C4, and crassulacean acid metabolism, each producing different carbon isotope fractionations (Boutton 1991). Most plant matter in soils is supplied by the C3 and C4 plants; contributions by crassulacean acid metabolism plants, which are largely succulents, are minor. Soil carbon isotope systematics are satisfactorily characterized, therefore, by considering only C3 and C4 plant inputs (Cerling 1984).

Photosynthesis in C3 plants produces a 3-carbon compound and plant matter having $\delta^{13}\text{C}$ values ranging from -32 to -22 and averaging -27‰ (Boutton 1991). Plants following the C4 pathway evolved during the Cenozoic, possibly in response to lowered levels of atmospheric CO_2 and higher temperatures, stresses that they endure more readily than C3 plants. Photosynthesis in C4 plants produces a 4-carbon compound and plant matter having isotopic compositions ranging from -17 to -9

and averaging -13‰ (Boutton 1991). Hot, dry lowlands are dominated by C4 plants, largely grasses, whereas wetter and cooler uplands may be occupied almost exclusively by C3 plants, which include most trees, shrubs, herbs, and other grasses (Quade, Cerling et al. 1989, page 469, provide a partial list of C3 and C4 plants of the Southern Great Basin).

Fossil pedogenic carbonate found in soils retains, in its $\delta^{13}\text{C}$ values, a clear indication of the types of plants that lived in the overlying soils. This was clearly demonstrated by Quade, Cerling et al. (1989) in a study of recent pedogenic carbonate in Southern Nevada. They found a direct correlation between elevation and pedogenic carbonate $\delta^{13}\text{C}$ values, with higher elevations displaying much lower $\delta^{13}\text{C}$ values because C3 plants were predominant (Figure 4.2-25). In the same sense that plant assemblage C3/C4 ratios vary with altitude, that ratio also varies with changes in past climate. Wetter and cooler climates in the past at Yucca Mountain, comparable to modern climates found at higher elevations, will produce infiltration with lower dissolved inorganic carbon $\delta^{13}\text{C}$ values; conversely, drier climates will result in higher $\delta^{13}\text{C}$ values in infiltration dissolved inorganic carbon. Unsaturated zone secondary calcite formed from past percolation fluxes retains, therefore, evidence of the climate that prevailed at the time of its formation.

4.2.5.2.2 Controls on Infiltration $\delta^{18}\text{O}$ Values

The $\delta^{18}\text{O}$ values of meteoric water (rain or snow) at any geographic location are chiefly controlled by air and water temperatures at the moisture source and by the precipitation history of the air mass preceding its arrival at a study site (see Subsection 4.2.2.1.3). Oxygen isotope fractionation between water and water vapor increases as temperature decreases, with the light isotope (^{16}O) enriched in the vapor phase. Air masses originating over cold seas will, therefore, produce lower $\delta^{18}\text{O}$ precipitation than warm-sea air masses because of the cooler temperatures of evaporation. Even air mass vapor with high tropical $\delta^{18}\text{O}$ values become isotopically lighter as they move north due to the isotopic fractionation effects of rain out along its path. Although isotopic depletion of ^{18}O in water vapor during evaporation is partially balanced by ^{18}O -enrichment during condensation and precipitation, meteoric waters are depleted in ^{18}O with respect to the ocean. It follows that condensation and precipitation will cause further ^{18}O -depletion in the air mass and that this depletion will be greater at cooler temperatures (and, therefore, larger $\text{H}_2\text{O}_l\text{-H}_2\text{O}_v$ isotopic fractionations). Meteoric waters from air masses with long precipitation histories (rain-out effects) or which have condensed and precipitated at cooler temperatures, such as during winter or at higher elevations, will have more negative $\delta^{18}\text{O}$ values than coastal or summer precipitation. The fractionation process is amplified during glacial periods when as a consequence of resident polar air masses the thermal gradient between tropical moisture sources and the Yucca Mountain region is much steeper (see Subsection 4.2.3.1, Devils Hole).

Measurements of precipitation $\delta^{18}\text{O}$ values from sites on and near Yucca Mountain and tracks of the air mass trajectories that produced the precipitation (Milne et al. 1987) were used by Benson and Klieforth (1989) to define the isotopic signatures of the air mass sources responsible for present day precipitation in the area. Modern extremes of precipitation $\delta^{18}\text{O}$ values in the Yucca Mountain region range from arctic and continental-polar air masses of -17 to -14‰ to maritime air masses of ~-11‰; modern precipitation is dominated by maritime moisture sources (Benson and Klieforth 1989). During the colder climates of glacial periods, arctic and polar air masses would have played a more important role in bringing moisture into the Yucca Mountain region. Thus, glacial climates

should be reflected by lower (more negative) $\delta^{18}\text{O}$ values of infiltrating waters – and a similar lowering of the $\delta^{18}\text{O}$ values of secondary calcite formed from those waters.

Secondary calcite $\delta^{18}\text{O}$ values are also affected by the gentle warming of percolating waters during their descent through the unsaturated zone. Reconnaissance stable isotope studies of unsaturated zone calcite by Szabo and Kyser (1990) indicated that calcite $\delta^{18}\text{O}$ values decrease regularly with depth which they attributed to decrease of the calcite-water O-isotopic fractionation factor as the fluids warmed. Subsequent studies of secondary minerals have verified the decrease of calcite $\delta^{18}\text{O}$ values with depth (Figure 4.2-26) and supported this conclusion (e.g., Whelan and Stuckless 1992; Whelan, Vaniman et al. 1994).

4.2.5.2.3 Formation and Distribution of Secondary Minerals

Precipitation of both calcite and opal is likely related to loss of volatiles from percolating waters. Carbon dioxide evasion is the most likely driver of calcite precipitation, whereas evaporation probably drives opal precipitation. Localization of secondary minerals in open fractures and lithophysal cavities indicates that open space itself together with open connections for volatile escape are necessary for mineral formation. In the PTn, those fractures that do occur are tight, not open, and percolation waters must move largely through the matrix of the bedded units. Consequently, volatile loss is restricted in the PTn and that unit contains much less secondary mineralization than the TCw and TSw units. See Section 5 for the hydrolithologic definitions of PTn, TCw, and TSw.

Mineral precipitation may not, however, be solely a function of open-space pathways, percolation flux, and volatile loss. Changes in the seasonality of infiltration, percolation fluxes, or soil type and chemistry in response to changes in climate may have varied the chemistry of percolating waters. For instance, cool and (or) wet climates with thicker vegetation cover might form more humus-rich soils. Coupled with higher infiltration rates, such soils could potentially result in infiltration of water with lower pH and initial calcite undersaturation. Similarly, climates generating summer infiltration may carry higher concentrations of dissolved species into the mountain than cold-season infiltration when soil CO_2 concentrations are much lower.

Infiltration waters percolate readily through the welded and fractured TCw and calcite stable isotopic signatures should faithfully record concurrent climate. Percolation moves through the matrix of the PTn much more slowly than through the fractured units. Fabryka-Martin et al. (1997) suggest that percolation may take 500 to 20,000 years to travel through the PTn depending on flux rates, and strontium isotopic compositions of PTn pore waters indicate extensive water-rock interaction as percolation moves through it (Marshall et al. 1997). Such travel times will result in century-scale and even millennial-scale averaging of stable isotope values in calcite precipitated in the underlying TSw. The basic glacial and interglacial signature of climate seen in other records throughout the region should none the less be preserved as long as calcite precipitates from all waters moving through Yucca Mountain.

4.2.5.3 Secondary Mineral Evidence of Past Climates

Pleistocene Climates Responsible for Calcite-depositing Percolation Flux

Carbon Isotopes—Typical $\delta^{13}\text{C}$ values of younger unsaturated zone calcite fall in a range of -8 and -4‰. Other heavier $\delta^{13}\text{C}$ values are known, especially from the older calcite, and those values are thought to be related to non-climate processes. Theoretical calculations, however, permit soil respiration processes to result in $\delta^{13}\text{C}$ values ranging up to about +4‰ (Cerling 1984) and this is then taken as the upper $\delta^{13}\text{C}$ limit of calcite that could have precipitated directly from percolation (Figure 4.2-27).

Correlations between soil carbonate isotopic values, elevation, and predominant plant species as determined by Quade, Cerling et al. (1989) show that the $\delta^{13}\text{C}$ values of secondary calcite are consistent with past climates that were colder and/or wetter than the present day. Figure 4.2-27 shows that ~60 percent of the $\delta^{13}\text{C}$ values fall between -8 and -4‰ with a pronounced mode around -6‰. This range is essentially identical to that of the pedogenic carbonates found in the massive calcretes on and around Yucca Mountain. Quade and Cerling (1990) concluded that the carbonate in pedogenic calcrete filling the Bow Ridge fault, and exposed in the near surface at Trench 14, formed during climates that were colder and wetter than the present. They correlated these $\delta^{13}\text{C}$ values to those of modern soil carbonate forming at elevations of 1,800 to 2,000 m, which is comparable, in today's climate terms, to the flanks of the Rainier Mesa. These correlations, therefore, suggest calcite deposition within Yucca Mountain occurred predominantly during colder and wetter climates in the past that had higher infiltration rates and percolation fluxes.

Oxygen Isotopes—Unsaturated zone calcite $\delta^{18}\text{O}$ values display a 4 to 5‰ range at all depths (Figure 4.2-26). It seems unlikely that past climate-induced changes in the temperature or flux of infiltration would significantly alter the geothermal gradient, hence the modern gradient should provide a reasonable estimate of calcite precipitation temperatures. The $\delta^{18}\text{O}$ range at any depth, therefore, reflects variations in the $\delta^{18}\text{O}$ of percolation flux caused by the range of past climates. Modern extremes of precipitation $\delta^{18}\text{O}$ values range from about -17 to -14‰ in arctic and continental polar air masses to near -11‰ in maritime air masses (Benson and Klieforth 1989). Modern precipitation appears to be dominated by maritime sources (Benson and Klieforth 1989). Logically, past glacial climates should have received significantly greater contributions from arctic and continental polar weather systems (see discussion under Owens Lake and Devils Hole above). The $\delta^{18}\text{O}$ value of calcite within the mountain is a function of the $\delta^{18}\text{O}$ content of the infiltrating waters and the temperature of the water within the mountain at the time of calcite deposition. The $\delta^{18}\text{O}$ values of infiltration will be related to the $\delta^{18}\text{O}$ of the precipitation, which expresses the climate signal (see Benson and Klieforth 1989 and Subsection 4.2.3.1) and to whether or not the precipitation evaporated before becoming infiltration. Evaporation would have the effect of increasing the $\delta^{18}\text{O}$ values of the infiltration, resulting in erroneous indication of warmer climates. Studies of soil moisture isotopes, however, show that $\delta^{18}\text{O}$ values change little during drying; it is unlikely, therefore, that evaporation significantly affects the $\delta^{18}\text{O}$ of infiltration. The Yucca Mountain thermal gradient should remain more or less constant through time and so the temperature at which calcite precipitates will be a function of depth within Yucca Mountain (see discussion above). So, presuming little or no evaporation, the range of calcite $\delta^{18}\text{O}$ values permit some generalizations about the climates responsible for calcite-precipitating percolation fluxes.

The mean annual temperature of a region provides an estimate of the air masses that are resident throughout the year, for example, arctic, polar, and tropical air masses have their own temperature characteristics. The relatively high modern mean annual temperature at Yucca Mountain reflects the rarity or absence of the arctic air masses and the commonness of subtropical air masses. Modern mean annual temperature thus provides a good estimate of a warm climate precipitation and a value of about 5°C (from Owens Lake and Local Records section) a good estimate of glacial mean annual temperature. The temperature dependence of the equilibrium oxygen isotopic difference between calcite and water $\delta^{18}\text{O}$ values is well known (Kim and O'Neil 1997). Using that relation and using the modern geothermal gradient and past mean annual temperature to estimate rock temperatures at depth allows the $\delta^{18}\text{O}$ values of past percolation to be estimated from measurements of the unsaturated zone calcite $\delta^{18}\text{O}$ values. At a modern mean annual temperature of ~15°C (written communication, July 1997, from J.A. Hevesi, USGS, to R.M. Forester, USGS) and an estimated geothermal gradient of around 34°C/km (Szabo and Kyser 1990), the calcite at 100 m depth reflects percolation flux (i.e., meteoric) water $\delta^{18}\text{O}$ values of -13.5 to -8.5‰. During glacial times and at an mean annual temperature of 5°C, this calcite would indicate a range of about -15.7 to -10.7‰. Percolation flux $\delta^{18}\text{O}$ values estimated from calcite found at 500 m depth, which ranges in $\delta^{18}\text{O}$ from about 14 to 18‰, are -12.7 to -8.7‰ for modern meteoric waters and -14.7 to -10.7‰ for glacial-stage waters. These estimated isotopic relations are shown in Table 4.2-2.

In general, these estimates suggest that younger unsaturated zone calcites have formed during both modern-like and glacial climates. The highest water $\delta^{18}\text{O}$ values of about -8‰ may reflect some evaporation of infiltrating waters or record infiltration during some past climate characterized by precipitation with fairly ^{18}O -enriched mean annual precipitation, perhaps a climate state with greater infiltration inputs from summer precipitation. However, because summer precipitation is typically taken up by plants, past infiltration by summer rain implies very high levels of precipitation. The water table elevation record from Browns Room at the Devils Hole site contains the best dated records from the last interglacial and shows a high water table, which was attributed to climate (Szabo et al. 1994). A wet interglacial could then produce these ^{18}O -enriched waters. These estimates also indicate that, if arctic moisture sources with $\delta^{18}\text{O}$ values of ~-17‰ (Benson and Klieforth 1989) were predominant during any past climate states, they either did not produce significant infiltration or produced infiltration that deposited little secondary calcite, again assuming the infiltration and percolation was not evaporatively enriched.

Climate states producing the most calcite were not necessarily those producing the highest percolation fluxes. Wetter or cooler climates that generated greater percolation fluxes, but which were calcite undersaturated and left no mineral record, are certainly possible.

Million-Year-Scale Climate Trends at Yucca Mountain—Uranium-lead ages of secondary opal and chalcedony reported by Paces, Whelan et al. (1997) range back to ~9 Ma. Preliminary determinations of the $\delta^{13}\text{C}$ of the calcite associated with the dated materials (Figure 4.2-28) confirm the correlation between paragenetic position and $\delta^{13}\text{C}$ indicated in Figure 4.2-27.

Secondary calcite deposited during the Pleistocene has $\delta^{13}\text{C}$ values ranging from -4.5 to -7.5‰ (Figure 4.2-28). Quade, Cerling et al. (1989), in studies of Holocene pedogenic carbonate formation in Southern Nevada, demonstrated a clear inverse correlation between $\delta^{13}\text{C}$ and elevation; i.e., soil calcite $\delta^{13}\text{C}$ values decreased with increasing elevation (Figure 4.2-25). Using this relation,

unsaturated zone calcite $\delta^{13}\text{C}$ values may be used to estimate climate variability on Yucca Mountain during the Pleistocene. A $\delta^{13}\text{C}$ of $\sim -4.5\text{‰}$ corresponds to a modern Southern Nevada microclimate with an elevation of about 1,400 m, and a plant assemblage including creosote bush, bursage, and ephedra, comparable to the present day southern end of Yucca Crest. By comparison, a $\delta^{13}\text{C}$ of $\sim -7.5\text{‰}$ implies a modern Southern Nevada elevation of $\sim 1,800$ m and a pinyon-juniper-sagebrush plant community like that found on Shoshone Mountain or the flanks of Rainier and Pahute Mesas.

Secondary calcite with $\delta^{13}\text{C}$ values less than -6‰ apparently was not formed prior to ~ 3.0 to 3.5 Ma (Whelan, J.F. and Moscati, R.J., *Origins and Paleoclimatic Implications of Secondary Calcite and Opal Within the Tuffs of Yucca Mountain, Nye County, Nevada*, USGS-OFR, Figure 4.2-28, in press). In plant community terms, this is equivalent to a decrease in the C3/C4 plant ratio. Older secondary calcite has $\delta^{13}\text{C}$ values that range between about -5 and $+2\text{‰}$ and seemingly increase with age. In paragenetic terms, this interval of time, and range of $\delta^{13}\text{C}$ values, represent the "Middle" mode in Figure 4.2-27).

Thompson (1991) in reviewing possible Pliocene climate in the Western United States, suggests that climates were generally milder, wetter, and less seasonal prior to ~ 2 Ma. Constrained by these broad climate conditions, modern climates forming soil carbonate of -5 to $+2\text{‰}$ include prairie settings such as found from Kansas to Minnesota, and tropical savannas and wooded grasslands such as found in Africa (Cerling and Quade 1993).

Winograd, Szabo et al. (1985) demonstrated a sharp decrease in the δD values of travertine-hosted fluid inclusions at about 1 Ma and suggested that it might reflect a regional shift in climate patterns related to uplift of the Sierra Nevada Mountain ranges. Other studies of paleosol carbonate (Rogers et al. 1992), Searles Lake salinity (Smith 1984), and Lake Tecopa water depths (Larson et al. 1991) also indicate a significant shift in regional climate 1 to 2 Ma. These regional records, therefore, broadly support the unsaturated zone calcite record of an apparent change in climate state beginning sometime in the Pliocene and culminating by ~ 1 Ma with the climate range produced by cyclic continental glaciations of the Pleistocene.

INTENTIONALLY LEFT BLANK

4.3 FUTURE CLIMATE VARIATION

Climate is the primary driver of hydrological change and provides insights into future exposure pathways. Hydrological change within Yucca Mountain in the future is a central issue confronting the program. Current studies by the national labs and the USGS seek to collect and model data to provide an understanding of past and future unsaturated zone and saturated zone hydrology. That information provides a basis for understanding how the total Yucca Mountain hydrologic system may behave under various future climates. Specifically, paleoclimate studies provide information about: 1. Past climate characteristics (MAT, MAP) including variability of the climate system of past glacial and interglacial periods, 2. Climate time series, 3. Climate parameters maps for the last glacial period, 4. Estimates of vegetation types and distributions during the last glacial, 5. Analog sites that serve as a source of meteorological data for models and, 6. Identification of the location of past ground-water discharge, wetland, and stream sites. This information is provided to TSPA-VA and LA or others needing it for input to numeric models or to serve as bounding parameters to limit output from numeric models.

Estimates of future climate may be gotten by prediction using climate models that employ the basic physics of climate or forecasting based on an understanding and documenting of the natural cyclicity of the climate system. The latter approach offers a means to forecast future climate based on knowledge of past climate. The National Center for Atmospheric Research sought to "predict" (simulate) past climate from a regional-scale climate model and ran two future scenarios based on high atmospheric levels of greenhouse gases. The USGS studied past climate cyclicity to potentially forecast future climate. The National Center for Atmospheric Research's emulation of past climate was designed as a test of the models resolving power and as a means of validating the model results from paleoclimate proxy data.

4.3.1 Modeling

Schelling and Thompson (1997) summarize the results of the climate modeling simulations derived from a regional-scale climate model, which is nested within a global-scale model called Genesis. Genesis begins a simulation under some past set of climate boundary conditions, such as sea surface-temperature reconstructions, insolation levels, and continental ice volume. The global climate simulation then produces climate parameter output for a gridded network covering earth. The global climate model output for nodes in the vicinity of the regional climates domain then becomes the input to the regional climate model. The regional model in turn generates climate output to its own higher resolution gridded network.

Four climate simulations were generated with the regional-scale model, present-day, the full-glacial (21 ka) and two greenhouse scenarios: a double CO₂ and six times CO₂ world. The two greenhouse scenarios provide insight into human-induced climate-change related to CO₂ loading of the atmosphere at higher rates than the oceans can take it up (Schelling and Thompson 1997). High levels of atmospheric CO₂ contribute to a rise in global air temperatures that then result in a gain in atmospheric water vapor, which is another and yet more important greenhouse gas. Because excess loading of CO₂ in the atmosphere will, within centuries, be taken up by the oceans, human modification of climate must be considered as a short-term deviation from long-term climate change discussed above. Indeed, Broecker (1997) suggests human-related climate perturbations may

accelerate change in the climate system toward a glacial state. The model output suggests that CO₂ loading of the atmosphere could result in an increase in precipitation within the Yucca Mountain region by about 20 percent. A part or all of the gain in precipitation would occur during growing seasons and would be accompanied by higher temperatures, change in infiltration would depend on the vegetation cover and level of temperature change.

The full-glacial scenario was run to provide a modeled input for various hydrologic models and to evaluate the output of the climate model for a non-modern climate against climate reconstructions based on climate-proxy data. A strong correspondence between modeled and database climate reconstructions would establish confidence in the climate model output, thus establishing a basis for using the climate model to predict future climate.

The results of the 21 ka experiment (Schelling and Thompson 1997) suggest a modest decrease in winter temperatures by about 1 to 3°C and a 2 to 6°C decrease for summer temperatures. Precipitation increases relative to the model control for most months of the year showing an average gain in annual precipitation relative to the model control of about 70 percent at Yucca Mountain, but ranging from about 0 to 170 percent throughout the region.

The temperature reconstructions derived from pack-rat middens (see Subsection 4.2.4.1 for average values) suggest colder temperatures than indicated by the model output. Aside from issues of model versus data reconstruction validity, the two sets of results can be evaluated in terms of the types of trees living on the 21 ka landscape versus those living in the region today. As discussed in Subsection 4.2.4.1, pinyon and ponderosa pine are common in the region today above about 1,800 m, but are absent on the 21 ka landscape in the Yucca Mountain region. Thompson (1990) shows that the modern-day northern limits of pinyon pine in the Great Basin are situated near Elko, Nevada. As at least an approximate estimation, winter average low temperatures determine the northern and the high-elevation limits of these trees. By contrast, the lower elevation limit for pinyon and other trees is typically determined by moisture availability. Because the record shows trees are moving downslope, moisture availability is not a limiting criteria. Inspection of weather data from the Elko airport shows an average January temperature of about -5°C. Average January temperature on Yucca Mountain is about 5°C (see Subsection 4.1.3.3), so a depression of that temperature by 3°C would produce a temperature well within the tolerance limits of pinyon pine. The absence of pinyon pine from the Yucca Mountain region therefore suggests temperature depressions by about or possibly more than 10°C (Yucca Mountain region today minus Elko). Thompson and Anderson (R.S. Thompson, USGS, and K.H. Anderson, INSTAAR, written communication to R.M. Forester, USGS, August 1997) report an average January temperature anomaly (value below modern) for the Yucca Mountain region around 21 ka of about -6.8°C from their packrat midden analyses. That value is also too warm relative to these calculations, but is closer to the limiting temperatures for pinyon pine than the temperatures generated from the model.

The model output for mean annual precipitation (see Schelling and Thompson 1997) suggests an approximate gain in precipitation over the model control (modern-day model simulation) of about 70 percent at Yucca Mountain. Thompson and Anderson (R.S. Thompson, USGS, and K.H. Anderson, INSTAAR, written communication to R.M. Forester, USGS, August 1997; and Subsection 4.2.4.1) show a similar gain in precipitation for the 1,600 m elevation and so the site comparison of model and data interpretations are similar. However, a more detailed comparison of

the modeled versus reconstructed levels of precipitation need to be made to access the similarity or dissimilarity of the two outputs. A visual inspection of the 21 ka precipitation maps (see Schelling and Thompson 1997) suggests the correspondence between model and data at Yucca Mountain may worsen on a regional basis.

Air temperature plays a significant role in determining infiltration, because it directly affects evaporation and indirectly affects the type of precipitation a region receives, i.e., cold temperatures favor snow rather than rain and snow typically results in higher rates of infiltration. As a consequence of the importance of temperature to infiltration and the apparent poor correspondence between model temperature output with the data, prediction of future climate based on models would seem unwarranted at this time. The apparent lack of a technical basis for models to predict future climate change is consistent with the NRC's regulatory position that future climate change should be based on paleoclimate information as stated in IRSR "UZ and SZ Flow Under Isothermal Conditions" and "Methods to Evaluate Future Climate Change and Associated Effects at Yucca Mountain."

4.3.2 Forecasting Using Paleoclimate Data

Forecasting climate using paleoclimate data requires that climate, at least in general terms, is cyclical, so characteristics of past climate may be used to bound future climate as the cycle repeats itself. Subsection 4.2.2 identified many of the known factors related to climate change on many time scales. Clearly, long-term earth-based climate drivers such as tectonics or ocean-land configurations are not cyclical. Long-term climate drivers, however, operate on million-year time scales, so the present configuration of, for example, mountain ranges and land ocean relations, should not change a lot in the next one-hundred or so thousands of years. Therefore, in the context of the YMP, the long-term drivers of climate change are nearly constant.

The earth orbital parameters, of eccentricity, obliquity, and precession, change over various millennial time scales (see Subsection 4.2.2.1.1) from high to low values in a predictable way and so are cyclical in character. Figure 4.2-3 shows the repetitive relation between eccentricity and precession and Figure 4.2-5 shows how eccentricity over the past 500 k.y. resembles eccentricity for the next 500 k.y. The long eccentricity cycle is composed of four approximately 100 k.y. long subcycles, although based on the Devils Hole record each of the four subcycle series are progressively longer than the last (Winograd, Coplen et al. 1992). Similarly, the degree of eccentricity (circular-shaped orbit low- and elliptical high-eccentricity) and consequent insolation change systematically through the 400 k.y. cycle. The first eccentricity subcycle describes a relatively circular orbit, so seasonal insolation differences through the subcycle are minimal. By contrast, later subcycles are more elliptical, so seasonal insolation differences through those subcycles are maximal (compare Figures 4.2-3 and 4.2-4). The orbital and consequent insolation characteristics of the eccentricity subcycles are different, but comparison of other 400 k.y. cycles (compare Figures 4.2-3 and 4.2-4) show that each subcycle has broadly repetitive characteristics. Although not identical, the next 100 k.y. has insolation characteristics that most closely resemble the period from about 400 to 300 ka, that is the earth is entering the beginning of a new 400 k.y. cycle (Figure 4.3-1).

The reconstruction of paleoclimate from the Owens Lake record (Subsection 4.2.3.2) for the past 400 k.y. reveals that just as the eccentricity/insolation values for various subcycles differ, so do the climate characteristics for those subcycles within the Yucca Mountain region. The last two glacials appear to have been cold and variously wet to dry glacials, whereas the previous two appear to have been temperate-wet glacials. Therefore, there is a possible correlation, if not cause and effect, between the nature of particular glacial climates and the progressions of orbital parameters within the eccentricity cycle. Change in eccentricity and hence insolation, however, should not by itself be considered a driver of climate change. Rather insolation should be viewed as a timer of change that in unknown ways may work with earth-based forcing functions to cause climate change (see Subsection 4.2.2). If, however, future insolation interacts with earth based climate forcing functions to create climates with characteristics similar to their past counterparts, then past climate can be used to forecast future climate. This expected repetition is the basis for using past climate to forecast future climate.

The OIS-10 glacial, based on preliminary climate reconstruction from the Owens Lake record, was wet and relatively cool, whereas OIS-8 was drier than OIS-10 and somewhat cooler. OIS-6 was wet, but probably not as wet as OIS-10, and the coldest of the glacials during the last 400 k.y., and OIS-2 was the driest of the glacials and about as cold as OIS-6. Similarly, the interglacials from the past 400 k.y. also had different climate characteristics, some like the Holocene (OIS-1) are very warm and dry as it appears was OIS-11. On the other hand, OIS-5 and -7 probably were warm wet interglacials.

Presuming a relationship exists between climate characteristics and either eccentricity and its other orbital correlates or the position of the glacial in the long 400 k.y. cycle, then the next glacial climate will be most similar to the OIS-10 glacial and least like the last two glacials. Under the latter assumptions detailed studies of the Owens Lake record from about 410 to 350 ka, which represent the wettest phase during the OIS-10 glacial, are in progress and will provide a detailed reconstruction of that glacial. More generally, all climates during the past 400 k.y. are under investigation to establish maximal estimates of climate change, the so called super-pluvial, to provide appropriate input terms for various hydrological models. Climates from farther back in time, beyond 400 ka, are also known, but may be of less value for input to hydrological models, because older climates would exist under different long-term climate drivers.

The Devils Hole stable isotope record, because of its well-constrained chronology, provides a means of examining the timing and rates of change of glacial and interglacial transitions in the Yucca Mountain area. Winograd, Coplen et al. (1992) identified Termination Events II through and including V and the timing for those events. A termination event by convention marks the waning phase of a glacial period (see also Winograd, Landwehr et al. 1997, for additional discussion) and is followed by an interglacial. All of the interglacials can be identified from the Devils Hole stable oxygen isotope record (see Figure 4.2-12). Similarly, the isotope data from Devils Hole identifies the end of the interglacials and the transition climate states between interglacials and full glacials. The duration of the interglacial and glacial periods, as defined from Devils Hole, are shown in Figure 4.3-2. As that figure shows, the interglacials are initiated as the shape of the earth's orbit changes from circular towards elliptical. The transitions from interglacials towards glacials take place before the orbital shape reaches its maximum elliptical form for a particular subcycle or as the orbital shape moves towards a circular shape. Full glacial periods are associated with the circular

orbit phase of the eccentricity curves. Presuming these relations persist into the future then from Figure 4.3-2, a transition to the next glacial should be in the immediate future with a maximal phase being about 20 k.y. in the future and a termination in about 60 k.y.

Assuming the interglacial to glacial transition that occurred in the Yucca Mountain region about 400 ka provides an analog for the future, then inspection of the Devils Hole data for that transition should provide insights into the rate of that climate change. The $\delta^{18}\text{O}$ data from Devils Hole from 430 ka to 330 ka is shown in Figure 4.3-3. Values of about 14.5 or larger signify interglacial conditions and the shaded rectangle identifies a cluster of values that remain more or less constant and may be analogous to the relatively stable climate conditions common to the present interglacial for the past 9 ka (Broecker 1997). The latter climate characteristics do not represent the full interglacial as defined by Winograd, Landwehr et al. (1997), but rather identify what should be the warmest phase of that interglacial. $\delta^{18}\text{O}$ values in stratigraphic sequence that are getting larger (transition toward an interglacial) or smaller (transition toward a glacial) signify climate change. The magnitude of that change must be determined from surface records such as Owens Lake, because change in the stable isotope values may be related to a number of factors from which extraction of parameters such as air temperature or precipitation data is not straightforward. The rate of change from the interglacial to glacial however is rapid and occurs between 398 and 397 ka.

The chronology of the Owens Lake record does not allow identification of the interglacial to glacial transition noted above in absolute years, because ages come from an age model rather than from absolute dates. Determination of the approximate rate of change from an interglacial state to a transition state is possible, and it occurs in less than about 2 k.y. (based on the sediment accumulation chronology between samples having scenario D proxies to samples with scenario B/C proxies, see Subsection 4.2.3.2 for scenario definition) or in about the same order of magnitude as is indicated from the Devils Hole record. In the case of Owens Lake, the system goes from a saline lake to a through flowing freshwater lake. The ostracode occurring in that time frame suggest a transition from modern-like conditions to one in which the Polar front was resident at Yucca Mountain latitudes in most winters, suggesting climate changed to a wetter and somewhat cooler, but not extremely cold, state. Examination of the rate and magnitude (Devils Hole and Owens Lake records) for other interglacial to glacial transitions from the Owens Lake record suggest similar rates of change.

Interpretation of the paleoclimate proxy data discussed above infers differing levels of past precipitation and air temperatures. Figure 4.3-4 provides a preliminary and highly simplified summary of relative change in mean annual precipitation and mean annual temperature for the past 500 k.y. based on the various climate proxies discussed in this report. Because more climate proxy records are available for study from the last glacial period and the Holocene the basis for both the mean annual precipitation and mean annual temperature values for those periods is better than for the older parts of the record.

INTENTIONALLY LEFT BLANK

4.4 SUMMARY

The purpose of this document is to summarize what is known about past, present, and future climate in the vicinity of Yucca Mountain. Subsections 4.1, 4.2, and 4.3 cover the present, past, and future, respectively.

Subsection 4.1 discusses the dynamics of modern-day weather and climate from the global-scale characteristics of atmospheric circulation to the particulars of site scale weather. The weather data characterizes the very dry arid to semi-arid nature of the site, establishing the basis for the limited infiltration under today's climate. The discussion of regional weather/climate shows, on a synoptic scale, how air mass dynamics (circulation) in the Pacific can result in local weather patterns that range from large storms to one or more wet years as well as in limited storminess and unusually dry years. The discussion of modern-day global circulation characteristics provides the basis to understand modern climate and from that a basis to understand how features of the modern system move in the response to global climate change, thereby linking this section to the other two sections.

Subsection 4.2 provides information on the features of the global climate system and factors correlated with global change. Long regional records, Owens Lake, Devils Hole, and Death Valley are discussed in terms of each other and in terms of the global system. Fossil and isotopic data show that past climate in the region changes in tandem with global climate change and that such changes are correlated, at the beginning of a glacial, with change in the earth's orbital parameters, but may not be well correlated at the end of a glacial. Climates wetter and/or colder than modern climates dominate the paleoclimate record and were in residence about 80 percent of the time during the past 400 k.y. During those periods winters were colder than modern winters and snow accumulation was more common than today. Summers were cooler than modern, perhaps being similar to modern-day winter or spring seasons (see section 4.2.4.1). Basins throughout the southwest, that today are dry or contain shallow water bodies, often supported lakes of various depths and most would have reached their maximum levels during some or all glacial periods. Surface water bodies supported by both runoff and groundwater discharge were common in the region. Figure 4.3-4 summarizes the data discussed in this subsection in terms of key climate parameters.

Subsection 4.3 discusses how climate information present and past may be used to develop possible future climate scenarios. Scenarios that could be used to bound potential variability within the climate system, limiting future climate over the next 100 k.y. to some subset of total past climate change so as to set bounds for the hydrological models. Models offer a way of looking at the future based on an understanding of modern-day atmospheric physics. Past records provide a way to look for climate cycles and from those cycles argue that the future will be likely be represented by a certain part of a past cycle. The strengths and weaknesses of the effort to model climate are discussed and in particular the estimates of precipitation are consistent with proxy data, at least in some parts of the region, but the estimates of past temperature appear to be relatively warm when compared with the proxy data. Long climate records show that past glacial periods have different climate characteristics (see Figure 4.3-4) and that those characteristics may be correlated with differences in the orbital parameters within the long 400 k.y. eccentricity cycle. If the latter correlation can be extended to the future, then interglacial and glacial climates that occurred from about 410 ka through about 350 ka may serve as a generalized view of future climate, that is the next glacial period from the near future to 50 to 60 kap.

INTENTIONALLY LEFT BLANK

4.5 REFERENCES

NOTE: For each reference either a document accession number (NNA.19xxxxxx.xxxx) or a technical information center number (TIC xxxxxx) is provided. If a number is not currently available, it is noted by TBD (to be determined).

4.5.1 References Cited

- AEC (U.S. Atomic Energy Commission) 1972. *Onsite Meteorological Programs*. Safety Guide 23. Washington, D.C.: U.S. Government Printing Office. TIC 222667.
- Ahrens, C.D. 1985. *Meteorology Today, An Introduction to Weather, Climate, and the Environment*. Second Edition. St. Paul, Minnesota: West Publishing. TIC 237196.
- Alley, R.B.; Gow, A.J.; Johnsen, S.J.; Kipfstuhl, J.; Meese, D.A.; and Thorsteinsson, T. 1995. "Comparison of Deep Ice Cores." *Nature*, 373, 393-394. London, England: MacMillan. TIC 239104.
- Anderson, R.Y. 1992. "Long-Term Changes in the Frequency of El Niño Events." Diaz, H.F. and Markgraf, V., Eds. *El Niño-Historical and Paleoclimatic Aspects of the Southern Oscillation*, 193-200. Cambridge, England: Cambridge University Press. TIC 239208.
- ASHRAE 1993. *ASHRAE Handbook: Climate Design Information, Fundamentals*, Chapter 26. Atlanta, Georgia: American Society of Heating, Refrigeration, and Air-Conditioning Engineers, Inc. TBD On Order.
- Barry, R. and Chorley, R. 1992. *Atmosphere, Weather, and Climate*. New York, New York: Routledge. TBD
- Bedinger, M.S.; Harrill, J.R.; and Thomas, J.M. 1984. *Maps Showing Ground-Water Units and Withdrawal, Basin and Range Province, Nevada*. U.S. Department of the Interior, USGS Water Resources Investigations Report 83-4119-A. Denver, Colorado: U.S. Geological Survey. NNA.19920131.0260.
- Bedinger, M.S.; Langer, W.H.; and Moyle, W.R. 1984. *Maps Showing Ground-Water Units and Withdrawal, Basin and Range Province, Southern California*. U.S. Department of the Interior, USGS Water Resources Investigations Report 83-4116-A. Denver, Colorado: U.S. Geological Survey. TBD
- Bell, G.D. and Basist, A.N. 1994. "The Global Climate of December 1992 - February, 1993. Part I: Warm ENSO Conditions Continue in the Tropical Pacific; California Drought Abates." *Journal of Climate*, 7, 1581-1605. Boston, Massachusetts: American Meteorological Society. TIC 236883.
- Benson, L. and Klieforth, H. 1989. "Stable Isotopes in Precipitation and Ground Water in the Yucca Mountain Region, Southern Nevada: Paleoclimatic Implications." Peterson, D.H., Ed. *Aspects of*

Climate Variability in the Pacific and the Western Americas. American Geophysical Union Monograph 55, 41-59. Washington, D.C.: American Geophysical Union. TIC 224413.

Benson, L.V. and McKinley, P.W. 1985. *Chemical Composition of Ground Water in the Yucca Mountain Area, Nevada, 1971-84.* USGS-OFR-85-484. Denver, Colorado: U.S. Geological Survey. NNA.19900207.0281.

Benson, L.V.; Burdett, J.W.; Kashgarian, M.; Lund, S.P.; Phillips, F.M.; and Rye, R.O. 1996. "Climatic and Hydrologic Oscillations in the Owens Lake Basin and Adjacent Sierra Nevada, California." *Science*, 274, 746-749. Washington, D.C.: American Association for the Advancement of Science. TIC 236824.

Benson, L.V.; Burdett, J.; Lund, S.; Kashgarian, M.; and Mensing, S. 1997. "Nearly Synchronous Climate Change in the Northern Hemisphere During the Last Glacial Termination." *Nature*, 388, 263-265. London, England: MacMillan. TIC 236823.

Berger, A. and Loutre, M.F. 1991. "Insolation Values for the Climate of the Last 10 Million of Years." *Quaternary Science Reviews*, 10, n. 4, 297-317. New York, New York: Elsevier. Science Publishing. TIC 234261.

Bischoff, J.L.; Stafford, T.W.; and Rubin, M. 1997. "A Time-Depth Scale for Owens Lake Sediments of Core OL-92: Radiocarbon Dates and Constant Mass-Accumulation Rate." Smith, G.I. and Bischoff, J.L., Eds. *An 800,000-year Paleoclimatic Record from Core OL-92, Owens Lake, Southeast California.* Geological Society of America Special Paper 317, 91-98. Boulder, Colorado: Geological Society of America. TIC 236857.

Bish, D.L. and Aronson, J.L. 1993. "Paleogeothermal and Paleohydrologic Conditions in Silicic Tuff from Yucca Mountain, Nevada." *Clays and Clay Minerals*, 41, n. 2, 148-161. Long Island, New York: Pergmon Press. TIC 224613.

Blumen, W. 1990. *Atmospheric Processes Over Complex Terrain.* Meteorological Monograph, 23, n. 45. Boston, Massachusetts: American Meteorological Society. TIC 237113.

Bond, G.C.; Broecker, W.S.; Johnsen, S.; Jouzel, J.; Labeyrie, L.D.; McManus, J.; and Taylor, K. 1993. "Correlations Between Climate Records from North Atlantic Sediments and Greenland Ice." *Nature*, 365, 143-147. London, England: MacMillan. TBD

Boutton, T.W. 1991. "Stable Carbon Isotope Ratios of Soil Organic Matter and Their Use as Indicators of Vegetation and Climate Change." *Mass Spectrometry of Soils.* Boutton, T.W. and Yamasaki, S., Eds., 43-78. New York, New York: Marcel Dekker, Inc. TIC 236912.

Bradbury, J.P. 1997. "A Diatom-Based Paleohydrologic Record of Owens Lake Sediments from Core OL-92." Smith, G.I. and Bischoff, J.L., Eds. *An 800,000-year Paleoclimatic Record from Core OL-92, Owens Lake, Southeast California.* Geological Society of America, Special Paper 317, 99-112. Boulder, Colorado: Geological Society of America. TIC 233989.

- Bradley, R.S. and Jones, P.D., Eds. 1992. *Climate Since A.D. 1500*. New York and London: Routledge. TIC 238650.
- Brennan, R. and Quade, J. 1997. "Reliable Late-Pleistocene Stratigraphic Ages and Shorter Groundwater Travel Times from ^{14}C in Fossil Snails from the Southern Great Basin." *Quaternary Research*, 47, 329-336. New York, New York: Academic Press. TIC 237063.
- Broecker, W.S. 1997. "Thermohaline Circulation, the Achilles Heel of Our Climate System: Will Man-Made CO_2 Upset the Current Balance." *Science*, 278, 1582-1588. Washington, D.C.: American Association for the Advancement of Science. TIC 236560.
- Broxton, D.E.; Bish, D.L.; and Warren, R.G. 1987. "Distribution and Chemistry of Diagenetic Minerals at Yucca Mountain, Nye County, Nevada." *Clays and Clay Minerals*, 35, n. 2, 89-110. Long Island City, New York: Pergamon Press. TIC 203900.
- Bryson, R.A. 1989. "Late Quaternary Volcanic Modulation of Milankovitch Climate Forcing." *Theoretical and Applied Climatology*, 39, 115-125. New York, New York: Springer-Verlag. TIC 237005.
- Carroll, M.R. 1997. "Volcanic Sulfur in the Balance." *Nature*, 389, 543-544. London, England: MacMillan. TIC 239759
- Cayan, D.R. and Webb, R.H. 1992. "El Niño/Southern Oscillation and Stream Flowing the Western United States." Diaz, H.F. and Markgraf, V., Eds. *El Niño-Historical and Paleoclimatic Aspects of the Southern Oscillation*, 29-68. Cambridge, England: Cambridge University Press. TIC 239347.
- Cerling, T.E. 1984. "The Stable Isotopic Composition of Modern Soil Carbonate and its Relationship to Climate." *Earth and Planetary Science Letters*, 71, n. 3, 229-240. Amsterdam, Netherlands: Elsevier Science Publishing. TIC 225414.
- Cerling, T.E. and Quade, J. 1993. "Stable Carbon and Oxygen Isotopes in Soil Carbonates in Climate Change." *Continental Isotopic Records*. Geophysical Monograph 78, 217-231. Washington, D.C.: American Geophysical Union. TIC 236947.
- Crowley, T.J. 1996. "Remembrance of Things Past: Greenhouse Lessons from the Geologic Record." *Consequences*, 2, n. 1, 3-12. Saginaw, Michigan: Saginaw Valley State University. TIC 237662.
- CRWMS M&O (Civilian Radioactive Waste Management System Management and Operating Contractor) 1997a. *Engineering Design Climatology and Regional Meteorological Conditions Report*. B00000000-01717-5707-00066. Las Vegas, Nevada: Author. MOL.19980304.0028.
- CRWMS M&O 1997b. *Regional and Local Wind Patterns Near Yucca Mountain*. B00000000-01717-5705-00081. Las Vegas, Nevada: Author. MOL.19980204.0319.

- Cuffey, K.M.; Clow, G.D.; Alley, R.B.; Stuiver, M.; Waddington, E.D.; and Saltus, R.W. 1995. "Large Arctic Temperature Change at the Wisconsin-Holocene Glacial Transition." *Science*, 270, 455-458. Washington, D.C.: American Association for the Advancement of Science. TIC 236946.
- Delorme, L.D. 1970. "Freshwater Ostracodes of Canada. Part IV: Families Ilyocyprididae, Notodromadidae, Darwinulidae, Cytherideidae, and Entocytheridae." *Canadian Journal of Zoology*, 48, n. 6, 1251-1259. Ottawa, Canada: National Research Council of Canada. TIC 234265.
- Dickens, J.M. 1993. "Climate of the Late Devonian to Triassic." *Paleogeography, Palaeoclimatology, Palaeoecology*, 100, 89-94. Amsterdam/New York: Elsevier. TIC 237518.
- DOE (U.S. Department of Energy) 1997. *Quality Assurance Requirements and Description*. DOE/RW-0333P, Revision 7. Washington, D.C: Department of Energy. MOL.19970731.0427.
- DON (U.S. Department of the Navy) 1994. *Global Historical Fields*. Version 1.0. Washington, D.C: U.S. Department of the Navy, Fleet Numerical Meteorology and Oceanography Detachment and National Climatic Center. TIC 225727.
- Donn, W.L. 1987. "Terrestrial Climate Change from Triassic to Recent." Rampino, M.R., et al., Eds., *Climate, History, Periodicity, and Predictability*, 343-352. New York, New York: Van Nostrand Reinhold. TIC 237663.
- Dublyansky, Y.; Reutsky, V.; and Shugurova, N. 1996. *Fluid Inclusions in Calcite from the Yucca Mountain Exploratory Tunnel: Sixth Biennial Pan American Conference on Research in Fluid Inclusions, May 30 - June 1, 1996*. Brown, P.E. and Hagemann, S.G., Eds. Program and Abstracts. Madison, Wisconsin: Department of Geology, University of Wisconsin. TIC 237704.
- Eddy, J.A. 1976. "The Maunder Minimum." *Science*, 192, 1189-1202. Washington, D.C.: American Society for the Advancement of Science. TIC 237060.
- Emiliani, C. 1955. "Pleistocene Temperatures." *Journal of Geology*, 63, 538-578. Chicago, Illinois: University of Chicago Press. TIC 237459.
- EPA (Environmental Protection Agency) 1987a. *Ambient Monitoring Guidelines for Prevention of Significant Deterioration (PSD)*. EPA-450/4-87-007. Research Triangle Park, North Carolina: Office of Air Quality Planning and Standards. TIC 228381.
- EPA 1987b. *On-Site Meteorological Program Guidance for Regulatory Modeling Applications*. EPA-450/4-87-013. Research Triangle Park, North Carolina: Office of Air Quality Planning and Standards. TIC 210292.
- Fabryka-Martin, J.T.; Flint, A.L.; Sweetkind, D.S.; Wolfsberg, A.V.; Levy, S.S.; Roemer, G.J.C.; Roach, J.L.; Wolfsberg, L.E.; and Duff, M.C. 1997. *Evaluation of Flow and Transport Models of Yucca Mountain, Based on Chlorine-36 Studies for Fiscal Year 97*. YMP Milestone Report SP2224M3. Los Alamos, New Mexico: Los Alamos National Laboratory. MOL.19980204.0916.

Fairbridge, R.W. 1961. "Convergence of Evidence on Climatic Change and Ice Ages." *Annals of the New York Academy of Science*, 95, 542-579. New York, New York: Academy of Science. TIC 237066.

Finley, Jr., R.B. 1990. *Woodrat Ecology and Behavior and the Interpretation of Paleomiddens: The Last 40,000 Years of Biotic Change*. Betancourt, J.L.; Van Devender, T.R.; and Martin, P.S., Eds. Chapter 4, 43-58. Tucson, Arizona: The University Press. TIC 237689.

Flint, A.L.; Hevesi, J.A.; and Flint, L.E. 1996. *Conceptual and Numerical Model of Infiltration for the Yucca Mountain Area, Nevada*. Milestone Report 3GUI623M, DTN GS960908312211.003. USGS Water Resources Investigations Report 96-4123. Denver, Colorado: U.S. Geological Survey. MOL.19970409.0087.

Forester, R.M. 1983. "Relationship of Two Lacustrine Ostracode Species to Solute Composition and Salinity: Implication for Paleohydrochemistry." *Geology*, 11, 435-438. Boulder, Colorado: Geological Society of America. TIC 222805.

Forester, R.M. 1986. "Determination of the Dissolved Anion Composition of Ancient Lakes from Fossil Ostracodes." *Geology*, 14, 796-798. Boulder, Colorado: Geological Society of America. TIC 224393.

Forester, R.M. 1987. "Late Quaternary Paleoclimate Records from Lacustrine Ostracodes," in Ruddiman, W.F. and Wright, Jr., H.E., Eds., "North America and Adjacent Oceans During the Last Deglaciation." *The Geology of North America, K-3*, Chapter 12, 261-276. Boulder, Colorado: Geological Society of America. TIC 222481.

Forester, R.M. and Smith, A.J. 1994. "Late Glacial Climate Estimates for Southern Nevada, the Ostracode Record." *High Level Radioactive Waste Management, Proceedings of the Fifth Annual International Conference, Las Vegas, Nevada, May 22-26, 1994*, 2553-2561. La Grange Park, Illinois: American Nuclear Society. TIC 233174.

Forester, R.M.; Bradbury, J.P.; Carter, C.; Elvidge, A.B.; Hemphill, M.L.; Lundstrom, S.A.; Mahan, S.A.; Marshall, B.D.; Neymark, L.A.; Paces, J.B.; Sharpe, S.E.; Whelan, J.F.; and Wigand, P.E. 1996. *Synthesis of Quaternary Responses of the Yucca Mountain Unsaturated and Saturated Zone Hydrology to Climate Change*. USGS Yucca Mountain Project Branch 1996 Milestone Report 3GCA102M. Submitted to USGS OFR 1996. Denver, Colorado: U.S. Geological Survey. MOL.19970211.0026.

Forester, R.M.; Delorme, L.D.; and Bradbury, J.P. 1987. "Mid-Holocene Climate in Northern Minnesota." *Quaternary Research*, 28, 263-273. New York, New York: Academic Press. TIC 237903.

Friedman, I.; Smith, G.I.; and Hardcastle, K.G. 1976. "Studies of Quaternary saline lakes-II. Isotopic and Compositional Changes During Desiccation of the Brines in Owens Lake, California, 1969-1971." *Geochimica et Cosmochimica Acta*, 40, 501-511. Oxford/New York: Pergamon Press. TIC 239139.

- Fritz, S.C.; Juggins, S.; and Battarbee, R.W. 1993. "Diatom Assemblages and Ionic Characterization of Lakes of the Northern Great Plains, North America: A Tool for Reconstructing Past Salinity and Climate Fluctuations." *Canadian Journal Fishery Aquatic Sciences*, 50, 1844-1856. Ottawa, Canada: Canadian Department of Fisheries and Oceans. TIC 234180.
- Gale, H.S. 1914. *Salines in the Owens, Searles, and Panamint Basins, Southeastern California*. USGS Bulletin 580-L, 251-323. Denver, Colorado: U.S. Geological Survey. TIC 225824.
- Gill, A.E. 1982. "Atmosphere-Ocean Dynamics." *International Geophysical Series*, 30. New York, New York: Academic Press. TIC 238648.
- Glantz, M. 1996. *Currents of Change: El Niño's Impact on Climate and Society*. New York, New York: Cambridge University Press. TIC 237232.
- Grasso, D.N. 1996. *Hydrology of Modern and Late Holocene Lakes, Death Valley, California*. USGS Water Resources Investigations Report 95-4237. Denver, Colorado: U.S. Geological Survey. MOL.19970204.0218.
- GRIP (Greenland Ice Core Project) members 1993. "Climate Instability During the Last Interglacial Period Recorded in the GRIP Ice Core." *Nature*, 364, 203-207. London, England: Macmillan Journals Inc. TIC 234197.
- Grove, J.M. 1988. *The Little Ice Age*. London, England: Methuen. TIC 238258.
- Hansen, E.M.; Schwarz, F.K.; and Riedel, J.P. 1981. *Meteorology of Important Rainstorms in the Colorado River and Great Basin Drainages*. Hydrometeorological Report 50. Silver Spring, Maryland: National Oceanic and Atmospheric Administration. TIC 234708.
- Hollett, K.J.; Danskin, W.R.; McCaffrey, W.F.; and Walti, C.L. 1991. *Geology and Water Resources of Owens Valley, California*, Chapter B. USGS Water-Supply Paper 2370. Denver, Colorado: U.S. Geological Survey. TIC 234646.
- Houghton, J.G.; Sakamoto, C.M., and Gifford, R.O. 1975. *Nevada's Weather and Climate*. Special Publication No. 2. Reno, Nevada: Nevada Bureau of Mines and Geology. TIC 225666.
- Huschke, R.E. 1980. *Glossary of Meteorology*. Boston, Massachusetts: American Meteorological Society. TIC 217595.
- Imbrie, J. and Imbrie, K.P. 1986. *Ice Ages: Solving the Mystery*. Cambridge, Massachusetts and London, England: Harvard University Press. TBD
- Imbrie, J.; Hays, J.D.; Martinson, D.G.; McIntyre, A.; Mix, A.C.; Morley, J.J.; Pisias, N.G.; Prell, W.L.; and Shackleton, N.J. 1984. "The Orbital Theory of Pleistocene Climate: Support from a Revised Chronology of the Marine $\delta^{18}\text{O}$ Record." Berger, A.L., Imbrie, J., Hays, J., Kukla, G., and Saltzman, B., Eds., *Milankovich and Climate*, Part I, 269-305. Boston, Massachusetts: D. Reidel Publishing Company. TIC 225740.

Imbrie, J.; Mix, A.C.; and Martinson, D.G. 1993. "Milankovitch Theory Viewed from Devils Hole." *Nature*, 363, 531-533. London, England: Macmillan Journals, Inc. TIC 234192.

Jackson, J.A. 1997. *Glossary of Geology*, 4th edition. Alexandria, Virginia: American Geological Institute. TIC 236393.

Karlen, W. and Kuylenstierna, J. 1996. "On Solar Forcing of Holocene Climate: Evidence from Scandinavia." *The Holocene*, 6, 359-365. Seven Oaks, Kent, England: E. Arnold (Distributed in North America by Cambridge University Press). TIC 236965.

Kay, P.A. 1982. "A Perspective on Great Basin Paleoclimates." Madsen, D.B. and O'Connell, J.F., Eds., *Man and the Environment in the Great Basin*. Society of American Archaeology Papers, n. 2, 76-81. Washington, D.C.: Society of American Archaeology. TIC 234650.

Kim, S.T. and O'Neil, J.R. 1997. "Equilibrium and Nonequilibrium Oxygen Isotope Effects in Synthetic Carbonates." *Geochimica et Cosmochimica Acta*, 61, 3461-3475. Oxford/New York: Pergamon Press. TIC 236999.

Kutzbach, J.E. and Guetter, P.J. 1986. "The Influence of Changing Orbital Parameters and Surface Boundary Conditions on Climate Simulations for the Past 18000 yrs." *Journal of the Atmospheric Sciences*, 43, 1726-1759. Lancaster, Pennsylvania: American Meteorological Society. TIC 221722.

La Marche, Jr., V.C. 1974. "Paleoclimatic Inferences from Long Tree-Ring Records." *Science*, 183, 1043-1048. Washington, D.C.: American Association for the Advancement of Science. TIC 225741.

Landwehr, J.M.; Coplen, T.B.; Ludwig, K.R.; Winograd, I.J.; and Riggs, A.C. 1997. *Data for Devils Hole Core DH-11*. USGS OFR 97-792. Denver, Colorado: U.S. Geological Survey. TBD

Larsen, E.E.; Patterson, P.E.; and Luiszer, F. 1991. *Paleoclimate Record from ~2.4 to ~0.5 Ma, Tecopa Basin, SE California*. Geological Society of America, Abstracts with Programs, 23, A301. Boulder, Colorado: Geological Society of America. TIC 237437.

Li, J.; Lowenstein, T.K.; Brown, C.B.; Ku, T-L.; and Luo, S. 1996. "A 100 ka Record of Water Tables and Paleoclimates from Salt Cores, Death Valley, California." *Palaeogeography, Palaeoclimatology, Palaeoecology*, 123, 179-203. Amsterdam/New York: Elsevier. TIC 236544.

Litwin, R.J.; Adam, D.A.; Frederiksen, N.O.; and Woolfenden, W.B. 1997. "An 800,000-year Pollen Record from Owens Lake, California: Preliminary Analyses," in Smith, G.I. and Bischoff, J.L., Eds., *An 800,000-year Paleoclimatic Record from Core OL-92, Owens Lake, Southeast California*. Geological Society of America, Special Paper, 317, 127-142. Boulder, Colorado: Geological Society of America. TIC 236857.

Lowenstein, T.K. 1997. "Death Valley Salt Core: 200,000-year Paleoclimate Record from Sedimentary Structures, Saline Mineralogy, Fluid Inclusions in Halite, and Ostracodes." *Great*

- Basin Aquatic System History, Program, Abstracts Field Guide*, unpaginated. Salt Lake City, Utah: University of Utah. TBD
- Lutgens, F. and Tarbuck, J. 1995. *The Atmosphere: An Introduction to Meteorology*. Sixth Edition. Figures 7-5, 7-6, and 7-7; pp 175, 177, 178. Englewood Cliffs, New Jersey: Simon and Schuster Co. TBD
- Marshall, B.D.; Futa, K.; and Peterman, Z.E. 1997. "Hydrologic Inferences from Strontium Isotopes in Pore Water from the Unsaturated Zone at Yucca Mountain, Nevada." Abstract. *EOS, Transactions of the American Geophysical Union, 1997 Fall Meeting, San Francisco, California, December 8-12, 1997*, F308. Washington, D.C.: American Geophysical Union. TIC 237795.
- McGlone, M.S.; Kershaw, A.P.; and Markgraf, V. 1992. "El Niño / Southern Oscillation Climatic Variability in Australasian and South American Paleoenvironmental Records." Diaz, H.F. and Markgraf, V., Eds. *El Niño-Historical and Paleoclimatic Aspects of the Southern Oscillation*, 435-462. Cambridge, England: Cambridge University Press. TIC 239210.
- Meko, D.M. 1992. "Spectral Properties of Tree-Ring Data in the United States Southwest as Related to El Niño/Southern Oscillation." Diaz, H.F., and Markgraf, V., Eds. *El Niño-Historical and Paleoclimatic Aspects of the Southern Oscillation*, 227-241. Cambridge, England: Cambridge University Press. TIC 239207.
- Milankovitch, M. 1938. "Astronomische Mittel zur Erforschung Dererdgeschichtlichen Klimate." *Handbuch der Geophysik*, 9, B. Guttenberg, Ed., 593-698 Berlin, Germany. TBD
- Miller, A. and Thompson, J. 1970. *Elements of Meteorology*. Columbus, Ohio: Charles E. Merrill Publishing Company. TBD
- Milne, W.K.; Benson, L.; and McKinley, P.W. 1987. *Isotope Content and Temperature of Precipitation in Southern Nevada, August 1983 - August 1986*. USGS-OFR-87-463. Denver, Colorado: U.S. Geological Survey. TIC 202638.
- Mock, C. 1996. "Climatic Control and Spatial Variations of Precipitation in the Western United States." *Journal of Climate*, 9, 1111-1125. Boston, Massachusetts: American Meteorological Society. TIC 237445.
- Neftel, A.H.; Oeschger, H.; and Stauffer, B. 1988. "CO₂ Record in the Byrd Ice Core 50,000 - 5,000 yrs B.P." *Nature*, 331, 609-611. London, England: Macmillan Journals Inc. TIC 236205.
- Neymark, L.A.; Amelin, Y.V.; Paces, J.B.; and Peterman, Z.E. 1998. "U-Pb Dating of Opal at Yucca Mountain: Evidence for Long-term Stability of the Unsaturated Zone." *High Level Radioactive Waste Management, Proceedings of the Eighth Annual International Conference, Las Vegas, Nevada, May 11-14, 1998*, 85-87. La Grange Park, Illinois: American Nuclear Society. TIC 237082.

- NOAA (National Oceanic and Atmospheric Administration) 1973. *NOAA Atlas 2: Precipitation-Frequency Atlas of the Western United States*. Volume VII - Nevada. Silver Spring, Maryland: Department of Commerce. TIC 206081.
- NOAA 1997. *Analysis of Extreme Precipitation Events in Southern Nevada*. Technical Memorandum ERL ARL-221, Randerson, D., April 1997. Silver Spring, Maryland: Department of Commerce. TIC 233167.
- NRC (U.S. Nuclear Regulatory Commission) 1977. *Methods for Estimating Atmospheric Transport and Dispersion of Gaseous Effluents in Routine Releases from Light-Water-Cooled Reactors*. Regulatory Guide 1.111. Washington, D.C: Nuclear Regulatory Commission. TIC 222639.
- NRC 1987. *Standard Review Plan for the Review of Safety Analyses Reports for Nuclear Power Plants*. Section 2.3.1, Regional Climatology; Section 2.3.2, Local Meteorology. NUREG-800. Washington, D.C: U.S. Nuclear Regulatory Commission. TIC 203894.
- NWS (National Weather Service) 1977. *Probable Maximum Precipitation Estimates, Colorado River and Great Basin Drainage*. Hydrometeorological Report 49. Silver Spring, Maryland: National Weather Service. TIC 220224.
- Paces, J.B.; Neymark, L.A.; Marshall, B.D.; Whelan, J.F.; and Peterman, Z.E. 1996. *Ages and Origins of Subsurface Secondary Minerals in the Exploratory Studies Facility (ESF)*. USGS Yucca Mountain Project Branch 1996 Milestone Report 3GQH450M. Denver, Colorado: U.S. Geological Survey. MOL.19970324.0052.
- Paces, J.B.; Taylor, E.M.; and Bush, C. 1993. "Late Quaternary History and Uranium Isotopic Compositions of Ground Water Discharge Deposits, Crater-Flat, Nevada." *High Level Radioactive Waste Management, Proceedings of the Fourth Annual International Conference, Las Vegas, Nevada, April 26-30, 1993*, 1573-1580. La Grange Park, Illinois: American Nuclear Society. GS921208315215.037; TIC 225325.
- Paces, J.B.; Whelan, J.F.; Forester, R.M.; Bradbury, J.P.; Marshall, B.D.; and Mahan, S.A. 1997. *Summary of Discharge Deposits in the Amargosa Valley*. U.S. Geological Survey Level 4 Milestone Report SPC333M4 to DOE-YMPSCO. Denver, Colorado: U.S. Geological Survey. TBD.
- Pyke, C.B. 1972. *Some Meteorological Aspects of the Seasonal Distribution of Precipitation in the Western United States and Baja California*. University of California Water Resources Center, Contribution 139. Los Angeles, California: University of California Water Resources Center. TIC 217366.
- Quade, J. 1986. "Late Quaternary Environmental Changes in the Upper Las Vegas Valley, Nevada." *Quaternary Research*, 26, n. 3, 340-357. New York, New York: Academic Press. TIC 218889.
- Quade, J. and Cerling, T.E. 1990. "Stable Isotopic Evidence for a Pedogenic Origin of Carbonates in Trench 14 near Yucca Mountain, Nevada." *Science*, 250, 1549-1552. Washington, D.C.: American Association for the Advancement of Science. TIC 222617.

Quade, J. and Pratt, W.L. 1989. "Late Wisconsin Groundwater Discharge: Environments of the Southwestern Indian Springs Valley, Southern Nevada." *Quaternary Research*, 31, n. 3, 351-370. New York, New York: Academic Press. TIC 223977.

Quade, J.; Cerling, T.E.; and Bowman, J.R. 1989. *Systematic Variations in the Carbon and Oxygen Isotopic Composition of Pedogenic Carbonate Along Elevation Transects in the Southern Great Basin, United States*. Geological Society of America Bulletin, 101, n. 4, 464-475. Boulder, Colorado: Geological Society of America. TIC 224417.

Quade, J.; Mifflin, M.D.; Pratt, W.L.; McCoy, W.; and Burckle, L. 1995. *Fossil Spring Deposits in the Southern Great Basin and Their Implications for Changes in Water Table Levels Near Yucca Mountain, Nevada, During Quaternary Time*. Geological Society of American Bulletin, 107, n. 2, 213-230. Boulder, Colorado: Geological Society of America. TIC 234256.

Randerson, R. 1984. *Atmospheric Science and Power Production*. DE84005177. Springfield, Virginia: National Technical Information Center. TIC 223438.

Roberts, S.M. 1996. *Paleoclimate of Death Valley, California (100 - 200 ka): Record from Cored Sediments, Homogenization Temperatures of Fluid Inclusions in Halite, and Stable Isotopes of Fluid Inclusions*. Doctoral dissertation. Calgary, Canada: University of Calgary. TBD

Roberts, S.M. and Spencer, R.J. 1995. "Paleotemperatures Preserved in Fluid Inclusions in Halite." *Geochemica et Cosmochemica Acta*, 59, 3929-3942. Oxford/New York: Pergamon. TIC 236546.

Roberts, S.M.; Spencer, R.J.; and Lowenstein, T.K. 1994. "Late Pleistocene Saline Lacustrine Sediments, Badwater Basin, Death Valley, California." Lomando, A.J., Schreiber, B.C., and Harris, P.M., Eds. *Lacustrine Reservoirs and Depositional Systems, Society of Economic Petrologists and Mineralogists (SEPM), Core Workshop 19*, 61-103. Tulsa, Oklahoma: Society for Sedimentary Geology. TIC 237003.

Roedder, E.; Whelan, J.F.; and Vaniman, D.T. 1994. "Fluid Inclusion Studies of Calcite Veins from Yucca Mountain, Nevada, Tuffs: Environment of Formation." *High Level Radioactive Waste Management, Proceedings of the Fifth Annual International Conference, Las Vegas, Nevada, May 22-26, 1994*, 1854-1860. La Grange Park, Illinois: American Nuclear Society. TIC 222135.

Rogers, K.L.; Larsen, E.E.; Smith, G; and 9 others. 1992. "Pliocene and Pleistocene Geologic and Climatic Evolution in South-Central Colorado." *Palaeogeography, Palaeoclimatology, and Palaeoecology*, 94, 55-86. Amsterdam, Netherlands: Elsevier. TIC 236885.

Sarna-Wojcicki, A.M.; Meyer, C.M.; and Wan, E. 1997. "Tephra Layers, Position of the Brunhes-Matuyama Boundary, and Effects of Bishop Ash Eruption on Owens Lake Sediments: Core OL-92," in Smith, G.I. and Bischoff, J.L. Eds., *An 800,000-year Paleoclimatic Record from Core OL-92, Owens Lake, Southeast California*. Geological Society of America Special Paper 317, 79-90. Boulder, Colorado: Geological Society of America. TIC 239731.

Schelling, F.J. and Thompson, S.L. 1997. "Future Climate Modeling Scenarios." Milestone Report SLTR97-0001 Department 6850 Letter Report-May 23 1997. Prepared for the USDOE-YMSCO by TRW Environmental Safety Systems. Albuquerque, New Mexico: Sandia National Laboratories. MOL.19971021.0607.

Self, S.; Rampino, M.R.; and Barbera, J.J. 1981. "The Possible Effects of Large 19th and 20th Century Eruptions on Zonal and Hemispheric Surface Temperatures." *Journal of Volcanology and Geothermal Research*, 11, 41-60. Amsterdam, Netherlands: Elsevier Science Publishers. TIC 237312.

Shackleton, N.J. and Opdyke, N.D. 1973. "Oxygen Isotope and Paleomagnetic Stratigraphy of Equatorial Pacific Core V28-238: Oxygen Isotope Temperatures and Ice Volumes on a 10^5 and 10^6 Year Cycle." *Quaternary Research*, 3, 39-55. New York, New York: Academic Press. TIC 225720.

Shaffer, J.A.; Cereny, R.S.; and Dorn, R.I. 1996. "Radiation Windows as Indicators of an Astronomical Influence on the Devils Hole Chronology." *Geology*, 24, 1017-1020. Boulder, Colorado: Geological Society of America. TIC 237308.

Sharpe, S.E.; Whelan, J.F.; Forester, R.M.; and McConnaughey, T. 1994. "Molluscs as Climate Indicators: Preliminary Stable Isotope and Community Analysis." *High Level Radioactive Waste Management, Proceedings of the Fifth Annual International Conference, Las Vegas, Nevada, May 22-26, 1994*, 2538-2544. La Grange Park, Illinois: American Nuclear Society. TIC 222141.

Siegenthaler, U. 1989. "Glacial-Interglacial Atmospheric CO_2 Variations," in Bradley, R.S., Ed., *Global Changes of the Past*, 245-260. Boulder, Colorado: University Corporation for Atmospheric Research. TIC 237911.

Smith, G.I. 1976. "Paleoclimatic Record in the Upper Quaternary Sediments of Searles Lake, California, U.S.A." Horie, S., Ed., *Paleolimnology of Lake Biwa and the Japanese Pleistocene*, 4, 577-604. Kyoto, Japan: Kyoto University. TIC 234339.

Smith, G.I. 1984. "Paleohydrologic Regimes in the Southwestern Great Basin, 0-3.2 my Ago, Compared with Other Long Records of 'Global' Climate." *Quaternary Research*, 22, 1-17. New York, New York: Academic Press. TIC 219152.

Smith, G.I. 1997. "Stratigraphy, Lithology, and Sedimentary Structures of Owens Lake Core OL-92." Smith, G.I. and Bischoff, J.L., Eds., *An 800,000-year Paleoclimatic Record from Core OL-92, Owens Lake, Southeast California*. Geological Society of America Special Paper 317, 9-24. Boulder, Colorado: Geological Society of America. TIC 239730.

Smith, G.I. and Bischoff, J.L. 1997. "Core OL-92 from Owens Lake: Project Rationale, Geologic Setting, Drilling Procedures, and Summary." Smith, G.I. and Bischoff, J.L. Eds., *An 800,000-year Paleoclimatic Record from Core OL-92, Owens Lake, Southeast California*. Geological Society of America, Special Paper 317, 1-8. Boulder, Colorado: Geological Society of America. TIC 237295.

- Smith, G.I.; Bischoff, J.L.; and Bradbury, J.P. 1997. "Synthesis of the Paleoclimatic Record From Owens Lake Core OL-92." Smith, G.I. and Bischoff, J.L. Eds., *An 800,000-year Paleoclimatic Record from Core OL-92, Owens Lake, Southeast California*. Geological Society of America, Special Paper 317, 143-160. Boulder, Colorado: Geological Society of America. TIC 233995.
- Spaulding, W.G. 1990. "Vegetational and Climatic Development of the Mojave Desert: The Last Glacial Maximum to the Present." *Packrat Middens: The Last 40,000 Yrs of Biotic Change*. Betancourt, J.L., Van Devender, T.R., and Martin, P.S., Eds. Chapter 9, 166-199. Tucson, Arizona: The University Press. TIC 234344.
- Stauffer, B.; Hofer, H.; Oeschger, H.; Schwander, J.; and Siegenthaler, U. 1984. "Atmospheric CO₂ Concentration During the Last Glaciation." *Annals of Glaciology*, 5, 160-164. Cambridge, Cambridgeshire, England: International Glaciological Society. TIC 237454.
- Swadley, W.C. and Carr, W.J. 1987. Geological Map of the Quaternary and Tertiary Deposits of the Big Dune Quadrangle, Nye County, Nevada, and Inyo County, California. USGS Miscellaneous Series Map, I-1767. Denver, Colorado: U.S. Geological Survey. TIC 203089.
- Szabo, B.J. and Kyser, T.K. 1990. *Ages and Stable-Isotope Compositions of Secondary Calcite and Opal in Drill Cores from Tertiary Volcanic Rocks of the Yucca Mountain Area, Nevada*. Geological Society of America Bulletin, 102, n. 12, 1714-1719. Boulder, Colorado: Geological Society of America. TIC 221927.
- Szabo, B.J.; Kolesar, P.T.; Riggs, A.C.; Winograd, I.J.; and Ludwig, K.R. 1994. "Paleoclimatic Inferences from a 120,000-yr Calcite Record of Water-Table Fluctuation in Browns Room of Devils Hole, Nevada." *Quaternary Research* 41, 59-69. New York, New York: Academic Press. TIC 234642.
- Taylor, K.C.; Lamorey, G.W.; Doyle, G.A.; Alley, R.B.; Grootes, P.M.; Mayewski, P.A.; White, J.W.C.; and Barlow, L.K. 1993. "The 'Flickering Switch' of Late Pleistocene Climate Change." *Nature*, 361, 432-436. London, England: Macmillan Journals Inc. TIC 234169.
- Thompson, R.S. 1990. "Late Quaternary Vegetation and Climate in the Great Basin." *Packrat Middens: The Last 40,000 Yrs of Biotic Change*. Betancourt, J.L., Van Devender, T.R., and Martin, P.S., Eds. Chapter 10, 200-239. Tucson, Arizona: The University Press, Tucson, Arizona. TIC 236704.
- Thompson, R.S. 1991. "Pliocene Environments and Climates in the Western United States." *Quaternary Science Reviews*, 10, 115-132. New York, New York: Elsevier. TIC 234260.
- U.S. Climate Division. U.S. Climate Division Plotting Page [Electronic database] (No date). National Oceanic and Atmospheric Administration [July 20, 1998]. Available: <http://www.cdc.noaa.gov/USclimate/USclimdivs.html>. TIC 240136
- van Devender, T.R. 1990a. "Late Quaternary Vegetation and Climate of the Chihuahuan Desert, United States and Mexico." *The Last 40,000 Yrs of Biotic Change*. Betancourt, J.L., Van Devender,

T.R., and Martin, P.S., Eds. Chapter 7, 104-133. Tucson, Arizona: The University Press. TIC 237728.

van Devender, T.R. 1990b. "Late Quaternary Vegetation and Climate of the Sonoran Desert, United States and Mexico." *The Last 40,000 Yrs of Biotic Change*. Betancourt, J.L., Van Devender, T.R., and Martin, P.S., Eds. Chapter 8, 133-165. Tucson, Arizona: The University Press. TIC 237691.

Vaniman, D.T. and Whelan, J.F. 1994. "Inferences of Paleoenvironment from Petrographic, Chemical, and Stable Isotope Studies of Calcretes and Fracture Calcites." *High Level Radioactive Waste Management, Proceedings of the Fifth Annual International Conference, Las Vegas, Nevada, May 22-26, 1993*, 2730-2737. LaGrange Park, Illinois: American Nuclear Society. TIC 222137.

Whelan, J.F. and Moscati, R.J. 1998. "9 m.y. Record of Southern Nevada Climate from Yucca Mountain Secondary Minerals." *High Level Radioactive Waste Management, Proceedings of the Eighth International Conference, Las Vegas, Nevada, May 11-14, 1998*, 12-15. La Grange Park, Illinois: American Nuclear Society. TIC 239553.

Whelan, J.F. and Stuckless, J.S. 1992. "Paleohydrologic Implications of the Stable Isotopic Composition of Secondary Calcite Within the Tertiary Volcanic Rocks of Yucca Mountain, Nevada." *High Level Radioactive Waste Management, Proceedings of the Third Annual International Conference, Las Vegas, Nevada, April 12-16, 1993*, 1572-1581. LaGrange Park, Illinois: American Nuclear Society. NNA.19930121.0109; TIC 237577.

Whelan, J.F.; Vaniman, D.T.; Stuckless, J.S.; and Moscati, R.J. 1994. "Paleoclimatic and Paleohydrologic Records from Secondary Calcite: Yucca Mountain, Nevada." *High Level Radioactive Waste Management, Proceedings of the Fifth Annual International Conference, Las Vegas, Nevada, May 22-26, 1994*, 2738-2745. La Grange Park, Illinois: American Nuclear Society. TIC 222138.

Wigand, P.E. 1997. "A Late Holocene Pollen Record from Lower Pahranaagat Lake, Southern Nevada, USA: High-Resolution Paleoclimatic Records and Analysis of Environmental Responses to Climate Change." Isaacs, C.M. and Tharp, V.L. Eds., *Proceedings of the Thirteenth Annual Pacific Climate (PACLIM) Workshop, April 15-18, 1996*, 63-77. Sacramento, California: California Department of Water Resources. TIC 236898.

Wigley, T.M.L. and Kelly, P.M. 1990. "Holocene Climate Change, 14-C Wiggles and Variations in Solar Irradiance." *Philosophical Transactions of the Royal Society of London, Series A*, 330, 547-560. London, England: Philosophical Transactions of the Royal Society of London. TIC 237434.

Williams, D.F.; Thunell, R.C.; Tappa, E.; Rio, D.; and Raffi, I. 1988. "Chronology of the Pleistocene Oxygen Isotope Record: 0-1.88 m.y. B.P." *Palaeogeography, Palaeoclimatology, and Palaeoecology*, 64, 221-240. Amsterdam/New York: Elsevier. TIC 236879.

- Willson, R.C. 1997. "Total Solar Irradiance Trend During Solar Cycles 21 and 22." *Science*, 277, 1963-1965. Washington, D.C.: American Association for the Advancement of Science. TIC 237442.
- Willson, R.C. and Hudson, H.S. 1988. "Solar Luminosity Variations in Solar Cycle 21." *Nature*, 332, 810-812. London, England: Macmillan Journals Inc. TBD
- Winograd, I.J. and Riggs, A.C. 1984. *Recharge to the Spring Mountains, Nevada: Isotopic Evidence*. Geological Society of America Bulletin Abstracts with Programs 16, 698. Boulder, Colorado: Geological Society of America. TIC 217345.
- Winograd, I.J. and Thordarson W. 1975. *Hydrogeologic and Hydrochemical Framework, South-Central Great Basin, Nevada-California, with Special Reference to the Nevada Test Site*. USGS Professional Paper 712-C. Denver, Colorado: U.S. Geological Survey. NNA.19870406.0201. TIC 206787.
- Winograd, I.J.; Coplen, T.B.; Landwehr, J.M.; Riggs, A.C.; Ludwig, K.R.; Szabo, B.J.; Kolesar, P.T.; and Revesz, K.M. 1992. "Continuous 500,000-year Climate Record from Vein Calcite in Devils Hole, Nevada." *Science*, 258, 255-260. Washington, D.C.: American Association for the Advancement of Science. TIC 237563.
- Winograd, I.J.; Landwehr, J.M.; Ludwig, K.R.; Coplen, T.B.; and Riggs, A.C. 1997. "Duration and Structure of the Past Four Interglaciations." *Quaternary Research*, 48, 141-154. New York, New York: Academic Press. TIC 236777.
- Winograd, I.J.; Szabo, B.J.; Coplen, T.B.; and Riggs, A.C. 1988. "A 250,000-year Climate Record from Great Basin Vein Calcite: Implications for Milankovitch Theory." *Science*, 242, 1275-1280. Washington, D.C.: American Association for the Advancement of Science. TIC 222215.
- Winograd, I.J.; Szabo, B.J.; Coplen, T.B.; Riggs, A.C.; and Kolesar, P.T. 1985. "Two-Million-Year Record of Deuterium Depletion in Great Basin Ground Waters." *Science*, 227, 519-511. Washington, D.C.: American Association for the Advancement of Science. TIC 216799.
- Winter, T. and Woo, M.K. 1990. "Hydrology of Lakes and Wetlands." *Geology of North America*, Wolman, M.G. and Riggs, H.C., O-1, Chapter 8. Boulder, Colorado: Geological Society of America. TIC 234262.
- Yang, I.C.; Yu, P.; Rattray, G.W.; and Thorstenson, D.C. 1998. *Hydrogeochemical Investigations and Geochemical Modeling in Characterizing the Unsaturated Zone at Yucca Mountain, Nevada*. USGS Water Resources Investigation Report. Denver, Colorado: U.S. Geological Survey. TBD

4.5.2 Codes, Standards, Regulations

- ASTM D5741-96. *Standard Practice for Characterizing Surface Wind Using a Wind Vane And Rotating Anemometer*. 1996. (Annual Book of Standards. Vol. 11.03: *Atmospheric Analysis*.) West Conshohocken, Pennsylvania: American Society for Testing and Materials. TIC 236772.

TABLES

	Page
4.1-1 Regional Meteorological Stations	T4.1-1
4.1-2 1986 -1996 Precipitation Statistics for Three Sites	T4.1-1
4.1-3 1965 -1996 Precipitation Statistics for Two Sites	T4.1-2
4.1-4 Temperature Summaries	T4.1-2
4.1-5 R/EFPD Meteorological Monitoring Sites	T4.1-2
4.1-6 R/EFPD Precipitation-Only Monitoring Sites	T4.1-3
4.1-7 Equipment Descriptions	T4.1-3
4.1-8 Reported Data - Hourly	T4.1-4
4.1-9 Reported Data - 10-minute	T4.1-5
4.1-10 Reported Data - Daily	T4.1-5
4.1-11 R/EFPD Site 1 (NTS-60) Monthly and Annual Climatological Summaries	T4.1-6
4.1-12 R/EFPD Site 2 (Yucca Mountain) Monthly and Annual Climatological Summaries	T4.1-7
4.1-13 R/EFPD Site 3 (Coyote Wash) Monthly and Annual Climatological Summaries	T4.1-8
4.1-14 R/EFPD Site 4 (Alice Hill) Monthly and Annual Climatological Summaries	T4.1-9
4.1-15 R/EFPD Site 5 (Fortymile Wash) Monthly and Annual Climatological Summaries	T4.1-10
4.1-16 R/EFPD Site 6 (WT-6) Monthly and Annual Climatological Summaries	T4.1-11
4.1-17 R/EFPD Site 7 (Sever Wash) Monthly and Annual Climatological Summaries	T4.1-12
4.1-18 R/EFPD Site 8 (Knothead Gap) Monthly and Annual Climatological Summaries	T4.1-13
4.1-19 R/EFPD Site 9 (Gate 510) Monthly and Annual Climatological Summaries	T4.1-14
4.1-20 Yearly Climatological Data Summary	T4.1-15
4.1-21 Climatological Summary for Austin and Battle Mountain	T4.1-16
4.1-22 Climatological Summary for Caliente and Desert Rock	T4.1-17
4.1-23 Climatological Summary for Elko and Ely	T4.1-18
4.1-24 Climatological Summary for Las Vegas and Tonopah	T4.1-19
4.1-25 Annual Precipitation for NWS Sites: 1921 - 1947	T4.1-20
4.1-26 Annual Precipitation for NWS Sites: 1948 - 1995	T4.1-21
4.1-27 ASHRAE Table for the R/EFPD Meteorological Sites	T4.1-22
4.2-1 Correspondence of Ages for Oxygen Isotope Stages from the Spectral Mapping Project and Owens Lake Records	T4.2-1
4.2-2 Estimation of the $\delta^{18}\text{O}$ Composition of Infiltration for a Modern or Glacial Climate	T4.2-1

INTENTIONALLY LEFT BLANK

Table 4.1-1. Regional Meteorological Stations

Station Name	Latitude ¹ Longitude ¹ (deg° min' sec")	Elevation (feet msl)	Period of Operation	Approximate Distance and Direction from Yucca Mountain
Amargosa Farms (Garey)	36° 34'N 116° 28'W	2450	Dec 1965 to present	30 km S, (10 km S of Site 9)
Austin, NV	39° 30'N 117° 04'W	6605	1921 to present	290 km NNW
Beatty (location moved in 1957)	36° 54'N 116° 45'W and 36° 55'N 116° 45'W	3310 3300	1948 - 1957 and 1957 - Nov 1972	25 km WNW
Beatty 8N	37° 00'N 116° 43'W	3550	Dec 1972 to present	25 km WNW
Caliente, NV	37° 37'N 114° 31'W	4403	Aug 1928 to present	170 km NE
Desert Rock Airport (DRA)	36° 37'N 116° 01'W	3300	Apr 1984 to present	45 km SE
NOAA/ARL/SORD 4JA (Second Location)	36° 47'05"N 116° 17'20"W	3422	1967 to present	15 km ESE
Area 12 Mesa	37° 11'00"N 116° 13'00"W	7490	1959 to 1993	44 km NNE

¹NAD27 (North American Datum of 1927)

Table 4.1-2. 1986 - 1996 Precipitation Statistics for Three Sites

	R/FFPD Site 1	Beatty 8N	Amargosa Farms
Mean	4.97	5.63	4.21
Maximum (year occurred)	9.17 (1995)	8.45 (1995)	6.09 (1992)
Minimum (year occurred)	1.44 (1989)	2.43 (1989)	0.72 (1989)
Standard Deviation	2.22	1.74	2.14

NOTE: Precipitation statistics are in inches

Table 4.1-3. 1965 - 1996 Precipitation Statistics for Two Sites

Mean	Amargosa Farms	Beatty
	4.21	5.53
Maximum (year occurred)	10.37 (1983)	11.49 (1983)
Minimum (year occurred)	0.72 (1989)	1.98 (1971)
Standard Deviation	2.66	2.31

NOTE: Precipitation statistics are in inches

Table 4.1-4 Temperature Summaries

Month	Statistic (degree C)	Site 1	Site 5	Desert Rock	Austin	Caliente
January	Mean Max	10.9	12.6	12.4	4.9	7.8
	Mean Min	2.4	1.8	0.4	-7.4	-8.2
July	Mean Max	34.2	36.3	36.9	30.6	35.3
	Mean Min	22.1	21.8	21.3	12.1	13.6

Table 4.1-5. R/EFPD Meteorological Monitoring Sites

Site	Latitude ¹ (deg° min' sec")	Longitude ¹ (deg° min' sec")	Elevation (above mean sea level)
Site 1 (NTS-60)	36°50'34"N	116°25'50"W	3750 ft 1143 m
Site 2 (Yucca Mountain)	36°51'19"N	116°27'56"W	4850 ft 1478 m
Site 3 (Coyote Wash)	36°51'17"N	116°27'06"W	4195 ft 1279 m
Site 4 (Alice Hill)	36°51'51"N	116°24'15"W	4050 ft 1234 m
Site 5 (Fortymile Wash)	36°45'52"N	116°23'26"W	3125 ft 953 m
Site 6 (WT-6)	36°53'40"N	116°26'45"W	4315 ft 1315 m
Site 7 (Sever Wash)	36°50'49"N	116°24'28"W	3545 ft 1081 m
Site 8 (Knothead Gap)	36°49'42"N	116°25'35"W	3710 ft 1131 m
Site 9 (Gate-510)	36°40'17"N	116°24'08"W	2750 ft 838 m

¹ NAD27 (North American Datum of 1927)

Table 4.1-6 R/EFPD Precipitation-Only Monitoring Sites

Site	Latitude ¹ (deg° min' sec")	Longitude ¹ (deg° min' sec")	Elevation (above mean sea level)
401	36°53'16"N	116°27'42"W	5125ft/1562m
402	36°51'28"N	116°25'3"W	3683ft/1123m
403	36°48'22"N	116°26'25"W	3686ft/1123m
404	36°52'44"N	116°25'29"W	3980ft/1213m
405	36°49'50"N	116°28'3"W	4882ft/1488m
406	36°48'7"N	116°31'47"W	3367ft/1026m
407	36°52'10"N	116°27'40"W	4440ft/1353m
409	36°49'25"N	116°24'54"W	4010ft/1222m
410	36°50'26"N	116°24'2"W	3476ft/1060m
411	36°48'47"N	116°23'32"W	3342ft/1019m
412	36°50'6"N	116°26'5"W	3820ft/1164m
413	36°46'54"N	116°26'16"W	3514ft/1071m
414	36°47'23"N	116°24'18"W	3275ft/998m
415	36°48'47"N	116°27'39"W	4725ft/1440m
417	36°48'43"N	116°29'23"W	3696ft/1126m
418	36°50'48"N	116°28'54"W	4268ft/1301m
419	36°53'19"N	116°23'14"W	3775ft/1151m

¹ NAD27 (North American Datum of 1927)

Table 4.1-7. Equipment Descriptions

Parameter	Measurement Method
Wind speed	Cup anemometer with photochopper
Wind direction	Vane, with potentiometer at Sites 2 through 9 and resolver at Site 1
Temperature and Delta-temperature	Mechanically aspirated shields with thermistor (Sites 2 through 9) or platinum wires (Site 1)
Relative humidity	Capacitance sensors at Sites 2 through 9
Dew point	Chilled mirror at Site 1
Barometric pressure	Aneroid wafer
Precipitation	Tipping bucket, 0.01-inch per tip
Solar radiation	Pyranometer
Vertical wind speed	Propeller anemometer with generator or optical chopper

Table 4.1-8. Reported Data - Hourly

Parameter	Calculation Method	Units
Wind speed	scalar average	meters per second
	maximum of 1-second averages	
	maximum of 3-second averages	
Wind direction	average (unit vector)	degrees
Sigma-A	root-mean-square of 15-minute standard deviation of horizontal wind direction	degrees
Sigma-w	standard deviation of vertical wind speed	meters per second
Temperature	average	degrees Celsius
Delta-temperature	average of differences: 10m - 2m at Sites 1 through 9; and 60m - 10m at Site 1	Celsius degrees
Barometric pressure	average	millibars
Relative humidity	average: measured at Sites 2 through 9; calculated for Site 1	percent
Solar radiation	average	Watts per square meter
Precipitation	total	inches
Dew point	average: measured at Site 1; calculated for Sites 2 through 9	degrees Celsius

Table 4.1-9. Reported Data - 10-minute

Parameter	Calculation Method	Units
Wind speed	scalar average	meters per second
	maximum of 3-second running averages	
	maximum 1-minute average	
Sigma-u	standard deviation of horizontal wind speed	meters per second
Wind direction	average (unit vector)	degrees
	1-minute average direction during maximum 1-minute wind speed	
Sigma-A	standard deviation of wind direction	degrees
Vertical wind speed	average	meters per second
Sigma-w	standard deviation of vertical wind speed	meters per second
Temperature	average	degrees Celsius
Relative Humidity	average: measured at Sites 2 through 9; calculated for Site 1	percent
Dew point	average: measured at Site 1; calculated for Sites 2 through 9	degrees Celsius
Barometric Pressure	average	millibars
Delta-temperature	average of difference: 10m - 2m temperatures.	Celsius degrees
Solar radiation	average	Watts per square meter

Table 4.1-10. Reported Data - Daily

Parameter	Calculation Method	Units
Wind speed	maximum 3-second running average	meters per second
	maximum 1-minute average	
Temperature	maximum 1-minute average	degrees Celsius
	minimum 1-minute average	degrees Celsius
Precipitation	total	inches

Table 4.1-11. R/EFPD Site 1 (NTS-60) Monthly and Annual Climatological Summaries

	JAN	FEB	MAR	APR	MAY	JUN	JUL	AUG	SEP	OCT	NOV	DEC	YEAR
Temperature (C)													
Extreme Maximum (2)	20.5	26.3	26.2	31.7	36.0	39.8	40.9	40.3	37.3	34.7	26.2	20.3	40.9
Mean Maximum (2)	10.9	13.4	16.1	21.1	24.9	31.0	34.2	33.7	29.0	23.5	15.5	10.6	22.0
Mean (2)	6.3	8.7	11.3	15.9	19.5	25.3	28.6	27.9	23.5	18.0	10.4	6.0	16.8
Mean Minimum (2)	2.4	4.4	6.5	10.2	13.4	18.6	22.1	21.7	17.7	12.8	5.9	2.1	11.5
Extreme Minimum (2)	-7.0	-11.1	-3.9	0.8	0.3	4.5	10.9	13.9	6.9	-0.3	-6.1	-11.7	-11.7
Number of Days													
Precipitation													
0.01 inch or more	4.5	4.3	5.2	2.9	4.2	2.7	1.9	3.2	2.8	3.5	2.8	3.8	41.8
Temperature (2)													
32°C (90°F) and above	0	0	0	0	3	13.8	22.9	21.5	6.4	2.7	0	0	70.3
0°C (32°F) and below	7.2	6	2.6	0	0	0	0	0	0	0	3.7	10.1	29.6
Barometric Pressure (mb)													
Mean (2)	888.4	886.7	884.6	884.2	882.4	883.1	885.1	885.7	885.7	886.7	888.4	888.8	885.8
Mean Relative Humidity (%)													
Hour 0400 (PST) (2)	44.6	45.3	41.5	32.3	31.5	22.8	23.5	25.5	25.9	28.0	37.2	45.9	33.7
Hour 1000 (2)	39.8	40.0	34.7	25.4	22.7	18.3	18.0	20.0	21.2	22.4	30.3	38.7	27.6
Hour 1600 (2)	33.1	30.9	26.2	18.8	17.1	13.0	13.4	14.3	14.8	18.1	25.1	31.9	21.4
Hour 2200 (2)	41.9	40.6	35.5	25.8	23.8	16.8	17.3	19.2	20.1	24.5	33.4	42.8	28.5
Precipitation (in)													
Max 1-hour total	0.19	0.16	0.58	0.21	0.27	0.12	0.47	0.66	0.12	0.19	0.40	0.23	0.66
Max 6-hour total (3)	0.77	0.49	0.84	0.71	0.42	0.16	0.86	1.18	0.39	0.48	0.66	0.70	1.18
Max 24-hour total (3)	1.39	0.76	1.33	1.32	0.46	0.24	1.22	1.18	0.44	0.62	1.29	1.00	1.39
Total	0.92	0.61	0.90	0.25	0.39	0.09	0.25	0.53	0.09	0.25	0.24	0.45	4.97
Wind													
Mean Speed (m/s) (2)	2.8	3.2	3.7	4.0	4.0	3.9	3.7	3.5	3.3	3.0	3.2	2.8	3.4
Fastest 1-minute (1)													
Speed (m/s)	n/a												
Direction (deg)	n/a												
Peak 3-sec Gust (m/s)	n/a												

NOTE 1: Values derived from 1-second data averaged over 1 minute.

NOTE 2: Values derived from 1-second data averaged over 1 hour.

NOTE 3: Continuous running period which may encompass more than one calendar day.

T4.1-6

Yucca Mountain Site Description
B00000000-01717-5700-00019 REV 00

September 1998

Table 4.1-12. R/EFPD Site 2 (Yucca Mountain) Monthly and Annual Climatological Summaries

	JAN	FEB	MAR	APR	MAY	JUN	JUL	AUG	SEP	OCT	NOV	DEC	YEAR
Temperature (C)													
Extreme Maximum (1)	18.5	23.6	24.0	29.8	34.2	39.9	39.7	39.1	36.1	33.5	24.3	18.9	39.9
Mean Maximum (1)	8.6	11.0	14.0	19.0	22.9	29.1	32.3	31.6	27.1	21.0	13.0	8.3	19.8
Mean (2)	5.6	7.4	10.2	14.6	18.2	23.9	27.1	26.7	22.7	17.1	9.5	5.5	15.7
Mean Minimum (1)	2.9	4.3	6.9	10.5	13.7	19.1	22.4	22.4	18.6	13.6	6.5	2.9	12.0
Extreme Minimum (1)	-10.1	-12.5	-3.7	-0.6	-1.2	2.4	10.2	12.7	5.6	-1.5	-7.3	-12.3	-12.5
Number of Days													
Precipitation													
0.01 inch or more	5.4	5.7	5.4	1.4	2.3	1.0	1.1	1.1	1.0	1.4	1.7	3.7	31.4
Temperature (2)													
32°C (90°F) and above	0	0	0	0	0.2	6.7	16.2	12.4	2.6	0.1	0	0	38.2
0°C (32°F) and below	7.3	5.6	2	0.3	0.2	0.1	0	0	0	0.3	2.9	6.7	25.4
Barometric Pressure (mb)													
Mean (2)	851.5	850.8	849.7	849.1	848.3	849.8	852.1	852.6	852.6	852.1	852.6	851.5	851.1
Mean Relative Humidity (%)													
Hour 0400 (PST) (2)	45.6	42.3	40.1	28.5	27.5	16.0	18.5	22.2	23.2	27.4	35.9	41.4	30.7
Hour 1000 (2)	43.2	41.2	38.0	25.5	22.9	13.6	14.9	19.2	19.8	25.1	33.0	38.7	27.9
Hour 1600 (2)	38.8	33.5	29.5	18.2	16.5	8.6	10.6	13.2	13.8	19.9	27.1	34.3	22.0
Hour 2200 (2)	43.8	39.4	34.7	23.7	22.0	12.3	14.4	17.9	18.4	24.5	32.4	39.9	27.0
Precipitation (in)													
Max 1-hour total	0.31	0.21	0.32	0.13	0.21	0.36	0.20	0.50	0.17	0.12	0.26	0.23	0.50
Max 6-hour total (3)	0.63	0.64	0.92	0.22	0.37	0.58	0.26	0.56	0.34	0.42	0.71	1.03	1.03
Max 24-hour total (3)	1.31	1.20	1.70	0.48	0.45	0.67	0.28	0.56	0.34	0.75	1.17	1.78	1.78
Total	1.29	1.51	1.55	0.14	0.22	0.14	0.11	0.23	0.09	0.23	0.31	0.74	6.56
Wind													
Mean Speed (m/s) (2)	3.6	4.1	4.5	5.0	4.8	4.6	4.2	4.6	4.2	4.1	4.0	3.8	4.3
Fastest 1-minute (1)													
Speed (m/s)	23.2	26.3	28.7	28.9	21.6	30.0	23.0	19.7	20.9	29.4	25.0	26.1	30.0
Direction (deg)	326	312	307	237	285	324	99	268	316	325	269	319	239
Peak 3-sec Gust (m/s)	27.2	31.0	34.8	38.2	27.2	33.4	28.5	25.2	24.1	33.3	31.9	31.6	38.2

NOTE 1: Values derived from 1-second data averaged over 1 minute.

NOTE 2: Values derived from 1-second data averaged over 1 hour.

NOTE 3: Continuous running period which may encompass more than one calendar day.

T4.1-7

Table 4.1-13. R/EFPD Site 3 (Coyote Wash) Monthly and Annual Climatological Summaries

	JAN	FEB	MAR	APR	MAY	JUN	JUL	AUG	SEP	OCT	NOV	DEC	YEAR
Temperature (C)													
Extreme Maximum (1)	19.5	24.9	25.0	30.9	34.6	40.4	39.9	39.6	36.6	33.6	25.2	19.7	40.4
Mean Maximum (1)	9.9	12.5	15.1	20.3	23.8	30.0	33.0	32.5	28.2	22.1	14.4	9.5	20.9
Mean (2)	6.3	8.6	10.8	15.6	19.0	24.8	28.0	27.5	23.4	17.8	10.3	5.9	16.5
Mean Minimum (1)	3.0	4.9	6.4	10.5	13.6	18.8	22.2	22.1	18.4	13.4	6.4	2.5	11.8
Extreme Minimum (1)	-7.9	-10.7	-4.3	-0.3	0.1	4.2	10.5	14.3	7.2	0.3	-5.9	-12.2	-12.2
Number of Days													
Precipitation													
0.01 inch or more	5.1	4.6	5.3	1.4	3.3	1.1	1.3	1.3	1.6	1.4	2.3	4.6	33.3
Temperature (2)													
32°C (90°F) and above	0	0	0	0	0.5	9.6	17.5	16.6	4.5	0.3	0	0	49.0
0°C (32°F) and below	6.8	4.1	1.9	0.1	0	0	0	0	0	0	1.9	8.2	23.0
Barometric Pressure (mb)													
Mean (2)	872.9	871.8	870.1	869.6	867.9	868.7	870.8	871.3	871.6	872.0	873.2	872.7	871.0
Mean Relative Humidity (%)													
Hour 0400 (PST) (2)	45.1	44.5	43.4	33.9	33.1	21.9	22.9	26.2	28.9	31.4	37.6	45.4	34.5
Hour 1000 (2)	39.4	39.6	37.3	27.2	24.7	16.8	16.8	20.8	22.3	25.1	30.8	38.3	28.3
Hour 1600 (2)	35.4	31.8	29.6	19.9	18.4	12.4	13.0	15.1	16.4	21.4	26.5	34.7	22.9
Hour 2200 (2)	42.9	40.8	38.0	26.9	25.2	16.6	17.1	20.3	22.5	27.9	33.8	42.9	29.6
Precipitation (in)													
Max 1-hour total	0.32	0.20	0.43	0.14	0.23	0.29	0.18	0.31	0.27	0.17	0.57	0.26	0.57
Max 6-hour total (3)	0.74	0.61	1.13	0.21	0.36	0.60	0.18	0.62	0.27	0.53	0.77	0.77	1.13
Max 24-hour total (3)	1.53	1.22	1.89	0.31	0.41	0.67	0.18	0.67	0.27	0.79	1.60	1.12	1.89
Total	1.33	1.29	1.57	0.14	0.33	0.14	0.09	0.20	0.15	0.31	0.39	0.75	6.70
Wind													
Mean Speed (m/s) (2)	2.2	2.4	2.7	2.8	2.8	2.8	2.6	2.4	2.4	2.4	2.6	2.3	2.5
Fastest 1-minute (1)													
Speed (m/s)	16.3	15.9	16.0	17.0	13.7	17.3	18.6	11.7	13.9	18.0	15.2	14.6	18.6
Direction (deg)	300	306	309	302	290	299	107	294	89	307	310	302	107
Peak 3-sec Gust (m/s)	23.3	21.8	25.2	24.5	19.2	24.3	21.0	17.3	19.5	26.2	21.5	22.0	26.2

NOTE 1: Values derived from 1-second data averaged over 1 minute.

NOTE 2: Values derived from 1-second data averaged over 1 hour.

NOTE 3: Continuous running period which may encompass more than one calendar day.

T4.1-8

Table 4.1-14. R/EFPD Site 4 (Alice Hill) Monthly and Annual Climatological Summaries

	JAN	FEB	MAR	APR	MAY	JUN	JUL	AUG	SEP	OCT	NOV	DEC	YEAR
Temperature (C)													
Extreme Maximum (1)	20.7	25.3	26.5	32.3	36.8	42.3	41.6	41.0	38.0	34.8	26.5	20.4	42.3
Mean Maximum (1)	10.4	12.8	15.8	20.6	24.4	30.5	33.7	33.5	28.9	22.6	14.7	10.0	21.5
Mean (2)	6.5	8.6	11.2	15.6	19.2	25.2	28.4	28.1	23.6	17.6	10.3	6.2	16.7
Mean Minimum (1)	2.9	4.5	6.8	10.3	13.8	19.2	22.7	22.5	18.1	12.5	6.2	2.6	11.8
Extreme Minimum (1)	-7.3	-11.0	-4.1	-0.0	-0.3	4.0	11.2	14.1	7.4	0.0	-6.0	-12.6	-12.6
Number of Days													
Precipitation													
0.01 inch or more	5.8	4.6	5.4	1.6	2.4	1.4	0.9	1.3	0.9	1.6	2.2	4.0	32.0
Temperature (2)													
32°C (90°F) and above	0	0	0	0	1	11.2	20.3	18.5	6	0.4	0	0	57.4
0°C (32°F) and below	5.3	4.3	1.4	0.1	0.1	0	0	0	0	0	1.4	6.3	18.9
Barometric Pressure (mb)													
Mean (2)	877.7	876.5	874.5	873.9	872.2	873.2	875.3	876.0	876.4	876.5	878.3	878.1	875.7
Mean Relative Humidity (%)													
Hour 0400 (PST) (2)	46.5	46.0	43.0	30.4	30.2	18.9	20.4	22.7	25.1	30.9	37.8	45.1	33.1
Hour 1000 (2)	43.7	42.7	37.7	24.4	22.3	14.7	15.5	18.0	20.3	24.9	32.9	40.0	28.1
Hour 1600 (2)	36.2	33.2	28.3	17.3	15.7	9.9	12.6	12.7	14.1	19.4	26.1	33.1	21.6
Hour 2200 (2)	44.0	42.1	37.3	24.2	22.3	13.9	15.3	17.6	19.9	26.8	33.3	42.4	28.3
Precipitation (in)													
Max 1-hour total	0.29	0.22	0.33	0.17	0.14	0.12	0.33	0.38	0.24	0.19	0.42	0.23	0.42
Max 6-hour total (3)	0.69	0.61	0.95	0.35	0.31	0.43	0.36	0.53	0.49	0.43	0.81	0.81	0.95
Max 24-hour total (3)	1.19	1.13	1.76	0.53	0.50	0.49	0.37	0.56	0.58	0.74	1.51	1.86	1.86
Total	1.49	1.16	1.43	0.21	0.22	0.12	0.16	0.17	0.11	0.32	0.37	0.84	6.57
Wind													
Mean Speed (m/s) (2)	3.7	4.2	4.6	5.2	5.1	4.8	4.3	4.1	4.1	4.1	4.5	3.7	4.4
Fastest 1-minute (1)													
Speed (m/s)	24.4	25.3	27.8	29.3	24.6	26.8	25.1	19.9	22.9	33.2	25.6	23.7	33.2
Direction (deg)	340	339	2	351	10	338	37	33	329	345	342	344	345
Peak 3-sec Gust (m/s)	28.0	29.2	31.4	32.2	29.3	30.0	28.3	28.5	24.9	37.2	29.8	27.9	37.2

NOTE 1: Values derived from 1-second data averaged over 1 minute.

NOTE 2: Values derived from 1-second data averaged over 1 hour.

NOTE 3: Continuous running period which may encompass more than one calendar day.

Table 4.1-15. R/EFPD Site 5 (Fortymile Wash) Monthly and Annual Climatological Summaries

	JAN	FEB	MAR	APR	MAY	JUN	JUL	AUG	SEP	OCT	NOV	DEC	YEAR
Temperature (C)													
Extreme Maximum (1)	22.9	27.9	28.6	34.6	38.8	43.6	43.5	42.8	39.9	36.9	28.3	22.2	43.6
Mean Maximum (1)	12.6	15.3	18.4	23.4	27.2	33.1	36.3	35.7	31.3	25.6	17.5	12.3	24.1
Mean (2)	6.8	9.5	12.5	17.0	20.9	26.4	29.6	28.9	24.5	18.8	11.2	6.4	17.7
Mean Minimum (1)	1.8	4.3	6.5	10.2	13.6	18.3	21.8	21.4	17.4	12.6	5.7	1.4	11.2
Extreme Minimum (1)	-7.1	-11.8	-4.7	0.5	1.4	2.6	11.1	13.0	5.5	-0.7	-6.6	-13.1	-13.1
Number of Days													
Precipitation													
0.01 inch or more	4.7	4.6	4.9	1.6	2.7	0.9	1.0	1.3	0.7	1.1	1.4	3.3	28.1
Temperature (2)													
32°C (90°F) and above	0.0	0.0	0.0	0.6	3.1	18.8	27.4	25.0	13.3	2.8	0.0	0.0	91.0
0°C (32°F) and below	7.5	3.7	0.7	0.0	0.0	0.0	0.0	0.0	0.0	0.1	2.0	8.5	22.6
Barometric Pressure (mb)													
Mean (2)	908.1	906.7	904.5	903.5	901.5	901.9	903.6	904.5	904.8	905.9	908.2	908.2	905.1
Mean Relative Humidity (%)													
Hour 0400 (PST) (2)	49.1	47.3	46.1	33.2	34.0	21.4	22.5	25.4	25.8	29.2	36.8	44.4	34.6
Hour 1000 (2)	40.7	38.0	34.5	23.2	21.9	14.4	15.1	18.4	18.7	21.1	27.5	34.6	25.7
Hour 1600 (2)	32.2	28.8	26.3	16.6	15.8	9.4	10.5	12.4	12.5	15.9	20.7	26.6	19.0
Hour 2200 (2)	47.1	43.9	40.1	27.2	25.0	15.2	16.4	19.0	20.4	25.6	32.6	41.9	29.5
Precipitation (In)													
Max 1-hour total	0.23	0.26	0.16	0.22	0.10	0.19	0.50	0.38	0.33	0.25	0.16	0.23	0.50
Max 6-hour total (3)	0.50	0.59	0.53	0.26	0.25	0.50	0.72	0.53	0.74	0.49	0.70	0.78	0.78
Max 24-hour total (3)	1.02	0.89	0.94	0.26	0.49	0.53	0.72	0.53	0.84	0.97	1.05	1.63	1.63
Total	1.14	0.94	0.89	0.12	0.20	0.10	0.15	0.12	0.14	0.26	0.23	0.79	5.10
Wind													
Mean Speed (m/s) (2)	3.7	4.1	4.3	4.6	4.6	4.5	4.3	4.3	4.3	4.1	4.2	3.9	4.2
Fastest 1-minute (1)													
Speed (m/s)	17.2	19.7	19.7	21.6	20.3	20.9	18.4	16.7	16.7	25.3	18.2	18.4	25.3
Direction (deg)	350	185	349	346	317	344	82	227	178	337	336	178	337
Peak 3-sec Gust (m/s)	20.7	23.1	24.9	26.4	24.8	25.1	26.5	20.0	20.7	30.4	21.7	22.1	30.4

NOTE 1: Values derived from 1-second data averaged over 1 minute.

NOTE 2: Values derived from 1-second data averaged over 1 hour.

NOTE 3: Continuous running period which may encompass more than one calendar day.

T4.1-10

Table 4.1-16. R/EFPD Site 6 (WT-6) Monthly and Annual Climatological Summaries

	JAN	FEB	MAR	APR	MAY	JUN	JUL	AUG	SEP	OCT	NOV	DEC	YEAR
Temperature (C)													
Extreme Maximum (1)	19.8	23.1	24.5	30.4	34.7	39.6	39.6	41.9	36.3	33.7	25.5	18.5	41.9
Mean Maximum (1)	9.8	12.3	16.2	19.8	24.2	30.5	33.9	33.9	29.1	22.1	14.2	10.0	21.3
Mean (2)	4.7	6.8	10.1	13.4	17.5	23.3	27.4	26.6	22.0	15.5	8.3	5.1	15.1
Mean Minimum (1)	0.2	1.5	4.1	6.4	9.9	14.6	18.4	18.3	14.5	9.4	2.7	-0.1	8.3
Extreme Minimum (1)	-9.9	-9.9	-6.9	-1.4	-0.3	2.3	11.0	12.0	6.2	-1.0	-7.8	-7.2	-9.9
Number of Days													
Precipitation													
0.01 inch or more	7.5	5.8	4.3	1.5	4.0	1.5	1.0	1.0	1.3	1.0	2.3	3.5	34.5
Temperature (2)													
32°C (90°F) and above	0.0	0.0	0.0	0.0	0.8	12.3	23.0	22.0	5.8	0.5	0.0	0.0	64.3
0°C (32°F) and below	12.3	10.8	3.0	0.0	0.0	0.0	0.0	0.0	0.0	0.0	6.0	13.3	45.3
Barometric Pressure (mb)													
Mean (2)	867.4	866.5	866.5	865.2	864.4	866.3	868.3	868.2	867.9	867.4	868.9	868.9	867.1
Mean Relative Humidity (%)													
Hour 0400 (PST) (2)	61.7	61.2	55.2	41.7	45.8	30.4	29.8	30.4	31.6	36.0	45.8	56.2	43.8
Hour 1000 (2)	49.2	45.3	38.7	26.3	26.2	18.3	16.5	17.3	18.7	23.8	31.4	39.6	29.3
Hour 1600 (2)	46.4	37.7	29.5	18.5	19.3	11.6	11.4	11.4	12.8	18.8	27.7	36.2	23.4
Hour 2200 (2)	59.3	57.9	47.1	33.4	34.9	22.0	20.3	21.5	23.2	31.0	41.9	53.0	37.1
Precipitation (in)													
Max 1-hour total	0.44	0.27	0.25	0.19	0.34	0.27	0.31	0.28	0.28	0.17	0.25	0.24	0.44
Max 6-hour total (3)	1.24	0.56	1.16	0.40	0.39	0.58	0.40	0.61	0.36	0.39	0.87	1.10	1.24
Max 24-hour total (3)	1.54	1.27	2.14	0.51	0.41	0.69	0.40	0.64	0.38	0.76	1.45	1.78	2.14
Total	2.35	1.50	1.52	0.34	0.38	0.25	0.21	0.26	0.17	0.36	0.68	0.68	8.69
Wind													
Mean Speed (m/s) (2)	3.4	3.6	4.1	4.6	4.2	4.2	4.1	4.0	4.0	3.8	3.8	3.6	4.0
Fastest 1-minute (1)													
Speed (m/s)	17.6	18.4	20.2	21.4	19.7	22.7	17.5	16.0	19.1	19.8	19.9	20.8	22.7
Direction (deg)	336	335	346	147	145	341	114	142	135	345	337	337	149
Peak 3-sec Gust (m/s)	21.5	25.7	26.1	28.7	26.5	28.8	23.6	21.1	24.0	27.0	26.7	23.6	28.8

NOTE 1: Values derived from 1-second data averaged over 1 minute.

NOTE 2: Values derived from 1-second data averaged over 1 hour.

NOTE 3: Continuous running period which may encompass more than one calendar day.

T4.1-11

Yucca Mountain Site Description
B0000000-01717-5700-00019 REV 00

September 1998

Table 4.1-17. R/EFPD Site 7 (Sever Wash) Monthly and Annual Climatological Summaries

	JAN	FEB	MAR	APR	MAY	JUN	JUL	AUG	SEP	OCT	NOV	DEC	YEAR
Temperature (C)													
Extreme Maximum (1)	22.2	25.3	27.1	33.3	37.8	42.3	42.8	42.3	39.3	36.1	27.8	20.5	42.8
Mean Maximum (1)	11.9	14.7	18.9	22.6	27.3	33.5	36.9	36.8	32.0	24.5	16.3	11.9	24.0
Mean (2)	5.0	7.4	11.1	14.7	18.9	24.5	28.4	27.6	22.6	15.6	8.5	5.1	15.8
Mean Minimum (1)	-1.6	-0.0	2.8	5.3	8.9	13.0	16.9	16.8	12.4	6.7	0.2	-2.4	6.6
Extreme Minimum (1)	-11.3	-10.8	-6.6	-1.7	-0.8	0.2	10.6	9.2	3.8	-5.0	-9.7	-12.8	-12.8
Number of Days													
Precipitation													
0.01 inch or more	5.8	5.3	4.8	1.5	3.5	1.3	1.0	1.0	1.0	1.8	3.3	2.8	32.8
Temperature (2)													
32°C (90°F) and above	0.0	0.0	0.0	0.3	2.0	19.3	30.3	28.5	14.0	2.3	0.0	0.0	96.5
0°C (32°F) and below	17.3	11.5	3.5	0.8	0.3	0.0	0.0	0.0	0.0	0.3	10.8	18.8	63.0
Barometric Pressure (mb)													
Mean (2)	893.1	891.9	891.6	890.2	888.8	890.0	891.7	891.7	891.9	892.2	893.8	894.0	891.7
Mean Relative Humidity (%)													
Hour 0400 (PST) (2)	66.9	67.5	59.9	44.9	48.8	32.9	31.8	31.4	33.5	39.5	50.4	62.5	47.5
Hour 1000 (2)	48.7	44.6	35.6	23.2	23.3	15.8	14.2	15.1	16.3	21.0	29.3	39.1	27.2
Hour 1600 (2)	41.9	34.3	25.9	16.4	16.5	9.4	9.1	9.4	10.5	16.2	23.8	31.5	20.4
Hour 2200 (2)	62.5	62.2	49.9	34.5	34.2	21.5	20.2	21.4	23.5	31.4	44.2	56.2	38.5
Precipitation (in)													
Max 1-hour total	0.41	0.23	0.24	0.15	0.18	0.12	0.59	0.33	0.05	0.20	0.40	0.28	0.59
Max 6-hour total (3)	0.97	0.52	0.94	0.26	0.24	0.46	0.60	0.50	0.07	0.48	0.81	0.93	0.97
Max 24-hour total (3)	1.18	1.25	1.69	0.37	0.35	0.49	0.60	0.55	0.08	0.73	1.49	2.15	2.15
Total	1.90	1.32	1.11	0.30	0.28	0.16	0.22	0.19	0.03	0.36	0.57	0.74	7.17
Wind													
Mean Speed (m/s) (2)	2.5	2.8	3.3	3.9	3.6	3.6	3.4	3.3	3.1	2.9	2.9	2.5	3.2
Fastest 1-minute (1)													
Speed (m/s)	15.8	16.7	18.1	21.3	18.9	18.5	15.6	15.2	16.9	23.2	18.0	17.1	23.2
Direction (deg)	320	328	329	331	163	162	165	152	218	331	333	162	333
Peak 3-sec Gust (m/s)	20.5	20.7	22.3	25.5	23.0	24.8	23.5	21.5	26.9	27.7	21.9	20.6	27.7

NOTE 1: Values derived from 1-second data averaged over 1 minute.

NOTE 2: Values derived from 1-second data averaged over 1 hour.

NOTE 3: Continuous running period which may encompass more than one calendar day.

Table 4.1-18. R/EFPD Site 8 (Knothead Gap) Monthly and Annual Climatological Summaries

	JAN	FEB	MAR	APR	MAY	JUN	JUL	AUG	SEP	OCT	NOV	DEC	YEAR
Temperature (C)													
Extreme Maximum (1)	21.2	24.7	26.2	32.8	37.1	41.9	42.0	41.3	38.2	35.6	27.2	19.7	42.0
Mean Maximum (1)	11.4	14.1	18.3	21.9	26.6	32.8	36.2	36.2	31.3	24.0	15.8	11.5	23.4
Mean (2)	5.2	7.5	11.1	14.6	19.0	24.7	28.7	27.9	23.0	15.8	8.8	5.5	16.0
Mean Minimum (1)	-0.5	1.0	3.8	6.3	10.1	14.4	18.5	18.4	14.0	8.3	1.7	-0.7	7.9
Extreme Minimum (1)	-9.9	-9.5	-6.6	-1.0	0.0	2.5	12.0	11.1	5.9	-3.1	-8.0	-9.6	-9.9
Number of Days													
Precipitation													
0.01 inch or more	6.0	5.0	4.8	1.5	3.3	1.3	1.3	1.5	1.3	1.0	2.5	2.8	32.0
Temperature (2)													
32°C (90°F) and above	0.0	0.0	0.0	0.0	1.5	17.5	29.8	27.8	11.8	1.8	0.0	0.0	90.0
0°C (32°F) and below	11.8	10.5	2.0	0.0	0.0	0.0	0.0	0.0	0.0	0.3	7.5	14.3	46.3
Barometric Pressure (mb)													
Mean (2)	888.8	887.7	887.1	885.6	883.9	884.8	886.3	886.4	886.8	887.5	889.1	889.4	887.0
Mean Relative Humidity (%)													
Hour 0400 (PST) (2)	62.7	64.0	57.0	41.6	45.1	30.1	28.9	29.3	31.1	36.8	46.8	58.2	44.3
Hour 1000 (2)	47.6	44.4	35.4	22.9	23.2	15.4	13.9	15.2	16.0	20.5	29.0	38.3	26.8
Hour 1600 (2)	41.4	34.1	26.2	15.7	16.5	9.1	9.0	9.2	10.2	16.1	23.9	32.0	20.3
Hour 2200 (2)	59.2	57.5	47.0	32.2	32.8	20.0	18.8	19.9	21.9	30.1	41.3	52.9	36.1
Precipitation (in)													
Max 1-hour total	0.43	0.21	0.22	0.23	0.26	0.14	0.29	0.39	0.04	0.13	0.40	0.23	0.43
Max 6-hour total (3)	1.06	0.47	0.84	0.23	0.31	0.58	0.31	0.69	0.08	0.53	0.76	1.02	1.06
Max 24-hour total (3)	1.18	1.25	1.43	0.29	0.38	0.62	0.31	0.73	0.11	0.84	1.42	2.43	2.43
Total	1.94	1.36	1.14	0.25	0.32	0.19	0.20	0.27	0.04	0.22	0.52	0.56	6.99
Wind													
Mean Speed (m/s) (2)	2.4	2.7	3.2	3.8	3.6	3.5	3.3	3.2	2.9	2.7	2.7	2.4	3.0
Fastest 1-minute (1)													
Speed (m/s)	16.6	18.9	17.7	19.9	17.3	19.7	15.5	15.0	16.7	21.3	16.4	17.1	21.3
Direction (deg)	327.9	331.1	189.9	204.1	171.1	337.2	322.5	168.2	167.4	332.3	4.1	200.7	220
Peak 3-sec Gust (m/s)	20.5	22.6	25.0	27.6	20.7	23.9	20.5	18.9	21.4	27.3	21.9	20.8	27.6

NOTE 1: Values derived from 1-second data averaged over 1 minute.

NOTE 2: Values derived from 1-second data averaged over 1 hour.

NOTE 3: Continuous running period which may encompass more than one calendar day.

Table 4.1-19. R/EFPD Site 9 (Gate 510) Monthly and Annual Climatological Summaries

	JAN	FEB	MAR	APR	MAY	JUN	JUL	AUG	SEP	OCT	NOV	DEC	YEAR
Temperature (C)													
Extreme Maximum (1)	22.9	26.6	29.2	35.4	39.5	45.1	44.7	43.8	40.5	37.8	28.5	22.5	45.1
Mean Maximum (1)	13.4	16.5	20.8	24.6	29.2	35.6	39.5	38.9	33.9	26.0	18.2	14.2	25.9
Mean (2)	7.0	9.7	13.3	16.8	21.3	27.6	31.4	30.5	25.4	17.8	10.5	7.1	18.2
Mean Minimum (1)	1.0	3.3	5.9	8.2	12.3	16.4	21.2	21.0	16.4	9.8	3.4	1.2	10.0
Extreme Minimum (1)	-7.6	-5.3	-3.8	0.0	1.2	2.5	12.2	13.8	7.5	0.6	-6.8	-7.7	-7.7
Number of Days													
Precipitation													
0.01 inch or more	6.5	5.0	4.5	2.0	3.5	0.8	1.0	0.5	0.3	1.0	1.8	2.5	29.3
Temperature (2)													
32°C (90°F) and above	1.5	1.0	1.3	3.0	8.5	24.5	31.0	30.8	21.0	3.3	1.8	1.3	128.8
0°C (32°F) and below	7.8	5.8	1.0	0.0	0.0	0.0	0.0	0.0	0.0	0.0	6.0	10.8	31.3
Barometric Pressure (mb)													
Mean (2)	919.7	918.4	918.2	916.6	914.4	915.0	916.3	916.3	916.5	917.7	919.5	920.5	917.4
Mean Relative Humidity (%)													
Hour 0400 (PST) (2)	61.0	59.3	53.9	39.1	42.5	26.4	23.7	24.2	26.6	32.6	44.6	55.1	40.7
Hour 1000 (2)	46.9	42.7	34.3	21.1	23.5	14.1	12.6	14.0	15.6	19.2	28.4	37.6	25.8
Hour 1600 (2)	39.0	30.9	23.3	14.2	16.0	7.8	7.2	8.2	9.1	14.0	21.2	28.5	18.3
Hour 2200 (2)	57.1	53.0	43.6	30.6	30.1	17.0	15.4	16.6	19.0	25.8	37.6	49.5	33.0
Precipitation (in)													
Max 1-hour total	0.13	0.29	0.12	0.16	0.18	0.32	0.02	0.04	0.01	0.19	0.16	0.20	0.32
Max 6-hour total (3)	0.39	0.57	0.40	0.16	0.43	0.68	0.03	0.05	0.02	0.44	0.50	0.42	0.68
Max 24-hour total (3)	0.65	0.94	0.61	0.18	0.57	0.68	0.04	0.05	0.02	0.63	0.63	0.97	0.97
Total	1.11	0.84	0.58	0.15	0.28	0.21	0.02	0.02	0.01	0.27	0.26	0.49	4.20
Wind													
Mean Speed (m/s) (2)	3.8	4.2	4.4	4.8	4.7	4.7	4.6	4.7	4.4	4.1	4.1	4.0	4.4
Fastest 1-minute (1)													
Speed (m/s)	16.5	19.3	19.1	19.9	18.5	17.8	19.2	20.5	16.8	19.1	16.7	19.8	20.5
Direction (deg)	320	182	171	195	163	356	85	137	164	335	335	167	354
Peak 3-sec Gust (m/s)	20.2	24.7	22.7	25.4	23.6	26.7	23.2	25.1	20.1	23.0	19.2	23.2	26.7

NOTE 1: Values derived from 1-second data averaged over 1 minute.

NOTE 2: Values derived from 1-second data averaged over 1 hour.

NOTE 3: Continuous running period which may encompass more than one calendar day.

T4.1-14

Table 4.1-20. Yearly Climatological Data Summary

	Site 1	Site 2	Site 3	Site 4	Site 5	Site 6	Site 7	Site 8	Site 9
Temperature (C)									
Extreme Maximum (1)	40.9	39.9	40.4	42.3	43.6	41.9	42.8	42.0	45.1
Mean Maximum (1)	22.0	19.8	20.9	21.5	24.1	21.3	24.0	23.4	25.9
Mean (2)	16.8	15.7	16.5	16.7	17.7	15.1	15.8	16.0	18.2
Mean Minimum (1)	11.5	12.0	11.8	11.8	11.2	8.3	6.6	7.9	10.0
Extreme Minimum (1)	-11.7	-12.5	-12.2	-12.6	-13.1	-9.9	-12.8	-9.9	-7.7
Number of Day									
Precipitation									
0.01 inch or more	41.8	31.4	33.3	32.0	28.1	34.5	32.8	32.0	29.3
Temperature (Hourly Averaged)									
32°C (90°F) and above	70.3	38.2	49.0	57.4	91.0	64.3	96.5	90.0	128.8
0°C (32°F) and below	29.6	25.4	23.0	18.9	22.6	45.3	63.0	46.3	31.3
Mean Relative Humidity (%)									
Hour 0400 (PST) (2)	33.7	30.7	34.5	33.1	34.6	43.8	47.5	44.3	40.7
Hour 1000 (2)	27.6	27.9	28.3	28.1	25.7	29.3	27.2	26.8	25.8
Hour 1600 (2)	21.4	22.0	22.9	21.6	19.0	23.4	20.4	20.3	18.3
Hour 2200 (2)	28.5	27.0	29.6	28.3	29.5	37.1	38.5	36.1	33.0
Precipitation (in)									
Max 1-hour total	0.66	0.50	0.57	0.42	0.50	0.44	0.59	0.43	0.32
Max 6-hour total	1.18	1.03	1.13	0.95	0.78	1.24	0.97	1.06	0.68
Max 24-hour total	1.39	1.78	1.89	1.86	1.63	2.14	2.15	2.43	0.97
Total	4.97	6.56	6.70	6.57	5.10	8.69	7.17	6.99	4.20
Wind									
Mean Speed (m/s) (2)	3.4	4.3	2.5	4.4	4.2	4.0	3.2	3.0	4.4
Fastest 1-minute (2)									
Speed (m/s)	n/a	30.0	18.6	33.2	25.3	22.7	23.2	21.3	20.5
Direction (deg)	n/a	239	307	345	337	149	333	220	354
Peak 3-sec Gust (m/s)	n/a	38.2	26.2	37.2	30.4	28.8	27.7	27.6	26.7

NOTE 1: Values derived from 1-second data averaged over 1 minute.

NOTE 2: Values derived from 1-second data averaged over 1 hour.

Table 4.1-21. Climatological Summary for Austin and Battle Mountain

	JAN	FEB	MAR	APR	MAY	JUN	JUL	AUG	SEP	OCT	NOV	DEC	YEAR
Austin													
Temperature (C)													
Extreme Maximum	18.3	21.1	23.3	28.3	32.8	36.1	40.6	37.8	36.1	30.0	23.9	21.1	40.6
Mean Maximum	4.9	6.7	9.1	13.6	18.7	24.7	30.6	29.5	24.5	17.8	9.9	5.9	16.4
Mean Minimum	-7.4	-5.9	-4.1	-0.8	3.2	7.4	12.1	11.3	7.1	2.1	-3.3	-6.4	1.3
Extreme Minimum	-31.7	-27.8	-21.1	-16.1	-11.1	-5.0	2.2	-1.1	-7.8	-16.7	-21.7	-28.9	-31.7
Precipitation (Inches)													
Mean Monthly	1.18	1.15	1.61	1.62	1.53	0.97	0.56	0.61	0.60	0.96	1.03	1.20	13.51
Monthly Maximum	4.00	2.95	5.36	5.96	5.85	3.55	2.53	2.45	3.45	3.72	3.73	4.19	22.37
Maximum Daily	1.64	1.60	1.76	2.01	1.57	1.57	1.99	1.25	1.65	2.04	1.18	1.19	2.04
Snowfall (Inches)													
Mean Monthly	0.92	0.06	0.00	0.00	0.00	0.00	0.00	0.00	0.00	0.00	0.11	0.05	1.13
Monthly Maximum	16.70	1.40	0.10	0.00	0.00	0.00	0.00	0.00	0.00	0.00	4.00	2.00	16.70
Daily Maximum	24.0	16.8	19.0	22.0	12.0	8.0	0.0	0.0T	9.0	20.0	13.0	10.4	24.0
Battle Mountain													
Temperature (C)													
Extreme Maximum	19.4	22.2	26.7	32.2	36.1	40.0	42.8	41.1	38.9	33.9	26.7	19.4	42.8
Mean Maximum	4.8	8.8	12.2	17.3	22.7	28.1	33.9	32.8	27.5	20.2	10.9	5.4	18.9
Mean Minimum	-9.6	-6.1	-4.0	-1.2	3.3	7.1	10.4	8.7	3.8	-1.3	-5.6	-9.0	-0.2
Extreme Minimum	-37.2	-31.7	-19.4	-13.3	-10.0	-4.4	-0.6	-2.2	-11.7	-14.4	-22.8	-39.4	-39.4
Precipitation (Inches)													
Mean Monthly	0.65	0.58	0.69	0.78	1.01	0.88	0.28	0.32	0.51	0.64	0.68	0.75	7.60
Monthly Maximum	2.22	2.20	2.42	3.02	4.91	3.39	1.62	1.65	2.92	2.83	2.08	2.58	12.50
Maximum Daily	0.75	0.90	0.73	1.00	1.10	1.10	0.70	0.50	0.97	1.10	0.84	1.00	1.10
Snowfall (Inches)													
Mean Monthly	7.72	3.09	1.16	0.91	0.12	0.00	0.00	0.00	0.00	0.12	2.35	3.35	18.82
Monthly Maximum	33.00	13.00	5.00	5.00	2.00	0.00	0.00	0.00	0.00	2.00	18.00	10.00	54.00
Daily Maximum	7.8	10.0	7.0	12.0	3.9	0.0T	0.0	0.0	0.0T	3.0	6.0	12.4	12.4

Table 4.1-22. Climatological Summary for Caliente and Desert Rock

	JAN	FEB	MAR	APR	MAY	JUN	JUL	AUG	SEP	OCT	NOV	DEC	YEAR
Caliente													
Temperature (C)													
Extreme Maximum	21.7	27.2	32.2	33.3	36.7	42.8	42.8	42.2	41.1	34.4	26.7	21.7	42.8
Mean Maximum	7.8	11.3	15.6	20.7	25.8	31.5	35.3	33.9	29.8	23.1	14.8	9.0	21.6
Mean Minimum	-8.2	-5.3	-2.3	1.2	5.5	9.6	13.6	12.9	7.7	1.8	-4.0	-7.3	2.2
Extreme Minimum	-35.0	-28.3	-16.7	-9.4	-4.4	0.6	4.4	1.7	-3.9	-12.2	-17.8	-27.8	-35.0
Precipitation (inches)													
Mean Monthly	0.86	0.84	1.08	0.71	0.61	0.34	0.80	0.96	0.63	0.76	0.76	0.70	8.82
Monthly Maximum	3.47	3.15	4.59	3.71	2.27	1.95	5.36	4.18	3.14	4.29	3.38	3.76	18.73
Maximum Daily	1.41	1.90	1.35	1.15	1.48	0.99	1.51	1.70	1.56	2.13	1.80	2.11	2.13
Snowfall (inches)													
Mean Monthly	3.96	2.42	1.14	0.11	0.01	0.00	0.00	0.00	0.03	0.07	0.83	2.85	13.80
Monthly Maximum	31.00	27.60	9.50	3.70	0.50	0.00	0.00	0.00	2.00	4.00	12.00	20.00	46.60
Daily Maximum	12.0	14.0	8.0	2.5	0.5	0.0	0.0	0.0	2.0	4.0	5.0	11.0	14.0
Desert Rock													
Temperature (C)													
Extreme Maximum	22.8	28.3	28.9	33.9	38.9	43.9	44.4	42.8	39.4	35.6	29.4	22.2	44.4
Mean Maximum	12.4	15.5	18.8	23.9	28.2	33.9	36.9	36.1	31.8	25.6	16.8	12.3	24.6
Mean Minimum	0.4	2.6	5.2	8.8	13.0	17.9	21.3	20.7	16.1	10.3	3.4	-0.2	10.2
Extreme Minimum	-8.9	-11.7	-5.0	-1.1	0.6	4.4	11.7	12.8	4.4	0.0	-7.2	-14.4	-14.4
Precipitation (Inches)													
Mean Monthly	1.02	0.74	0.67	0.28	0.34	0.08	0.76	0.71	0.25	0.40	0.52	0.65	5.50
Monthly Maximum	3.37	3.29	2.39	1.50	1.94	0.41	3.64	3.14	1.43	1.65	1.76	1.91	8.56
Maximum Daily	0.87	1.15	0.65	0.72	0.92	0.39	2.03	1.10	1.25	0.67	1.48	0.91	2.03
Snowfall (inches)													
Mean Monthly	1.33	0.77	0.15	0.00	0.00	0.00	0.00	0.00	0.00	0.00	0.23	0.83	2.86
Monthly Maximum	5.10	6.00	0.50	0.00	0.00	0.00	0.00	0.00	0.00	0.00	1.50	6.60	8.80
Daily Maximum	4.3	6.0	0.5	0.0	0.0T	0.0	0.0	0.0	0.0	0.0	1.5	4.0	6.0

T4.1-17

Table 4.1-23. Climatological Summary for Elko and Ely

	JAN	FEB	MAR	APR	MAY	JUN	JUL	AUG	SEP	OCT	NOV	DEC	YEAR
Elko													
Temperature (C)													
Extreme Maximum	17.8	21.1	25.0	30.0	33.3	40.0	41.7	41.7	37.2	31.1	25.6	18.3	41.7
Mean Maximum	2.2	5.5	9.9	15.3	20.6	26.3	32.5	31.4	26.1	18.8	9.4	3.5	16.8
Mean Minimum	-11.4	-7.9	-4.6	-1.7	2.2	5.8	9.4	8.1	2.9	-2.0	-6.6	-10.2	-1.3
Extreme Minimum	-41.7	-38.3	-22.8	-18.9	-12.2	-5.0	-1.1	-6.7	-12.8	-16.1	-24.4	-38.9	-41.7
Precipitation (inches)													
Mean Monthly	1.09	0.81	0.90	0.81	1.00	0.80	0.35	0.44	0.48	0.69	0.99	1.02	9.38
MonthlyMaximum	3.35	2.49	2.39	2.17	4.09	2.61	2.35	4.61	3.22	2.76	2.80	4.21	18.34
Maximum Daily	1.25	0.89	0.79	1.07	1.73	1.05	1.04	4.13	2.25	1.31	1.33	1.60	4.13
Snowfall (inches)													
Mean Monthly	10.05	6.09	5.07	2.29	0.78	0.00	0.00	0.00	0.06	0.70	4.74	7.85	37.75
Monthly Maximum	29.20	26.10	23.20	15.60	11.30	0.00	0.00	0.00	2.00	5.60	20.00	33.20	85.40
Daily Maximum	16.3	9.0	8.2	9.3	7.8	0.0T	0.0T	0.0T	2.0	5.2	10.6	9.3	16.3
Ely													
Temperature (C)													
Extreme Maximum	20.0	19.4	22.8	27.8	31.7	37.2	37.8	36.1	33.9	28.9	23.9	19.4	37.8
Mean Maximum	3.8	6.1	9.0	14.2	19.3	25.6	30.4	29.2	24.4	17.6	9.6	4.8	16.3
Mean Minimum	-12.7	-9.7	-6.4	-3.3	0.8	4.6	8.7	8.1	3.0	-2.2	-7.6	-11.8	-2.3
Extreme Minimum	-32.8	-34.4	-25.0	-20.6	-13.9	-7.8	-1.1	-4.4	-9.4	-19.4	-26.1	-33.9	-34.4
Precipitation (inches)													
Mean Monthly	0.74	0.66	0.99	0.89	1.17	0.74	0.63	0.75	0.83	0.75	0.62	0.68	9.48
MonthlyMaximum	2.08	2.19	2.40	3.41	3.26	3.53	2.30	2.51	4.99	3.67	1.82	2.11	15.98
Maximum Daily	0.88	1.38	0.69	0.80	1.37	1.44	1.20	1.01	2.52	1.09	1.17	0.84	2.52
Snowfall (inches)													
Mean Monthly	9.43	7.27	9.35	6.12	2.67	0.14	0.00	0.00	0.33	2.34	5.31	7.69	50.55
Monthly Maximum	24.80	20.00	25.30	24.50	12.10	1.70	0.00	0.00	6.30	12.10	17.30	22.30	101.30
Daily Maximum	0.88	1.38	0.69	0.80	1.37	1.44	1.20	1.01	2.52	1.09	1.17	0.84	2.52

T4.1-18

Table 4.1-24. Climatological Summary for Las Vegas and Tonopah

	JAN	FEB	MAR	APR	MAY	JUN	JUL	AUG	SEP	OCT	NOV	DEC	YEAR
Las Vegas													
Temperature (C)													
Extreme Maximum	25.0	30.6	32.8	37.2	42.8	46.1	46.7	46.7	45.0	39.4	30.6	25.0	46.7
Mean Maximum	13.4	16.9	20.4	25.6	30.8	36.9	40.1	38.8	34.7	27.4	19.0	13.9	26.6
Mean Minimum	0.9	3.6	6.4	10.6	15.5	20.7	24.6	23.6	19.0	12.2	5.4	1.2	12.0
Extreme Minimum	-13.3	-8.9	-5.0	-0.6	4.4	8.9	15.6	13.3	7.8	-3.3	-6.1	-11.7	-13.3
Precipitation (Inches)													
Mean Monthly	0.58	0.47	0.48	0.18	0.20	0.10	0.42	0.48	0.25	0.21	0.40	0.37	4.14
Monthly Maximum	3.00	2.52	4.80	2.44	0.96	0.97	2.48	2.59	1.58	1.22	2.22	1.71	9.88
Maximum Daily	0.74	1.29	1.20	0.97	0.83	0.82	1.36	2.58	1.07	1.05	1.09	0.95	2.58
Snowfall (Inches)													
Mean Monthly	0.92	0.06	0.00	0.00	0.00	0.00	0.00	0.00	0.00	0.00	0.11	0.05	1.13
Monthly Maximum	16.70	1.40	0.10	0.00	0.00	0.00	0.00	0.00	0.00	0.00	4.00	2.00	16.70
Daily Maximum	7.4	1.4	0.1	0.0T	0.0T	0.0T	0.0	0.0T	0.0	0.0T	3.0	2.0	7.4
Tonopah													
Temperature (C)													
Extreme Maximum	19.4	23.9	25.6	31.1	34.4	38.9	40.0	39.4	35.6	32.2	25.0	21.1	40.0
Mean Maximum	6.4	9.6	12.9	17.4	22.7	28.9	32.8	31.6	26.8	20.3	12.1	7.3	19.2
Mean Minimum	-7.6	-4.7	-2.3	0.7	5.5	10.3	13.4	12.5	8.3	2.8	-3.3	-7.0	2.4
Extreme Minimum	-26.1	-22.8	-15.6	-12.8	-7.2	-2.8	4.4	2.8	-3.9	-10.6	-15.6	-25.0	-26.1
Precipitation (Inches)													
Mean Monthly	0.40	0.45	0.53	0.38	0.61	0.30	0.55	0.53	0.46	0.37	0.44	0.27	5.33
Monthly Maximum	2.25	2.68	2.38	2.13	2.03	1.67	2.49	2.65	2.05	2.16	2.68	1.02	10.64
Maximum Daily	0.59	0.55	0.67	0.85	0.96	1.06	1.23	1.36	1.13	1.14	0.67	0.62	1.36
Snowfall (Inches)													
Mean Monthly	3.22	2.71	2.43	1.14	0.42	0.00	0.00	0.00	0.01	0.07	1.50	1.85	13.53
Monthly Maximum	16.50	13.60	16.40	7.50	5.00	0.00	0.00	0.00	0.40	1.50	9.60	17.00	31.30
Daily Maximum	7.1	9.7	9.0	7.2	5.0	0.0T	0.0	0.0T	0.4	1.0	8.0	7.6	9.7

Table 4.1-25. Annual Precipitation for NWS Sites: 1921 - 1947

Year	Amargosa Farms	Austin	Beatty	Beatty8N	Callente	Desert Natl WL Range	Desert Rock	Elko Municipal AP	Ely Yelland Field	Indian Springs	Las Vegas Mccrn Intl	Pahranagat W L REF	Pioche	Ruby Lake	Snowball Ranch	Tonopah AP	Tonopah	Winnemucca
1921		9.21																
1922		17.86																
1923		10.15																
1924		9.14																
1925		17.66																
1926		4.57																
1927		10.64																
1928		10.44						5.17								2.63		5.52
1929		10.65			1.84			6.84								3.36		3.85
1930		16.67			3.56			13.30								4.49		9.60
1931		11.77			9.49			6.07								6.53		4.87
1932		12.43			11.81			12.23								3.88		8.70
1933		10.16			8.16			6.65								2.19		5.67
1934		14.63			7.14			6.72								3.48		9.07
1935		16.26			9.43			8.23								3.40		10.59
1936		14.91			11.60			10.52								4.62		8.76
1937		7.03			6.84			7.12								4.39		9.35
1938		16.51			4.43			9.75								7.71		11.98
1939		10.46			9.41			7.78								6.25		7.79
1940		14.51			7.49			10.76								4.59		11.69
1941		19.36			18.73			16.27								6.29		13.24
1942		10.81			6.63			12.26								2.19		10.07
1943		11.89			11.70			9.58								6.56		6.60
1944		10.68			7.96			9.59								3.49		10.34
1945		16.31			11.60			12.62								5.77		14.54
1946		16.93			12.36			10.18								10.27		10.65
1947		6.40			7.47			7.25								3.66		6.24

Table 4.1-26. Annual Precipitation for NWS Sites: 1948 - 1995

Year	Anaogosa Farms	Austin	Beatty	Beatty/N	Callente	Desert Nell WL	Desert Rock	Elko Municipal AP	Ely Yelland Field	Indian Springs	Las Vegas Moorn Intl	Pahranagat W L REF	Pioche	Ruby Lake	Snowball Ranch	Tonopah AP	Tonopah	Winnemucca
1948		11.90			5.23	0.70		7.41					3.86	4.86		6.11		7.52
1949		9.10	5.43		10.03	6.28		7.10	6.88	7.04	4.42		15.36	10.73		5.85		6.23
1950		10.12	2.05		2.92	1.41		14.60	6.03	0.66	2.34		7.11	18.18		5.08		10.61
1951		11.38	2.60		10.15	4.21		7.97	7.29	1.84	2.81		13.98	12.84		4.99		8.63
1952		10.34	8.36		11.52	6.54		7.28	10.98	3.26	5.08		16.14	10.49		7.89		10.33
1953		6.73	0.69		4.66	1.00		6.85	5.22	1.41	0.56		7.26	10.18		2.91		6.28
1954		9.92	6.44		9.31	3.05		6.58	7.89	2.92	4.71		13.28	8.20				3.13
1955		11.02	4.31		7.13	3.64		9.52	8.76	1.73	5.40		14.09	11.92			4.13	7.28
1956		12.30	1.67		4.77	0.85		10.04	6.36	1.86	2.04		3.81	12.98			2.51	7.29
1957		12.70	5.91		9.11	5.87		10.10	9.14	4.70	4.98		17.14	14.54			5.10	10.02
1958		8.93	4.23		8.13	5.86		6.40	7.58	4.38	4.52		15.51	9.39			3.38	9.61
1959		5.91	3.39		4.83	3.94		5.51	5.97	3.50	4.17		10.41	9.76			2.37	4.07
1960		8.49	5.12		9.77	4.20		7.84	7.89	5.14	4.40		12.85	13.81			3.69	8.11
1961		9.38	3.29		8.80	5.76		7.60	7.29	2.75	3.17		9.62	10.98			2.90	7.79
1962		6.96	2.67		4.76	1.79		8.24	7.36	2.02	1.45		7.53	12.20			5.84	6.83
1963		16.61	5.00		10.15	4.27		15.03	11.14	2.91	3.87		12.80	14.35			6.03	10.86
1964		15.62	2.11		6.58	1.11		12.14	12.70		1.12		7.88	16.25			3.88	10.47
1965		19.28	7.33		10.61	7.41		11.17	10.77		7.96	7.80	17.99	13.63			5.58	7.75
1966	1.28	7.85	3.22		6.15	2.34		6.50	6.08		1.91	3.93	16.04	7.46			3.00	4.51
1967	1.42	10.22	4.88		12.86	4.93		8.62	14.73		5.54	8.83	14.46	12.14	11.20		7.68	7.70
1968	3.00	12.23	4.45		6.79	1.47		14.63	10.03		1.11	6.60	12.38	11.97	8.35		6.56	8.48
1969	6.95	15.16	6.53		9.76	7.53		9.71	11.45		5.09	8.35	18.66	15.81	11.14		5.16	9.67
1970		13.95	3.00		8.39	2.60		15.19	10.69		4.29	4.41	18.07	13.97	8.37		3.11	9.09
1971		20.71	1.98		8.75	1.50		13.67	9.42		2.54	3.93	12.88	14.61	8.08		3.36	9.17
1972		11.85			7.20	6.57		8.47	6.59		4.85	5.36	8.99	9.89	6.02		5.59	6.62
1973		15.71		6.72	9.75	4.58		9.10	11.23		4.68	7.14	12.51	13.07	7.44		5.11	7.92
1974		10.92		5.80	8.01	4.77		4.77	4.22		4.52	5.45	10.28	5.94	5.32		4.43	6.33
1975		20.35		4.84	7.56	5.15		11.34	9.77		3.47	5.01	12.22	15.95	8.06		4.38	8.59
1976		13.58		7.82	10.74	6.35		7.10	8.25		6.77	8.16	11.78	10.24	10.93		7.14	7.31
1977		12.62		6.44	8.51	3.03		6.46	9.19		3.97	4.03	9.38	12.52	10.43		7.34	8.08
1978		19.42		10.80	16.83	6.88		11.14	12.47		7.65	9.46	27.29	17.84	11.63		10.64	8.10
1979	2.16	12.60		4.71	9.31	1.95		7.74	7.39		6.79	0.00	10.60	14.70	7.47		5.94	8.73
1980	6.24	12.67		6.01	11.67	4.54		12.81	12.78		5.63	5.58	18.38	19.41	13.16		4.18	7.36
1981	3.20	11.84		3.73	9.60	3.26		8.78	10.29		3.14	6.58	11.81	11.22	6.87		9.21	8.44
1982	4.30	16.82		6.07	12.90	4.87		13.72	15.98		3.99	9.87	17.50	16.87	10.57		6.29	9.04
1983	10.37	22.37		11.49	12.21	6.34		18.34	14.84		4.86	11.54	18.78	23.86	14.24		9.64	14.47
1984	8.80	17.72		6.53	13.11	10.38		10.36	14.84		6.85	8.86	9.40	17.78	8.27		6.95	12.87
1985	1.00	15.83		2.79	7.89	2.58	4.77	7.30	9.89		1.27	4.84	12.22	10.84	6.98		5.96	7.01
1986	3.75	5.98		5.22	7.94	4.66	6.92	6.08	8.60		2.65	4.37	11.36	12.00	6.35		2.53	5.51
1987	8.18	18.98		7.38	12.08	7.21	8.56	8.62	12.30		6.59	7.71	17.42	11.20	10.35		8.33	9.04
1988	5.59	16.53		6.21	6.22	3.12	5.84	6.72	8.66		2.29	5.32	6.69	9.34	10.21		5.67	6.73
1989	0.72	9.56		2.43	5.20	1.51	1.25	7.88	6.60		2.11	2.23	7.31	10.28	6.18		3.00	5.56
1990	2.58	13.32		4.92	8.93	2.82	4.88	9.43	8.76		3.75	5.70	2.06	9.78	7.25		5.18	6.37
1991	3.40	14.01		5.15	7.49	4.07	5.55	7.85	9.98		4.06	5.52	8.72	11.89	10.14		5.79	7.80
1992	6.09	8.83		7.37	12.00	8.85	6.35	7.56	9.78		9.88	9.66	15.75	10.62	7.30		3.30	4.14
1993	5.68	8.00		5.71	11.83	4.91	7.55	7.66	10.06		5.05	6.82	17.91	13.67	6.66		4.45	7.27
1994	2.27	13.47		3.44	9.00	3.89	3.28	8.32	9.22		2.56	6.27	14.36	12.02	8.76		4.10	7.58
1995	5.27	15.42		8.45	7.98	4.53	7.90	11.46	12.10		3.69	7.53	15.27	18.70	9.75		6.75	9.82

Table 4.1-27. ASHRAE Table for the R/EFPD Meteorological Sites

State and Station	Latitude	Longitude	Elev. Meters	Winter, C		Summer, C							Prevailing Winds		Temp, C	
				Design Dry-Bulb		Design Dry-Bulb and Mean Coincident Wet-Bulb			Mean Daily Range	Design Wet-Bulb			Winter	Summer	Median of Annual Extr.	
				99%	97.5%	1%	2.5%	5%		1%	2.5%	5%			M/S	
Site 1 (NTS - 60)	36° 50' 34" N	116° 25' 50" W	1143	-5	-3	37/16	36/16	35/15	12	18	17	16	NNW 3	S	39	-6
Site 2 (Yucca MT)	36° 51' 19" N	116° 27' 56" W	1478	-6	-4	35/13	34/13	33/13	9	17	16	15	NE 6	WSW	36	-7
Site 3 (Coyote Wash)	36° 51' 17" N	116° 27' 06" W	1279	-5	-3	36/15	35/15	34/15	10	19	18	17	WNW 3	SSE	38	-7
Site 4 (Alice Hill)	36° 51' 51" N	116° 24' 15" W	1234	-5	-3	37/16	36/16	34/15	10	18	18	17	NNE 5	S	38	-6
Site 5 (Fortymile Wash)	36° 45' 52" N	116° 23' 26" W	953	-4	-2	39/15	38/15	37/15	14	20	19	18	N 4	S	41	-9
Site 6 (WT - 6)	36° 53' 40" N	116° 26' 45" W	1315	-4	-2	36/15	35/14	34/14	14	18	17	16	NW 3	SSE	38	-6
Site 7 (Sever Wash)	36° 50' 49" N	116° 24' 28" W	1081	-6	-5	39/15	38/15	37/15	18	19	18	17	WNW 1	S	41	-10
Site 8 (Knothead Gap)	36° 49' 42" N	116° 25' 35" W	1131	-5	-4	39/15	38/14	36/14	16	18	18	17	NNW 1	S	41	-8
Site 9 (Gate - 510)	36° 40' 17" N	116° 24' 17" W	838	-3	-2	42/16	40/16	39/16	17	20	19	18	NNE 4	SW	44	-6

T4.1-22

Table 4.2-1. Correspondence of Ages for Oxygen Isotope Stages from the Spectral Mapping Project and Owens Lake Records

OIS Stage No.	Owens Lake Age (ka)	SPECMAP Age (ka)
1	10 - 0	10 - 0
2	24 - 10	25 - 10
3	64 - 24	55 - 25
4	70 - 64	70 - 55
5	120 - 70	128 - 70
6	170 - 120	185 - 128
7	220 - 170 ?	245 - 185
8	250 - 220 ?	280 - 245
9	355 - 320	340 - 280
10	400 - 350	400 - 340

NOTE: Owens Lake chronology from Bischoff, Stafford et al. (1997). Owens Lake stage boundaries determined by microfossil stratigraphy (Figures 4.2-16 and 4.2-17).

Table 4.2-2. Estimation of the $\delta^{18}\text{O}$ Composition of Infiltration for a Modern or Glacial Climate

Depth (m)	$\delta^{18}\text{O}$ Calcite	$\delta^{18}\text{O}_{\text{H}_2\text{O}}$ Modern Climate (MAT = 15°C)	$\delta^{18}\text{O}_{\text{H}_2\text{O}}$ Glacial Climate (MAT = 5°C)
100	16 to 21%	-13.5 to -8.5%	-15.7 to -10.7%
500	14 to 18%	-12.7 to -8.7%	-14.7 to -10.7%

INTENTIONALLY LEFT BLANK

FIGURES

	Page
4.1-1 Idealized Global Circulation for the Three-Cell Circulation Model of a Rotating Earth	F4.1-1
4.1-2 Idealized Global Circulation and Semi-Permanent Pressure Systems Locations	F4.1-2
4.1-3 Mean Zonal Winds	F4.1-3
4.1-4 ENSO Precipitation Anomalies in the Western United States	F4.1-4
4.1-5 ENSO Temperature Anomalies in the Western United States	F4.1-5
4.1-6 Average Surface Pressure (in millibars) and the Associated Global Circulation for January and July	F4.1-6
4.1-7 Examples of Upper Air Patterns for Southern Nevada Cyclone Passages	F4.1-6
4.1-8 Locations of the Regional Monitoring Sites	F4.1-7
4.1-9 Locations of the R/EFPD Monitoring Sites	F4.1-8
4.1-10 1986 to 1996 Annual Precipitation Totals for Site 1, Beatty 8N and Amargosa Farms	F4.1-9
4.1-11 1965 to 1996 Annual Precipitation Totals for Amargosa Farms and Beatty	F4.1-10
4.1-12 Wind Rose Plots for 10 m and 60 m at Site 1	F4.1-11
4.1-13 Wind Rose Plots for Sites 4 and 7	F4.1-12
4.1-14 Wind Rose Plots for Sites 3 and 9	F4.1-13
4.1-15 Wind Rose Plots for 850 and 700 mb Levels at Desert Rock	F4.1-14
4.1-16 Wind Rose Plots for 500 and 300 mb Levels at Desert Rock	F4.1-15
4.2-1 Generalized Depiction of Eccentricity, the Shape of the Earth's Orbit and Obliquity, the Tilt of the Earth's Spin Axis	F4.2-1
4.2-2 A Graphic Expression of Eccentricity (Shape of Earth's Orbit) for the past Million Years (a Large Value Signifies a More Elliptical Orbit and a Low Value a More Circular Orbit)	F4.2-2
4.2-3 A Graph Showing the Relation of Precession (the wobble of the Earth's Axis), the High Frequency Curve, to Eccentricity	F4.2-3
4.2-4 A Graph Showing June Insolation (the amount of heat arriving in the upper troposphere in watts per sq meter) for the Past and Next Million Years	F4.2-4
4.2-5 A Graph Showing Past and Future Eccentricity	F4.2-5
4.2-6 A Graph Showing Insolation Values for June and December at Different Latitudes and for the Last 500 k.y.	F4.2-6
4.2-7 The SPECMAP (Spectral Mapping Project) Record of Oxygen Isotope Variations for the Past 800 k.y.	F4.2-7
4.2-8 Record of Oxygen Isotopes in Water (Ice) Taken from the Greenland (Summit) Ice Core for the Past 160 k.y.	F4.2-8
4.2-9 The Greenland (GRIP) Ice Core Oxygen Isotope Record Between 10 ka and 50 ka and the Relative Abundance of Neogloboquadrina Pachyderma (Left Coiling = s) a Polar Foraminifera from the North Atlantic Sediment Core V23-81	F4.2-9

FIGURES (Continued)

	Page
4.2-10 Oxygen Isotope Records from Greenland (GISP-2) Ice Core and Owens Lake, California Showing Possible Millennial- And Sub-millennial-scale Correlations (tie lines between silhouettes) Between Lacustrine Environments at Owens Lake and Global Atmospheric Changes During the Late Glacial and Holocene Periods Between 6 ka B.P. and 13 ka B.P.	F4.2-10
4.2-11 Index Map Showing Sites in the Yucca Mountain Area Discussed in the Text ...	F4.2-11
4.2-12 Comparison of the $\delta^{18}\text{O}$ Record from Devils Hole to the Marine $\delta^{18}\text{O}$ Record (SPECMAP)	F4.2-12
4.2-13 Lithology and Age Control for Death Valley, California, Core DV93-1	F4.2-13
4.2-14 Maximum Homogenization Temperatures from Halite Fluid Inclusions from Death Valley Core DV93 Plotted Against Time and Sequence of Lacustrine Paleoenvironments Represented by Core Lithology and Lake Level Data	F4.2-14
4.2-15 Annual Discharge (in thousands of acre feet) on the Owens River, California, between Long Valley and Tinemaha, California, from June 1961 through September 1992	F4.2-15
4.2-16 Principal Ecologic Groups of Diatoms in the Owens Lake Core for the Past 525 k.y.	F4.2-16
4.2-17 Stratigraphic Distribution of Ostracode Species from the Owens Lake Core for the Past 400 k.y.	F4.2-17
4.2-18 Stratigraphic distribution of Fresh-Water, Planktic Diatoms from the Owens Lake Core for the Past 500 k.y. Compared to the SPECMAP and Devils Hole Oxygen Isotope Records	F4.2-18
4.2-19 Stratigraphic Distribution of Key Ostracode Species Compared to SPECMAP and Devils Hole Climate Records Based on Oxygen Isotopes	F4.2-19
4.2-20 Graph Showing the Stratigraphic Abundance Profiles of Key Ostracode Species Found in Samples Collected from Section OCI-11 in the Las Vegas Valley	F4.2-20
4.2-21 Graph Showing the Ostracode Species Data Combined into Two Environmental Groups, Wetland Taxa (Those Taxa That Typically Live in Shallow Standing to Low Flow Environments Supported By Groundwater Discharge) and Spring Stream Taxa	F4.2-21
4.2-22 Locality Map Showing the Location of the Two Sections from the Las Vegas Valley Discussed in the Text	F4.2-22
4.2-23 Graph Showing the Lithostratigraphic Section Measured just North of Cactus Springs, Nevada, Including the Stratigraphic Units Established by Quade, Mifflin et al. (1995).	F4.2-23
4.2-24 Histograms of Radiocarbon (from calcite) and U-series (from calcite and opal) Ages Obtained for Outermost Mineral Surfaces	F4.2-24
4.2-25 Stable O(a) and C(b) values of Pedogenic Carbonate from Southwestern Nevada as a Function of Elevation	F4.2-25
4.2-26 Plot of the $\delta^{13}\text{C}$ (circles) and $\delta^{18}\text{O}$ (crosses) Values of Calcite Versus Depth Below, or Height Above, the Water Table	F4.2-26
4.2-27 Histogram of Unsaturated Zone $\delta^{13}\text{C}$ Values from Calcite Occurrence in the Exploratory Studies Facility Tunnel and from Drill Core	F4.2-27

FIGURES (Continued)

	Page
4.2-28 Secondary Calcite $\delta^{13}\text{C}$ (‰) Values Plotted Against Ages (m.y.) Determined by U/Pb or $^{230}\text{Th}/\text{U}$ Techniques	F4.2-28
4.3-1 Graph Comparing June Insolation at 30°N Latitude for the Periods 400-300 ka and 0 to 100 kyap	F4.3-1
4.3-2 Graph Showing the Timing of Interglacials, Glacial Transitions, Ice Growth, and Ice Maxima Based on the Devils Hole Chronology, Excepting the Last 50 k.y. Where Data Comes from SPECMAP	F4.3-2
4.3-3 Graph Showing the Delta Oxygen-18 Values from Devils Hole for the Period 430 ka to 330 ka	F4.3-3
4.3-4 Climate Summary Graph Showing Relative Levels of MAP and MAT Based on All Climate Proxy Data, Primarily Diatoms, Ostracodes, Pollen, Plant Macrofossils from Packrat Middens, and Stable Isotope Data	F4.3-4

INTENTIONALLY LEFT BLANK

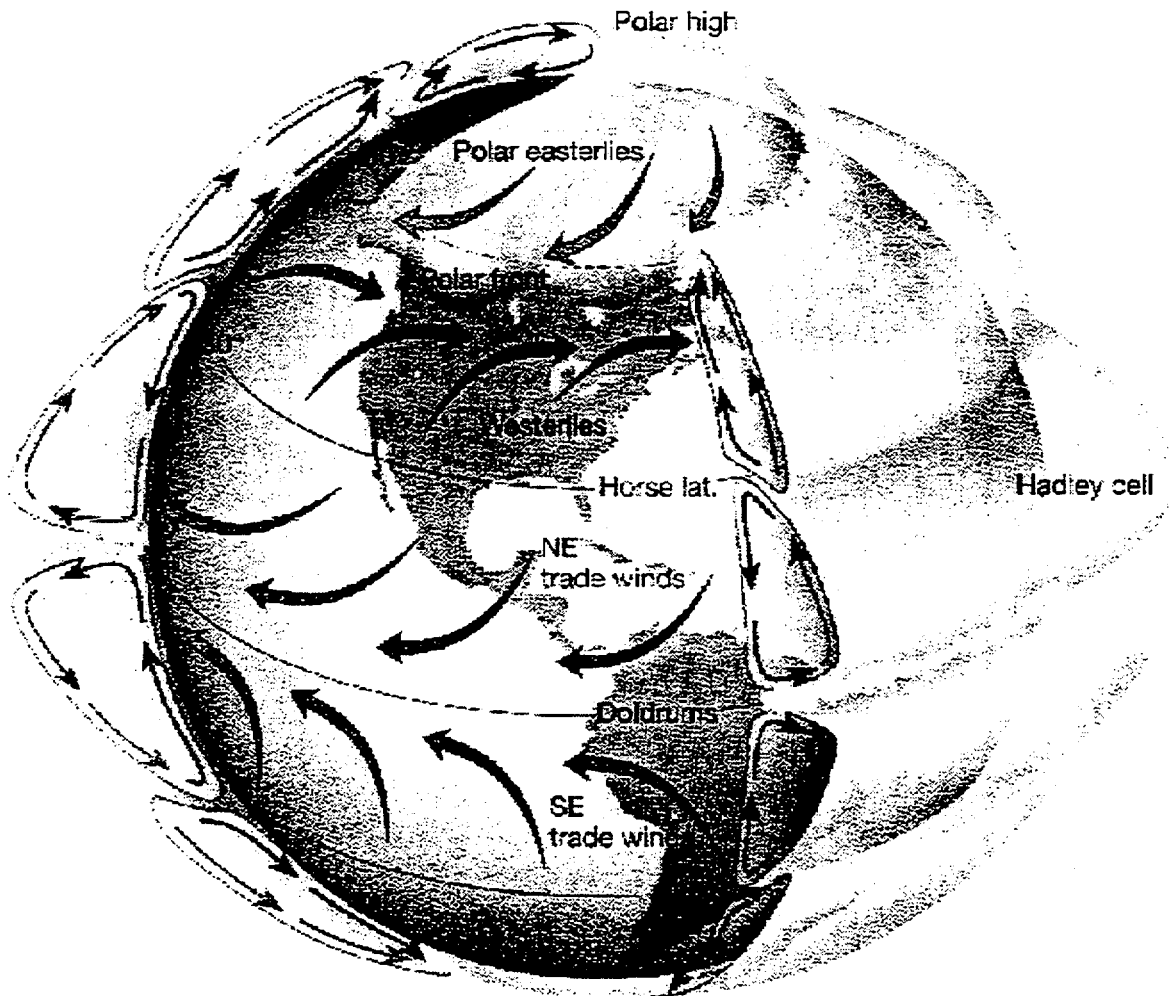


Figure 4.1-1. Idealized Global Circulation for the Three-Cell Circulation Model of a Rotating Earth (from Lutgens and Tarbuck 1995)

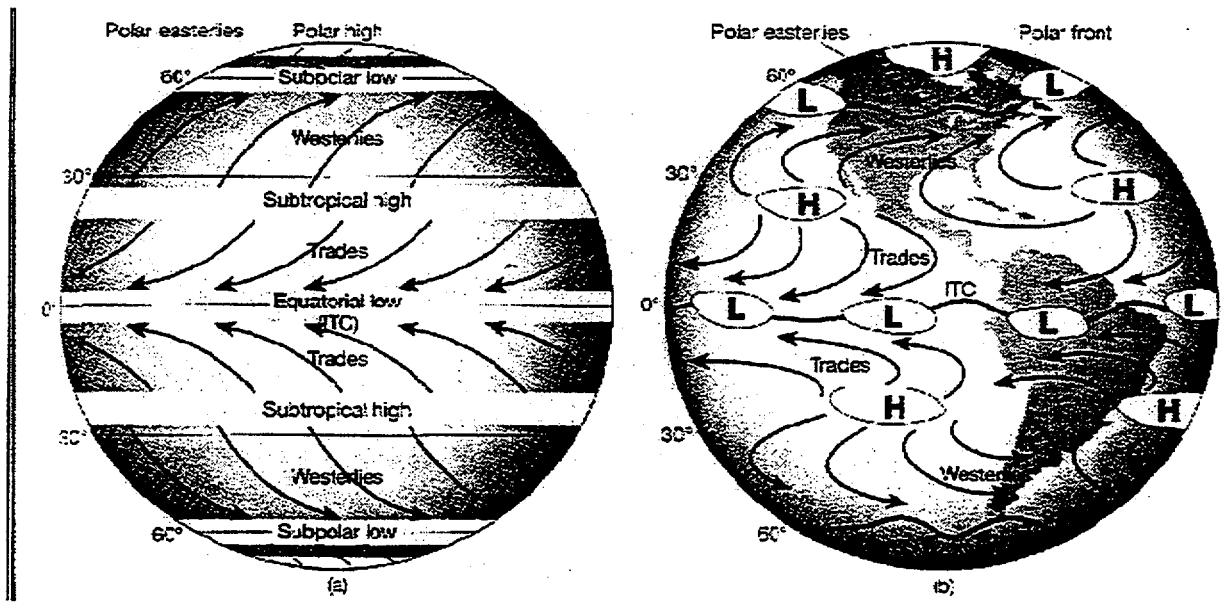


Figure 4.1-2. Idealized Global Circulation and Semi-Permanent Pressure Systems Locations (from Lutgens and Tarbuck 1995)

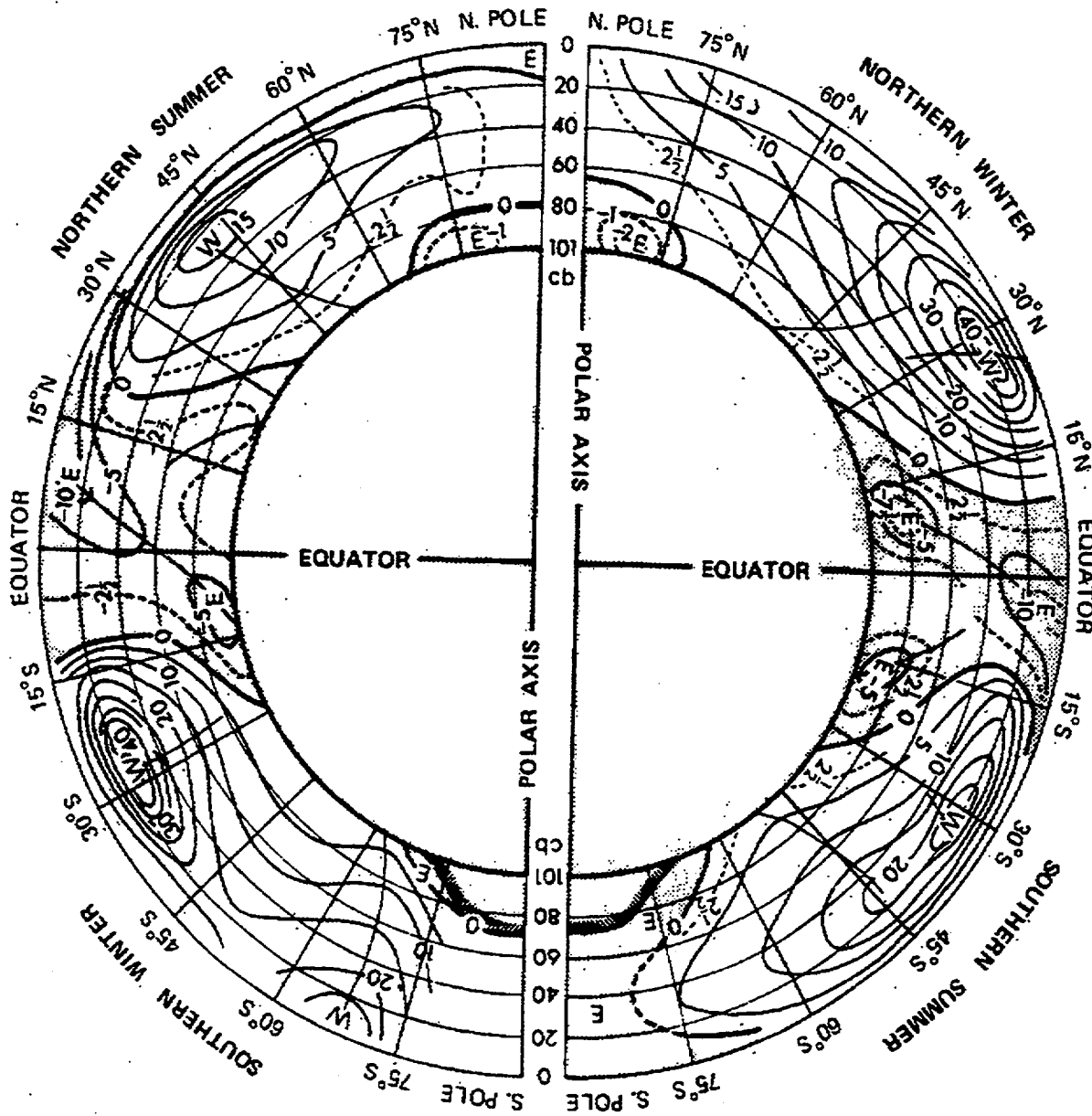


Figure 4.1-3. Mean Zonal Winds (from Barry and Chorley 1992)

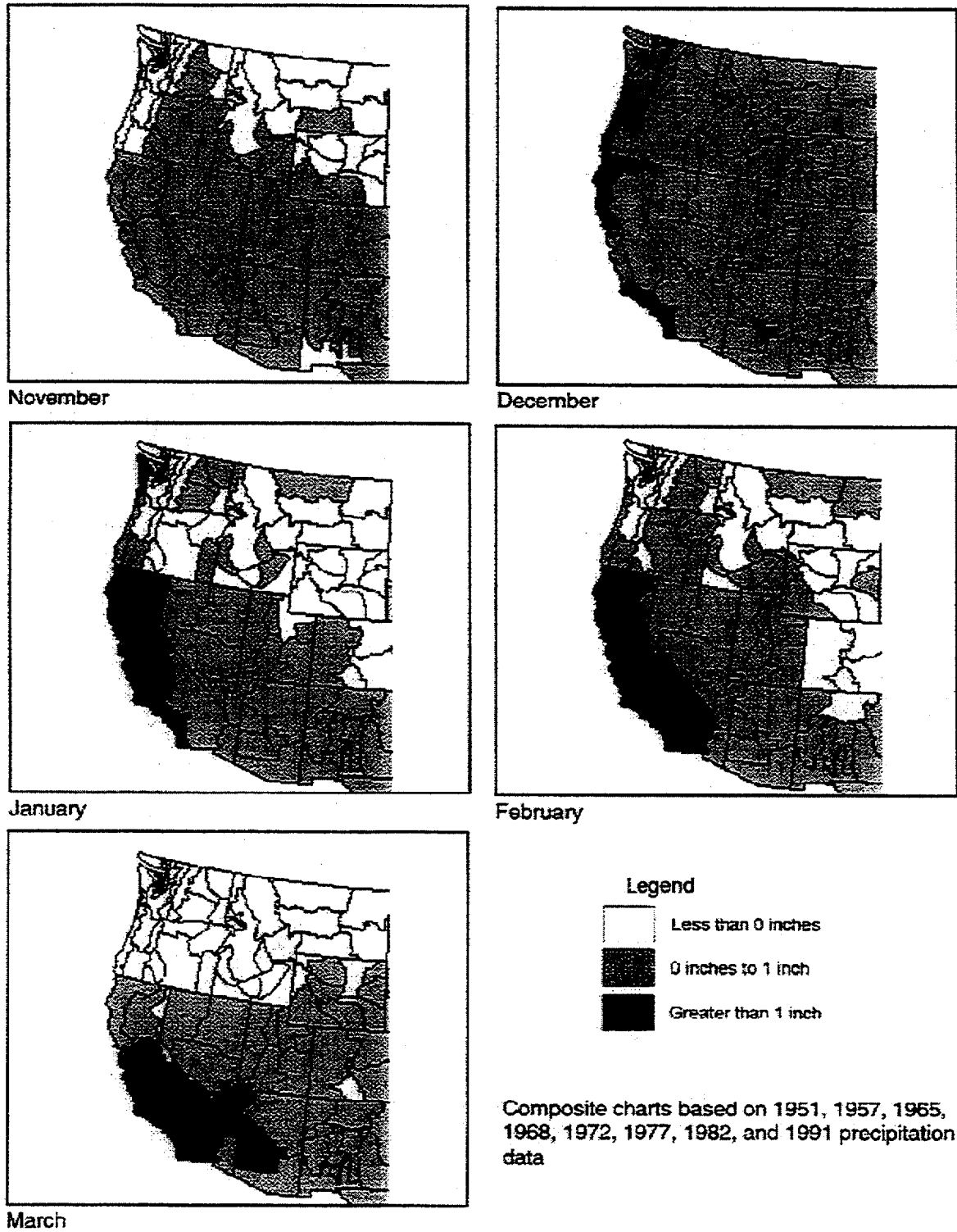


Figure 4.1-4. ENSO Precipitation Anomalies in the Western United States (after U.S. Climate Division)

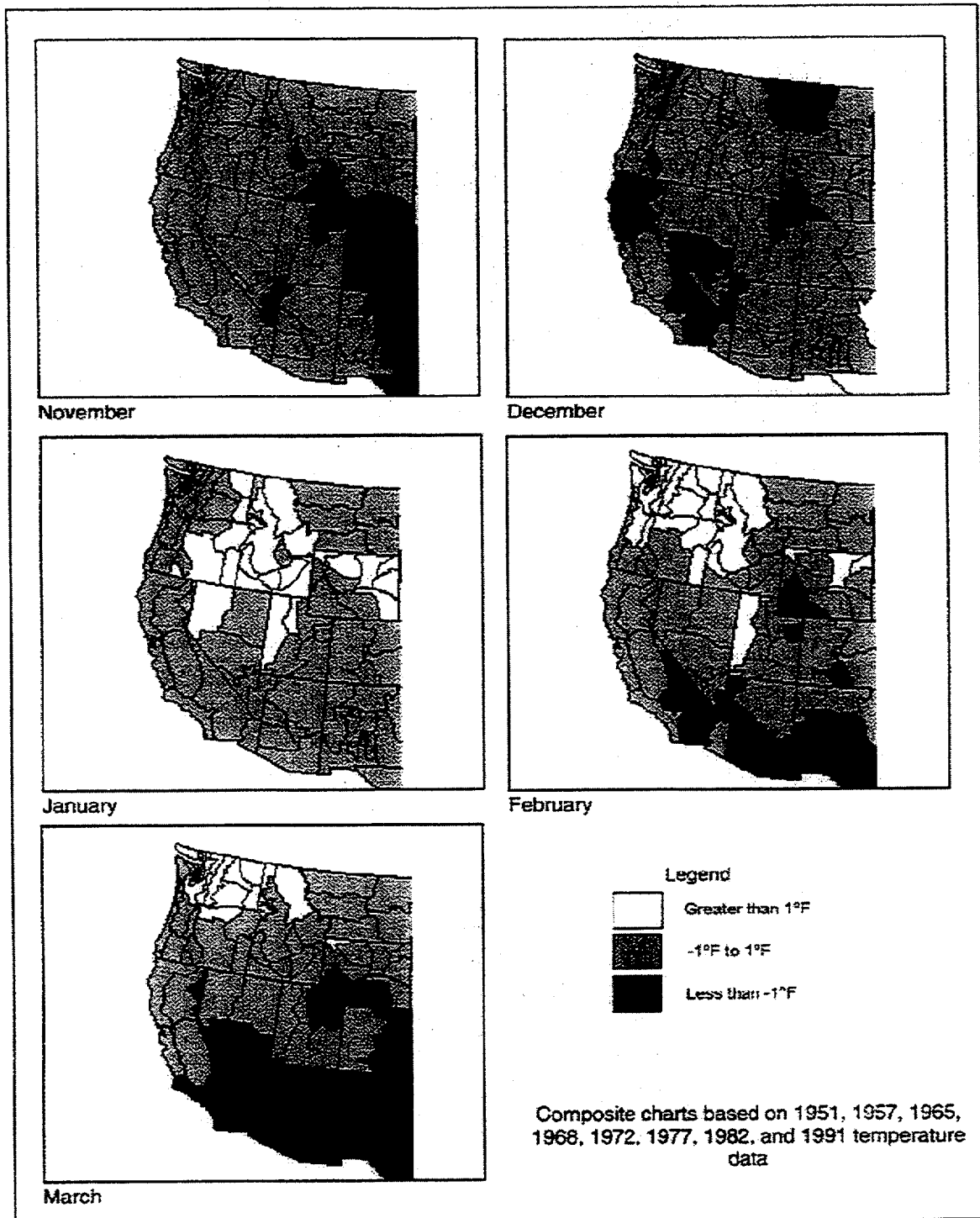


Figure 4.1-5. ENSO Temperature Anomalies in the Western United States (after U.S. Climate Division)

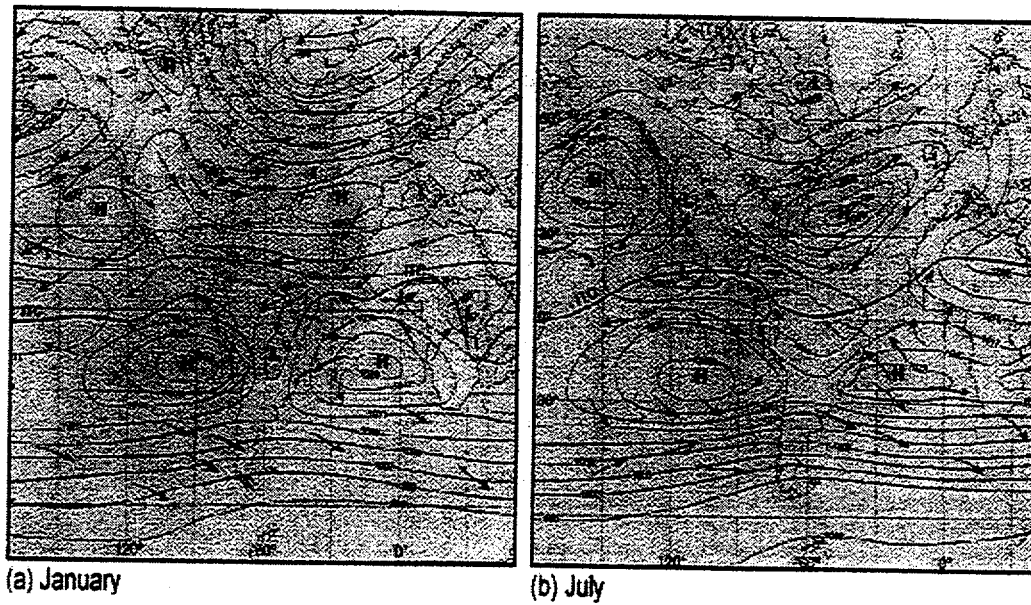
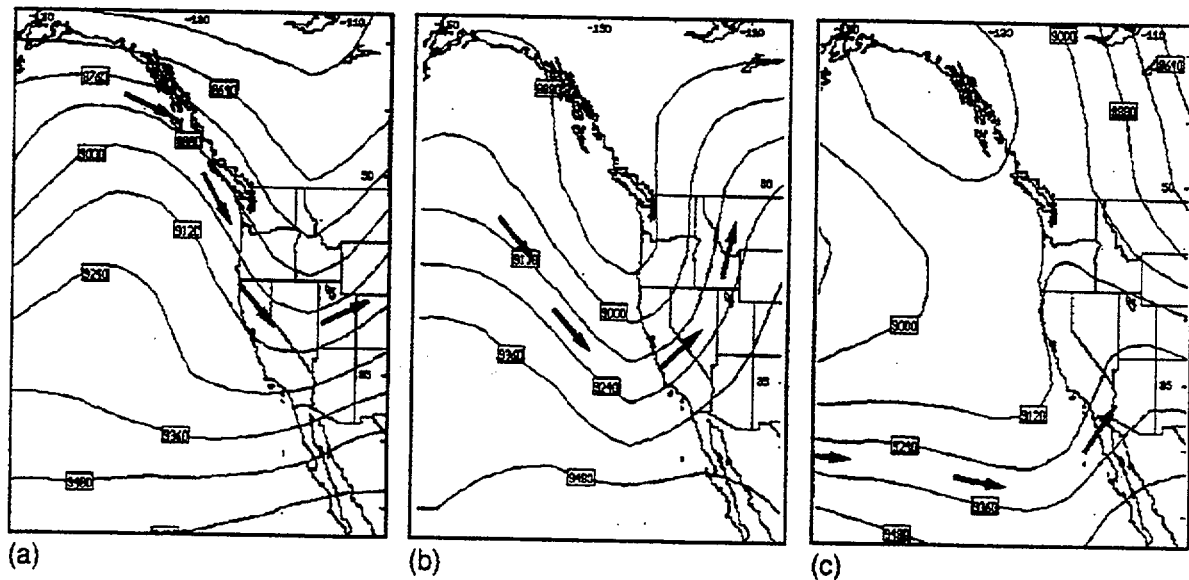


Figure 4.1-6. Average Surface Pressure (in millibars) and the Associated Global Circulation for January and July (from Lutgens and Tarbuck 1995)



NOTE: The boxed numbers indicate geopotential in meters.

Figure 4.1-7. Examples of Upper Air Patterns for Southern Nevada Cyclone Passages (DON 1994)

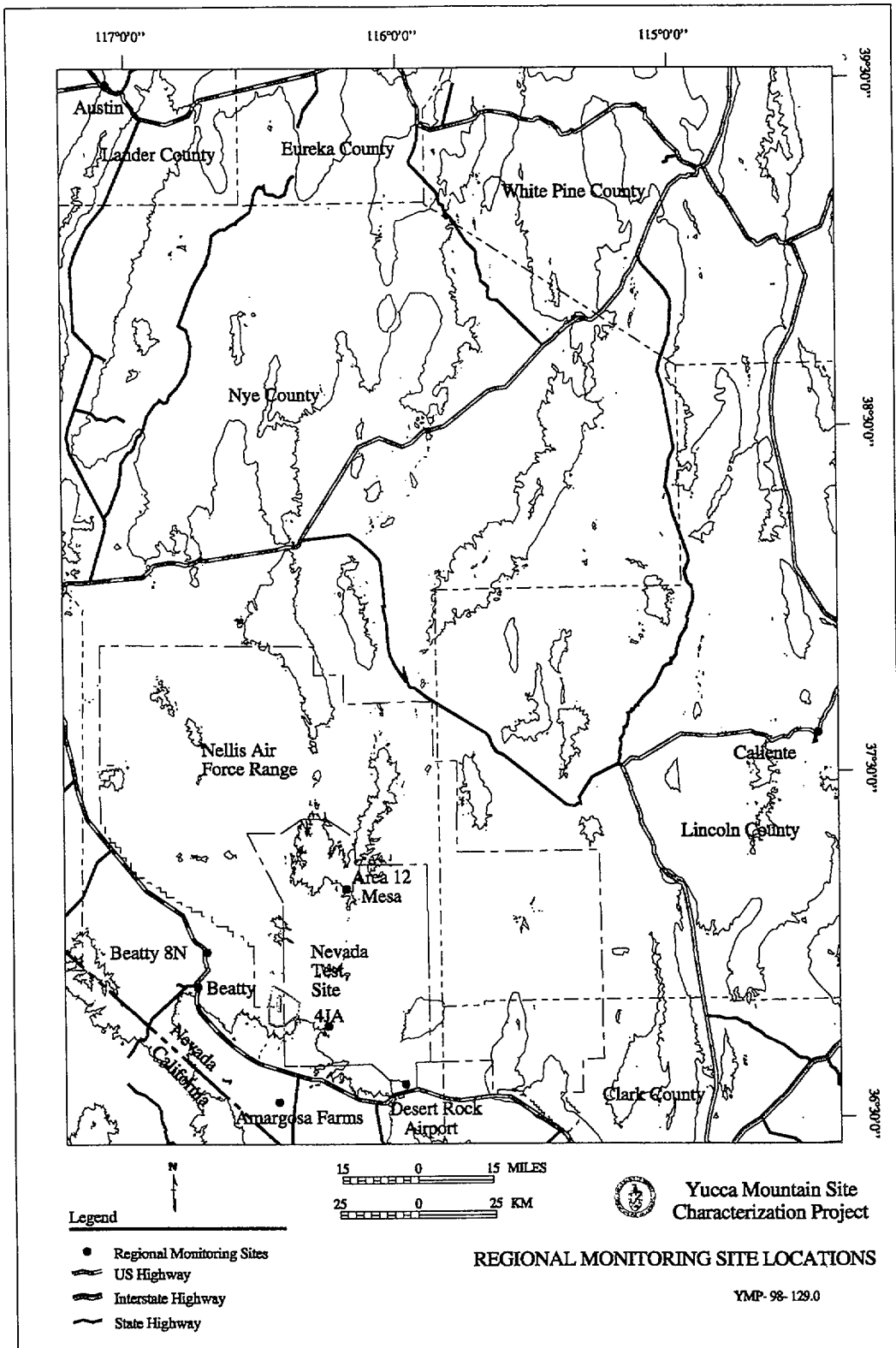


Figure 4.1-8. Locations of the Regional Monitoring Sites

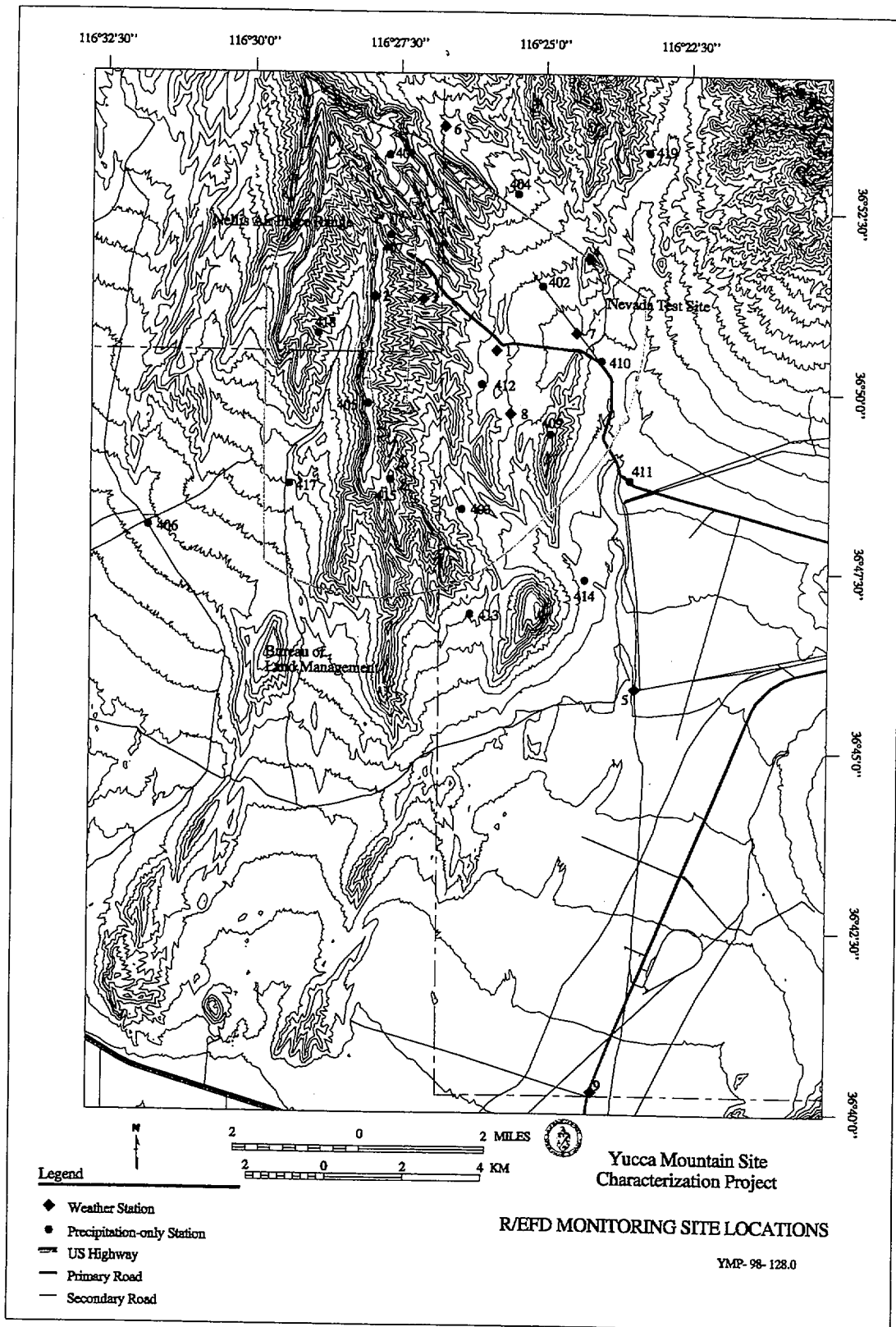


Figure 4.1-9. Locations of the R/EPD Monitoring Sites

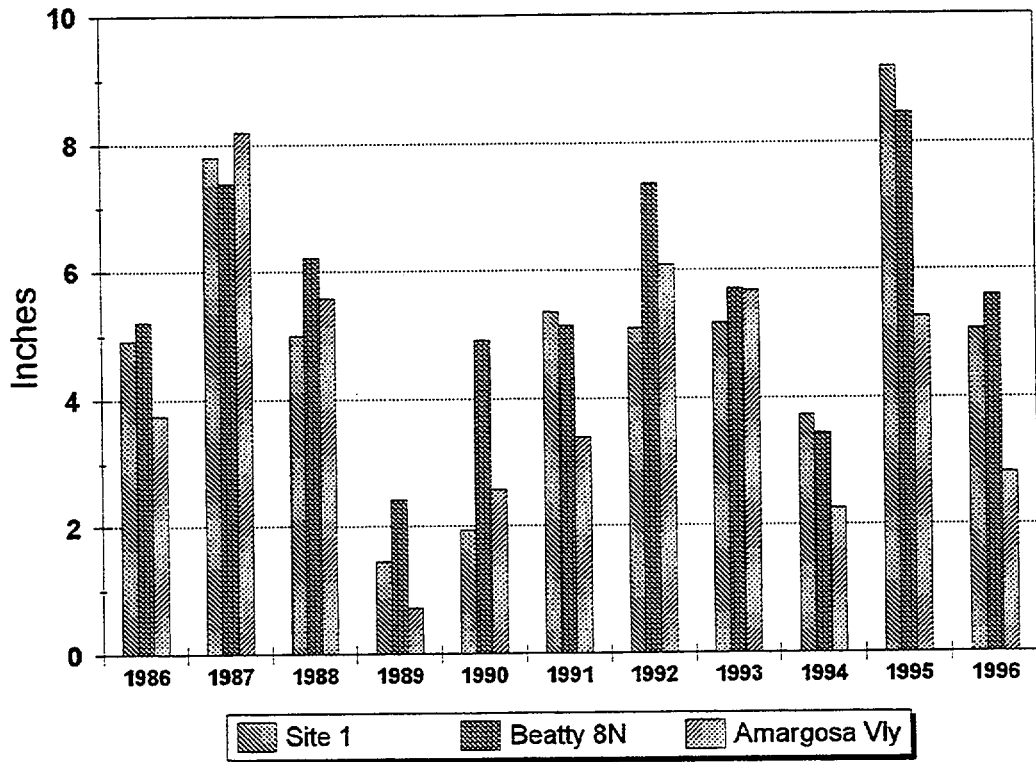


Figure 4.1-10. 1986 to 1996 Annual Precipitation Totals for Site 1, Beatty 8N and Amargosa Farms

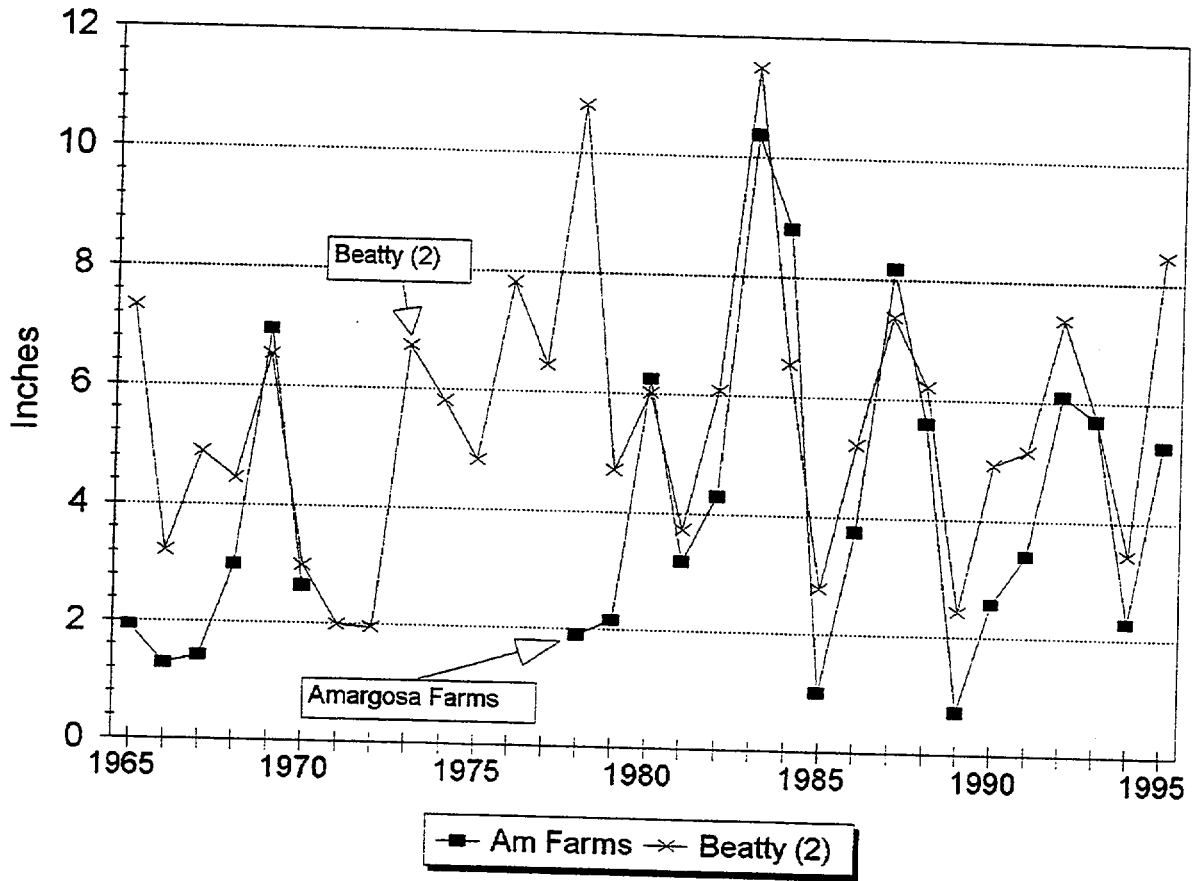


Figure 4.1-11. 1965 to 1996 Annual Precipitation Totals for Amargosa Farms and Beatty

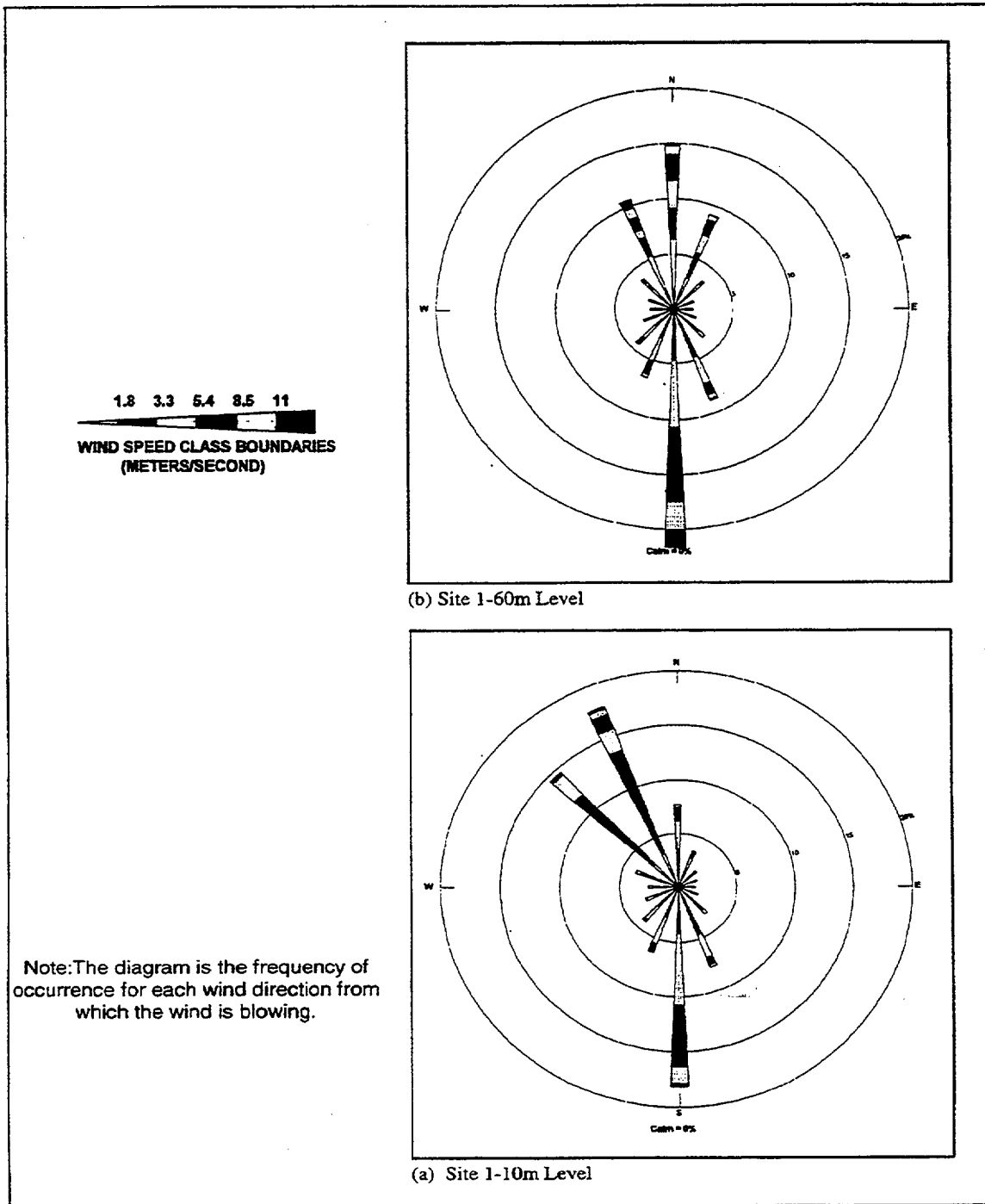


Figure 4.1-12. Wind Rose Plots for 10 m and 60 m at Site 1

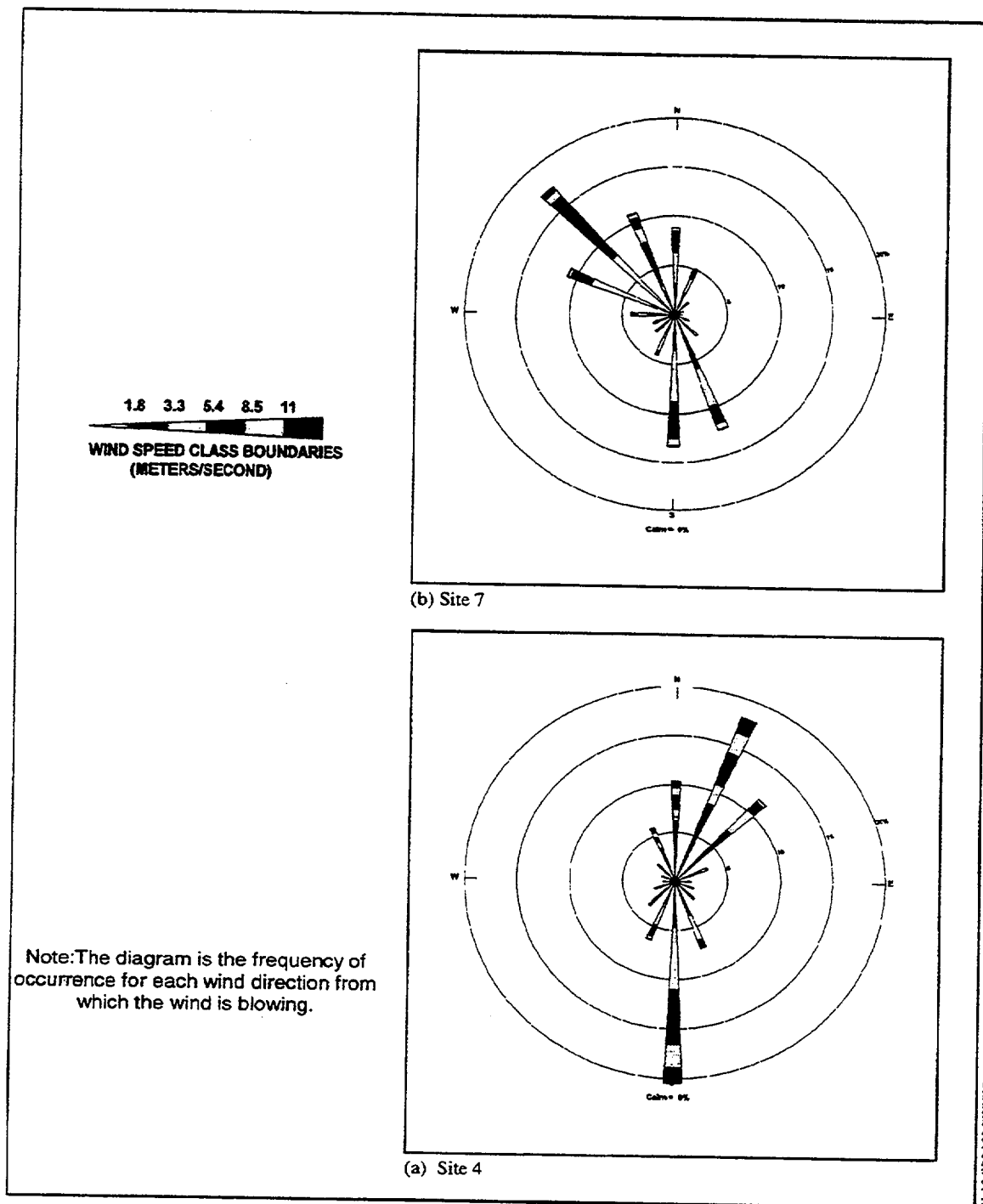


Figure 4.1-13. Wind Rose Plots for Sites 4 and 7

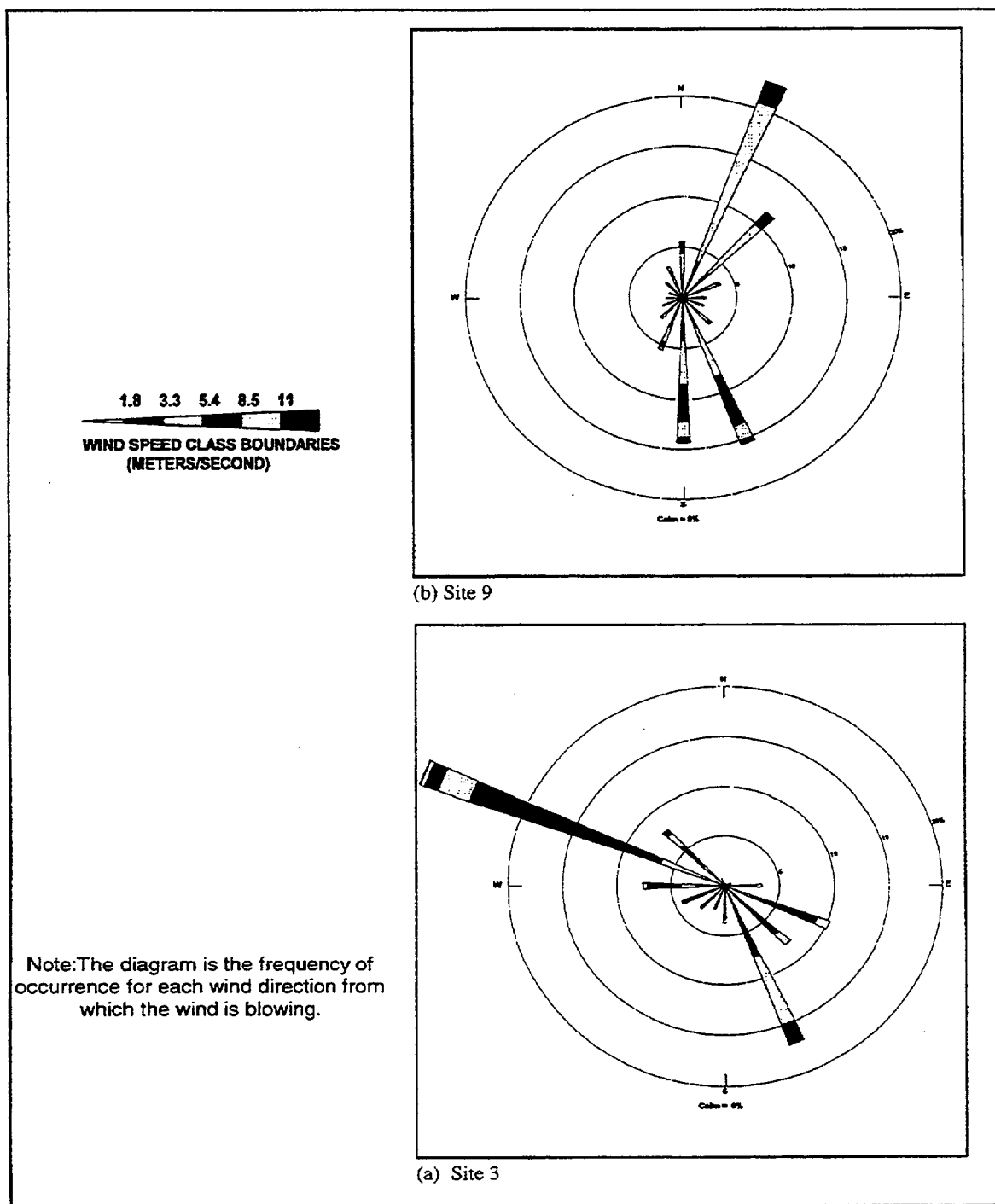


Figure 4.1-14. Wind Rose Plots for Sites 3 and 9

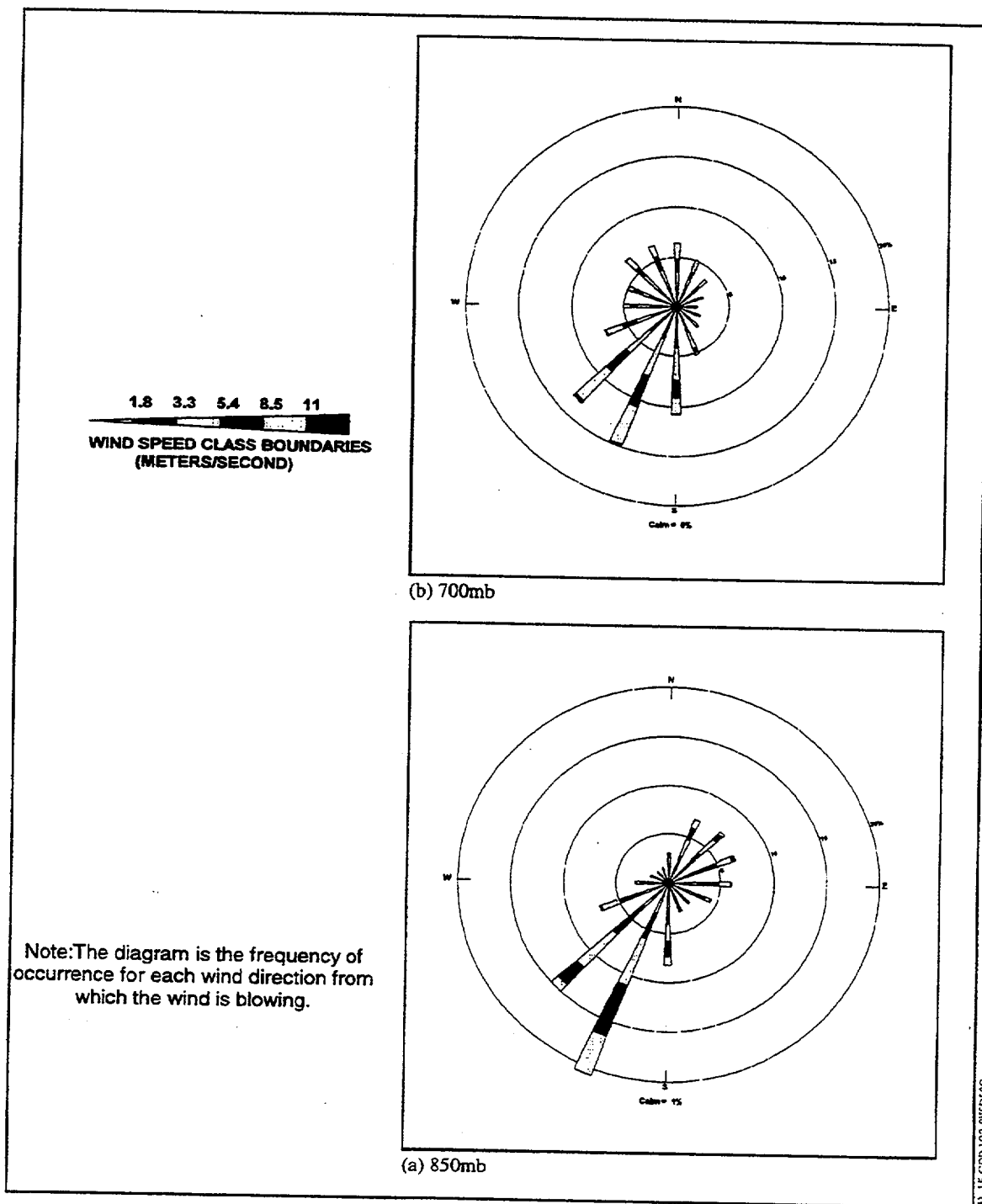


Figure 4.1-15. Wind Rose Plots for 850 and 700 mb Levels at Desert Rock

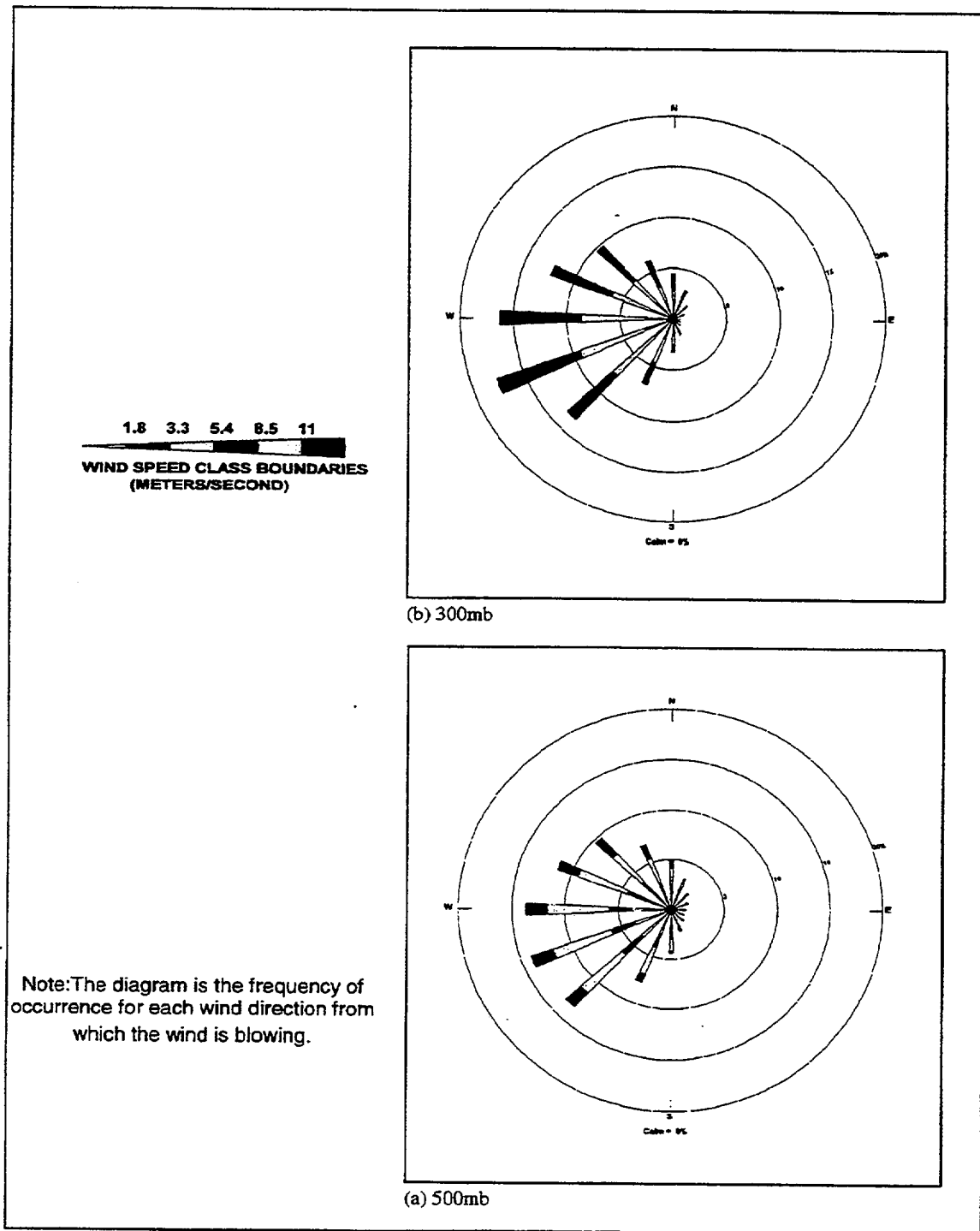
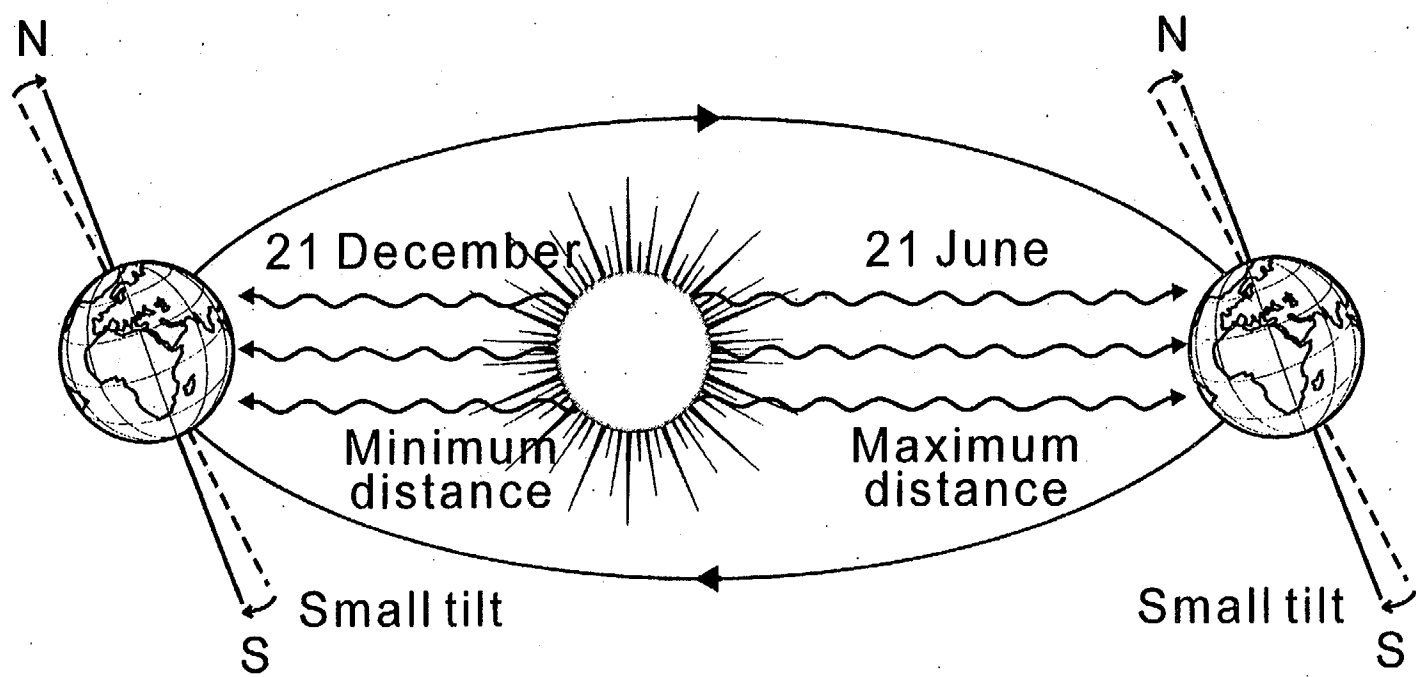


Figure 4.1-16. Wind Rose Plots for 500 and 300 mb Levels at Desert Rock

INTENTIONALLY LEFT BLANK



modified from Ahrens, 1985
42-01.CDR.123.SIIEDESC

NOTE: Notice that the distance between the Earth and Sun is at a minimum in the northern hemisphere winter and at a maximum in the summer, which in 12 k years will be exactly the opposite. The latter change over a 12 k period is due to the wobble of the earth's axis and is called precession.

Figure 4.2-1. Generalized Depiction of Eccentricity, the Shape of the Earth's Orbit and Obliquity, the Tilt of the Earth's Spin Axis

F4.2-1

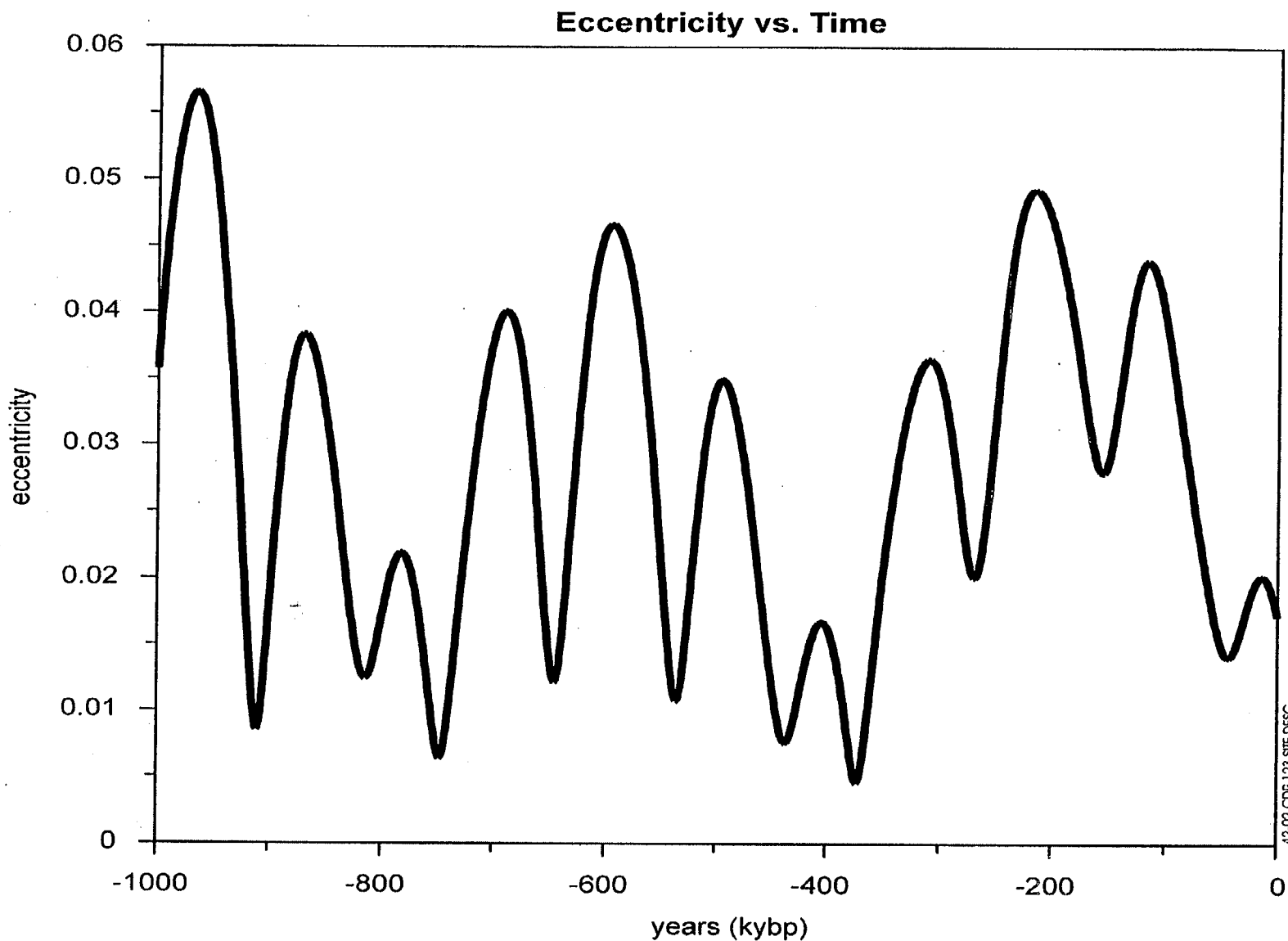


Figure 4.2-2. A Graphic Expression of Eccentricity (Shape of Earth's Orbit) for the past Million Years (a Large Value Signifies a More Elliptical Orbit and a Low Value a More Circular Orbit)

data after Berger and Loutre, 1991

F4.2-2

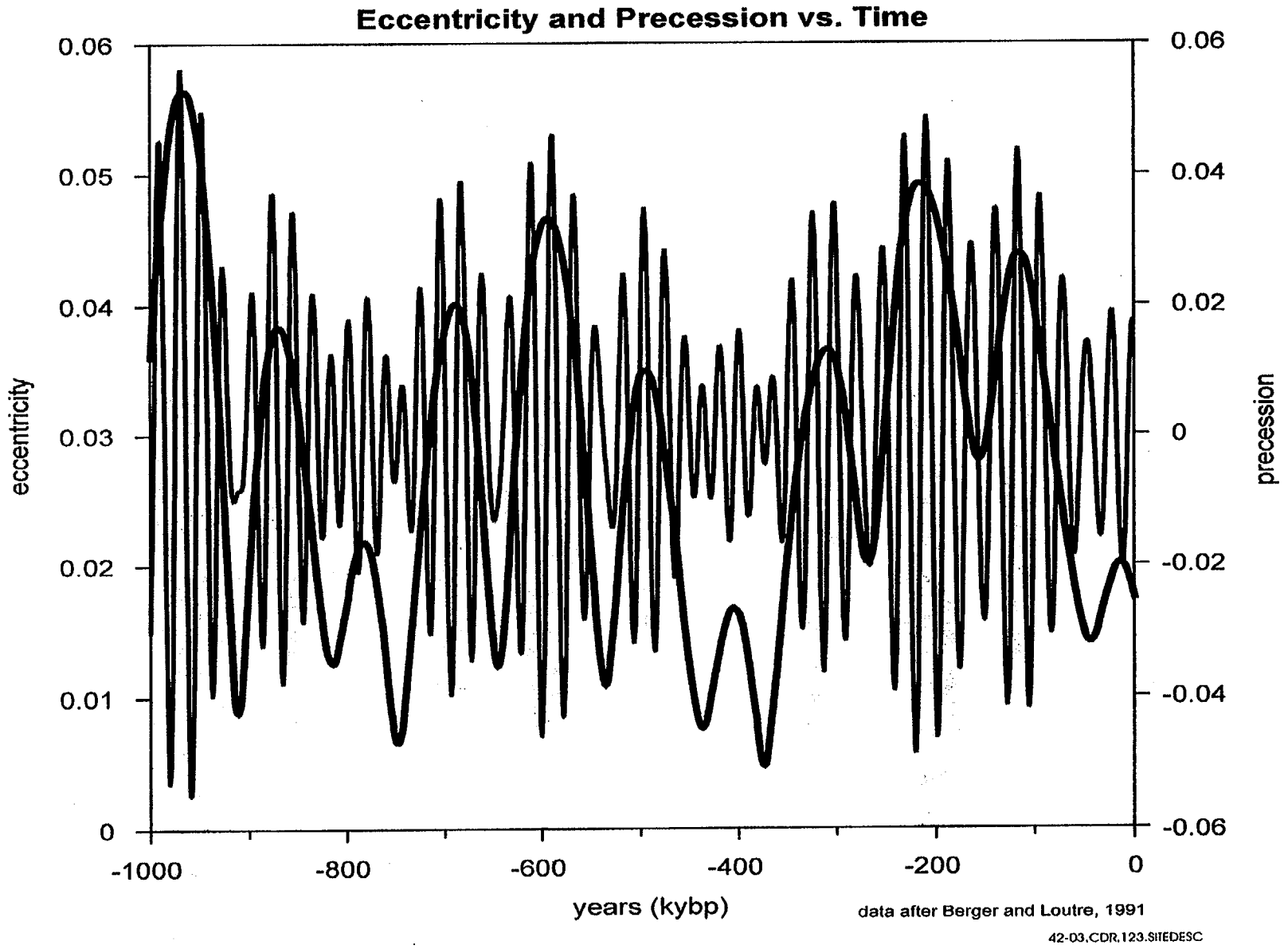
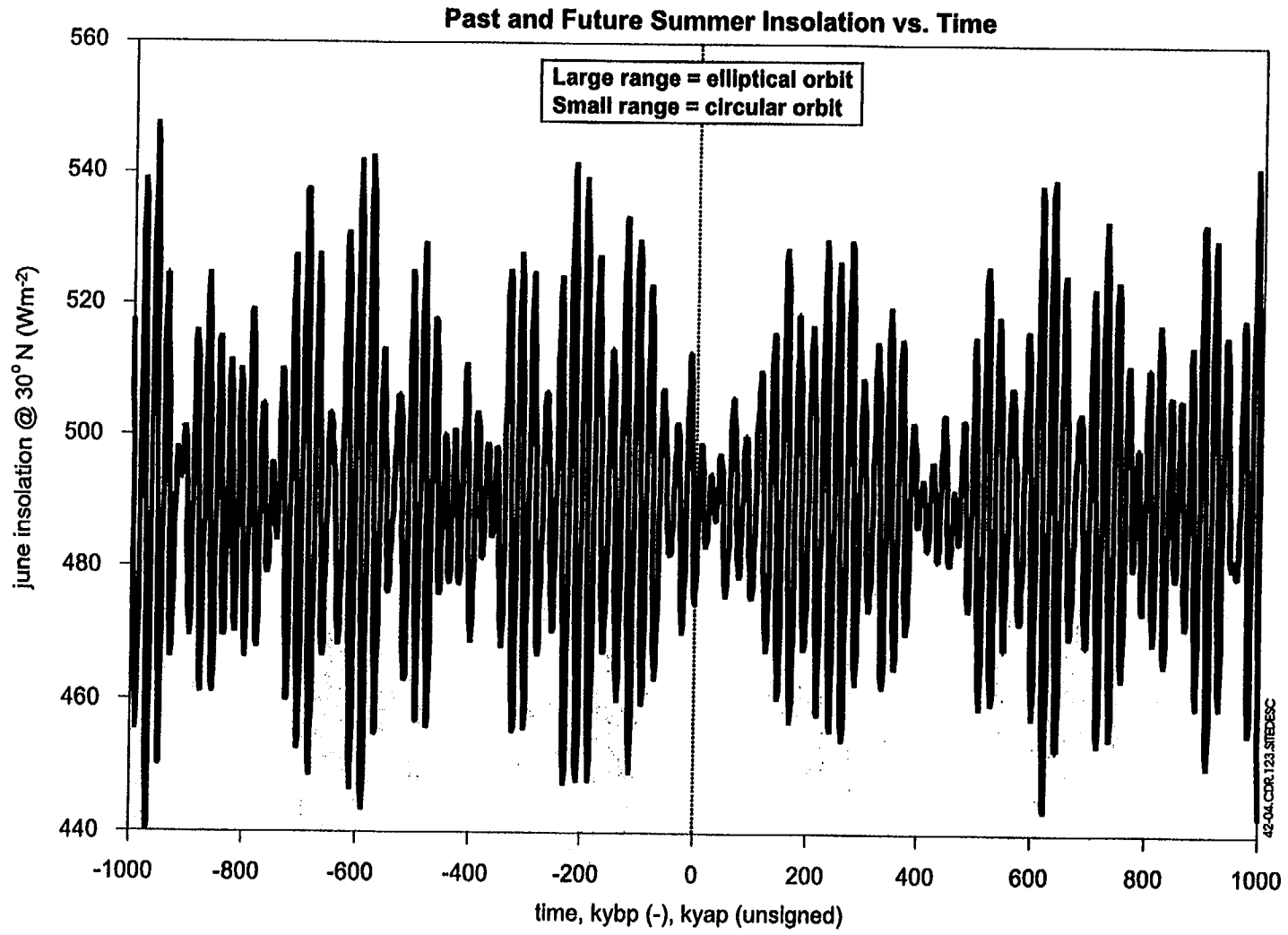


Figure 4.2-3. A Graph Showing the Relation of Precession (the wobble of the Earth's Axis), the High Frequency Curve, to Eccentricity

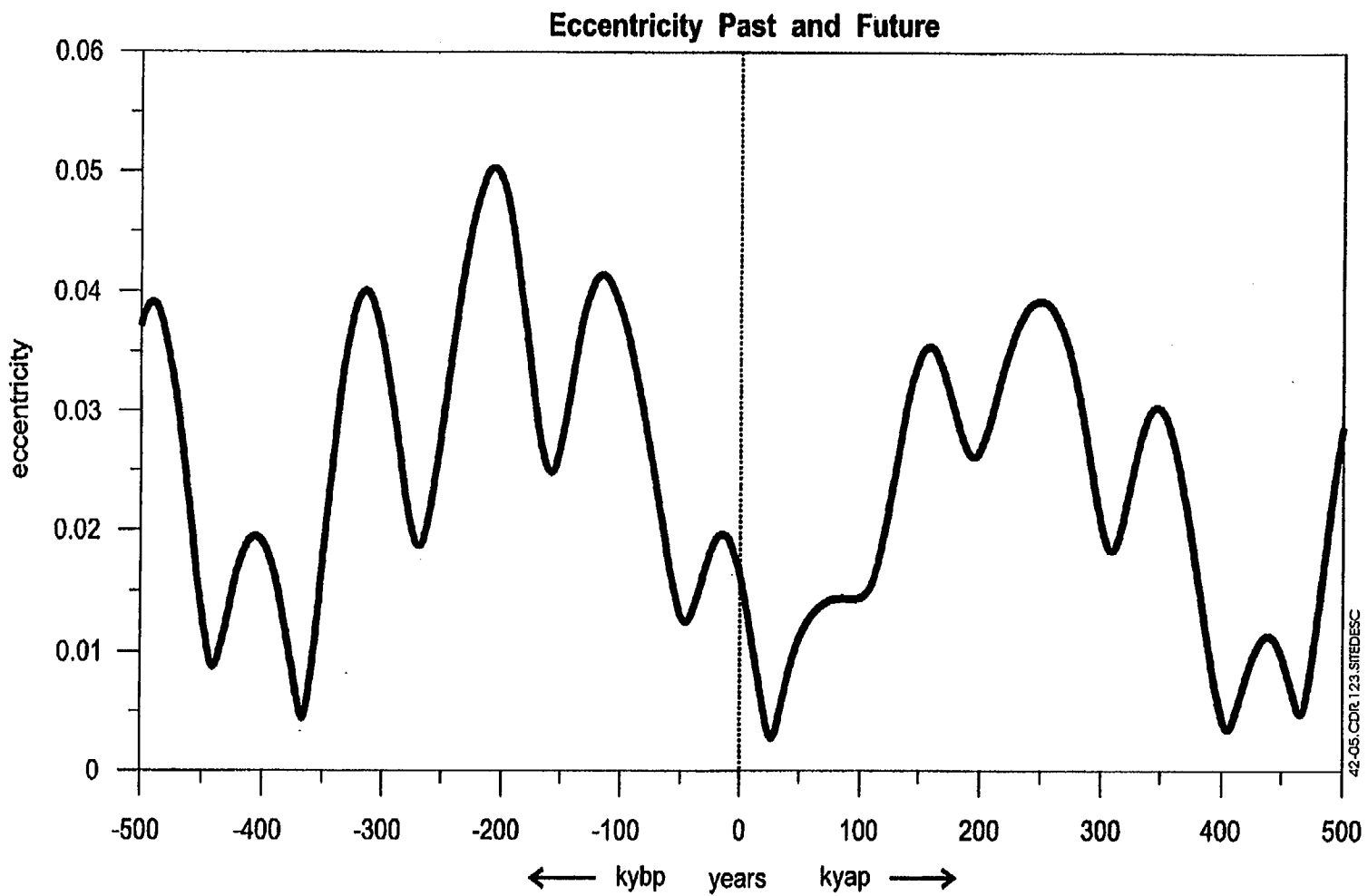
F4.2-3



NOTE: Notice that the change in insolation is related to eccentricity and precession.

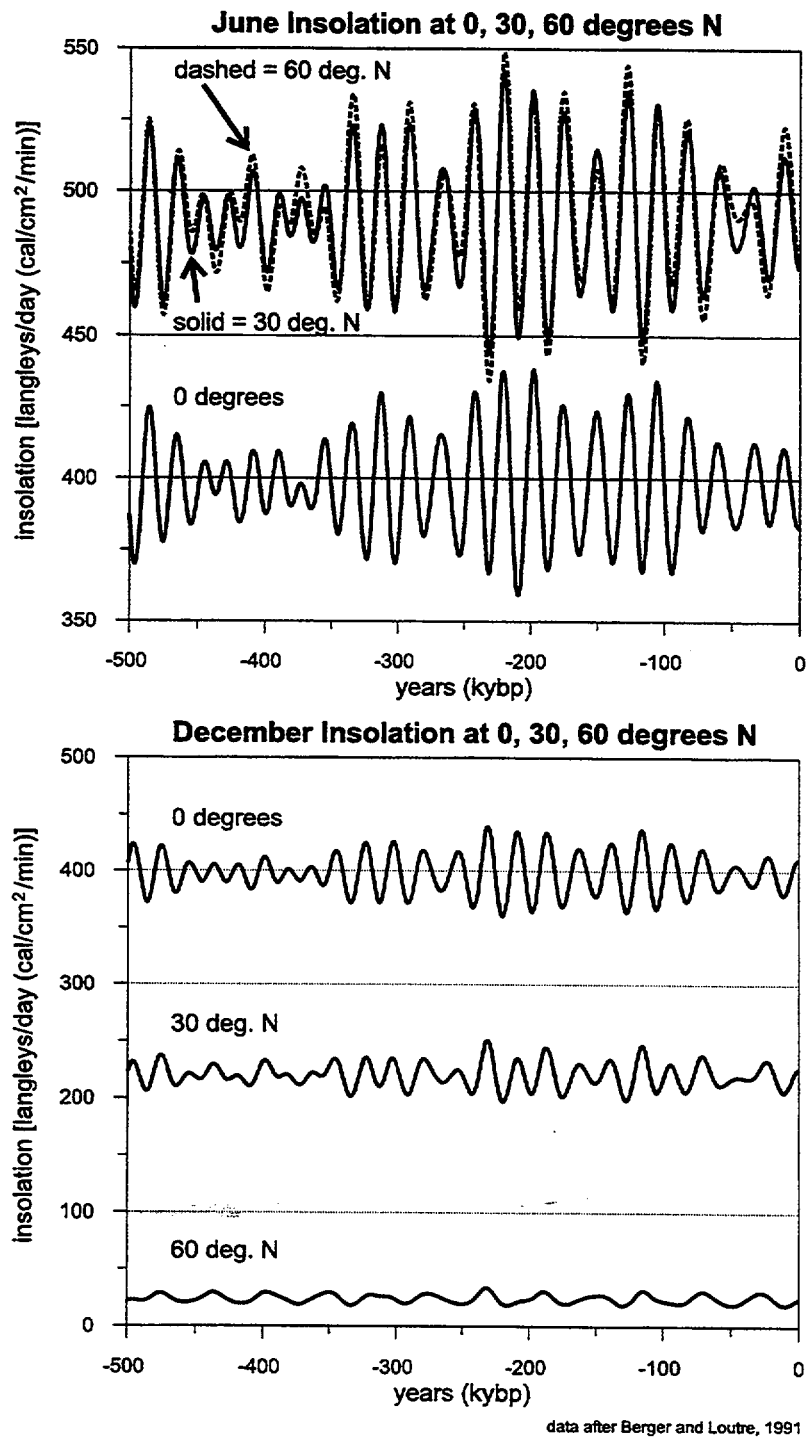
Figure 4.2-4. A Graph Showing June Insolation (the amount of heat arriving in the upper troposphere in watts per sq meter) for the Past and Next Million Years

F4.2-4



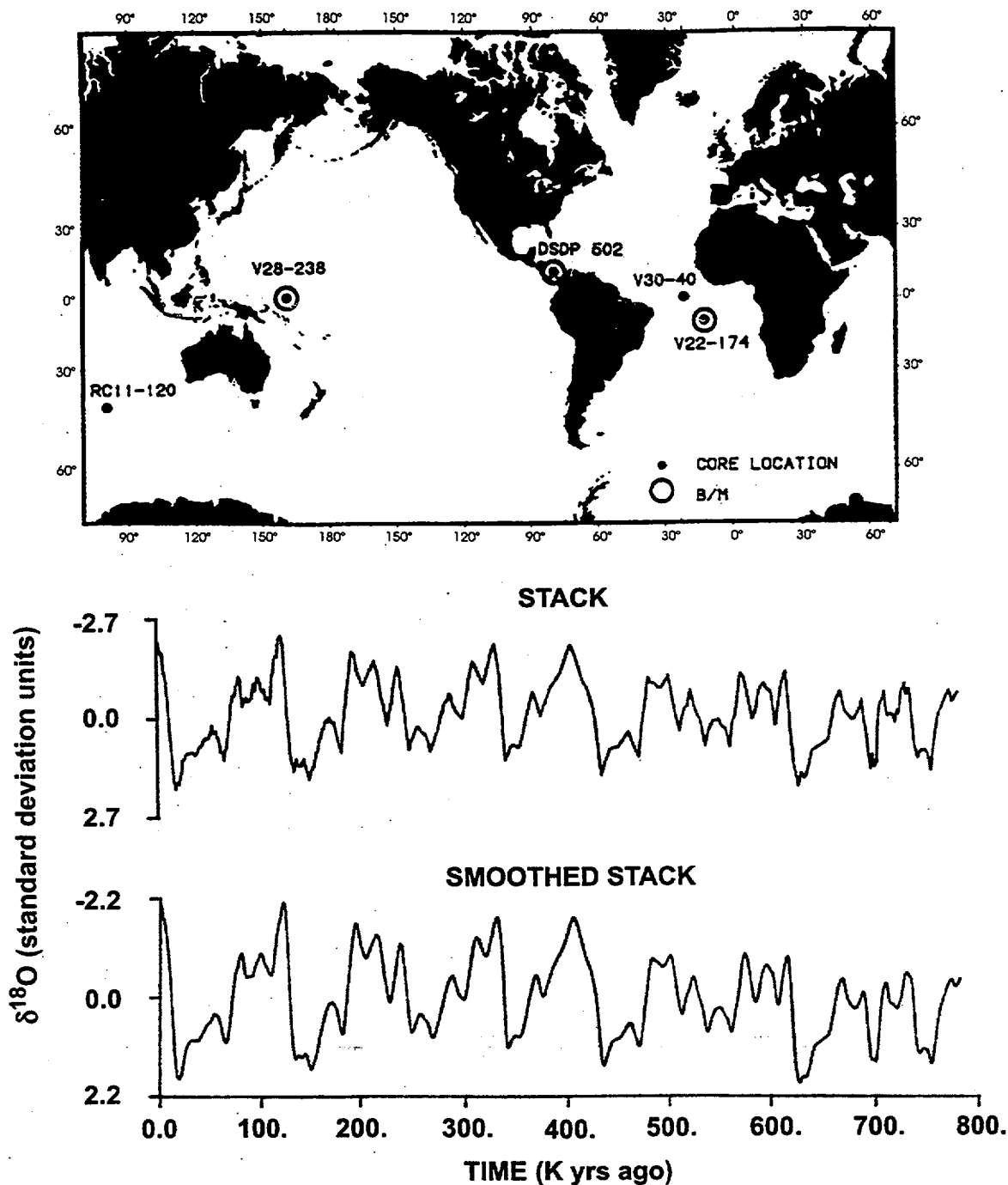
F4.2-5

Figure 4.2-5. A Graph Showing Past and Future Eccentricity



NOTE: Notice the eccentricity signature embedded within insolation is evident at the equator, but has an even larger signature at high latitudes.

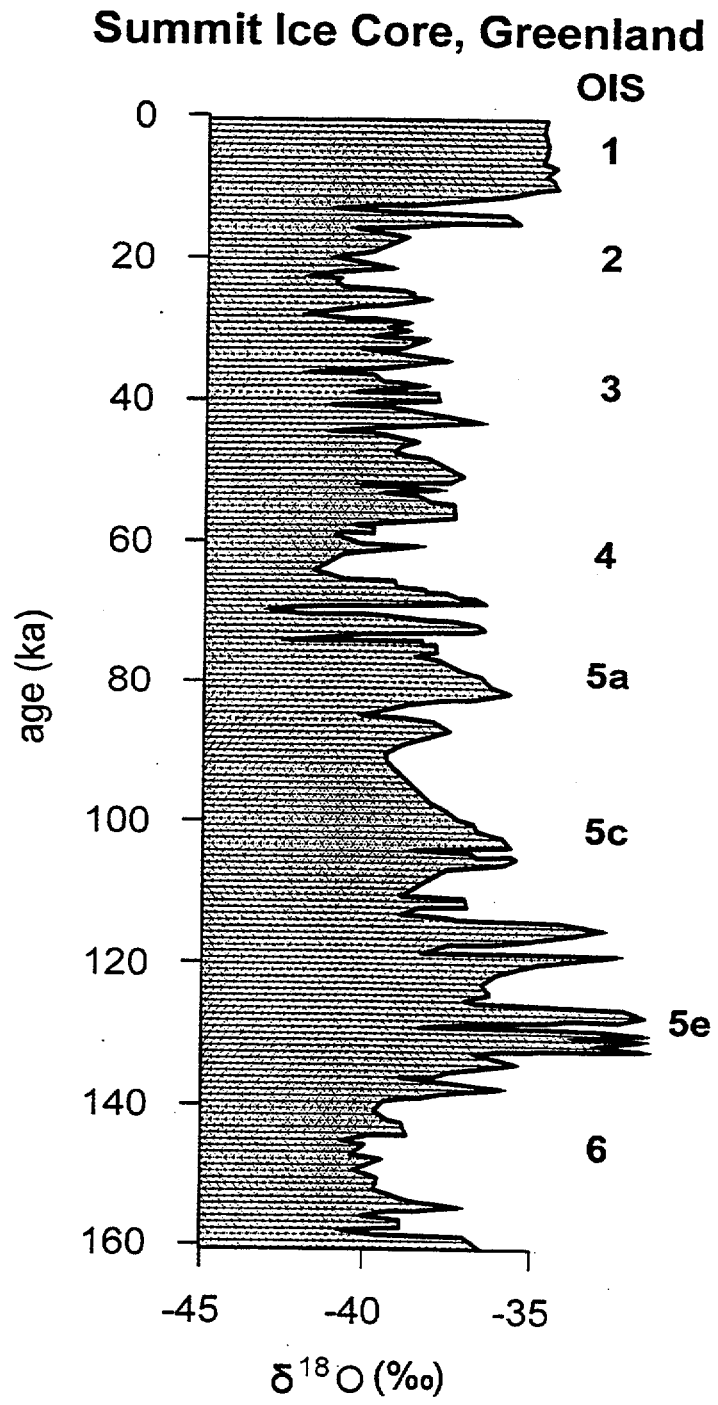
Figure 4.2-6. A Graph Showing Insolation Values for June and December at Different Latitudes and for the Last 500 k.y.



42-07.CDR.123.SITEDESC

NOTE: Map shows sites where marine cores were taken. The individual records were normalized and averaged to produce the "stack" record which was subsequently smoothed with a 9-point gaussian filter ("smoothed stack") to make the commonly used SPECMAP oxygen isotope curve for correlation and timing of Quaternary climate changes. (after Imbrie, Hays et al. 1984).

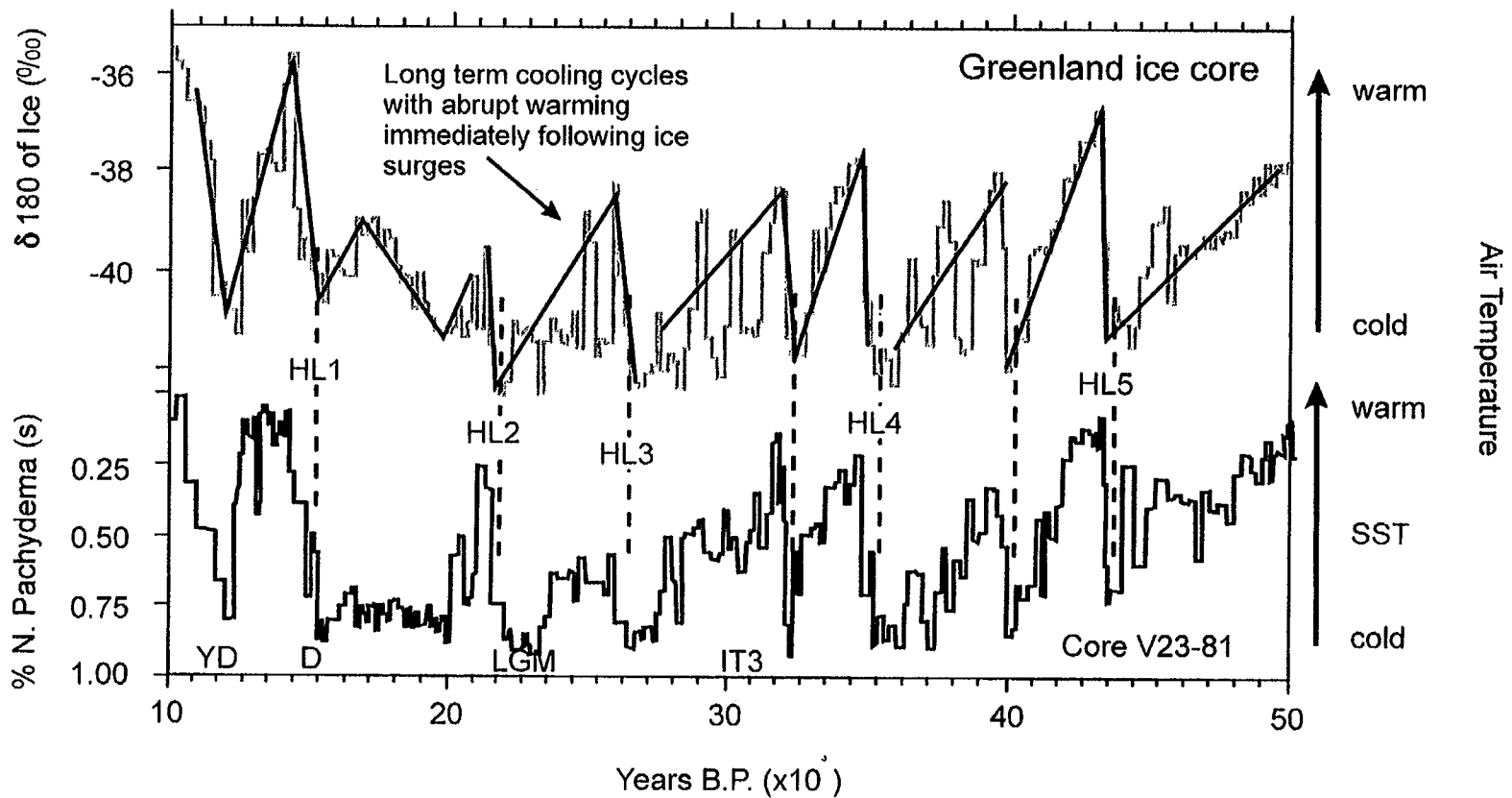
Figure 4.2-7. The SPECMAP (Spectral Mapping Project) Record of Oxygen Isotope Variations for the Past 800 k.y.



42-08.CDR.123.SITEDESC

NOTE: The fluctuations in oxygen isotopes mirror the oxygen changes from marine sediment cores and demonstrate the processes of isotope fractionation between the oceans and land as well as the global nature of climate change.

Figure 4.2-8. Record of Oxygen Isotopes in Water (Ice) Taken from the Greenland (Summit) Ice Core for the Past 160 k.y. (after GRIP members 1993)

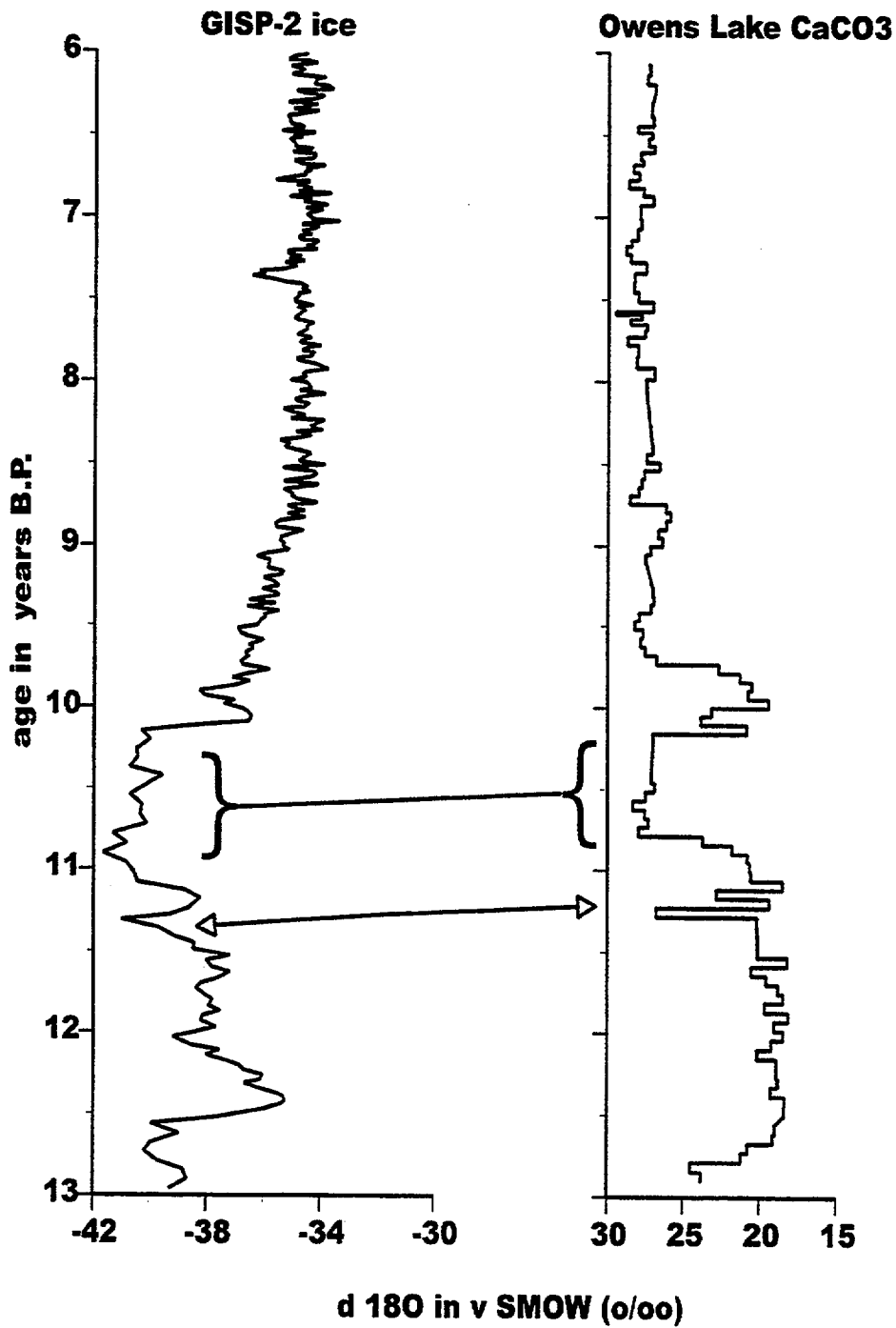


F4.2-9

42-09.CDR.123.SIIEDESC

NOTE: Greater abundance of the cold-water Foraminifera coincides with episodes of 18-O - depleted ice indicating extensive glaciation. Dashed tie lines mark Heinrich events or layers of sand in the core that were deposited by icebergs breaking off the ice sheet and entering the North Atlantic Ocean. This figure illustrates the close coupling of abrupt climate change in the glacial period atmosphere and the ocean. D (= Dryas) and YD (= Younger Dryas) are cold events in western European terrestrial pollen records. LGM (= Last Glacial Maximum) and HL (= Heinrich Layer) (after Bond et al. 1993).

Figure 4.2-9. The Greenland (GRIP) Ice Core Oxygen Isotope Record Between 10 ka and 50 ka and the Relative Abundance of *Neogloboquadrina Pachyderma* (Left Coiling = s) a Polar Foraminifera from the North Atlantic Sediment Core V23-81 (after Bond et al. 1993)



42-10.CDR.123.SITEDESC

Figure 4.2-10. Oxygen Isotope Records from Greenland (GISP-2) Ice Core and Owens Lake, California Showing Possible Millennial- And Sub-millennial-scale Correlations (tie lines between silhouettes) Between Lacustrine Environments at Owens Lake and Global Atmospheric Changes During the Late Glacial and Holocene Periods Between 6 ka B.P. and 13 ka B.P. (after Benson et al. 1997)

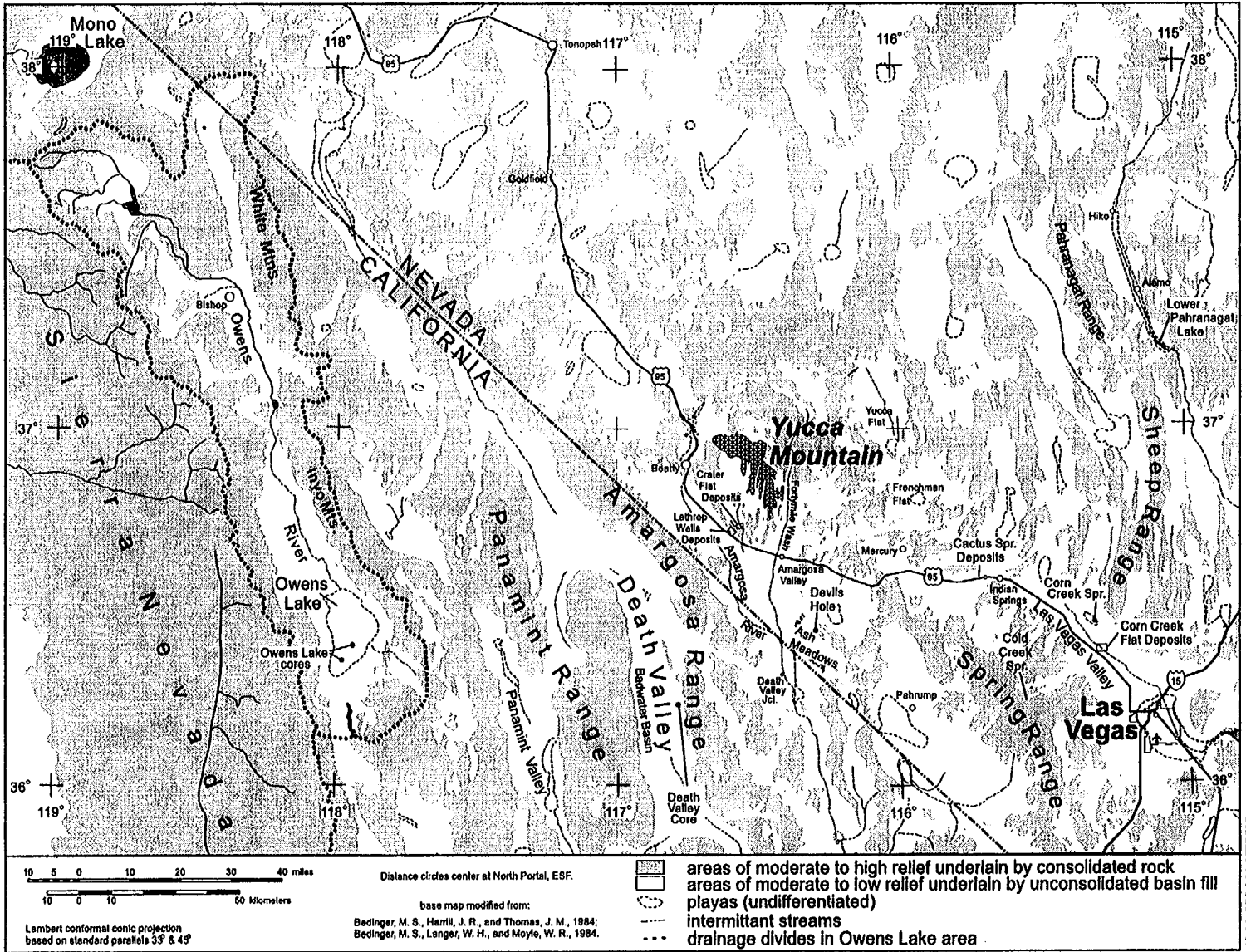
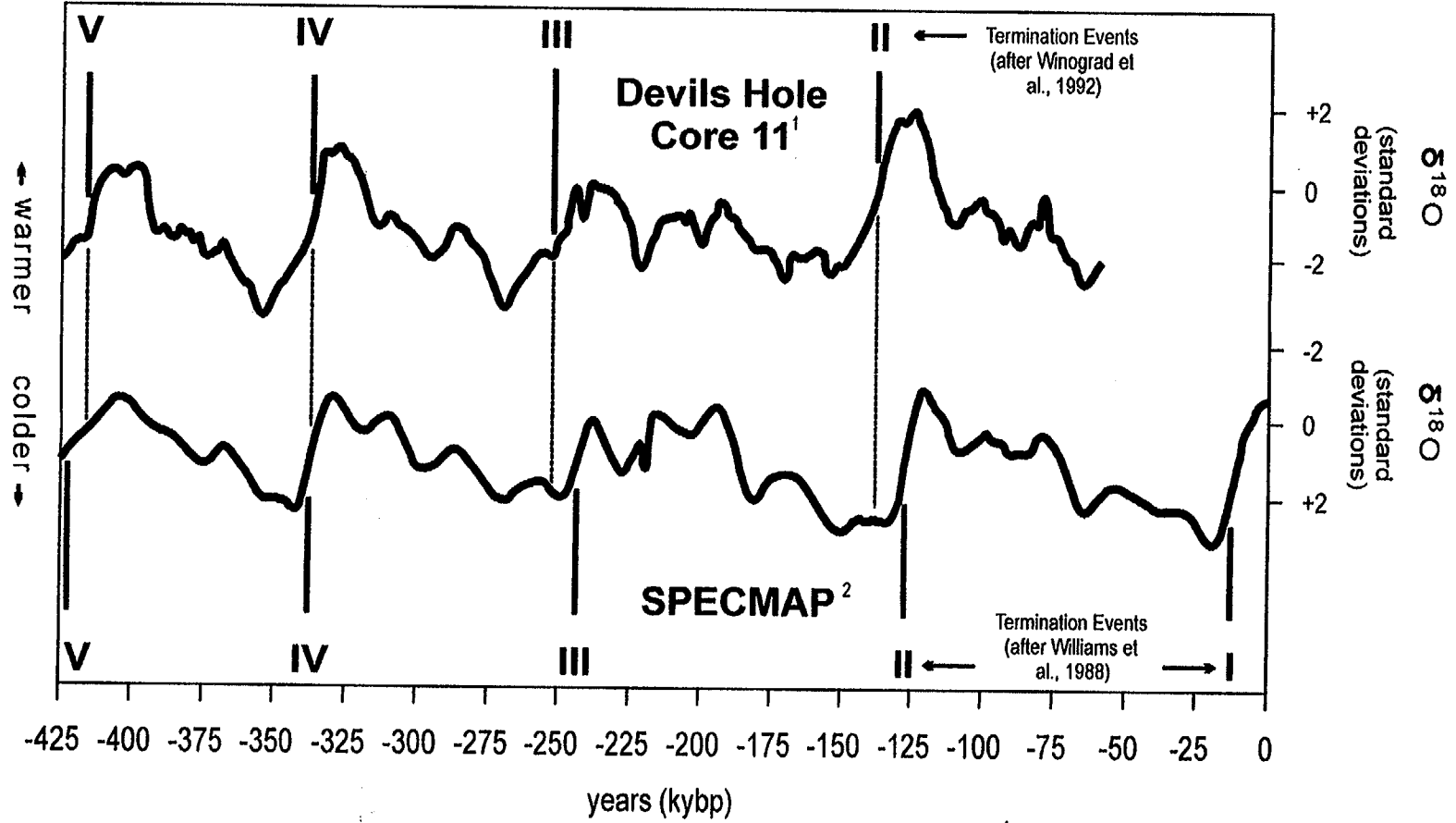


Figure 4.2-11. Index Map Showing Sites in the Yucca Mountain Area Discussed in the Text

Stable-Oxygen Isotope Records From Nevada and North Atlantic



¹ data after Winograd et al., 1992
² data after Imbrie et al., 1984

42-12.CDR.123.SHEDESC

Figure 4.2-12. Comparison of the $\delta^{18}O$ Record from Devils Hole to the Marine $\delta^{18}O$ Record (SPECMAP) (after Winograd, Coplen et al. 1992)

F4.2-12

Death Valley, CA, Core DV93-1

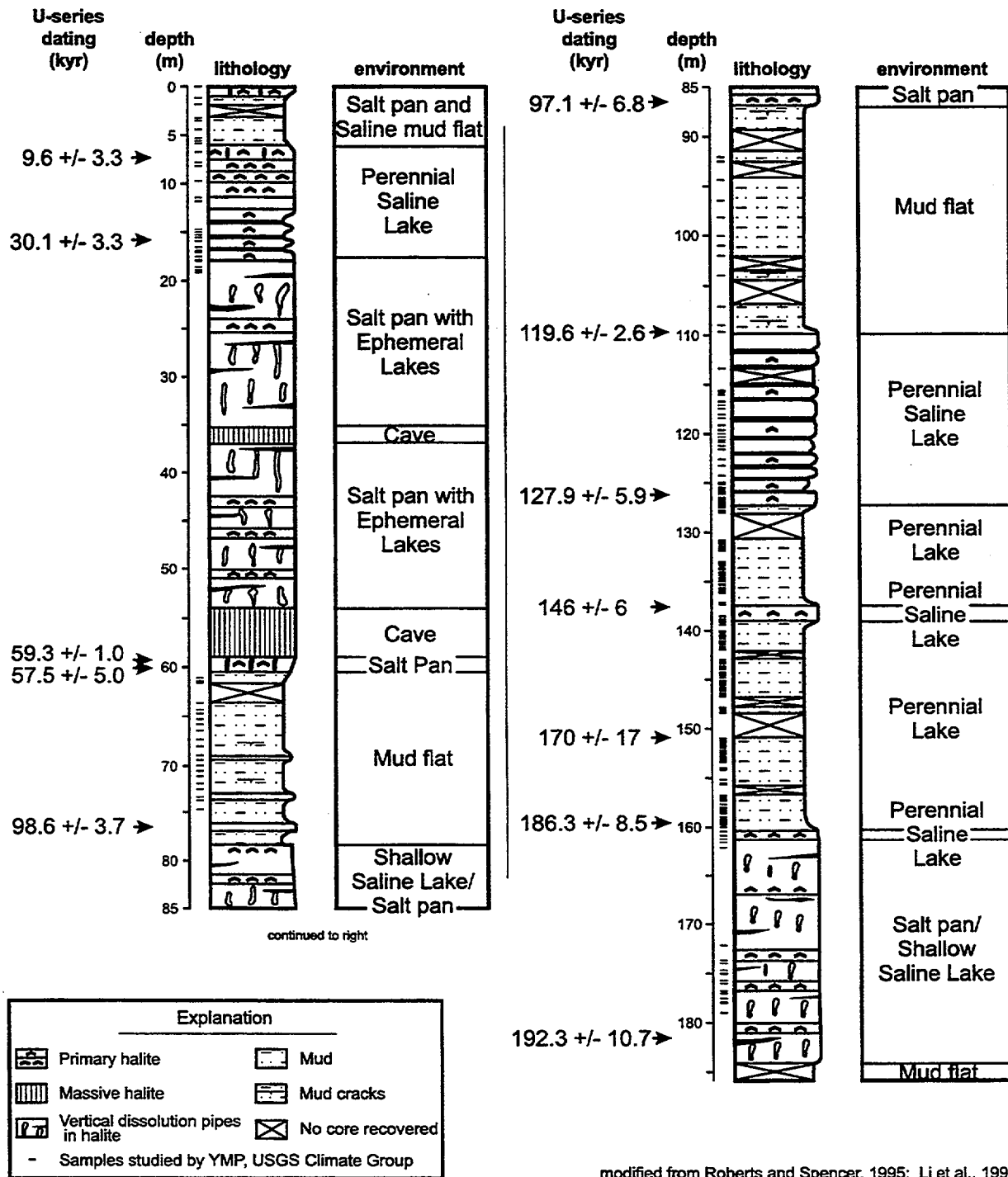
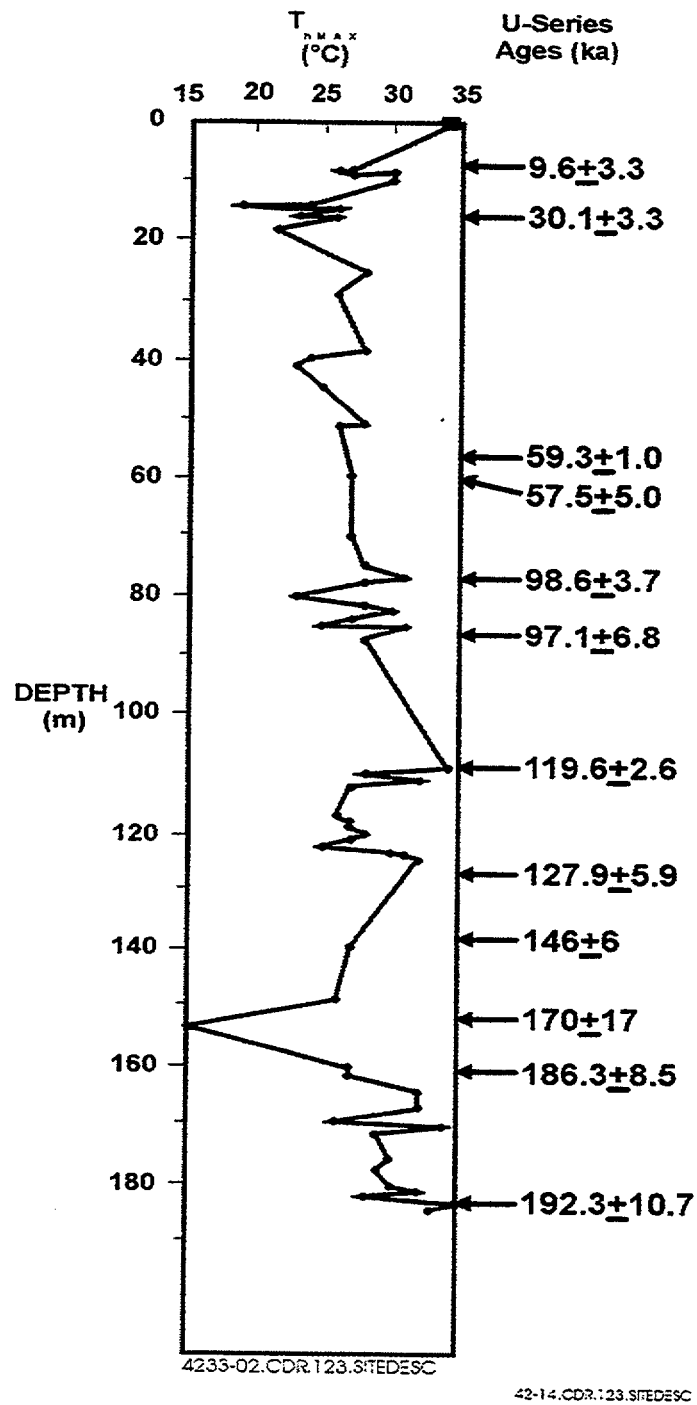
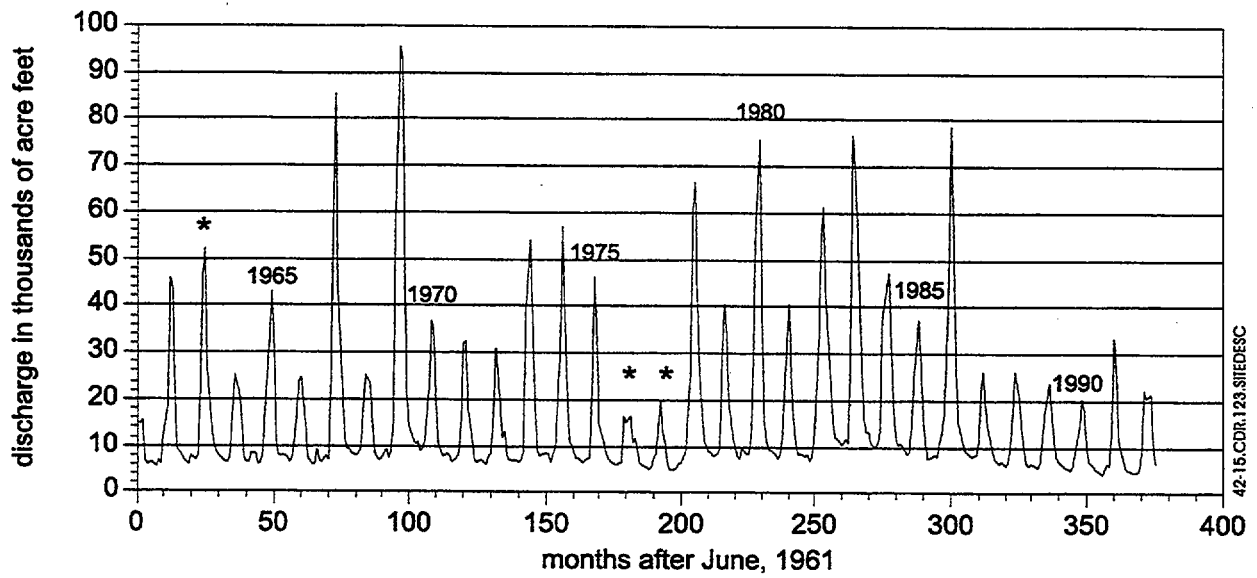


Figure 4.2-13. Lithology and Age Control for Death Valley, California, Core DV93-1 (after Roberts and Spencer 1995; Li et al. 1996)



NOTE: Maximum homogenization temperatures match the maximum brine temperatures during the crystallization of halite.

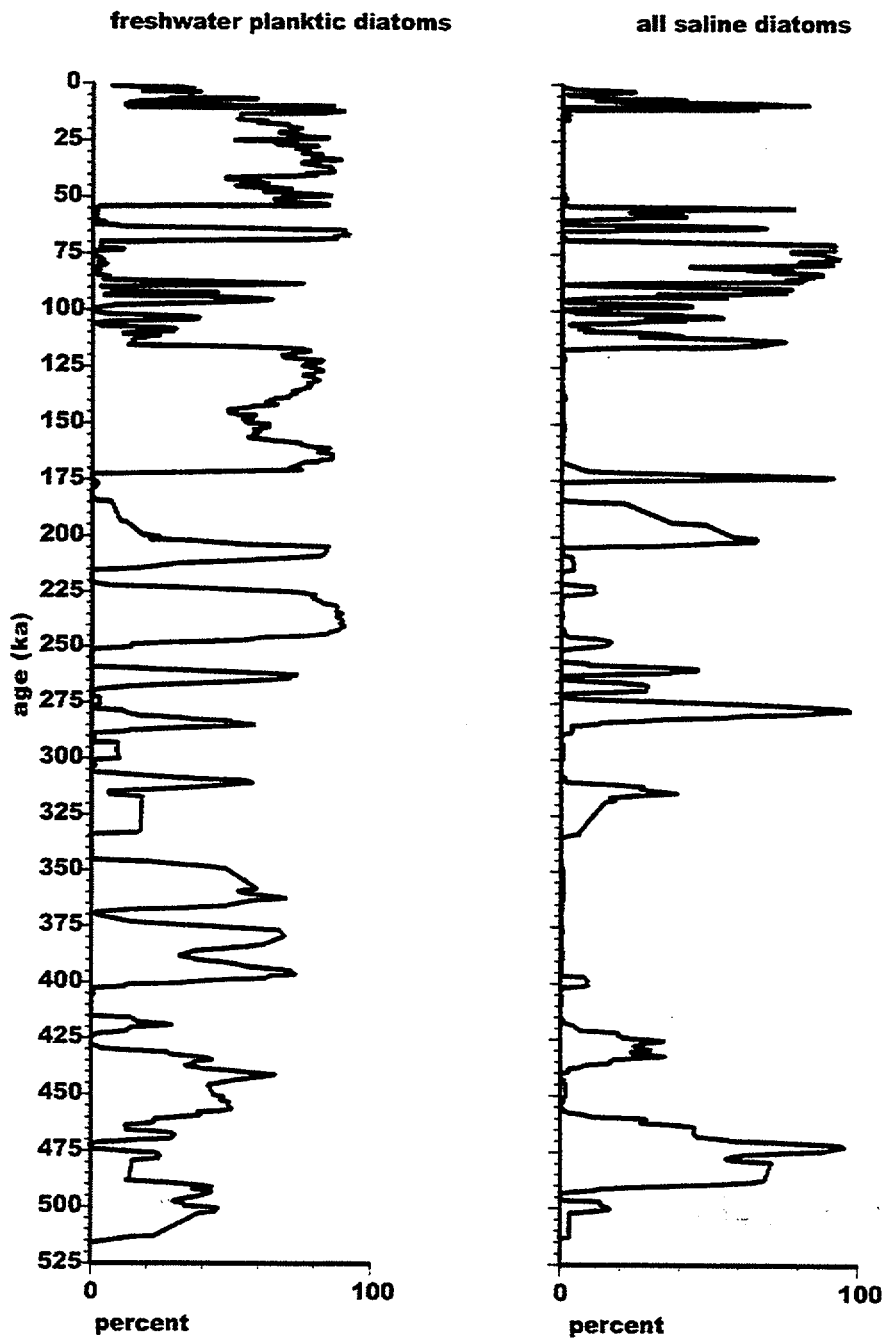
Figure 4.2-14. Maximum Homogenization Temperatures from Halite Fluid Inclusions from Death Valley Core DV93 Plotted Against Time and Sequence of Lacustrine Paleoenvironments Represented by Core Lithology and Lake Level Data (after Lowenstein et al. 1997)



* = years of high summer precipitation

NOTE: Data from California Department of Water Resources, Division of Flood Management. Asterisks indicate years of high summer precipitation that do not produce correspondingly high discharge in the Owens River.

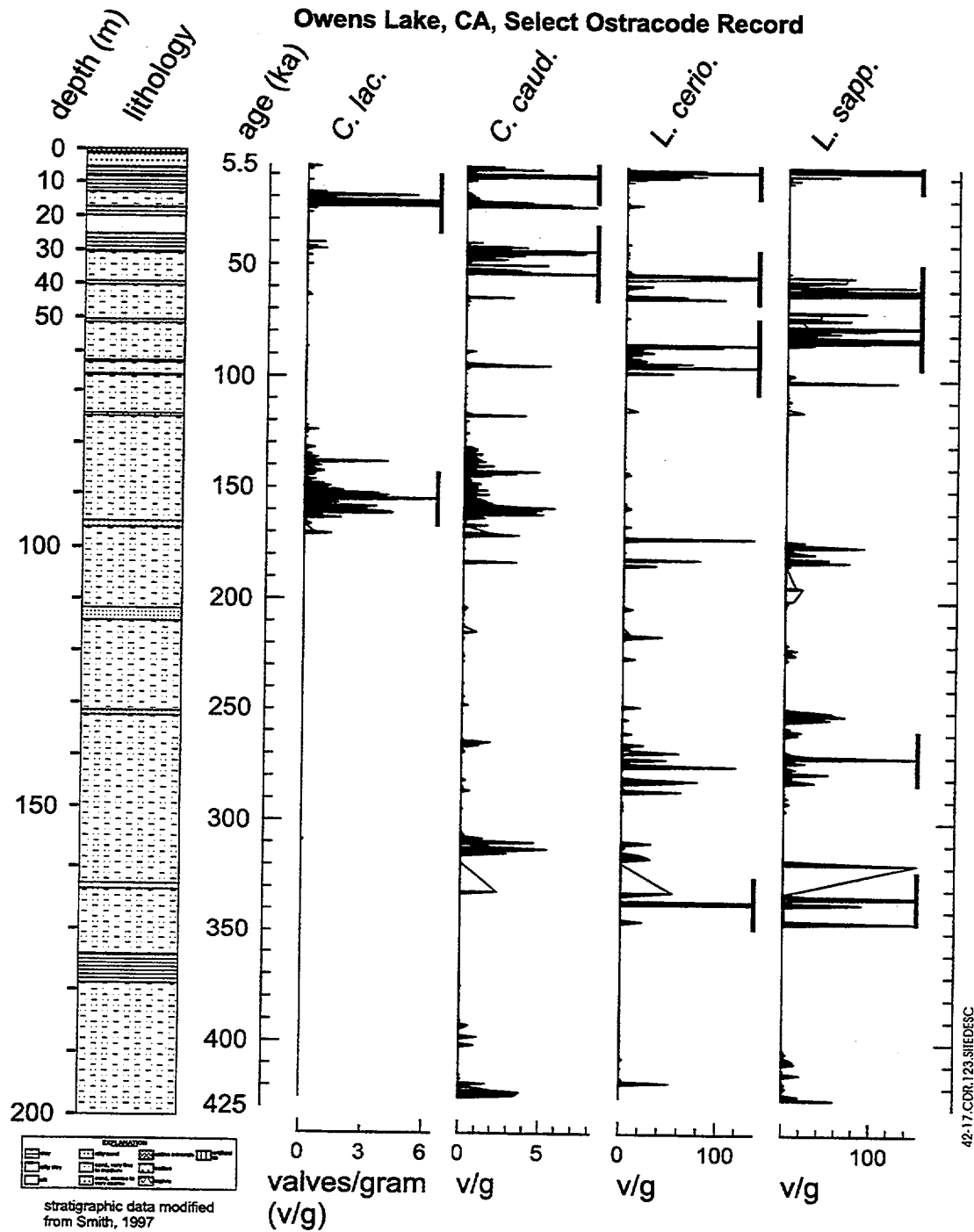
Figure 4.2-15. Annual Discharge (in thousands of acre feet) on the Owens River, California, between Long Valley and Tinemaha, California, from June 1961 through September 1992



42-16.CDR.123.STEDESC

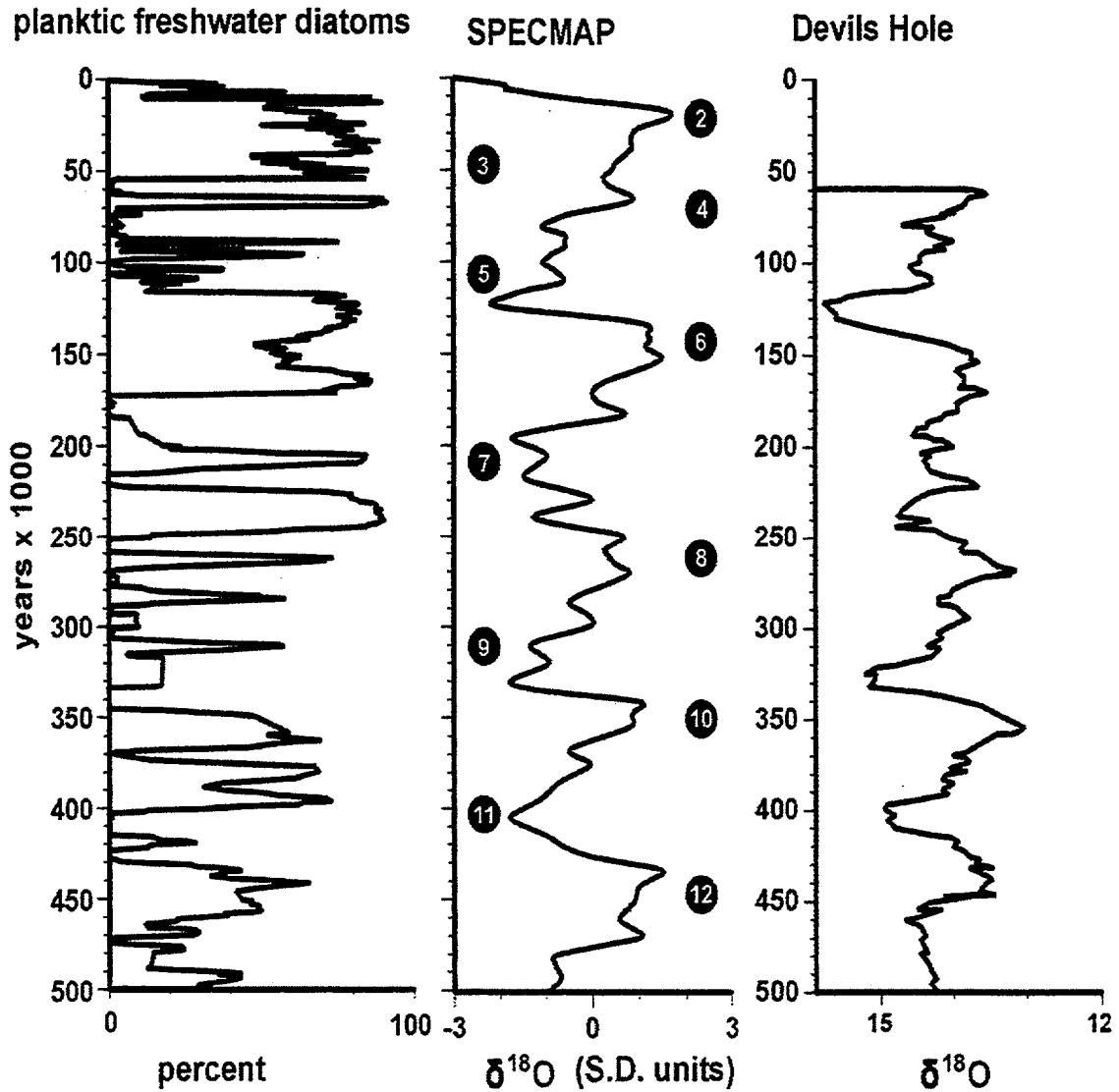
NOTE: The stratigraphic distribution of saline diatoms represents arid climates that approximate modern conditions. The distribution of freshwater planktic diatoms indicate a though-flowing fresh-water lake that spilled to basins downstream from Owens Lake. The freshwater planktic diatom profile documents periods during the past 525 k.y. when winter precipitation and mean annual temperatures were higher and lower respectively than today.

Figure 4.2-16. Principal Ecologic Groups of Diatoms in the Owens Lake Core for the Past 525 k.y.



NOTE: The ostracodes are aligned according to their salinity and hence climate preferences from fresh, cold and wet of the left (towards the stratigraphic column) to saline and dry on the right. *L. sappanensis* on the right lives in springs discharging onto the lake bed today.

Figure 4.2-17. Stratigraphic Distribution of Ostracode Species from the Owens Lake Core for the Past 400 k.y.

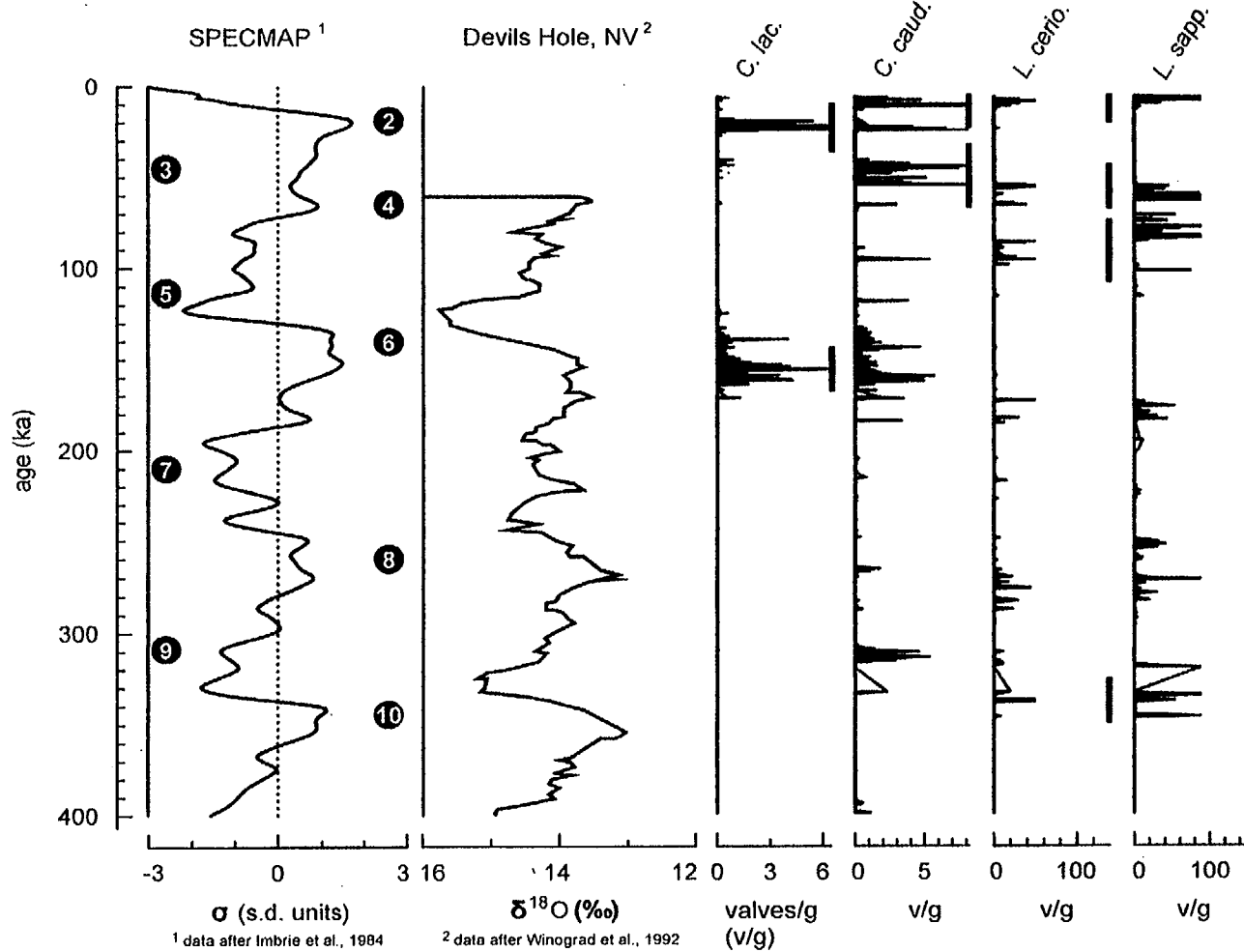


42-18.CDR123.STEDESC

NOTE: Even numbers in circles next to the SPECMAP profile identify the widely recognized oxygen isotope stages (OIS) that correspond to glacial periods; the odd numbers in circles identify the interglacial periods. Each number refers to a particular oxygen isotope stage. There is a general correspondence between large percentages of freshwater planktic diatoms and glacial periods represented by even-numbered OIS stages from the SPECMAP curve. Discrepancies in the correlation between the Owens Lake diatom record and the SPECMAP and Devils Hole oxygen isotope records may reflect the different chronological controls for the respective records or represent actual differences in the proxy climate records from these systems, or both.

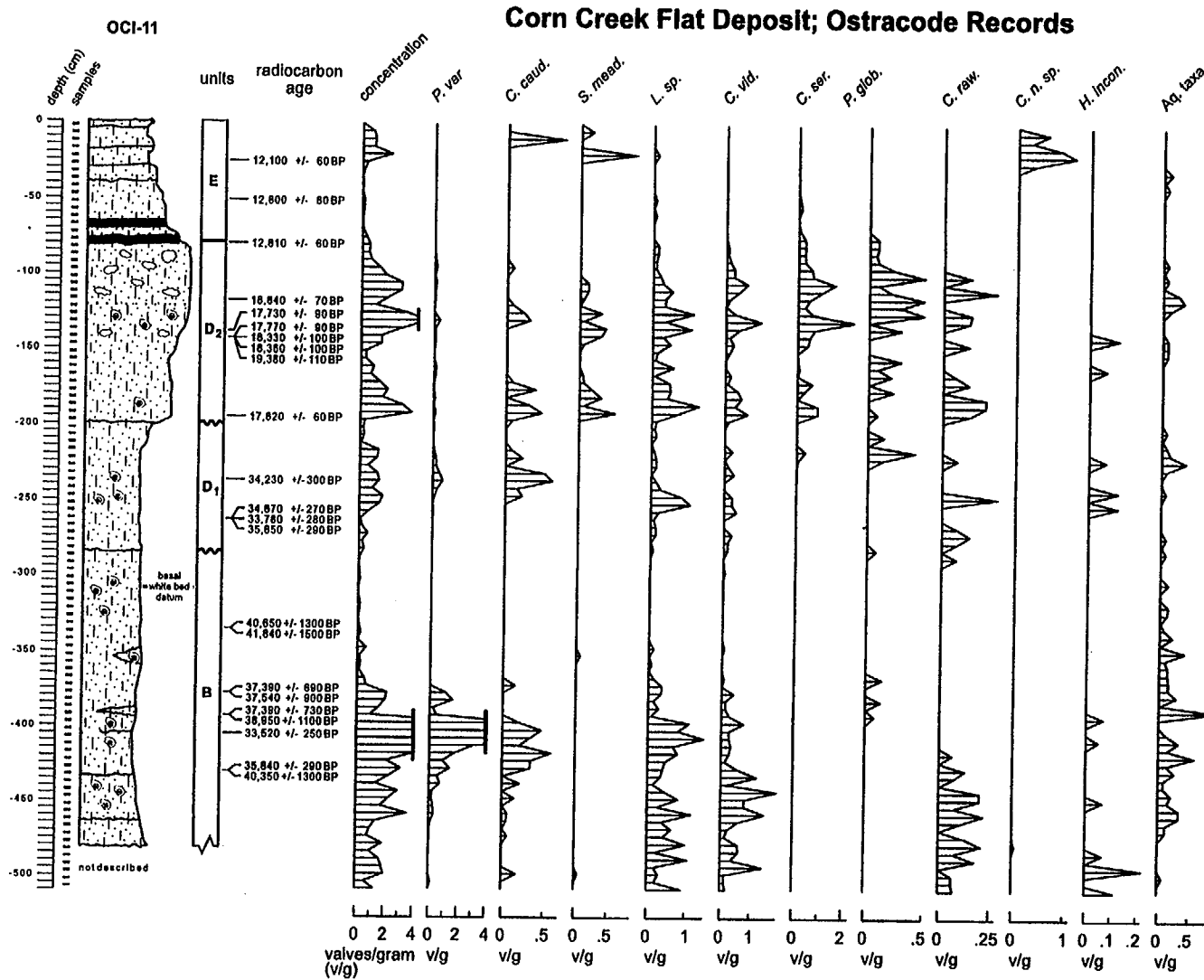
Figure 4.2-18. Stratigraphic distribution of Fresh-Water, Planktic Diatoms from the Owens Lake Core for the Past 500 k.y. Compared to the SPECMAP and Devils Hole Oxygen Isotope Records

Stable-Oxygen Isotope Records from North Atlantic and Nevada with Select Ostracode Records from Owens Lake, CA, cores OL 92-1, OL 92-2 & OL 92-3



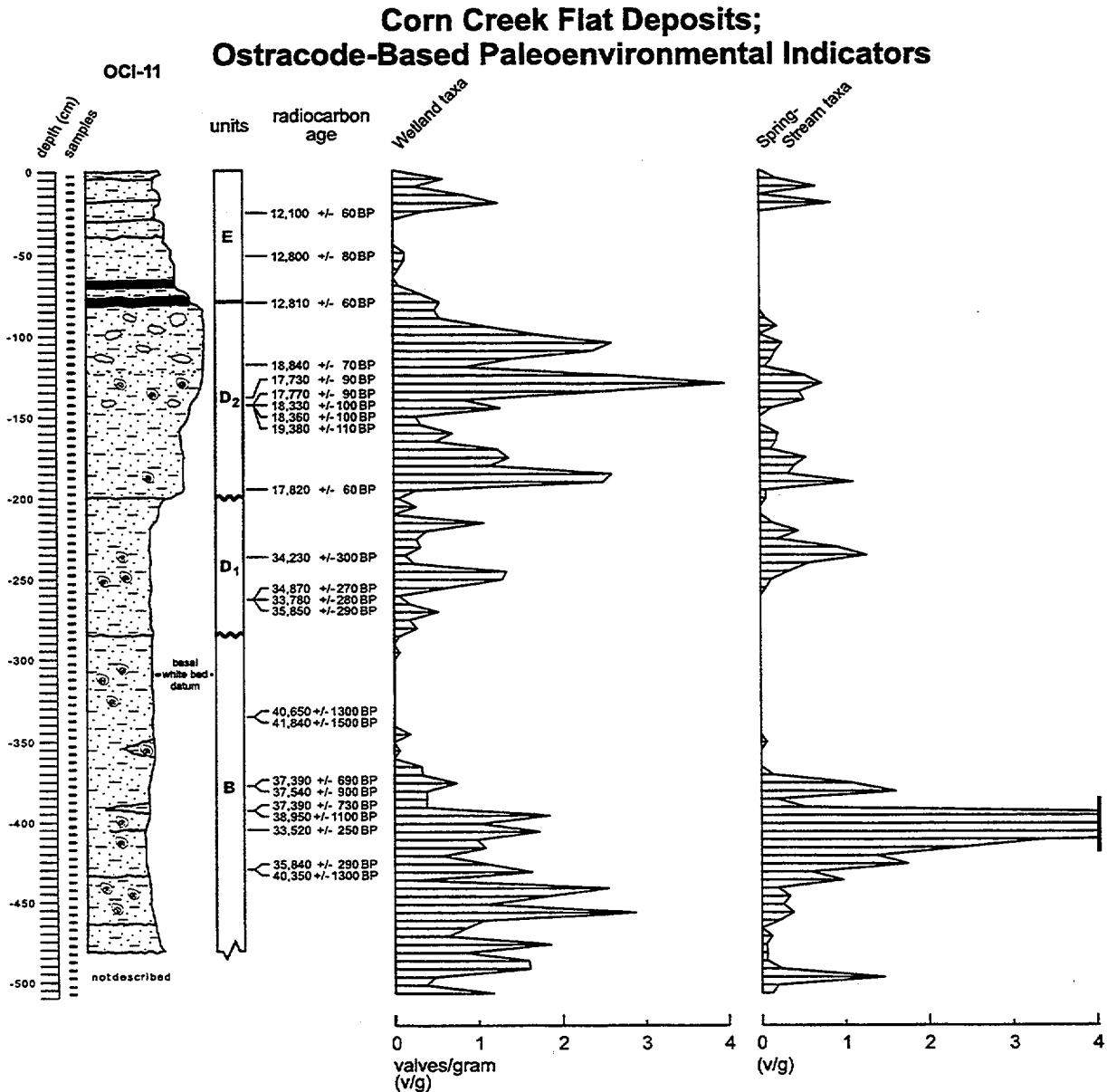
NOTE: Numbers in circles identify glacial and interglacial periods for the past 400 k.y. climate cycle.

Figure 4.2-19. Stratigraphic Distribution of Key Ostracode Species Compared to SPECMAP and Devils Hole Climate Records Based on Oxygen Isotopes



NOTE: Ostracode abundance expressed as number of adult valves per gram of sediment. Lithostratigraphic section shown on left of figure along with the key stratigraphic units established by Quade, Miffilin et al. (1995). Radiocarbon dates establish chronology for the section; see the text for discussion.

Figure 4.2-20. Graph Showing the Stratigraphic Abundance Profiles of Key Ostracode Species Found in Samples Collected from Section OCI-11 in the Las Vegas Valley



42-21.CDR.123.SITEDESC

Figure 4.2-21. Graph Showing the Ostracode Species Data Combined into Two Environmental Groups, Wetland Taxa (Those Taxa That Typically Live in Shallow Standing to Low Flow Environments Supported By Groundwater Discharge) and Spring Stream Taxa (Those Species That Commonly Live in Springs, Seeps, and Streams)

Topography, Outcrop Distribution, and Lithologic Section, Corn Creek Flat Deposits, NV

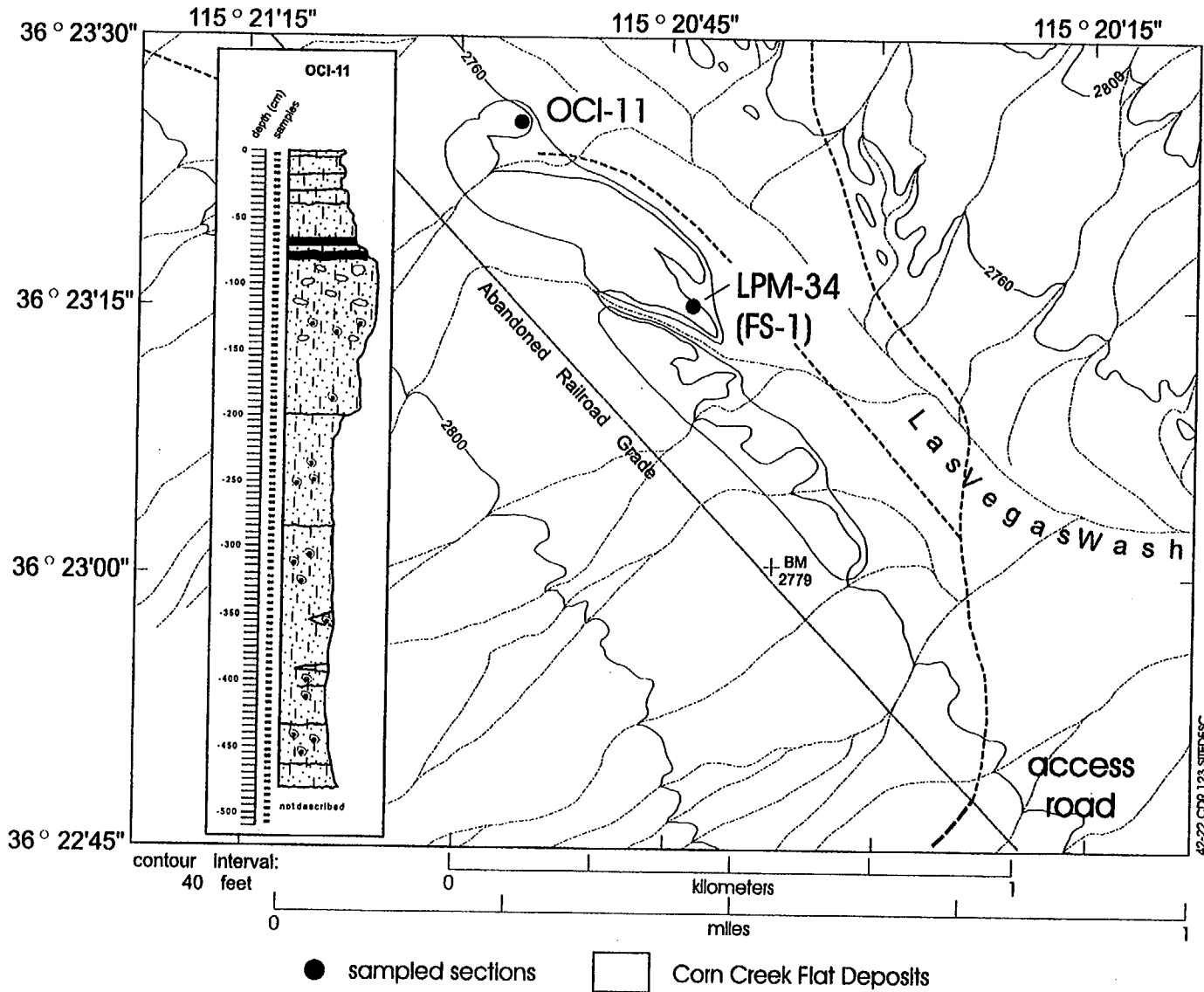
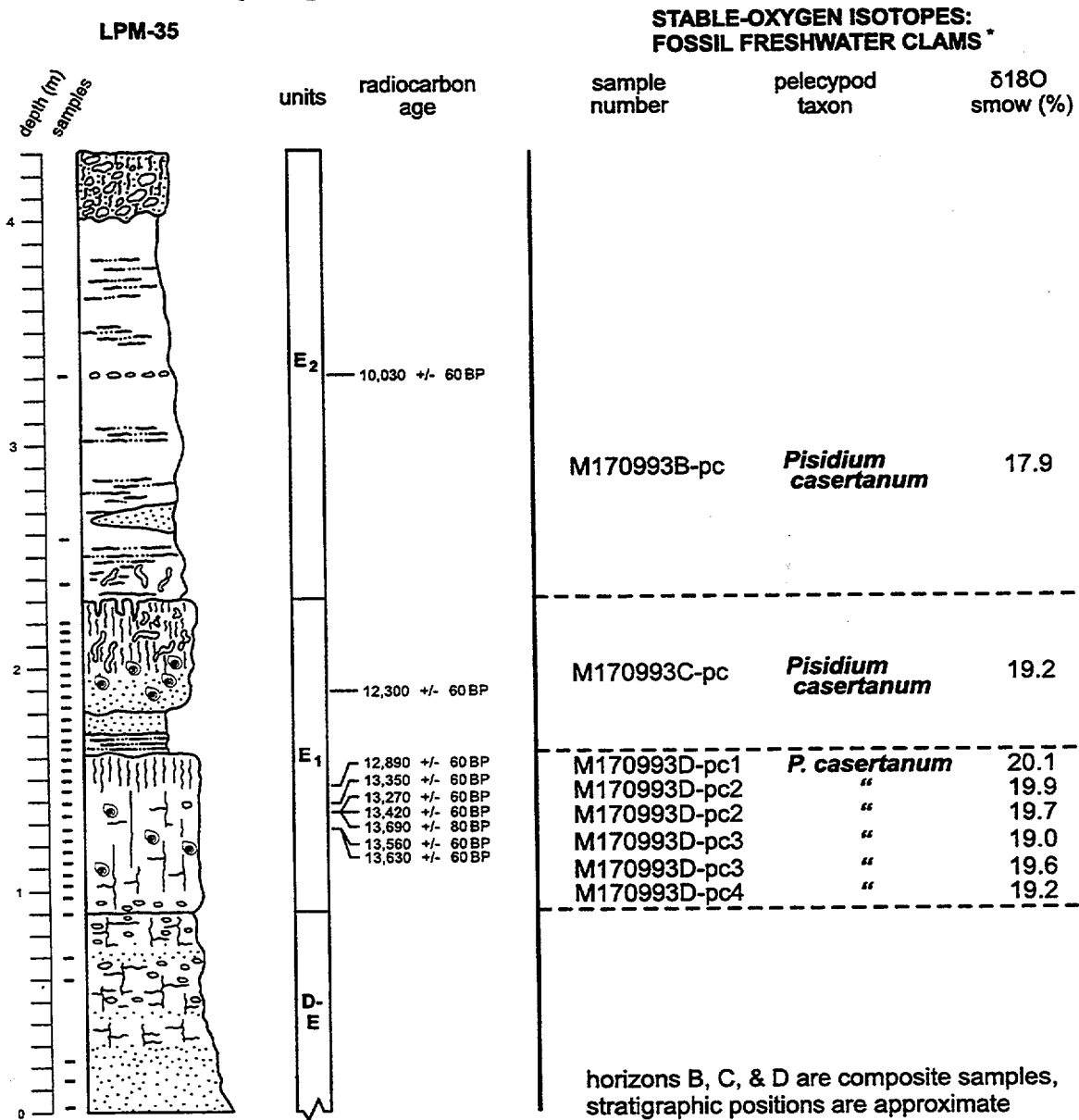


Figure 4.2-22. Locality Map Showing the Location of the Two Sections from the Las Vegas Valley Discussed in the Text

F4.2-22

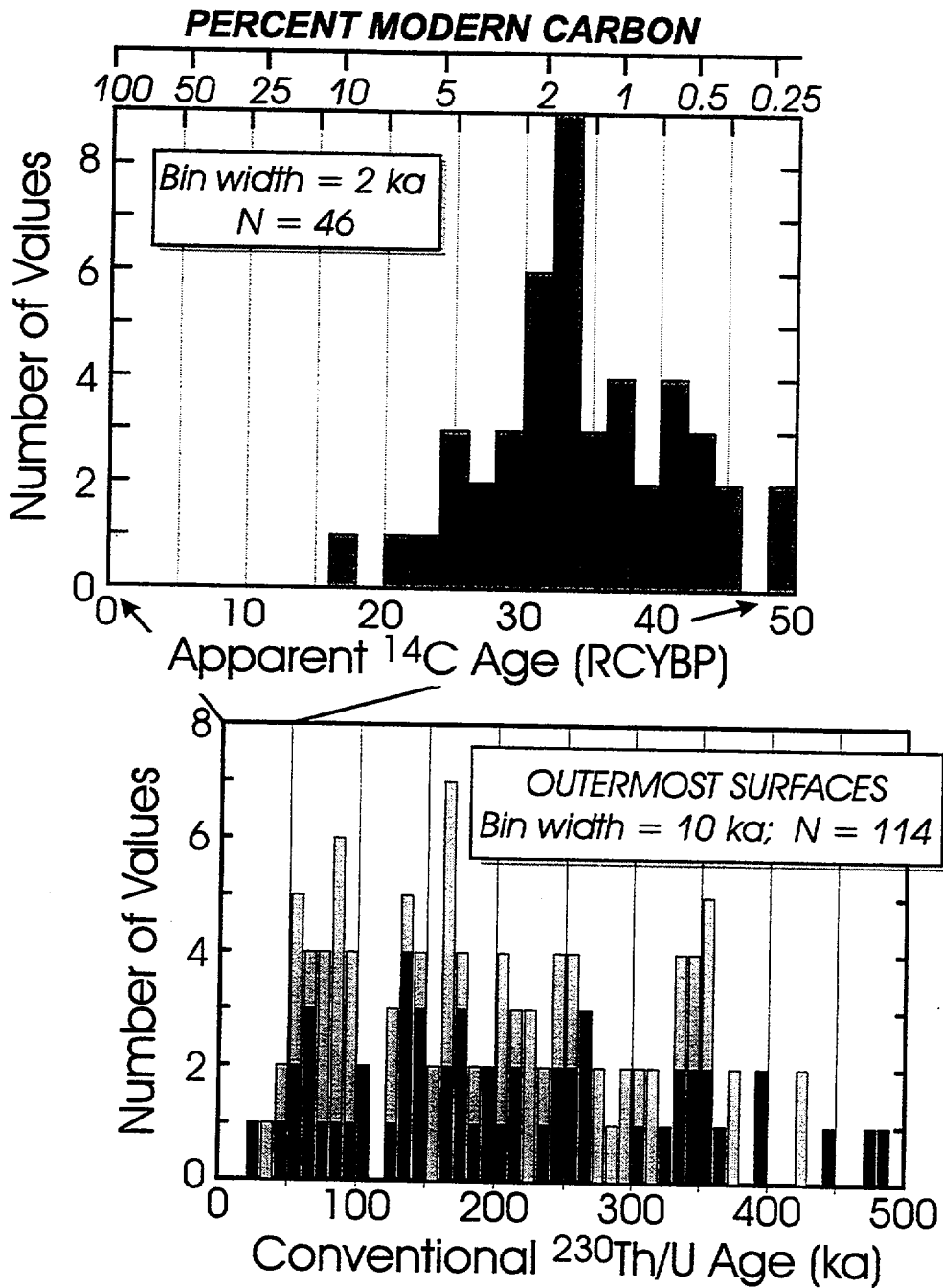
Cactus Springs Deposits; Stable-Oxygen Isotope Studies



* data from Sharpe et al. 1994.

NOTE: Stable isotope values (SMOW) and approximate stratigraphic position of the *P. casertanum*, a bivalve whose shell was the source of the isotope data.

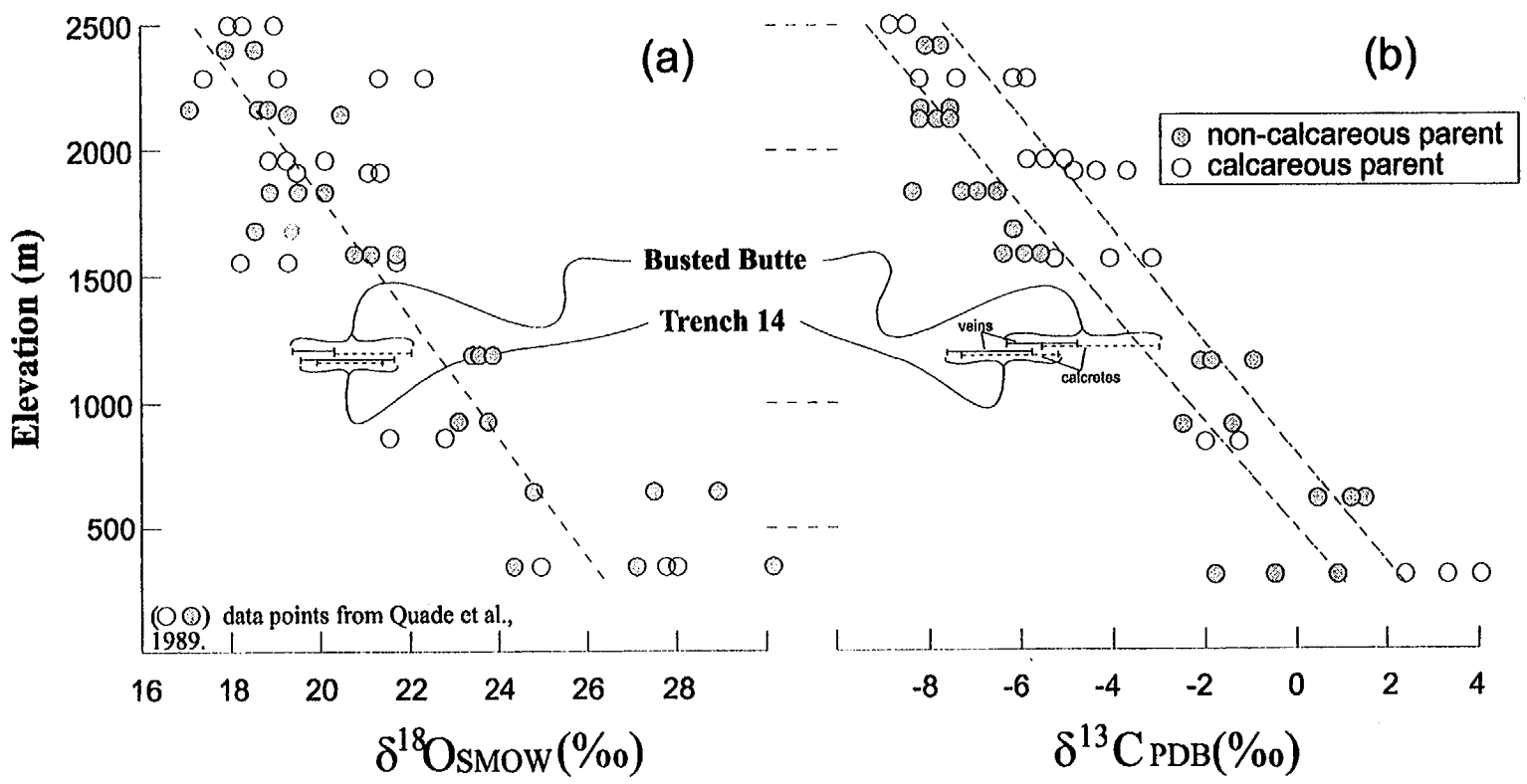
Figure 4.2-23. Graph Showing the Lithostratigraphic Section Measured just North of Cactus Springs, Nevada, Including the Stratigraphic Units Established by Quade, Mifflin et al. (1995).



42-24.CDR.123.SITEDESC

NOTE: U-series ages are shown for both lithophysal cavity (light bars) and fracture (dark bars) occurrences.

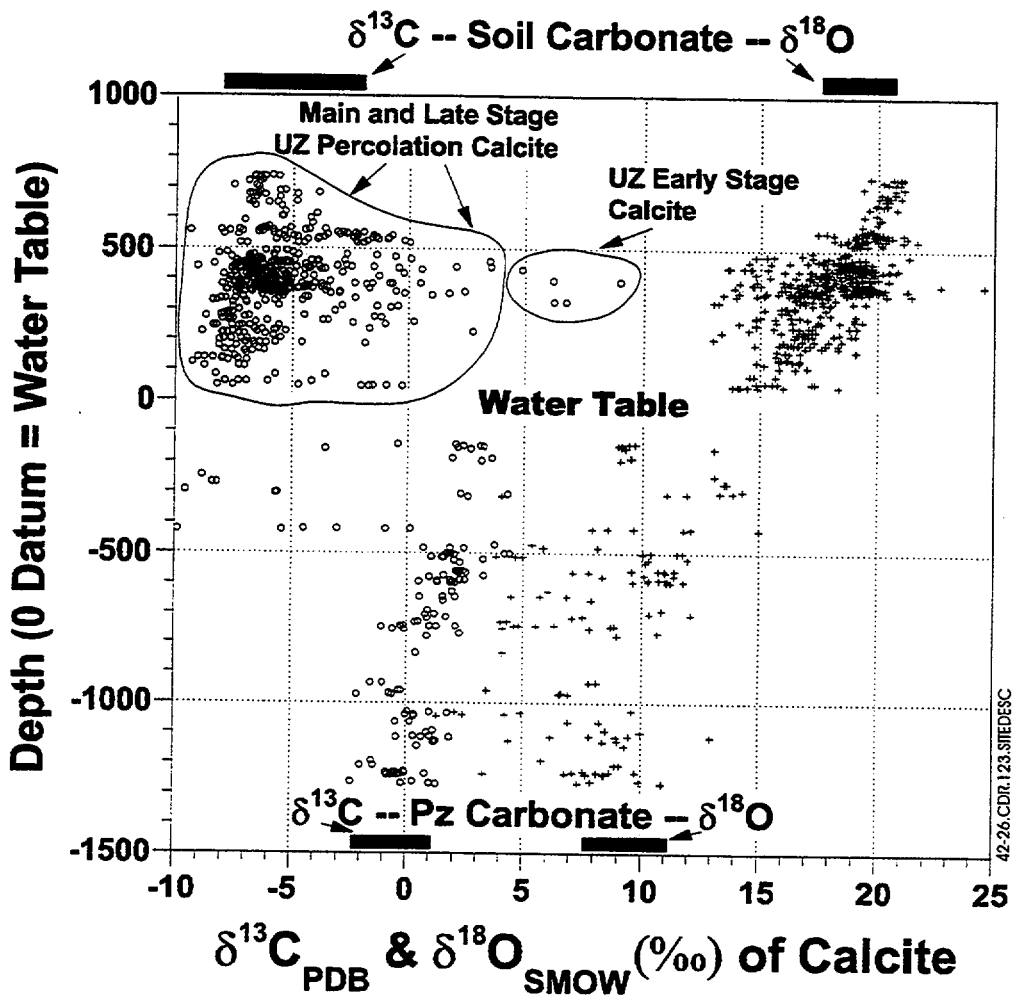
Figure 4.2-24. Histograms of Radiocarbon (from calcite) and U-series (from calcite and opal) Ages Obtained for Outermost Mineral Surfaces



42-25.CDR.123.SITEDESC

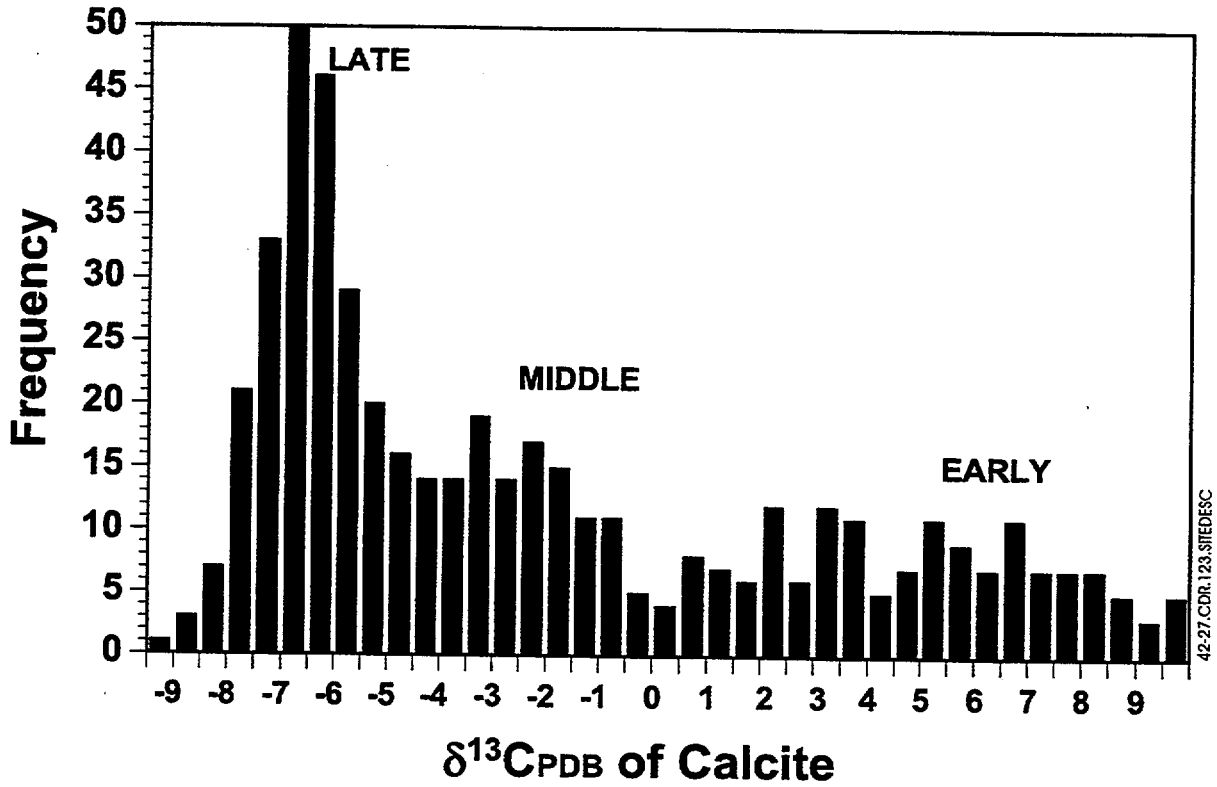
Figure 4.2-25. Stable O(a) and C(b) values of Pedogenic Carbonate from Southwestern Nevada as a Function of Elevation (after Quade, Cerling et al. 1989)

F4.2-25



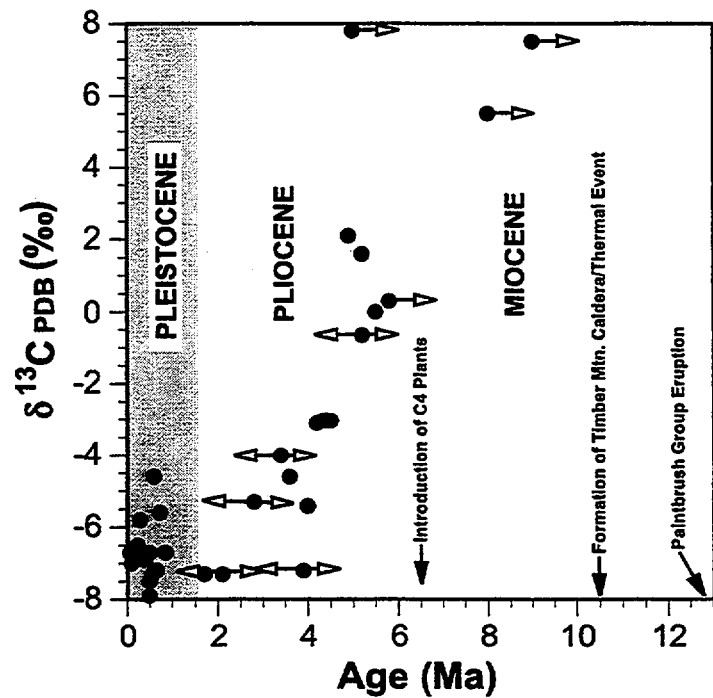
NOTE: The ranges of isotopic compositions of calcite in the thin soils occupying the surface of Yucca Mountain are shown, as are the isotopic compositions of calcite in equilibrium with ground waters of the underlying Paleozoic marine sedimentary section (Whelan, Vaniman et al. 1994). Fields of percolation-deposited calcite and early, probably non-percolation calcite are also outlined.

Figure 4.2-26. Plot of the $\delta^{13}\text{C}$ (circles) and $\delta^{18}\text{O}$ (crosses) Values of Calcite Versus Depth Below, or Height Above, the Water Table



NOTE: The data displays modes that are generally correlative with the Early, Middle, and Late paragenetic stages described in the text.

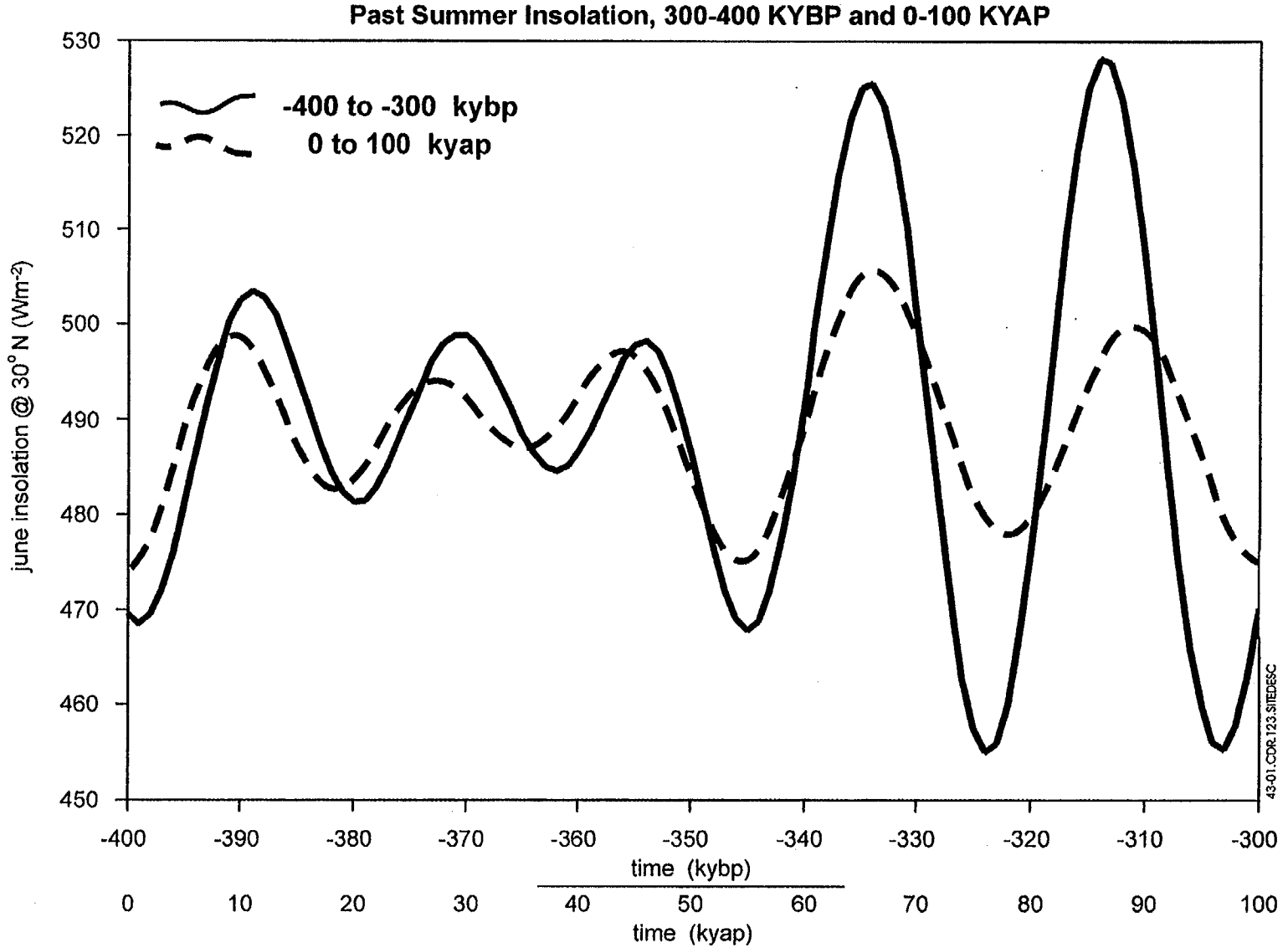
Figure 4.2-27. Histogram of Unsaturated Zone $\delta^{13}\text{C}$ Values from Calcite Occurrence in the Exploratory Studies Facility Tunnel and from Drill Core



42-28.CDR.123.SITEDESC

NOTE: Data from calcite samples bracketed by dated material are marked by double arrows and calcite samples underlying dated material (i.e., having a minimum age) are marked by single arrows to the right.

Figure 4.2-28. Secondary Calcite $\delta^{13}\text{C}$ (‰) Values Plotted Against Ages (m.y.) Determined by U/Pb or $^{230}\text{Th}/\text{U}$ Techniques (Whelan and Moscati 1998; Neymark et al. 1998)

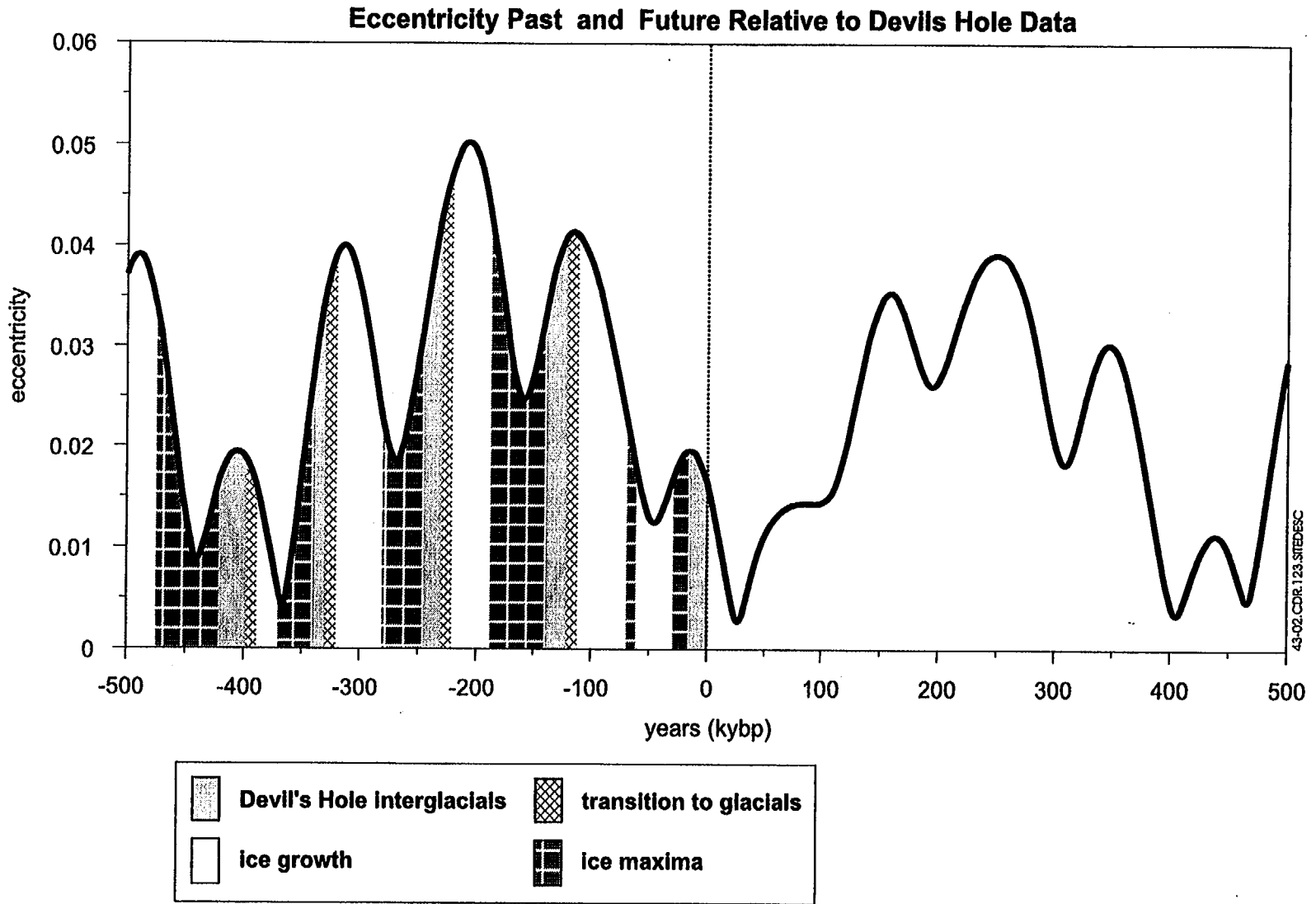


NOTE: Climate for the next 100 k years is being compared with the period 400-300 ka as a possible analog. See text for further discussion.

Figure 4.3-1. Graph Comparing June Insolation at 30°N Latitude for the Periods 400-300 ka and 0 to 100 kyap

F4.3-1

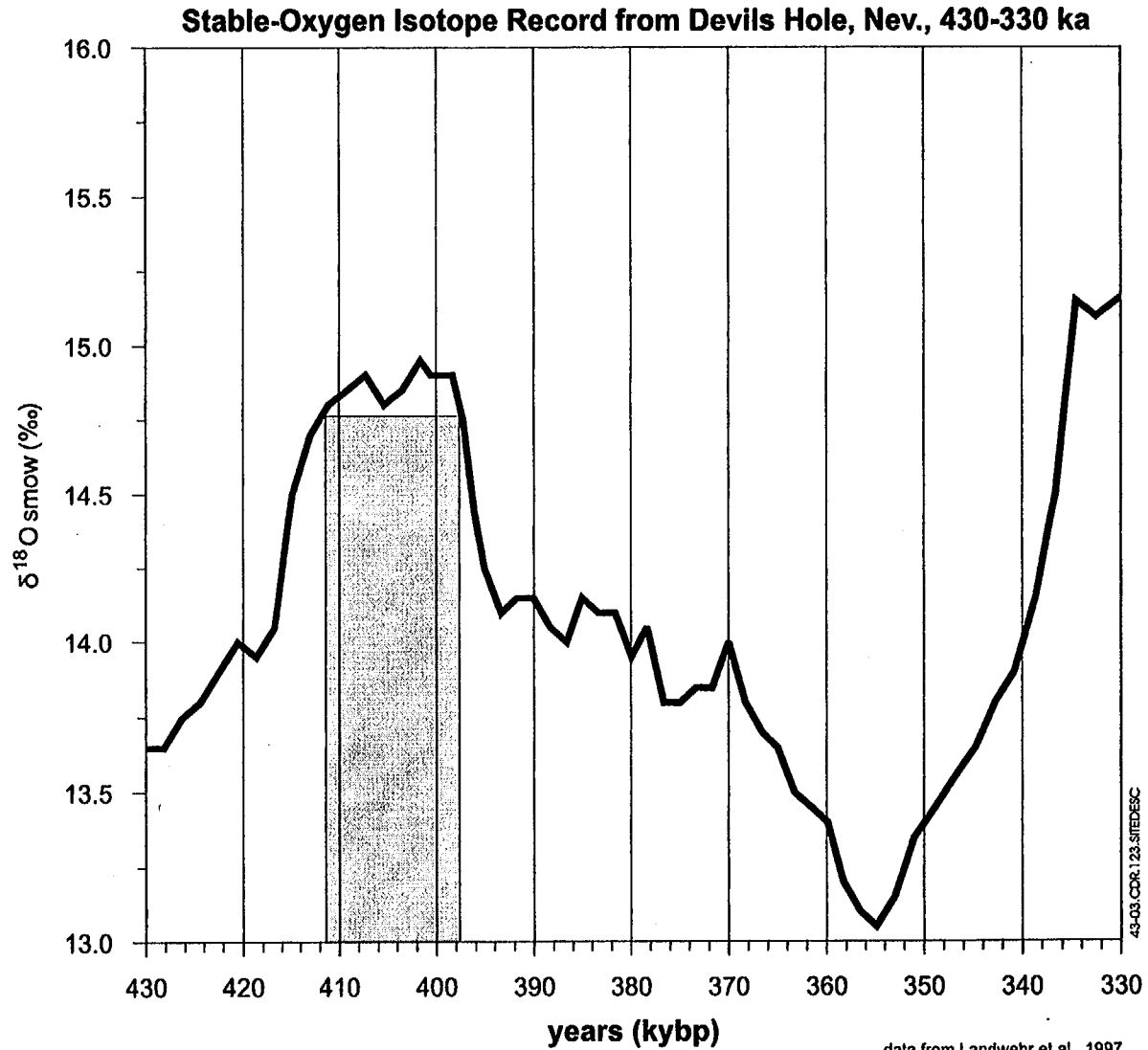
43-01.CDR.123.SITEDESC



NOTE: Presuming a similar relation for the future the interglacials will occur at high eccentricity and full glacial periods at low eccentricity.

Figure 4.3-2. Graph Showing the Timing of Interglacials, Glacial Transitions, Ice Growth, and Ice Maxima Based on the Devils Hole Chronology, Excepting the Last 50 k.y. Where Data Comes from SPECMAP

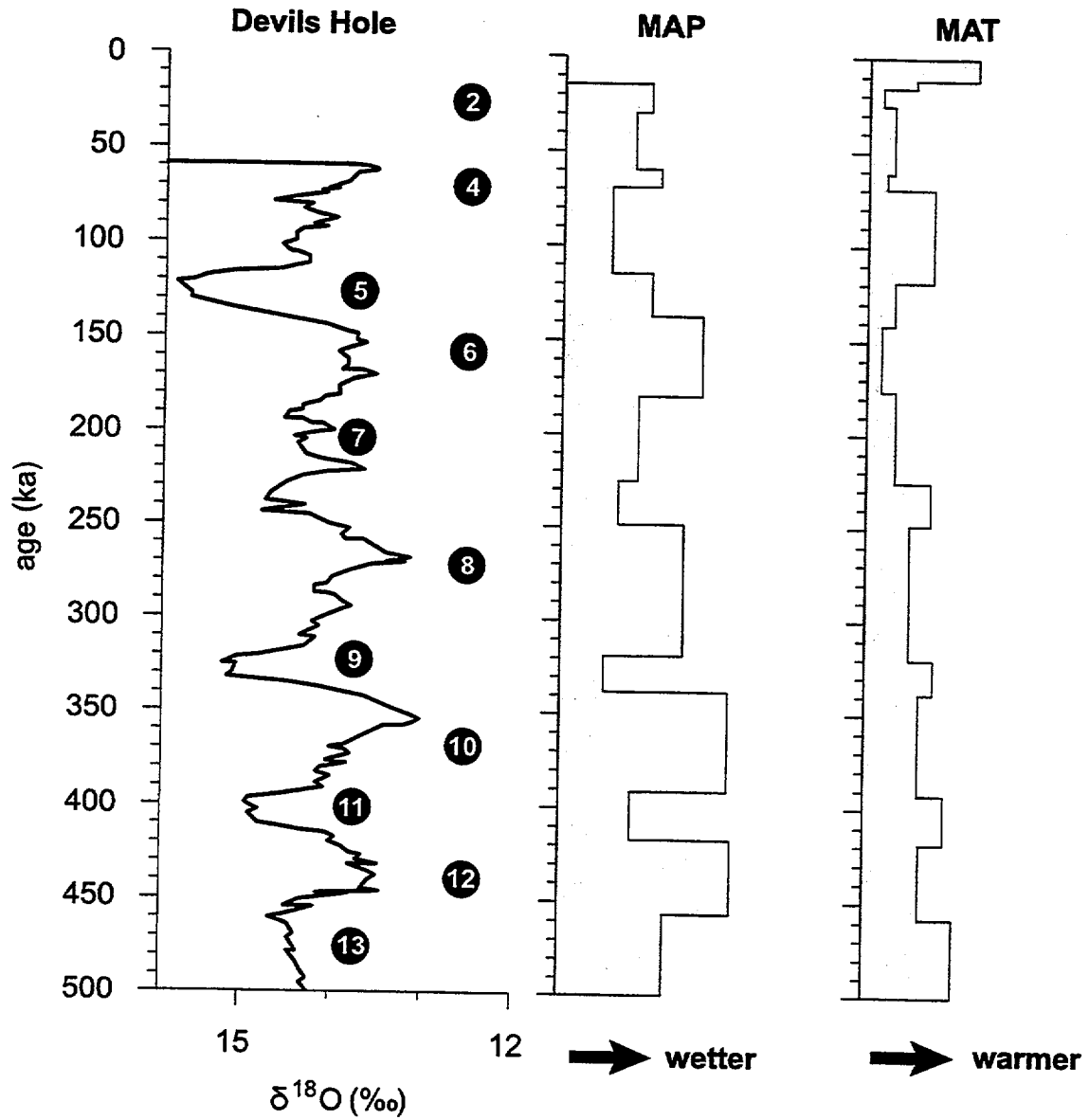
F4.3-2



NOTE: The shaded rectangle identifies the OIS -11 interglacial and the lower values to the right of the rectangle the OIS-10 glacial. (430 ka to 330 ka, an interglacial and glacial period that may serve to bound climate conditions for the next 50 kap.) See text for further discussion.

Figure 4.3-3. Graph Showing the Delta Oxygen-18 Values from Devils Hole for the Period 430 ka to 330 ka

Estimates of Mean Annual Precipitation and Mean Annual Temperature based on Devils Hole Core 11 Stable-Oxygen Isotopic Data



data from Landwehr et al., 1997

43-04CDR.123.SITEDESC

Figure 4.3-4. Climate Summary Graph Showing Relative Levels of MAP and MAT Based on All Climate Proxy Data, Primarily Diatoms, Ostracodes, Pollen, Plant Macrofossils from Packrat Middens, and Stable Isotope Data

5. HYDROLOGIC SYSTEM

5.1 SURFACE WATER HYDROLOGY

This section presents information to characterize the surface water hydrology of the Yucca Mountain vicinity and surrounding region. The hydrologic data described in this section focus on characterization of surface water runoff and streamflow occurrence and quantities in and around Yucca Mountain. Surface water quality data collection efforts and selected surface water chemistry information are also presented. These data help establish baseline (boundary) conditions for supporting other site characterization efforts, such as: studies of infiltration in the unsaturated zone; studies of past and possible future climate changes; paleohydrologic studies; evaluation of surface water/groundwater chemistry relationships; age dating of subsurface waters to assess subsurface percolation processes and rates; and unsaturated-zone modeling and synthesis. The information contained in this section relates to information presented in the following subsections: 3.4.4, Paleoenvironmental History of Yucca Mountain; 3.4.5, Erosion at Yucca Mountain and Vicinity; 5.3.4.1, Site Infiltration; and 6.2.4, Chemical and Isotopic Composition of Surface Water.

Quality Assurance Controls—Yucca Mountain Site Characterization Project (YMP) work summarized in this section comes under the control of the *Quality Assurance Requirements and Description* (DOE 1997b). Some of the information presented and discussed, however, was developed outside of the YMP and has been included here through examination of the hydrological literature. Thus, the quality assurance status of the data in this section is determined by the activities and reports from which they were synthesized. To determine the Q status of a particular data set, interested readers should consult the source document cited in the text.

5.1.1 Surface Water Bodies and Drainage Areas

Yucca Mountain is located in the Amargosa River drainage basin, a closed basin with Death Valley at the terminus (Hunt et al. 1966). The area drained by the Amargosa River and the surrounding drainage system features are depicted in Figures 5.1-1 and 5.1-2. Streamflow from Yucca Mountain can flow from local drainages to the Amargosa River and then to Death Valley. Since the Amargosa River and its tributaries are ephemeral streams, except where spring discharge flows into the channel system for short distances (Malmberg and Eakin 1962; Walker and Eakin 1963), flow rarely occurs throughout its entire reach. Water is lost to infiltration and evaporation as streamflow moves downstream.

5.1.1.1 Amargosa River System

The ephemeral streams on Yucca Mountain are tributary to the Amargosa River, the largest drainage basin of Death Valley. The eastern slope of Yucca Mountain drains via Yucca Wash, Drill Hole Wash, and Dune Wash (also known as Busted Butte Wash) to Fortymile Wash (Figures 5.1-3 and 5.1-4). Fortymile Wash spreads out into a distributary system in the Amargosa Desert and joins the Amargosa River about 18 km north of Death Valley Junction, California (Figure 5.1-3). An unnamed ephemeral channel in Crater Flat collects drainage from the western slope of Yucca Mountain. This channel also collects drainage from the southern slope of Yucca Mountain, and it then drains to the Amargosa River near its confluence with Fortymile Wash.

Jackass Flats, where support facilities for Yucca Mountain site characterization studies and other Nevada Test Site projects are located, is drained by Topopah Wash (Figure 5.1-4). Topopah Wash flows into the Amargosa River in the Amargosa Desert.

As the Amargosa River flows southward through the Amargosa Desert, the tributary Carson Slough joins the channel system (Figure 5.1-1). Carson Slough drains spring flow from the Ash Meadows regional groundwater discharge area in the eastern portion of the Amargosa Desert. The Amargosa River channel flows along the western side of the Franklin Lake Playa (also known as Alkali Flat), a discharge area for the regional groundwater flow system (Figure 5.1-1).

The Amargosa River drainage course passes through the small community of Tecopa, California, continues southward, and then turns to the northwest to enter the southern end of Death Valley. The channel continues northerly through Death Valley until it terminates in the central portion of Death Valley. Lakes have formed in Death Valley after significant streamflow runoff has flowed down the Amargosa River (Grasso 1996). Tributary inflow from the surrounding mountains and valleys occurs to the Amargosa River along its entire length.

Channels are formed in the alluvial material by erosion and deposition during flash flooding. Large floods alter channel characteristics over great distances. Smaller floods alter channel characteristics along short stretches. The current channel characteristics are some combination of when the last large flood and the last several small floods occurred.

Several flood-potential studies and indirect measurements contain data pertaining to channel characteristics in the Yucca Mountain area. In general, channel slopes are steeper in the headwater portion of the channels. Channel cross-sectional area generally increases downstream. Active channels with enough capacity to contain smaller floods are contrasted with larger channels that are formed by more infrequent large floods. Estimates of channel roughness, often characterized using a Manning roughness constant (n), are generally estimated to be in the range of $n \approx 0.030$ to 0.055 . Bedrock constrictions, that have the potential to backup flood waters and inundate previously dry areas, are found in the Amargosa River drainage, but are situated away from the Yucca Mountain area. Flat areas in tributary valleys are subject to inundation when large floods exceed channel capacity.

Christensen and Spahr (1980) documented ephemeral channel characteristics of Topopah Wash and its tributaries in Jackass Flats in their flood potential study. Forty seven cross-sections were field surveyed in the Topopah Wash drainage basin above Little Skull Mountain. Distances above the lowest part of the streambed in the cross-section were used in their computations. Selected cross-sections were displayed in graphical format (Christensen and Spahr 1980, Figure 7). The area, width, and maximum depth of the wetted channel for each cross-section were tabulated for the estimated 100-year, 500-year, and maximum potential floods. Slopes of the channel bottoms, used to estimate the slope of the energy-grade line in their slope-conveyance computations, were estimated for each cross-section from topographic contours on a map. Channel-roughness Manning constants (n) for each cross-section were estimated based on the author's engineering judgement. They documented ranges of estimated values of n for the main channel of Topopah Wash (0.030 to 0.050), and for flood plain of Topopah Wash (0.030 to 0.055).

In another flood potential study, Squires and Young (1984) documented ephemeral channel characteristics of Fortymile Wash and its tributaries, Yucca Wash, Drill Hole Wash, and Dune Wash (Busted Butte Wash) in the Yucca Mountain area. Cross-sections of the stream channels were field surveyed, including seven along Fortymile Wash, five along Yucca Wash, eleven along Drill Hole Wash, and nine along Dune Wash. Detailed altitudes across the surveyed cross-sections were not tabulated in the report, but selected cross-sections were displayed in graphical format (Squires and Young 1984, Figures 14 through 17). Altitudes in the cross-section figures were labeled as approximate and were probably computed from published topographic maps. The area, width, and maximum depth of the wetted channel for the each cross-section were tabulated for the estimated 100-year, 500-year and regional maximum floods. Longitudinal profiles along the four surveyed ephemeral channels were graphically shown in Figure 2 of Squires and Young (1984). Slopes of the channel bottoms, used to estimate the slope of the energy-grade line in their slope-conveyance computations, were not documented. Manning n constants for the various cross-sections were estimated based on the author's engineering judgement. They documented ranges of estimated values of n for Fortymile Wash (0.032 to 0.045), and for Yucca Wash, Drill Hole Wash, and Dune Wash (0.030 to 0.055).

Bullard (1986, Table 7; 1991, Table 5) documented estimated basin slopes for small drainages in the Drill Hole Wash drainage basin. Basin slopes were found to range from 40.3 to 268 m/km. Bullard used the basin slopes in probable maximum flood hydrograph computations for surface facility sites. Blanton (1992) extended Bullard's 1991 probable maximum flood study by computing flow depths, widths, and areas for seven cross-sections in Mid Valley Wash in Midway Valley east of Yucca Mountain, three cross-sections in Drill Hole Wash, three cross-sections in Coyote Wash, and four cross-sections at the Exploratory Studies Facility South Portal location (Blanton 1992, Tables 1 to 12). Cross-section elevations were surveyed to the 1927 North American Datum (Blanton 1992, Figures 2 to 9, 11 to 14, 16 to 19, and 21 to 25). Water surface profiles for the probable maximum flood and basin slopes were documented in Figures 10, 15, 20, and 26 of Blanton (1992). Channel roughness Manning n constants were estimated to be about equal (0.045) at all cross-sections.

Christensen and Spahr (1980) and Squires and Young (1984) described how channel characteristics can change during flood flows due to the presence of sediment in the flow. Savard (1995a, 1996) documented channel changes with photographs after small flood flows from the intermittent tributary from Delirium Canyon to Fortymile Wash in the Fortymile Canyon area northeast of Yucca Mountain.

Glancy (1994, Figures 12 and 13) documented channel surface features, longitudinal profiles and cross-section elevations relative to an arbitrary datum in Coyote Wash on Yucca Mountain. Evaluation of prehistoric flooding and potential future extreme flooding at Coyote Wash were the major objectives of the study. The land surface profiles and cross-sectional area were presented graphically but were not tabulated in the report.

Osterkamp et al. (1994) discussed the use of channel characteristics in the Amargosa River, Fortymile Wash, and Topopah Wash for use in developing a geomorphic/distributed parameter groundwater recharge water model. Channel widths were measured in the field with a hand-held tape. These width values were not documented in their report but were contained in technical files of the Yucca Mountain Site Characterization Office. Channel widths generally were found to

increase in the downstream direction of each stream within the study area. Due to infiltration and evaporation losses, active channel widths were found to decrease in the Amargosa River downstream of the Amargosa Narrows near Beatty and Fortymile Wash downstream of the mouth of Yucca Wash. The active channels were developed by smaller floods, such as floods having a 5-year recurrence interval. The Fortymile Wash distributary system of channels in the Northern Amargosa Desert, southeast of Yucca Mountain, spread the flood water into several channels; thus in the downstream direction, channel width decreased.

USGS files contain channel characteristics at the gauging stations where indirect streamflow measurements of peak discharge were made after flood flows. Channel cross-sections have been surveyed in to a local datum. Water surface profiles are surveyed periodically from high water marks measured at these stations. Channel slopes have been measured from previous channel surveys. Channel Manning n constants were estimated based on inspection of the site or photographs. The data obtained from these monitoring stations complement data obtained from the above-described individual channel flood-potential studies.

5.1.1.2 Perennial Surface Water

Perennial surface water in the Amargosa River drainage basin is associated with springs discharging groundwaters. The Oasis Valley, the Ash Meadows, Tecopa, and Badwater areas have flowing water either after precipitation/ runoff events, which occur infrequently and not on a perennial basis, or during the winter months when evapotranspiration is at a minimum. Some of the perennial water almost completely dries up during high evapotranspiration periods during the summer.

Numerous permanent or nearly permanent springs discharge along or near the Amargosa River channel in Oasis Valley. During winter and spring, several reaches of the main channel have sustained flow which diminishes or disappears due to evapotranspiration in the summer and fall (Malmberg and Eakin 1962; White 1979). The Amargosa River channel through the Amargosa Desert is ephemeral, but short reaches of persistent flow occur between Amargosa Desert and the channel enters Death Valley. Between Franklin Lake Playa and Death Valley, several springs discharge into the Amargosa River where perennial surface water exists (Hunt et al. 1966). Wet playas occur in the eastern (Amargosa or Peters Playa) and southernmost (Franklin Lake Playa or Alkali Flat) parts of Amargosa Desert (Figure 5.1-1).

The Ash Meadows groundwater system, which drains the region east of the Yucca Mountain area, discharges at several perennial springs that sustain small pools at Ash Meadows in the southeastern portion of Amargosa Desert. Winograd and Thordarson (1975) and Dudley and Larson (1976) describe the characteristics of these springs. Crystal Reservoir, a man-made structure, captures discharge from Crystal Spring and several springs in the Point of Rocks area. These bodies of water drain to the Amargosa River through Carson Slough.

Within the Amargosa Desert there are four small perennial ponds (Walker and Eakin 1963). These ponds occur in former clay mining pits. Groundwater discharge is greater than evapotranspiration resulting in the ponds formation.

Badwater is a spring discharge pool in the terminal area of the Amargosa River in Death Valley. Lakes occasionally occur in Death Valley from surface water runoff. The Amargosa River and other Death Valley tributaries contribute runoff to form these temporary standing water bodies, as does direct precipitation (Grasso 1996). These modern day lakes dry up in the spring and summer after the winter storms. The lakes do not occur frequently, and last occurred in 1969 and 1993.

5.1.2 Monitoring Network

Surface water flows are currently monitored at several different geographic locations representing varying drainage basin areas, elevations, and physical characteristics (soil types, percent bedrock exposed, different rock types, and vegetation types) both at Yucca Mountain and in the region (Figures 5.1-2, 5.1-3, and 5.1-4). The monitoring network consists of sites operated for the Yucca Mountain Project (Pabst et al. 1993, Kane et al. 1994) and regional sites operated for other projects. Data collected from all of these sites is pertinent to the Yucca Mountain Project objectives (USGS 1961 to 1993; Moosburner 1978; Waddell et al. 1984). Some of these regional sites where data were collected prior to the start of Yucca Mountain characterization studies provide an extended record of streamflow. Regional monitoring sites tend to be located near road crossings since these sites were operated in conjunction with the Nevada Department of Transportation. Sites shown in Figure 5.1-3 (subregional scale map) were generally operated with regional scale site surface water data collection investigations (Figure 5.1-2). Sites shown on the site scale map (Figure 5.1-4) were operated with regional (Figure 5.1-2) and subregional (Figure 5.1-3) scale site characterization hydrologic investigations. The sites utilized in the monitoring network (i.e., total number of sites monitored) vary depending on the operating budget and programmatic objectives. The following three types of sites have been used in the monitoring network:

- Continuous monitoring gauging stations that provide continuous discharge data (including peak discharge), streamflow volume and duration, and continuous gauge-height record
- Crest-stage gauges that provide peak discharge data and peak gauge-height record
- Miscellaneous sites that provide discharge (mostly peak) data at selected sites of importance

Station numbers, names, location by latitude/longitude, drainage areas, site type and periods of record are tabulated for the continuous monitoring stations, crest-stage gauges, and miscellaneous sites on Table 5.1-1. Records of gauge height and discharge are recorded and computed using standard USGS techniques.

Continuous monitoring gauging stations record pressure at an orifice opening mounted in a pipe attached to the stream bank. When streamflow fills the ephemeral channel, the pressure rise associated with the water rise over the orifice is converted to analog and digital signals and recorded. The analog signal is recorded on a paper chart. The digital signal is recorded on paper medium or in an electronic recorder. The digital signal is also transmitted back to the operations office for processing. A few stations use a float attached to a recorder with a calibrated pulley and tape system. When the float moves up and down from streamflow water entering and leaving the float well, the recorder registers the rise and fall. The same type of analog and digital recorders are used as those at the pressure orifice stations.

The record of streamflow height with time (usually referenced to some local gauge datum) constitutes the gauge-height record. These data are stored in USGS files and the extremes summarized in publications. The gauge-height record in the Yucca Mountain area exhibits flat behavior (no change with time) when there is no streamflow, which is the majority of the time. During periods of streamflow the change in water-level height with time is recorded. The gauge-height record can be affected by environmental factors (such as ice buildup on the float or sediment buildup over the orifice), animals that destroy pieces of the equipment, or instrument malfunction. The gauge-height record is examined for erroneous or missing data and then corrected or adjusted. Elevations of high water marks left by streamflow (such as wash lines and sediment/debris deposits) are surveyed to correlate to the gauge-height record and verify instrument readings. The elevations of low points in the ephemeral channel also are surveyed to determine minimum readings possible by the instruments (point of zero flow). Local datum benchmarks are established beyond the destructive power of the streamflow to provide a stable elevation reference over time.

Crest-stage gauges record peak gauge-height values during streamflows. A pipe, which contains a calibrated stick, is installed in the ephemeral stream channel. The stick is constrained so it will not move or float. During streamflow, water and sediment enter the pipe through the openings. Sediment deposits mark the peak gauge height reached on the stick during the streamflow. The stick is cleaned off during each inspection visit after the peak gauge height is noted. Inspection of the gauge and verification of high-water marks from the streamflow allow operators to evaluate the crest-stage gauge readings.

Miscellaneous sites are established after large streamflow events at sites other than gauging station locations. Peak discharges are determined at these sites by indirect measurements after the streamflow occurred. No gauge-height record is obtained at these sites. Table 5.1-2 presents dates and peak discharges at continuous gauging stations, crest-stage gages, and miscellaneous sites in the Yucca Mountain region. Tables 5.1-3, 5.1-4, and 5.1-5 provide data for the ten largest observed historical peak discharges in the Yucca Mountain region, the ten largest observed historical unit peak discharges in the Yucca Mountain region, and the ten largest observed historical unit peak discharges for sites with drainage areas greater than 10 square kilometers in the Yucca Mountain region, respectively.

Stream discharge (volume of water discharging per unit of time, such as cubic feet or cubic meters per second) is computed at the continuous gauging stations and crest-stage gauges from the gauge-height record and a rating curve for the channel. The rating curve is a function in which the water-level elevation in the ephemeral channel represents a unique stream discharge. A theoretical rating curve is developed for the gauges based on the slope, roughness, width, and depth of the channel. This curve is verified through actual measurements of streamflow discharge and gauge height during a flood, indirect measurements of peak stream discharge after a flood, and measurements of the point of zero flow. The theoretical curve is adjusted based on measurement data and applied to the gauge-height record to determine continuous streamflow discharge and peak discharge. Discharge is computed for 10-minute intervals if the gauge-height record is recorded electronically. The analog gauge-heights continuously recorded on a paper chart are subdivided into time intervals and a mean gauge height for the interval noted. A daily mean discharge value is computed from the interval discharges. The daily mean discharge is then stored in USGS databases and published for the continuous gauging stations. Peak discharge values are also published for the continuous and the

crest-stage gauges. Peak discharge values can be several orders of magnitude higher than daily mean discharge values. Streamflows last only several hours or days with rapid changes in gauge heights and discharges. This rapid change in discharge is a characteristic of the flash flooding that commonly occurs in the desert southwest.

The use of rating curves based on indirect measurements of streamflow (slope area and slope conveyance) is dependent on stable channel conditions. The large force of the streamflow and the readily available sediment can influence the channel shape, size, roughness, and slope during streamflow. Several gauging stations (e.g., Fortymile Wash at Narrows, and an unnamed tributary to Stockade Wash near Rattlesnake Ridge) are located in relatively stable channels (bedrock outcrops) where changes in channel conditions are expected to be minimal. Some gauging stations have scour chains installed which measure the total change in channel bottom elevation during a streamflow. The chains are vertically positioned in a hole in the channel bottom, so that the remaining chain left out of the backfilled hole can be measured. After streamflow occurs, the chain length left on the surface is remeasured. If erosion has occurred during the streamflow, more of the chain is exposed and measured. If deposition has occurred during the streamflow, the amount of fill removed to recover the chain is measured. The length of the exposed chain can be used to measure the combined effects of erosion during the early part of the streamflow and deposition in the late part of the streamflow. With several scour chains installed across the gauging station channel cross-section, the changes in channel depth during streamflow can be measured and the change in cross-sectional area computed. The change in cross-sectional area is part of the discharge computations in applying the rating curve to the gauge-height record. Inspection notes and photographs of the channel before and after streamflows allow changes in channel roughness to be incorporated into the discharge computations. Surveys of the channel before and after streamflows allow changes in channel shape, size, and slope to be incorporated into the discharge computations. The number of significant figures in the estimated peak discharge values are adjusted to account for the errors caused by channel instability.

Few measurement points are obtained during streamflow at gauging stations because of safety considerations, manpower and equipment limitations, and the short duration of events. During periods of streamflow, several events are happening for short periods of time at nearby stations and it is physically impossible to be at all sites to make direct measurements of discharge, especially the peaks. Bridge and cableway structures do not exist to safely make discharge measurements. Boat measurements cannot be conducted safely or practically.

5.1.3 Water-Control Structures and Diversions

No significant water-control structures are located in the Amargosa River system or its tributaries. Road crossings of river channels may become flooded with water and sediment during flash flooding. Culverts at road crossings may become choked with sediment and debris during floods, causing water and sediment to overflow the road crossing. U.S. Highway 95 was closed at the Fortymile Wash crossing in 1995 during streamflow (Beck and Glancy 1995). Release of impounded water behind choked road crossings would only have minor impacts on downstream streamflow during flash flooding. Erosion can occur at road crossings, especially unimproved ones, during streamflow. Road crossings can be partially damaged or destroyed during such events.

The impoundments in the Ash Meadows area of the Amargosa Desert, such as Crystal Reservoir, receive only local surface runoff and discharge from the springs. Release of the impounded water behind Crystal Reservoir would affect downstream locations only in the eastern Amargosa Desert and the Amargosa River below Franklin Lake Playa.

5.1.4 Drainage Development, Paleohydrology, and Flood History

The following subsections summarize the results of studies of the history of the ancient development of drainage system patterns, ancient and historical surface water flow conditions, and historical flood occurrences and flood discharges in the Yucca Mountain and surrounding areas. The data derived from these studies help in understanding past climatic, geomorphic, and streamflow conditions, and, in some cases, can be used as an analogue to help understand possible future climatic and surface hydrologic conditions within the region. In addition, age dating data of groundwater samples using radiological dating and stable isotopic analysis techniques generates data that, when compared to historical and ancient surface water hydrologic data, can lead to a better understanding of past and possible future recharge and infiltration processes and rates.

5.1.4.1 Drainage Development

In a regional study using maps, reports, and photographs, Huber (1988) analyzed the late Cenozoic evolution of the upper Amargosa River drainage area. Huber concluded that the basin regional drainage pattern was established soon after the collapse of the Timber Mountain Caldera and has changed little in the past 11 million years.

Lundstrom and Warren (1994) found new field evidence suggesting that the present day Fortymile Wash drainage pattern was established within approximately the last 3 million years. They found alluvial deposits in the Timber Mountain caldera suggesting a different drainage pattern than the present day one during the period between 3 and 11 million years ago. They also found mapped volcanic units in Fortymile Canyon to be a part of a big landslide deposit, concluding that Huber's interpretations based on the position of these volcanic units needed to be revised.

5.1.4.2 Paleohydrology

Studies of ancient and historical stream-flow processes and the physical and chemical conditions under which such paleo-stream processes occurred provide data regarding past climatic and hydrogeochemical and recharge conditions. This subsection summarizes work done to date to characterize these flow processes. Related subsections present additional information and interpretations resulting from such studies of paleo-flow processes (Subsection 3.4.4), paleoclimates (Subsection 4.2), and surface water chemistry (Subsection 6.2.4).

5.1.4.2.1 Site and Subregional Paleohydrologic Studies

Glancy (1994) discussed the geologic evidence found for prehistoric flooding in Coyote Wash on Yucca Mountain. Trenches excavated both across and along the modern-day channel exhibited sediments indicative of multiple flood events including debris-flow deposits. He concluded that moderately indurated sediments overlying the bedrock and underlying the stream terraces adjacent

to the channel probably were deposited during the late Pleistocene (over 10,000 years ago), and that nonindurated sediments overlying the older sediments were probably of Holocene age (less than 10,000 years old). Using surficial boulders near the trenches, he estimated the magnitude of the flood that deposited them during the Holocene. Assuming the flood was water dominated (Newtonian fluid) and all the boulders were emplaced by the same flood, a peak discharge of 68 cubic meters per second (2,400 cubic feet per second) was estimated to have occurred. The peak discharge could have been underestimated if the peak-flow rate was competent enough to move boulders larger than those available. Also the boulders considered could represent exhumed deposits from a non-Newtonian debris flow, and thus the estimated peak-flow discharge could be invalid.

Grasso (1996) developed a lake-water-budget model for a modern day (1969) lake in Death Valley. Inputs for the water-budget model were precipitation, runoff, and spring discharge. Output for the water-budget model was evaporation. Using the lake-water-budget model he computed the inputs and output needed to sustain a lake the size of the late Holocene perennial lake in Death Valley. Precipitation, runoff, and spring discharge inputs would have to increase 200 percent and evaporation output decrease 50 percent for the lake to form. With the changed climatic conditions, the lake could have formed over a 12-year period and could have been sustained.

Claassen's (1985) geochemical interpretation of groundwater in the West-Central Amargosa Desert indicates that most groundwater recharge occurred from streamflow in Fortymile Canyon and the Amargosa Desert during late Wisconsin time. Sodium, calcium, and magnesium concentrations in groundwater in the Amargosa Desert are not consistent with a presumed source of recharge in the bedrock aquifers to the north (Yucca Mountain and further north). Groundwater with the lowest concentrations of these constituents underlay modern day channels of Fortymile Wash and streamflow in the channels are the presumed source of the recharge. Carbon-, hydrogen-, and oxygen-isotope data indicate that major recharge occurred at the end of the Pleistocene and through early Holocene time.

Claassen's (1986) analysis of ^{14}C and stable isotope ($\delta^{18}\text{O}$ and δD) data indicated that recharge of the Amargosa Desert groundwater was from infiltration of runoff in paleostream channels from 17,000 to 10,000 years ago. The mean annual temperature 17,000 years ago (late Pleistocene) was approximately 8°C less than present-day mean annual temperature and recharge occurred during winter as well as summer. Mean winter temperatures 10,000 years ago (Holocene) were approximately 1°C less than present-day winter temperature and recharge occurred during winter but not during summer. Differences in ^{14}C between Yucca Mountain and Amargosa Desert groundwater indicate that groundwater ages are about the same and do not suggest movement of groundwater from the Yucca Mountain area to the west-central Amargosa Desert. No correlation was found between depth of saturated zone sampled and the ^{14}C age for seven groundwater sites in the west-central Amargosa Desert. The theory of younger groundwater from recharge overlying older groundwater moving from upgradient sources in the alluvial aquifer was not supported. A high correlation between the distance from assumed paleochannel locations to well locations and ^{14}C ages for six samples in the west-central Amargosa Desert support the concept of groundwater recharge from paleo-streamflow infiltration.

Benson and Klieforth's (1989) analysis of unadjusted ^{14}C ages of groundwater samples from the Yucca Mountain and Amargosa Desert area determined that the groundwater was derived from

recharge that occurred between about 9,000 and 18,500 years ago. Stable isotope ($\delta^{18}\text{O}$ and δD) analysis of modern-day precipitation and groundwater indicates that cold season precipitation was the source of the groundwater. They proposed that the groundwater recharge occurred as streamflow in Fortymile Canyon. They also inferred that the global ice sheets affected the position and persistence of the jet stream during this period which brought moisture into the Yucca Mountain area.

5.1.4.2.2 Regional Paleohydrologic Studies

Ely (1997) proposed that paleofloods that occurred in Arizona and Southern Utah over the last 5,000 years cluster into distinct time periods related to regional and global climatic fluctuations. For 29 drainage basins ranging in area from 285 km² to 279,350 km², high-magnitude floods were frequent during the periods between 3,800 and 2,200 BC, 400 BC and 1,100 AD, and 1,400 AD and the present. Modern-day high-magnitude floods (≥ 10 -year floods) for these size drainage basins generally result from winter storms and tropical cyclones. The winter storms and tropical cyclones are often associated with El Niño conditions. Ely (1997) emphasized the positive relationship between paleofloods and the long-term variations in the frequency of El Niño conditions over the last 1,000 years. He also indicated that there is a positive relationship between the paleofloods and warm coastal sea-surface temperatures, indicative of El Niño conditions, over the last 3,000 years.

5.1.4.3 Streamgauge Flood Record

Historical flood data for streams within and around the Yucca Mountain area include historical data collected from a few selected stream gauge monitoring stations in the general area and data collected from numerous stream courses at and around the Yucca Mountain site as part of Yucca Mountain site characterization activities. This subsection, and subsequent Subsections 5.1.4.4 and 5.1.5, present data obtained regarding stream flow volumes, average and annual peak discharges, and stream flood potential for streams in the Yucca Mountain vicinity and region.

5.1.4.3.1 Site and Subregional Paleohydrologic Floodstream Studies

Peak discharge data have been collected at 52 sites in the Yucca Mountain area (Table 5.1-2). The sites have different periods of record and represent varied terrain, geology, elevation, location, and drainage basin size. Peak discharge information at a number of sites was collected prior to the initialization of Yucca Mountain Site characterization activities. Some sites on and near Yucca Mountain associated with site characterization have been the source of data since 1983.

The largest observed peak discharge, 570 m³/s, in the Yucca Mountain area was at Fortymile Wash near Well J-13 (Table 5.1-3). Squires and Young (1984), in their flood potential study of Fortymile Wash, observed high-water marks along the channel near Well J-13. Based on the channel measurements they made, a peak discharge was computed. They assigned the February 25, 1969, date to the peak because of known peak discharges downstream in Fortymile Wash and in the Amargosa River on that date. The 10 largest observed peak discharges in the Yucca Mountain area are from drainage basins greater than 100 km² in area. Three of the largest peak discharges occurred during the summer in August, the other seven occurred during the winter/spring period in February and March.

The largest observed unit peak discharge, $9.66 \text{ m}^3/\text{s}/\text{km}^2$, in the Yucca Mountain area occurred at Split Wash below Quac Canyon on July 21, 1984 on Yucca Mountain (Table 5.1-4). The ten largest observed unit peak discharges in the Yucca Mountain area were from drainage basins smaller than 10 km^2 in size, except for the Frenchman Lake tributary at Old Mercury Highway on August 15, 1984, which was associated with a drainage basin of 16.4 km^2 in area. All of the top ten unit peak discharges occurred during the summer months of June, July, or August.

The largest observed unit peak discharge for sites in the Yucca Mountain areas with drainage basin areas greater than 10 km^2 , $1.90 \text{ m}^3/\text{s}/\text{km}^2$, was at Frenchman Lake tributary at Old Mercury Highway on August 15, 1984 (Table 5.1-5). Seven of the ten largest observed unit peak discharges for sites with drainage basin area greater than 10 km^2 occurred during the summer months of July and August, the other three occurred during the winter/spring months of February and March.

Hunt et al. (1966), in their study of the Death Valley hydrologic basin, briefly mention streamflow occurring in the Amargosa River from Eagle Mountain to Death Valley during the 1957 to 1958 winter season and the 1958 spring season. They observed continuous streamflow from the Eagle Mountain area to the saltpan. Normally only short stretches of this reach of the Amargosa River are perennial due to spring discharge. No mention is made of flood peaks or volumes of streamflow; however, the main subject of their study was the groundwater resources of Death Valley.

Moosburner (1978) tabulated flood peaks at gauged and ungauged sites through 1977 throughout Nevada. Dates and peak discharges were measured and recorded by the USGS for the Fortymile Wash, Amargosa River, and other nearby drainage basins for various programs. Most peak discharge data were collected for the Nevada Department of Highways at or near road crossings of stream channels. Prior to commencement of Yucca Mountain site characterization studies, some of the 1969 flood peak discharges in the Amargosa River drainage basin were documented by the USGS (1970) and Moosburner (1978) at four sites in the Yucca Mountain area (Amargosa River near Springdale, Beatty Wash near Beatty, Amargosa River Tributary near Lathrop Wells, and Fortymile Canyon near Lathrop Wells). The July 1964 peak discharge at the Indian Springs Valley tributary near Indian Springs, Nevada (10248490) previously published in the USGS annual data report was revised from 0.5 to $0.0 \text{ ft}^3/\text{s}$ due to new data or revised interpretations of the data. The August 13, 1972 peak discharge at Ralston Valley tributary near Tonopah, Nevada (10249140) was revised from 10.5 to $0.57 \text{ m}^3/\text{s}$ (370 to $20 \text{ ft}^3/\text{s}$) due to reinterpretation of the streamflow indicating the majority of the peak discharge came from an adjacent basin. Other peak discharges at sites near Yucca Mountain were not revised. Moosburner (1978) only presented the data but did not interpret it. A general conclusion that can be made from their data is that floods can occur during both the winter and summer seasons in the region around Yucca Mountain. Sometimes the exact day of the peak discharge cannot be determined and only the month and year are published. During some water years (October 1 through September 30) no discharge is observed and no annual peak discharge is published. Another general conclusion that can be made based on the available information is that flood peak discharge in the Yucca Mountain area is difficult to measure accurately. Most floods are listed as estimated or only reported to one or two significant figures (due to difficult field conditions and personnel and budget constraints). Large peak discharge measurements usually cannot be made safely by direct techniques if personnel are fortunate enough to be at a site for the short time duration streamflows (flash floods). Indirect techniques (such as slope to area, conveyance to slope, and culvert analyses) are usually used to estimate peak discharges. These indirect techniques may have

large errors due to limited water-surface profile data, unstable channel bed geometry (cross-sectional area of streamflow may be unknown during event due to erosion or deposition), unknown sediment load, and uncertainties associated with estimating channel roughness factors.

Only three continuous gauging stations—Penoyer Valley tributary near Tempiute, Nevada (10247860), Amargosa River near Beatty, Nevada (10251220), and Amargosa River at Tecopa, California (10251300)—were operated prior to startup of site characterization studies in the Yucca Mountain area. Streamflow volume and peak discharge are available for the periods of time these gauges were in operation.

After site characterization studies were initiated, more detailed streamflow data were collected than previously in the Yucca Mountain area. Streamflow data for the Yucca Mountain vicinity were documented by Pabst et al. (1993) for the water years 1983 to 1985, Kane et al. (1994) for the water years 1986 to 1990, Emmett et al. (1994) for the water years 1991 to 1993, Clary et al. (1995) for water year 1994, and Bauer et al. (1996) for water year 1995. Streamflow only occurs during and after precipitation events in the drainage basins of the usually dry washes. Flooding can occur during both the winter and summer seasons in the stream channels at and near Yucca Mountain.

Grasso (1996) discussed the Amargosa River at Tecopa discharge record, 1961 to 1983. Regional winter storms, usually during El Niño conditions, can cause basin-wide runoff which can cause a modern day lake to form in Death Valley. Peak discharge at the Amargosa River at Tecopa gauge during these winter storms can be large. The largest peak discharge observed at this gauge was from a summer storm. Remnants of Pacific Ocean hurricanes also have been known to pass through the Amargosa River drainage basin and can cause large peak discharges.

Beck and Glancy (1995) discussed the March 11, 1995 runoff in Fortymile Wash and Amargosa River. This runoff is important because it represents the first documented case during site-characterization studies in which Fortymile Wash and Amargosa River flowed simultaneously throughout their entire Nevada reaches. Hydrographs of four gauges—Stockade Wash near Fortymile Wash, Fortymile Wash at Narrows, Fortymile Wash near Well J-13, and Fortymile Wash near Amargosa Valley—for runoff during March 11, 1995 exhibited a rapid rise and fall of streamflow and short duration of runoff (Figure 5.1-5). Hydrographs of three gauges on Yucca Mountain—Wren Wash at Yucca Mountain, Pagany Wash near the Prow, and Pagany Wash #1 near Well UZ- 4—exhibited a similar rapid rise and fall of streamflow and short duration of runoff (Figure 5.1-6). The peak discharge in the Yucca Mountain streams was almost two orders of magnitude lower than in Fortymile Wash. Tributary inflow and losses from infiltration affected the hydrograph volumes between gauge locations on Fortymile Wash and Pagany Wash.

Savard (1994, 1995a, 1995b, 1996, 1998) discussed streamflow from small floods in Fortymile Canyon during February and March 1992, January and February 1993, and January and March 1995. The floods of February 1992, January 1993, January 1995, and March 1995 were of sufficient volume to reach the Fortymile Wash at Narrows gauging station. The March 1992 and February 1993 flood volumes were not large enough to reach the gauge but did cause groundwater recharge to occur from streamflow infiltration losses in the stream channels.

5.1.4.3.2 Regional Streamgauge Flood Studies

Moosburner and Williams (1991) presented a chronology of major floods in Nevada between 1907 and 1988 as part of a national water summary. Large floods have happened in Southern Nevada and have caused loss of life and economic loss. The Eldorado Canyon flood of September 14, 1974 (Glancy and Harmsen 1975) is included in the regional maximum flood envelope curve data set (Crippen and Bue 1977).

McKinley and Oliver (1994, 1995) document discharge in two small basins in Central Nevada. They collected the discharge data to quantify groundwater recharge processes in analog basins which are thought to be similar to Yucca Mountain during wetter climatic periods. No significant flood peaks were observed in the two small basins during 1987 to 1992. The 1987 to 1992 period was a relatively dry period compared to longer time periods.

At the South Twin River gauging station, approximately 20 km to the southeast of the East Stewart Basin, the 1987 to 1992 mean annual discharge was $0.110 \text{ m}^3/\text{s}$ and the 1966 to 1996 mean annual discharge was $0.186 \text{ m}^3/\text{s}$ (Figure 5.1-7). The 1987 to 1992 mean annual discharge was approximately 59 percent of the long-term mean annual discharge. The 1988 water year annual mean discharge, $0.195 \text{ m}^3/\text{s}$, was the only year to exceed the 1966 to 1996 mean annual discharge.

5.1.4.4 Streamgauge Volume Record

5.1.4.4.1 Site and Subregional Streamgauge Volume Studies

Besides streamflow peak discharges, streamflow volumes were computed for sites on and near Yucca Mountain. Before site characterization studies were initiated, streamflow volumes were computed only at three sites (Penoyer Valley tributary near Tempiute, Amargosa River near Beatty, and Amargosa River at Tecopa) in the Yucca Mountain region. After site characterization studies began, several sites on Yucca Mountain and in the Fortymile Wash/Amargosa River drainage basin were monitored for streamflow volumes as well as peak discharges. The number of sites where streamflow volumes were computed fluctuated during the 1983 to 1995 period as program priorities changed.

Prior to site characterization, streamflow data (including streamflow volumes) were documented for Penoyer Valley tributary near Tempiute, Nevada (water years 1966 to 1977); Amargosa River near Beatty, Nevada (water years 1963 to 1968); and Amargosa River at Tecopa, California (water years 1962 to 1983) in the Yucca Mountain vicinity, and are documented in USGS annual Water Data Reports for Nevada and California (USGS 1963 to 1984). After site characterization studies were initiated, two reports specific to the Yucca Mountain Site Characterization Project (YMP) were published: Pabst et al. (1993) for the water years 1983 to 1985, and Kane et al. (1994) for the water years 1986 to 1990. Streamflow data were then again published in the annual water data reports: Emmett et al. (1994) for the water years 1991 to 1993; Clary et al. (1995) for water year 1994; and Bauer et al. (1996) for water year 1995. Streamflow occurs for only short periods of time, typically on the order of hours to several days. Streamflow volume decreases because of infiltration losses in the channel as the flood moves downstream in the channel system (Savard and Beck 1994).

Tributary inflow can be greater than the streamflow infiltration losses in a reach and flood volume may therefore increase downstream in a reach.

Grasso (1996), in his study of Death Valley lake volumes, developed a relation between peak discharge and runoff volume for the area using data from 34 streamflow periods of the Amargosa River at the Tecopa gauge. The peak discharge and runoff volume data were log transformed and an ordinary least-squares regression was performed on the winter, summer, and all-storms data. Simple power-series equations were developed relating runoff volume to peak discharge. The all-storms equation relation they developed is:

$$Q_{vol} = 1.43(Q_{peak}^{0.99})$$

where Q_{vol} = runoff volume, in acre-feet and
 Q_{peak} = peak discharge, in cubic feet per second.

This equation was used to estimate runoff volume frequencies from the peak discharge frequencies for the Amargosa Basin and other basins tributary to Death Valley. The runoff volumes were then used in a water budget analysis of lake formation and evaporation. Helsel and Hirsch (1992) cautioned against using the ordinary least-square regression method for record extension studies. The reduction in variance of the predicted values and the difficulty in deciding the independent and dependent relations were their main concerns. They recommended the line of organic correlation regression method for record extension studies. Grasso acknowledged that his method is not exact in extrapolating the runoff volume to peak discharge relation to other Death Valley drainage basins and stated that his results were approximate.

5.1.4.4.2 Regional Streamgauge Volume Studies

Moosburner (1988) studied peak discharges and runoff volumes in his potential flood and debris hazard study at the Katherine Landing and Telephone Cove areas. These areas are tributary to Lake Mohave in the Lake Mead recreational area and are approximately 245 km to the southwest of Yucca Mountain. Moosburner estimates the 10, 25, 50, 100, and 500-year peak discharges from regional flood-frequency relations developed for Northwest Arizona. The extreme flood peak discharge was estimated using Crippen and Bue's (1977) regional maximum flood envelope curve. To evaluate the effect of the storage capacity of a borrow pit in South Katherine Landing Wash on flood peaks, Moosburner used a common technique in watershed hydrology relating runoff volume to peak discharge, drainage basin area, and the time of concentration by:

$$Q_{vol} = [Q_{peak}(T_c^{0.5} + 0.6(T_c))] / 484(A)$$

where

Q_{vol} = runoff volume, in inches of depth for the drainage basin area;

Q_{peak} = peak discharge, in cubic feet per second;

T_c = time of concentration, in hours; and

A = drainage basin area, in square miles.

The time of concentration was estimated by:

$$T_c = 0.00013(L^{0.77}/S^{0.385})$$

where L = drainage basin length in feet, and
 S = slope, ratio of total fall to L .

Moosburner did not provide data to verify the use of these equations and stated that his runoff volume estimate for the 100-year peak discharge was uncertain.

Glancy and Harmsen (1975), in their study of the September 14, 1974, Eldorado Canyon flood which occurred approximately 180 km southwest of Yucca Mountain, estimated the peak discharge to be 2,150 m³/s. They developed a hydrograph for the flood and estimated the runoff volume to be 2,466,000 m³. The U.S. Bureau of Reclamation estimated a similar runoff volume after analyzing the change in Lake Mohave elevation (Glancy and Harmsen 1975, p. 10).

McKinley and Oliver (1994, 1995) tabulated mean daily discharges for several sites in Central Nevada at their analog recharge sites. The streamflow mainly originated from spring discharge, but periods of streamflow attributed to snowmelt and precipitation excess have occurred. Their data were collected during a relatively dry period for Nevada and runoff volumes for the period could have been less than long-term averages.

Lichty and McKinley (1995) compared estimated runoff volumes from hydrologic modeling to measured volumes at sites in Central Nevada. Volcanic rock underlies the Three-Springs and East Stewart drainage basins. The drainage basins are considered to be analog recharge basins to Yucca Mountain under cooler and wetter climatic conditions. Estimation of groundwater recharge volumes from a water-balance equation was the main objective of the study. A precipitation-runoff modeling system was used to account for the spatial variability of hydrologic inputs, processes, and outputs. They compared measured runoff volumes at gauge locations and computed runoff volumes from the model to calibrate the model with a daily time step.

5.1.5 Flood Potential

Studies of stream flood potential conducted to date have included flood studies of streams located within the Yucca Mountain vicinity as well as a number of streams located in the central Nevada and Great Basin regions. These study efforts have resulted in data on average and peak annual discharges as well as estimates of probable maximum flood magnitudes and frequencies in these areas.

5.1.5.1 Site and Subregional Flood Potential Studies

Christensen and Spahr (1980) discussed flooding potential in Topopah Wash and tributaries in the eastern part of Jackass Flats. Peak discharge data for 71 gauged sites in Nevada were analyzed and the 10, 25, 50, and 100-year recurrence interval peak discharges were determined. Drainage basin area, mean basin altitude, and latitude of the basin are significant parameters used when estimating the flood-frequency relations:

$$\begin{aligned}Q_{10} &= 392(A^{0.66})(E^{-1.02})(L^{-0.33}); \\Q_{25} &= 1810(A^{0.61})(E^{-1.14})(L^{-0.70}); \\Q_{50} &= 4860(A^{0.58})(E^{-1.21})(L^{-0.94}); \\Q_{100} &= 11900(A^{0.55})(E^{-1.28})(L^{-1.16});\end{aligned}$$

where Q_{10} = peak discharge statistically expected to recur at least once in a 10-year period, in ft^3/s ;
 Q_{25} = peak discharge statistically expected to recur at least once in a 25-year period, in ft^3/s ;
 Q_{50} = peak discharge statistically expected to recur at least once in a 50-year period, in ft^3/s ;
 Q_{100} = peak discharge statistically expected to recur at least once in a 100-year period, in ft^3/s ; and
 A = drainage basin area, in square miles, and $0.2 < A < 100$;
 E = mean basin altitude, in thousands of feet, and $2 < E < 10$; and
 L = latitude of basin minus 35° latitude, and $1 < L < 7$.

The magnitude-frequency curve was estimated from the equations for selected sites in the Topopah Wash drainage basin. The 500-year flood discharge at a site was extrapolated from the magnitude-frequency curve. The regional maximum flood discharge, referred to as the maximum potential flood, at a site was estimated from an envelope curve of maximum observed peak discharges and drainage basin area from an analysis of regional data (Crippen and Bue 1977). Flood depth at a cross-section was estimated using Manning's equation for the peak discharge. Based on their analyses, the authors concluded that:

- The 100-year flood prone areas would probably closely parallel most stream channels with very few occurrences of out-of-bank flooding (Figure 5.1-8).
- Channel flood depths would range from 0.3 to 2.7 m and mean velocities would range from 0.9 to 2.7 m/s.
- Out-of-bank flood depths would be less than 0.6 m with mean velocities as much as 2.1 m/s.
- The 500-year flood would probably exceed the discharge capacities of all channels except for the main branch of Topopah Wash and some channels in the upstream reaches of a few tributaries.
- Channel flood depths would range from 0.3 to 3.7 m and mean velocities would range from 0.9 to 4.0 m/s.
- Out-of-bank flow depths between adjacent channels would be as much as 0.9 m with mean velocities more than 2.1 m/s.
- The regional maximum flood would probably inundate most of the eastern part of Jackass Flats.
- Channel flood depths would range from 0.6 to 7.0 m and mean velocities would range from 1.2 to 7.9 m/s.
- Out-of-bank flow depths between adjacent channels would be as much as 1.5 m with mean velocities as much as 4.0 m/s.

Squires and Young (1984) investigated flood potential in Fortymile Wash and its tributaries on Yucca Mountain. Peak discharges data for 12 gauged sites adjacent to the Nevada Test Site were analyzed and the 100- and 500-year recurrence interval peak discharges and regional maximum flood peaks were estimated. Drainage basin area was the only significant basin parameter used in their flood frequency relations:

$$Q_{100} = 482(A^{0.565});$$

$$Q_{500} = 2200(A^{0.571});$$

where Q_{100} = peak discharge statistically expected to recur at least once in a 100-year period, in ft³/s;
 Q_{500} = the peak discharge statistically expected to recur at least once in a 500-year period, in ft³/s; and
A = the drainage basin area, in square miles.

The equations used by Squires and Young differed from those used by Christensen and Spahr (1980) because the Topopah Wash study used regression equations that were limited to drainage basin sizes below 180 square kilometers and the periods of records were different. The magnitude-frequency curve was estimated from the equations for selected sites in the Fortymile Wash drainage basin. The regional maximum flood discharge at a site was estimated from the same analysis of regional data (Crippen and Bue 1977). Flood depth at a cross-section was estimated with Manning's equation for the peak discharge. The authors found that:

- In Fortymile Wash, the 100-year, 500-year, and regional maximum floods would remain in the incised channel.
- The regional maximum flood (Figure 5.1-9) would probably have flood depths of 8.8 m and mean flow velocities as great as 8.5 m/s.
- In Dune Butte and Drill Hole Washes, the 100-year flood would generally remain in the channel with flood depths of up to 1.2 m and mean velocities of 2.4 m/s.
- The 500-year flood would exceed stream-channel capacities at several places in both drainage basins with flood depths up to 3.0 m and mean velocities of 3.4 m/s.
- The regional maximum flood would inundate sizeable areas in both drainage basins.
- In Yucca Wash, the 100-year, 500-year, and regional maximum floods would remain within the stream channel.
- The regional maximum flood would probably have depths of 7.0 m and mean velocities of 6.7 m/s.

Thomas et al. (1994) discussed regional magnitudes and frequencies of floods which include the Yucca Mountain area. Their analysis did not include any streams on Yucca Mountain, but did include streams used by Christensen and Spahr (1980) and Squires and Young (1984) in their earlier

flood frequency studies. Thomas et al. (1994) developed a set of equations relating peak discharge to drainage area for different recurrence intervals (2, 5, 10, 25, 50, and 100 years) of the Southern Great Basin region (south of 37° latitude), which includes the Yucca Mountain site:

$$\begin{aligned}Q_2 &= 12(A^{0.58}); \\Q_5 &= 85(A^{0.59}); \\Q_{10} &= 200(A^{0.62}); \\Q_{25} &= 400(A^{0.65}); \\Q_{50} &= 590(A^{0.67}); \\Q_{100} &= 850(A^{0.69});\end{aligned}$$

where

Q_2 = peak discharge statistically expected to recur at least once in a 2-year period, in ft³/s;
 Q_5 = peak discharge statistically expected to recur at least once in a 5-year period, in ft³/s;
 Q_{10} = peak discharge statistically expected to recur at least once in a 10-year period, in ft³/s;
 Q_{25} = peak discharge statistically expected to recur at least once in a 25-year period, in ft³/s;
 Q_{50} = peak discharge statistically expected to recur at least once in a 50-year period, in ft³/s;
 Q_{100} = peak discharge statistically expected to recur at least once in a 100-year period, in ft³/s;
and
A = drainage basin area, in square miles.

The northern part of the Fortymile Wash drainage basin is in the Northern Great Basin region and they develop a different set of equations relating peak discharge to drainage area and mean basin elevation for different recurrence intervals:

$$\begin{aligned}Q_2 &= 0; \\Q_5 &= 32(A^{0.80})(E/1000)^{0.66}; \\Q_{10} &= 590(A^{0.62})(E/1000)^{-1.6}; \\Q_{25} &= 3200(A^{0.62})(E/1000)^{-2.1}; \\Q_{50} &= 5300(A^{0.64})(E/1000)^{-2.1}; \\Q_{100} &= 20000(A^{0.51})(E/1000)^{-2.3};\end{aligned}$$

where

Q_2 = peak discharge statistically expected to recur at least once in a 2-year period, in ft³/s;
 Q_5 = peak discharge statistically expected to recur at least once in a 5-year period, in ft³/s;
 Q_{10} = peak discharge statistically expected to recur at least once in a 10-year period, in ft³/s;
 Q_{25} = peak discharge statistically expected to recur at least once in a 25-year period, in ft³/s;
 Q_{50} = peak discharge statistically expected to recur at least once in a 50-year period, in ft³/s;
 Q_{100} = peak discharge statistically expected to recur at least once in a 100-year period, in ft³/s;
and
A = drainage basin area, in square miles ; and
E = mean basin elevation, in feet.

Due to a lack of sufficient historical annual peak discharge data, only a portion of the stations in the Great Basin can be analyzed using the U.S. Water Resources Council techniques (1981). The log

Pearson type III distribution cannot have very many low outliers or no-flow years in the systematic record to be used for the analysis. Two of the sites (Sarcobatus Flat tributary near Springdale, Nevada and Amargosa River tributary near Mercury, Nevada) in the Yucca Mountain region did have enough annual peak discharge data to be analyzed by the log Pearson type III technique.

Despite the above shortcomings, Vogel et al. (1993) found the log Pearson type III still appropriate to be used in the desert southwest (e.g., Great Basin Areas). They used a hybrid method to analyze the peak discharge data at stations with many years of no flow. Hjalmarson and Thomas (1992) developed the hybrid method to develop the regional regression equations. The hybrid method combines all recorded peak discharges for the region to form a single composite record. Peak discharges are standardized using drainage area in the Southern Great Basin and drainage area and mean basin elevation in the Northern Great Basin. For the hybrid method to work, three assumptions needed to be true: the annual peaks at gauging need to be independent; the drainage area and mean basin elevation need to be independent; and the data need to be normally distributed. Thomas et al. (1994) find all three assumptions need to be true. Both sets of equations were developed for drainage basins smaller than 200 square miles. The latter authors also describe the methodology to be used when a drainage basin spans both the Northern and Southern Great Basin or when a drainage basin spans the 7,500 foot elevation, the elevation used to differentiate between low- to middle-elevation sites and high-elevation sites. They cautioned that the equations should not be used when streams are part of a distributary-flow area, the drainage basin contains large areas of highly permeable rock, streams with basin and climatic characteristics outside of the range of explanatory variables used in the regression analyses, streams with lower base flow than nearby gauged streams, and streams with channel characteristics that cause a large quantity of floodflow attenuation.

Peak discharges differ between the systematic annual peak record and the three different flood frequency curve estimates for six gauges in the Yucca Mountain area (Figures 5.1-10 through 5.1-12). Sarcobatus Flat tributary and Amargosa River tributary peak discharges were used in the three flood frequency regression analyses to develop the equations. Squires and Young (1984) and Thomas et al. (1994) used the entire 1961 to 1981 Sarcobatus Flat tributary peak discharge record in their flood frequency analyses. Christensen and Spahr (1980) did not use the entire record since it was not available. Thomas et al. (1994) used the 1963 to 1982 and 1984 to 1986 Amargosa River tributary peak discharge record in their flood frequency analysis. Squires and Young (1984) used the 1963 to 1980 record and Christensen and Spahr (1980) used a undocumented record length from 1963 to pre-1980. The Yucca Wash, Drill Hole Wash, Dune Wash, and Topopah Wash sites were not installed or did not have a long enough period of record to be included in the three analyses.

For a site, the flood frequency curve estimates require drainage basin area, mean basin elevation, and gauge latitude. These data are published and readily available. For four sites (Yucca, Drill Hole, Dune, and Topopah washes) the mean basin elevation is not readily available, thus the elevation of the gauge is substituted for the mean basin elevation. For the statewide flood frequency curves presented by Christensen and Spahr (1980), this substitution had the greatest effect. The exponent for the mean basin elevation parameter in the equations is negative. The gauge elevation was lower than the mean basin elevation, thus peak discharges were over estimated for the four sites. The systematic annual peak discharges (all annual peaks from 1995 and before) were ranked and exceedence probabilities computed. The systematic annual peak discharges were plotted with both the Weibull and Cunnane annual exceedence probability plotting positions. The Weibull plotting

position is the traditional method used by hydrologists in the U.S. to plot flood exceedence probabilities (Helsel and Hirsch 1992). Thomas et al. (1994) favored the Cunnane plotting position. The annual exceedence probability, in percent, plotting position for a peak discharge of rank 'i' with 'n' number of years of annual peak discharges collected is $[(n+1)/i]/100$ for the Weibull method and $[(n+0.2)/(i-0.4)]/100$ for the Cunnane plotting position.

Annual peak discharges were recorded at Sarcobatus Flat tributary near Springdale, Nevada for the period 1961 to 1981. The site is approximately 45 km northwest of Yucca Mountain and has a drainage basin area of 96.1 km². The log Pearson III station analysis frequency curve (Thomas et al. 1994) is similar to the systematic annual peaks. This is expected since no new peaks were collected after 1981 and Thomas et al. used the 1961 to 1981 record in their analysis. They removed peaks considered to be low outliers for the log Pearson III analysis, but did not document which ones were removed. The reason for removing the low outliers from the data set is discussed later in this subsection. The region 6 frequency curve (Thomas et al. 1994) indicated larger estimated discharges compared to the systematic annual peaks. The weighted frequency curve, a combination of the log Pearson III and the region 6 frequency curves (Thomas et al. 1994), is similar to the systematic annual peaks. The Yucca Mountain area frequency curve (Squires and Young 1984) and the statewide regression frequency curve (Christensen and Spahr 1980) both indicated larger estimated discharges compared to the systematic annual peaks.

Annual peak discharges were recorded near the mouth of Yucca Wash, Nevada Test Site, Nevada for the period 1982 to 1995. The drainage basin is on the north side of Yucca Mountain and has a drainage basin area of 44 km². The region 10 frequency curve (Thomas et al. 1994) indicates slightly larger estimated discharge compared to the systematic annual peaks. The 100-year and 500-year peak discharge estimated from the Yucca Mountain area frequency curve (Squires and Young 1984) is somewhat in line with the systematic annual peak 14-year record. The statewide frequency curve (Christensen and Spahr 1980) is similar compared to the systematic annual peaks. The regional maximum flood (Squires and Young 1984) was larger than all measured and estimated peak discharges, which is expected.

Annual peak discharges were recorded at the mouth of Drill Hole Wash, Nevada Test Site, Nevada, for the period 1983 to 1995. The drainage basin is on the eastern side of Yucca Mountain and has a drainage basin area of 42.2 km². The region 10 (Thomas et al. 1994), the Yucca Mountain area (Squires and Young 1984), and the statewide (Christensen and Spahr 1980) frequency curves estimates are somewhat in line with the systematic annual peaks. Because only three annual peak discharges have been recorded at this site during the 13 years of record, any comparison is somewhat tenuous. The regional maximum flood (Squires and Young 1984) is larger than all measured and estimated peak discharges, which is expected.

Annual peak discharges were recorded at Dune Wash near Busted Butte, Nevada Test Site, Nevada for the period 1982 to 1995. The drainage basin is on the eastern side of Yucca Mountain and has a drainage basin area of 15.5 km². The region 10 (Thomas et al. 1994), the Yucca Mountain area (Squires and Young 1984), and the statewide (Christensen and Spahr 1980) frequency curves estimate larger discharges than the systematic annual peaks. Only five annual peak discharges have been recorded at this site during the 14 years of record and any comparison is somewhat tenuous.

The regional maximum flood (Squires and Young 1984) is larger than all measured and estimated peak discharges, which is expected.

Annual peak discharges were recorded at Topopah Wash at Little Skull Mountain, Nevada Test Site, Nevada for the period 1984 to 1995. The site is approximately 10 km east of Yucca Mountain and has a drainage basin area of 269 km². The region 10 (Thomas et al. 1994), the Yucca Mountain area (Squires and Young 1984), and the statewide (Christensen and Spahr 1980) frequency curves estimate larger discharges than the systematic annual peaks. The site is just downstream of Christensen and Spahr's most downstream cross-section (Topopah Wash 1). Christensen and Spahr use a drainage area of 272 km² compared to the 269 km² of the gauge site. The minor difference is probably due to different drainage area delineation and subsequent computation in the mountainous terrain around and in the flat expanses of Jackass Flats. The difference between the estimated statewide frequency curve 100-year peak discharge of 505 m³/s and Christensen and Spahr's estimated flood frequency curve 100-year peak discharge of 320 m³/s is probable due to using the gauge elevation instead of the mean basin elevation in the regression equation. Christensen and Spahr did not document what mean basin elevation they used in their computations. Increasing the elevation from the 975 m of the gauge to 1,410 m in the statewide frequency curve 100-year peak discharge estimate would result in a similar peak discharge to Christensen and Spahr's. The short period of record (12 years) also makes any comparisons tenuous. A factor which may influence the systematic annual flood peaks is human development in the drainage basin. A support facility area with impervious streets, parking lots, and roof areas, only 1 to 2 km upstream of the gauge site, can generate runoff from storms that do not seem to have natural runoff. Peak discharges from these events are then recorded by the gauge. The systematic annual peak record may not reflect natural conditions, especially at the high exceedence probability percentages. The systematic peak discharges may give a false indication of the natural shape of the flood frequency curve. The regional maximum flood (Christensen and Spahr 1980) is larger than all the measured and estimated peak discharges, which is expected.

Annual peak discharges were recorded at Amargosa River tributary near Mercury, Nevada for the periods 1963 to 1982 and 1984 to 1995. The site is approximately 45 km southwest of Yucca Mountain and has a drainage basin area of 285 km². Station data was analyzed using a log Pearson Type III frequency distribution procedure (Thomas et al. 1994). Thomas et al. only used the 1961 to 1982 and 1984 to 1985 records in their analysis. They removed peaks considered to be low statistical outliers for the log Pearson III analysis, but did not document which ones were removed. Such outliers can result from a number of factors including incorrect measurements, unknown changes in sampling conditions, etc. The low outliers were removed using the statistical procedure included in the Pearson Type III method, based on the authors' evaluation of the historical data presented in the flow distribution curve. The purpose of removing the low outliers was to generate better statistical parameters for data evaluation purposes (by removal of data points that did not fall into the same "family" as the other data points). Removing outliers in this way helps avoid skewing the theoretical flow probability distribution and allows an improved statistical estimate of the flow distribution curve to be developed that is more representative of actual flow conditions at the monitoring station location. The region 10 frequency curve (Thomas et al. 1994) estimates higher discharge compared to the systematic annual peaks. The weighted results, a combination of the log Pearson III and the region 10 results, is similar to the systematic annual peaks. The Yucca Mountain area frequency curve (Squires and Young 1984) is in line with systematic annual peaks. The

statewide frequency curve (Christensen and Spahr 1980) is larger than the systematic annual peaks. The 32 years of systematic record is one of the longest in the Yucca Mountain area, but still is short for making comparisons to 100-year and 500-year estimated peak discharges. The comparisons require caution in evaluating the different frequency curve estimates.

French (1984) considers the use of Manning's equation to compute streamflow depth in the flood potential studies of Topopah Wash and Fortymile Wash to be inappropriate because the assumptions needed for its use are probably violated. The assumption of steady or uniform streamflow during peak discharge is probably not valid. The short duration of the flows does not allow steady or uniform conditions to exist. The assumption of minimal sediment transport during large floods (100-year, 500-year, and maximum) is probably not valid. Large amounts of sediment are carried affecting the density of the flow, the cross-sectional area, and the channel roughness. The assumption of permanently entrenched channels is probably not valid. During the time span of many years channel locations can move around on alluvial fan surfaces, thus mapping of inundation areas based on channel location may not be valid. The assumption of stable channel geometry is probably not valid. Stable alluvial channels do not exist on alluvial fans because a state of equilibrium does not exist between the sediment supply and its transport through the channel system. French proposed an alternative methodology to better assess flood hazards, but the methodology still needs to be validated. Crippen (1979), Christensen and Spahr (1980), and Squires and Young (1984) acknowledge the problems in mapping inundation areas during large recurrence intervals or maximum floods.

Bullard (1986, 1991), and Blanton (1992) report on three probable maximum flood studies following U.S. Bureau of Reclamation procedures. Bullard (1986) estimated probable maximum flood hydrographs at 15 sites on Yucca Mountain. Eleven individual drainage basins and four sites at the confluence of drainage basins were selected based on facility designs when vertical shafts to the potential repository horizon were being considered. Bullard (1991) estimated probable maximum flood hydrographs at seven sites on Yucca Mountain. These drainage basin locations are based on facility designs when a tunnel to the potential repository horizon was proposed. Blanton (1992) bulked up Bullard's (1991) probable maximum flood hydrographs to account for entrained air, debris, and sediment. He then routed the probable maximum flood hydrographs through measured cross-sections and plotted probable maximum flood inundation areas (Figure 5.1-13).

Probable maximum precipitation estimates from Hydrometeorological Report 49 (National Weather Service 1984) were the input for probable maximum flood hydrograph estimates. Bullard (1986) considered both local and general storms. Bullard (1991) only considered local storms because in the 1986 study, local storms always created probable maximum floods with much larger peaks and larger volumes for the small drainage basins investigated. In support of this concept, the ten largest observed unit peak discharges in the Yucca Mountain area occurred after summer thunderstorm rainfall events (Table 5.1-4). The local storm was considered to be an isolated event and no large antecedent rainfall events are assumed to occur before the design storm. The same central location was used for both studies to determine values from Hydrometeorological Report 49 (latitude 36°52'30" and longitude 116°26'48"). Only one central point was chosen because the drainage basin under consideration are small and plot essentially at one point on the maps from Hydrometeorological Report 49. A value of 10.3 inches for 1^{mi} per 1 hour was estimated from the Hydrometeorological Report 49 map. A design storm for each drainage basin was estimated based

on corrections for 6-hour duration and drainage basin size (if larger than 1 mi²). Fifteen-minute precipitation increments were estimated first based on Hydrometeorological Report 49 procedures. The 15-minute incremental precipitation values were then broken into smaller increments and rearranged into the design storm. The 1986 study used 1- and 2-minute increments. The 1991 study used 3-minute increments.

The probable maximum flood computations required the use of a dimensionless hydrograph for extreme events representative of the Yucca Mountain area. A dimensionless hydrograph (called the Phoenix Mountain dimensionless graph) had been developed using flood reconstitution data for the New River near Rock Springs, Arizona and New River at New River, Arizona (U.S. Army Corps of Engineers 1974). For the Yucca Mountain probable maximum flood studies the original Phoenix Mountain S-graph was converted to a dimensionless hydrograph by doing a numerical differentiation and adjustment for units. The Bureau of Reclamation and Corps of Engineers flood hydrologists believed the Phoenix Mountain dimensionless hydrograph would be appropriate to use for probable maximum flood computations on Yucca Mountain.

The Phoenix Mountain dimensionless hydrograph is used to estimate a unit hydrograph for each drainage basin in the probable maximum flood computations. Two basin parameters, the drainage area and lag time, and the appropriate incremental time period (unit duration) are used for the computations. YMP topographic maps are used to measure drainage basin area and channel lengths. Elevations are also picked off the maps. Lag times are computed from an empirical equation based on the results of many historic flood observations and flood reconstitutions by the Bureau of Reclamation and Corps of Engineers. The lag time equation uses the channel length of the drainage basin, the longest channel length from the point of collection to a point opposite the centroid of the drainage basin area, the slope of the longest channel (change in channel elevation divided by the channel length), and hydrologic efficiency coefficient. The hydrologic efficiency coefficient is estimated to be 0.5 for local storms in the 1986 and 1991 studies and 0.6 for general storms in the 1986 study.

Retention rates (infiltration estimates) are subtracted from the design storm incremental precipitation estimates (1, 2, or 3 minutes) to compute a incremental runoff excess volume. An incremental hydrograph is computed by multiplying the drainage basin unit hydrograph by the incremental runoff excess volume. The incremental hydrographs are summed over the design storm period for the probable maximum flood hydrograph. Clear water conditions were assumed for the 1986 and 1991 studies. No effects of climate change on the probable maximum precipitation were considered.

Bullard (1986) developed probable maximum flood hydrographs for 11 sites on Yucca Mountain when vertical shafts were being planned to access the potential repository rock strata. He also developed four additional probable maximum flood hydrographs for sites just downstream of the confluence of two upstream drainage basins by adding the results of the upstream probable maximum flood hydrographs. Both local and general maximum precipitation events were used to compute probable maximum floods for the 11 small drainage basins. The drainage areas ranged from 0.026 to 11.16 km². Estimates of retention rates for the local storms are 1.00 inch (25.4 mm) of initial loss and a loss rate of 0.05 inch per hour (1.27 mm per hour). Estimates of retention rates for the general storms are 0.00 inch (0.00 mm) of initial loss and a loss rate of 0.05 inch per hour (1.27 mm per hour). The assumed initial loss for the general storms occurs during the less intensive

initial portion of the design storm with the precipitation occurring during the period not contributing to the probable maximum flood hydrograph. The initial portion of the general storm is at least 30 hours long and is not included in the probable maximum flood hydrograph computations. For the local probable maximum flood's peak, discharges ranged from 6.94 to 1,226 m³/s and volumes ranged from 8,631 to 3,817,000 m³. For the general probable maximum flood's peak, discharges ranged from 0.48 to 182 m³/s and volumes ranged from 4,932 to 2,674,000 m³. Local probable maximum floods always have larger peaks and larger volumes than general probable maximum floods. For design purposes the local probable maximum floods are preferred to general probable maximum floods. Probable maximum flood peak discharges are larger than a regional maximum flood envelope curve and a local gauge flood data, which is expected (Figure 5.1-14).

Bullard (1991) developed probable maximum flood hydrographs for seven sites on Yucca Mountain when tunnels were being planned to access the potential repository rock strata. Only local precipitation events were used to compute probable maximum floods for the small drainage basins of interest, since the 1986 study showed this is the preferred design storm. The drainage areas range from 0.052 to 11.53 km². Estimates of retention rates for the local storms are 1.00 or 2.00 inches (25.4 or 50.8 mm) of initial loss and a loss rate of 0.05 inch per hour (1.27 mm per hour). The 2.00-inch (25.4 mm) initial loss probable maximum floods have smaller peaks and volumes than the 1.00-inch (25.4 mm) initial loss probable maximum floods. For design purposes the 1.00-inch (25.4 mm) initial loss probable maximum flood is preferred. The probable maximum flood's peak discharges range from 10.2 to 949 m³/s and volumes range from 17,262 to 3,470,000 m³. As a quality assurance check of these results, a separately developed method was used to verify these results. Comparison between the probable maximum flood's estimates from the Corps of Engineers HEC-1 rainfall-runoff program and the probable maximum flood hydrographs from the Bureau of Reclamation show minor differences in peak discharges, time to peak, and hydrograph volume. Differences in curve fitting techniques between the two methods attribute to the minor differences. 1991 probable maximum flood peak discharges are also higher than a regional maximum flood envelope curve and a local gauge flood data, which is expected.

Blanton (1992) computed new probable maximum floods for Bullard's 1991 sites using a bulking factor for the entrained air, debris, and sediment load in the streamflow. The Bureau of Reclamation, in their flood inundation analyses, proposed that a bulking factor of 2 be used to account for increased flow depths caused by the presence of entrained air, debris, and sediment load relative to clear water flow. Using the Bureau of Reclamation-recommended approach, a multiplier of 2 was thus applied by Blanton to adjust the 1991 clear water probable maximum flood data for purposes of estimating new probable maximum floods for the 1991 sites. There is no known published rationale supporting the basis for selection of the bulking factor value of 2. Routing of the bulked up peak discharges through surveyed cross-sections determines the water surface profiles along a reach. Potential facility sites determined the four different reaches, each defined by several cross-sections. Cross-sectional elevation data was field surveyed. Channel roughness coefficients for all reaches and cross-sections was estimated to be " $n=0.045$ " for use in Manning's equation. Critical flow is reached in the reaches because of the steep gradient and the roughness estimate is not relatively important. The step backwater computations assumed critical flow at the downstream cross-section because of the steep slope. A critical elevation check at the next upstream cross-section prevents super critical flow conditions, and critical flow conditions were then used at the upstream cross-sections. The water surface profiles were transferred to site scale topographic maps

for portions of Mid-Valley Wash in Midway Valley, Drill Hole Wash, Coyote Wash, and the Exploratory Studies Facility South Portal area and flood inundation boundaries for the bulked up 1991 probable maximum floods were located.

Glancy (1994) discussed the flood potential in Coyote Wash on Yucca Mountain. Empirical estimates of peak discharge ranged from 25.4 to 73.6 m³/s for a 0.24 km² drainage area of North Fork Coyote Wash. Geologic evidence supports the discharge estimate, which would include both water and the accompanying debris and sediment.

Savard (1990, 1991a, 1991b, 1992) analyzed Yucca Mountain regional streamflow time series with chaos theory. If the streamflow time series exhibited chaotic behavior, then long-term predictability of streamflow would be impossible. No evidence of low-dimensional chaos was found; the dynamic system generating streamflow probably is random.

Savard (1995b, 1998) and Grasso (1996) discussed climatic and weather patterns responsible for Yucca Mountain region streamflow and the associated flooding. Winter/spring streamflow occurs during El Niño events when the track of Pacific cyclonic fronts passes the Yucca Mountain area. Summer streamflow occurs from thunderstorms, often when the summer monsoon in the Southwest U.S. extends into the Yucca Mountain area. Occasionally remnant hurricanes from the Pacific move into the Yucca Mountain area causing streamflow in the late summer and fall.

5.1.5.2 Regional Flood Potential Studies

Crippen and Bue (1977) developed regional maximum flood envelope curves for 17 physiographic flood regions in the U.S. The Yucca Mountain area is in their flood-region 16, which includes the Great Basin and the lower Colorado basins. Peak discharges from seven sites in the region (Arizona, New Mexico, Utah, Nevada, and California) define the drainage area, in square miles, to peak discharge, in cubic feet second, envelope curve. Crippen (1982) presents the mathematical formulation of this curve:

$$Q = 98,900 * (A^{1.029}) * [(A^{0.5}) + 5]^{-1.341}$$

or if $A < 0.05$ square miles, then

$$Q = 9,878 * A$$

where:

Q = peak discharge in cubic feet per second and
A = drainage basin area in square miles.

No exceedence probability or recurrence interval frequency is assigned to the peak discharge estimates from the envelope curve. Christensen and Spahr (1980) and Squires and Young (1984), estimate maximum floods from this equation for drainage basin in their flood potential study areas.

Crippen (1979), in a study of potential hazards from floods in the Furnace Creek area, modified the equation for the regional maximum flood envelope curve for use in the Death Valley area by changing the coefficient 98,900 to 66,000. The new coefficient was based on the peak discharge from the September 14, 1974 flood in Eldorado Canyon (Glancy and Harmsen 1975). The peak discharge of 76,000 ft³/s was approximately two-thirds of the regional maximum flood envelope curve discharge for a 22.8 mi² drainage basin, 116,000 ft³/s. The coefficient 98,900 was multiplied by two-thirds to obtain the new coefficient 66,000. Crippen (1981) in a study of potential hazards from floods in Wildrose Canyon (western slope of the Panamint Range, western mountain range of Death Valley), Bowers (1990) in a study of potential hazards from floods in Grapevine Canyon (around Scotty's Castle, Northern Death Valley), and Grasso (1996) in study of Death Valley lake formation, estimated maximum flood peak discharges with the modified equation.

Hjalmarson and Phillips (1997) reexamined the peak discharge of one of the points in Crippen and Bue's (1977) regional maximum flood envelope curve analysis for their flood-region 16, which includes the Yucca Mountain area. An eyewitness of the Bronco Creek near Wikieup, Arizona flood of August 19, 1971 observed floodwaves overtopping the highway bridge at the site. Translatory waves may have been responsible for the observed floodwaves and increased the previously published instantaneous peak by 32 percent (2,082 to 2,742 m³/s). Hjalmarson and Phillips caution the translatory wave technique needs verification by experiment, observation, and research. The regional maximum flood curve is drawn above the Bronco Creek data point and the proposed new peak discharge still is slightly below the regional maximum flood envelope curve (2,888 m³/s, 102,000 ft³/s, 19 mi²). The regional maximum flood envelope curve may need to be updated, if the increased instantaneous peak discharge is found to be correct.

5.1.6 Chemistry of Surface Water

The chemistry of surface water flows in the Yucca Mountain area and surrounding region has been evaluated through analytical testing of intermittent storm water runoff, spring discharges, or runoff or drip water samples comprised of mixed overland runoff and spring discharge water. In some cases, the surface water samples tested included a shallow infiltration water discharge water component. The chemistry of these waters provides an indication of the surface and shallow subsurface (meteoric) water chemical environment at the time of sampling. Such data reflect the chemical make-up of the surface and near-surface soils and/or the chemistry of the contributing groundwater and subsurface groundwater medium. This information provides data that can be used for assessing infiltration pathways, processes and rates, subsurface water-rock interactions, and near-surface and subsurface geochemical and mineralization processes.

Information on the chemistry of surface water flows is presented in the following subsections to characterize baseline surface water chemical conditions at and around the Yucca Mountain Repository Site. Subsections 5.2 and 5.3 include related discussions of chemical conditions in groundwater beneath Yucca Mountain and surrounding areas. Subsection 6.2 presents and compares the chemistry of precipitating waters, surface waters, and unsaturated zone waters (perched water and pore waters) and interpretations as to the relationships between these various water types.

Three general types of surface water chemistry data have been developed in the Yucca Mountain region depending on the source of the water: relatively dilute waters from runoff during precipitation

or snowmelt, relatively saline waters from groundwater discharge at large springs, and mixtures of the two preceding types. No studies with a description of surface water chemistry as the major objective exist. Preceding site characterization studies, a number of surface water samples were collected and tested over time to document groundwater chemistry from spring discharges. These samples are classified as surface water samples since the spring discharge represents emergent streamflow. These samples are documented in a number of publications. A limited number of samples have been collected to document streamflow chemistry during the occasional runoff event since Yucca Mountain site characterization studies were initiated. These sample analysis results are also documented in a number of publications. The physical characteristics and chemical composition of 27 surface water sites in the Yucca Mountain area have been compiled and are listed in Table 5.1-6. Twenty-four of the surface water sample results presented represent samples collected within the Amargosa River/Fortymile Wash drainage basin (Figure 5.1-15). The three additional surface water sample sites are located near Yucca Mountain on the Nevada Test Site (Whiterock Creek-Northern Yucca Flat and Rainer Mesa area, Yucca Lake-Yucca Flat, and Cane Springs Wash tributary-Frenchman Lake drainage basin). A compilation of hydrochemical data collected in the Death Valley region over the period 1910 to 1990 includes baseline data from rivers and playas in addition to springs and wells (Perfect et al. 1995). The compilation is presented in a digital format (Lotus 1-2-3). The main objective of compiling the data into such an electronic format was to both document and facilitate statistical analysis of groundwater quality in the Yucca Mountain area; however, surface water quality data were also compiled (which can also be analyzed using statistical methods). The chemical analyses in the compilation are taken from four general sources:

- USGS unpublished data files
- USGS National Water Information System database
- Published reports from Federal and State agency investigations
- Unpublished data

The compilation edited out duplicate samples and entries. A cation-anion balance was computed for each chemical analysis, then the analysis was assigned to one of three categories: the analysis balances to within ± 10 percent, not enough major ion information is available to calculate a balance, or the analysis balances over ± 10 percent. Samples from the salt pan area of Death Valley are included in the compilation but do not represent surface water quality found in the immediate Yucca Mountain area. Some surface water sample data included in the database is for groundwater spring discharge. As such, these water quality samples are probably more representative of groundwater than surface water originating from precipitation.

Surface water chemistry of samples taken in channels downstream of groundwater discharge points when there has been no recent precipitation or runoff component generally have specific conductances above 1,000 microsiemens per cm. The maximum specific conductance observed, 4,870 microsiemens per cm, was at the Amargosa River at Highway 127 (353953116174501) on March 21, 1967 (Table 5.1-6).

Hydrochemical data were reported for spring pools and discharge channels in Oasis Valley and Amargosa Desert groundwater studies (Walker and Eakin 1963; Dudley and Larson 1976; White 1979). Hydrochemical data along the upper and lower portion of the Amargosa River were tabulated

by Hunt et al. (1966) and Miller (1977). These data are dominated by the chemistry of the groundwater sources for the surface pools and channels.

Surface water chemistry of samples taken in channels during precipitation and runoff events when groundwater discharge is diluted generally have specific conductances below 300 microsiemens per cm (Table 5.1-6). The minimum specific conductance observed, 59 microsiemens per cm, was at Fortymile Wash at J-12 (364551116233700) on August 14, 1984. During periods of streamflow in August 1984, surface water samples were collected in Fortymile Wash, Drill Hole Wash, and Dune Wash. These were the first surface water samples collected during site characterization studies in the Yucca Mountain area.

During periods of streamflow in 1993, surface water quality samples were collected. Emmett et al. (1994) document analyses from dip samples of surface water in the Amargosa River drainage basin from six sampling sites. Three of the sites (Stockade Wash at Airport Road, Yucca Wash near mouth, and Cane Spring Wash) represent overland runoff during precipitation. The other three sites (Amargosa River near Beatty, Carson Slough at Stateline Road, and Amargosa River near Eagle Mountain) represent spring discharge from groundwater or mixing of overland runoff and spring discharge. Savard (1996) documents analyses from dip samples of Pah Canyon Wash and Delirium Canyon Wash in Fortymile Canyon. These two samples were taken during the later part of the streamflow hydrograph recession after peak discharge. The samples represent overland runoff from precipitation and possibly some mixing with discharge from shallow infiltration drainage in the soil and volcanic rock layers in the mountainous terrain of Fortymile Canyon.

During periods of streamflow in 1995, surface water quality samples were collected on Yucca Mountain and Fortymile Canyon (Table 5.1-6). The data from the dip samples have not been formally published previously but are contained in Yucca Mountain databases (DTN:GS960308312133.001, TBV). Six sites were in the Fortymile Canyon area (overland flow in Delirium Canyon, overland flow near the confluence of Fortymile Wash and Pah Canyon Wash, overland flow near Fortymile Wash raincan, Yucca Wash near mouth, Pah Canyon Wash, and Delirium Canyon Wash). Two sites were on Yucca Mountain (Wren Wash at Yucca Mountain and Split Wash below Quac Canyon). The sites on Yucca Mountain were sampled during overland runoff of precipitation. Some of the overland runoff from the hill slopes in the drainage basins infiltrated soil and volcanic rock layers, then reemerged as overland runoff. Some of the overland runoff also originated from disturbed areas in the drainage basins such as roads and drill pads where compaction of the surface material reduced infiltration and increased overland runoff. Some of the surface water quality samples in Fortymile Canyon were taken during overland runoff of precipitation and/or snowmelt, the others were taken during the recession period after peak discharge. All samples probably represent a mixing of overland runoff and shallow infiltration waters which discharge along the hill slopes.

Additional related information on the chemistry of percolating aqueous phase water recovered from the unsaturated zone, including both major-ion concentrations and isotopic compositions, is presented in Subsection 5.3.4. Subsection 5.3.5 includes a discussion of hydrogeochemical and isotopic data for the deep unsaturated zone/saturated zone that are relevant to evaluations of groundwater flowpaths and groundwater age. Surface water chemistry of samples taken in channels during precipitation and runoff events when groundwater discharge is diluted but not masked have

specific conductances above 300 microsiemens per cm. The specific conductance, 937 microsiemens per cm, at Carson Slough at Spring Meadows Road (362453116214501) on January 27, 1959, is probably this type of mixture. Five samples were taken during the winter of 1957 to 1958 when there was continuous flow along the lower portion of the Amargosa River during what Hunt et al. (1966, Table 15) described as a wet season. Total dissolved solids increased downstream, indicating a greater contribution of groundwater discharge to the total flow than surface water runoff.

Surface water data obtained for selected streams and springs at and east of the Yucca Mountain Repository Site are described in Subsection 6.2.4, summarized in Tables 6.2-5a and 6.2-5b, and plotted on trilinear diagrams and linear cross-chemical comparison plots shown in Figures 6.2-8 and 6.2-10, and 6.2-11. Additional comparisons of surface water, perched water, and groundwater chemistry data are presented on subsequent figures supporting Subsection 6.2.4, and key findings and conclusions developed from evaluation of these data are summarized in Subsection 6.2.4.

McKinley and Oliver (1994, 1995) tabulate water quality from sampling sites in two basins in Central Nevada: Three-Springs Basin and East Stewart Basin. The physical characteristics and chemical composition of surface water samples from their studies are tabulated in Tables 5.1-7 and 5.1-8. Three-Springs Basin is a semiarid basin in the Kawich Range east of Tonopah. East Stewart Basin is a subalpine basin in the Toiyabe Range north of Tonopah. The two basins were being studied as analog sites to Yucca Mountain during wetter and cooler periods. Water quality samples were collected from precipitation, springs, and surface water during the period 1986 to 1992. Springs in the basins are probably above the regional groundwater system and do not represent discharge from large groundwater basins, as at Ash Meadows in the Amargosa Desert. The water quality of the spring discharges does represent movement of water through unsaturated volcanic rock layers in the basins. Surface water samples can represent overland runoff from precipitation or snowmelt and also can represent mixing of spring discharge with overland runoff.

Most of the surface water quality samples were collected as dip samples near the waters edge since access across the stream was impossible or near the middle of the channel since the flow was so small. Dip samples may not represent an integrated sample for all of the surface water at a site for large flows, but probably are representative for small flows. An integrated sample from across the stream cross-section would be desirable because of stream chemistry variability across the cross-section. Tributary inflow upstream of the dip sampling point may influence the sample and not be representative of all the upstream drainage basin. Reaeration of surface water as it proceeds down the channel may also affect the chemistry. Some samples were analyzed for bicarbonate in the laboratory instead of at the site during collection. Transport of the samples can cause mixing with atmospheric gases and change the sample temperature. These procedures may effect the bicarbonate concentration which is in dynamic equilibrium with carbon dioxide. Some samples were collected at the site and bicarbonate changes are minimized.

Man-made disturbances influence sediment concentrations in surface water. During light precipitation events in 1995, fine sediment, which probably originated from the Exploratory Studies Facility north portal pad and tunnel waste piles, was transported down Drill Hole Wash, clogging infiltration pathways in the channel alluvial material. With the resulting reduction of infiltration, surface water runoff and sediment were being moved much greater distances than under natural

conditions. During some of the periods of runoff from the Exploratory Studies Facility pad no other runoff was noted in the area, indicating that the Exploratory Studies Facility pad and tunnel waste piles were influencing water quality and runoff characteristics.

5.1.7 Location, Quantity, and Quality of Surface Water Extracted

Since runoff from precipitation and snowmelt is intermittent throughout the Yucca Mountain area and surrounding region, no systemic extraction of surface water runoff is possible. The municipality of Tecopa pumps water from the Amargosa River channel, which is spring discharge, upstream of the Amargosa River at Tecopa gauging station (Clary et al. 1995). The quantity or the frequency of pumping is unknown.

Savard and Beck (1994) and Savard (1998) discusses natural streamflow infiltration losses from flood flows in Fortymile Wash. These infiltration losses recharge the groundwater system, from which water supplies are extracted.

5.1.8 Projected Surface Water Use

No known use of surface water is projected.

5.2 REGIONAL HYDROGEOLOGY

Subsection 5.2, Regional Hydrogeology, documents the status of understanding of the regional hydrogeologic system of the Death Valley region as of 1997. The boundaries of the Death Valley region used in this report are those defined by D'Agnese et al. (1997, p. 4). The Death Valley region has an area of approximately 50,000 km² and is located in Nevada and California (Figure 5.2-1). The region is part of the Basin and Range physiographic province (Basin and Range province) of the Southwestern United States and includes several large prominent valleys, namely Amargosa Valley, Pahrump Valley, and Death Valley (Figure 5.2-1). The region also includes several major mountain ranges including the Panamint Range, the Spring Mountains, the Sheep Range, the Amargosa Range, the Kawich Range, the Kingston Range, the Pahranaagat Range, the Timpahute Range, and the Last Chance Range (Figures 5.2-1 and 5.2-2).

The concepts and information of many investigators who have studied the hydrogeology of the Death Valley region are presented in Subsection 5.2. Conclusions reached about the hydrogeology of the Death Valley region are based on all of these previous investigations, however, most of the previous investigators presented information of localized hydrogeology, and only a few discussed the hydrogeology on a regional scale. Subsequently, most of the conclusions in Subsection 5.2 are based on those reports which dealt with the hydrogeology on a regional scale, with supportive documentation coming from the reports of the localized hydrogeology.

Quality Assurance Controls—Yucca Mountain Site Characterization Project (YMP) work summarized in this section comes under the control of the *Quality Assurance Requirements and Description* (DOE 1997b). Some of the information presented and discussed, however, was developed outside of the YMP and has been included here through examination of the hydrogeological literature. Thus, the quality assurance status of the data in this section is determined by the activities and reports from which the description was synthesized. To determine the Q status of a particular data set, interested readers should consult the source document cited in the text.

5.2.1 Flow System Boundaries and Hydrogeologic Units

Harrill, Welch et al. (1983, p. 6), stated that a basic premise in defining a unique flow system is that each flow system terminates in a sink. Consequently, in defining a flow system, the task is reduced to identifying areas that contribute groundwater to a particular sink. For local systems consisting of only one basin and for smaller regional systems consisting of a sink and one or more adjacent tributary basins, the task is simple. However, within the Great Basin province, some of the larger regional systems extend greater than 100 miles and have flowpaths that traverse many basins. In some instances, some water is discharged at intermediate points along flowpaths; consequently, only part of the groundwater flows all the way to the regional sink. In the simplest case, the intermediate discharge represents a circulation cell in the shallower part of a regional system. In many systems, however, the intermediate discharge represents flow derived from a group of areas that constitutes a regional-scale multibasin subsystem. This situation is dealt with by assuming that a large regional flow system has one principal sink area and that all flow in the system is generally toward this sink. Harrill, Welch et al. (1983, Figure 2) presented a general hierarchical scheme that could be used to delineate a multibasin flow system. With this hierarchical scheme and applying the general

procedures just discussed, Harrill, Welch et al. (1983, Figure 3) and Harrill, Gates et al. (1988, Figure 6) defined 39 groundwater flow systems in the Great Basin province.

In a study conducted by the USGS to evaluate potential hydrogeologic environments for isolation of high-level radioactive waste, the basin and range physiographic province was divided into six regions (Bedinger, Langer et al. 1989a, p. A2). The regions were selected on the basis of adopted guidelines and on information obtained on:

- The distribution of rock types that may be host media for radioactive waste
- Characteristics of the province related to tectonic stability–seismicity, late Cenozoic volcanism, Quaternary faulting, late Cenozoic regional uplift, and heat flow
- The hydrology of groundwater flow systems

One of these six regions was defined as the Death Valley region which was divided into nine groundwater units (Bedinger, Langer et al. 1989b, pp. F28, F29, plate 5). Two of these groundwater units (DV-02 and DV-03) were similar in area to two of the groundwater flow systems (Death Valley and Mesquite Valley, #28 and #36,) defined by Harrill, Welch et al. (1983, Figure 3) and Harrill, Gates et al. (1988, Figure 6).

In a report to document the regional hydrologic modeling studies conducted by the USGS as part of the site characterization activities at Yucca Mountain, D'Agnese et al. (1997, p. 4) characterizes the regional hydrogeology of the Yucca Mountain area and documents a numerical simulation of the present-day (1997) regional groundwater flow system. In their report, D'Agnese et al. defined the area and flow system boundary of the Death Valley Regional Groundwater Flow System (Figure 5.2-1). This area defined by D'Agnese et al. included the DV-02 and DV-03 groundwater units of the area defined as the Death Valley region by Bedinger, Langer et al. (1989b, plate 5), and also encompassed the Death Valley and Mesquite Valley groundwater flow systems defined by Harrill, Welch et al. (1983, Figure 3) and Harrill, Gates et al. (1988, Figure 6). Further, in defining the Death Valley Regional Groundwater Flow System, D'Agnese et al. defined Death Valley as being the ultimate groundwater sink of the flow system.

For the purpose of Subsection 5.2 of this report, the Death Valley Regional Groundwater Flow System¹ defined by D'Agnese et al. will be the area used to define the regional hydrogeology. The area defined by D'Agnese is used for two reasons:

- It is the smallest unique regional flow system which encompasses all of the Yucca Mountain area.

¹ Within Subsection 5.2, "Death Valley region" will be synonymous with the area defined as the Death Valley Regional Groundwater Flow System. However, it should be noted, that though the Death Valley Regional Groundwater Flow System defined by D'Agnese et al. (1997) is used in this subsection, the area referred to as the "Death Valley region" in the report by D'Agnese et al. is larger than and encompasses the Death Valley Regional Groundwater Flow System. Subsequently, if the reader refers to any of the reports referenced in Subsection 5.2, the "Death Valley Region" discussed in these reports will not be the same area as the "Death Valley Region" defined here.

- It is similar to unique flow system areas defined by Harrill, Welch et al. (1983) and Bedinger, Langer et al. (1989b).

The groundwater flow system of the Death Valley region is complex. Groundwater movement within the region may be classified as movement of perched water, intrabasin movement of water, and interbasin movement of water (Winograd and Thordarson 1975, p. C49). Movement of perched water, though important on a local scale, does not significantly affect the regional flow of groundwater. Intrabasin flow of groundwater can be described as groundwater moving laterally in valley-fill aquifers from recharge areas in the flanking mountains toward discharge areas in playas, streams, or adjacent valleys. Typically the bedrock underlying or flanking the valley fill is considered to be relatively impermeable in comparison to the valley fill (Winograd and Thordarson 1975, p. C53). Interbasin flow of groundwater can be described as flow through deep regional aquifers which are not controlled by topographic boundaries of individual valleys.

The southeastern portion of the Death Valley region lies within a hydrogeologic region known as the carbonate-rock province of the Great Basin (Prudic et al. 1993, pp. 1, 3, 4, Figure 1), which is characterized by thick sequences of carbonate rock. These rocks form a generally deep regional aquifer of the flow system, which allows interbasin transfer of groundwater in the Death Valley region (D'Agnese et al. 1997, p. 5). In the Yucca and Frenchman Flats areas Winograd and Thordarson (1975, p. C53) stated that the deep water table in these areas is due to the drainage of groundwater from the valley-fill into the underlying and surrounding carbonate rock aquifer. In other valleys, such as the Amargosa Desert, Southern Indian Springs Valley, and possible Eastern Jackass Flats, interbasin movement of groundwater is upward. Subsequently, a hydraulic connection can be assumed to exist between the valley-fill aquifers and deeper carbonate rock aquifer.

The northwestern portion of the Death Valley region is underlain by volcanic rock. The volcanic rock in this area is part of the southwest Nevada volcanic field (Laczniak et al. 1996, p. 15, Figure 4). The water-bearing properties of these volcanic deposits are governed chiefly by the mode of eruption and cooling, by the extent of primary and secondary fracturing, and by the degree to which secondary alteration (crystallization of volcanic glass and zeolite alteration) have affected primary permeability (Laczniak et al. 1996, p. 15). On a regional scale, the volcanic rocks are assumed to be in hydraulic connection with valley-fill aquifers and the carbonate aquifers. This hydraulic connection may be either a lateral (subbasin to subbasin flow) or vertical connection (valley-fill aquifers overlying the volcanic rock).

5.2.1.1 Boundaries of Regional Flow System

The Death Valley regional groundwater flow system defined by D'Agnese et al. (1997, p. 59) consists of groundwater moving through a 3-D body of consolidated and unconsolidated materials. Subsequently, three principal flow boundaries are defined for the Death Valley region: the upper boundary, the lower boundary, and the lateral boundaries. These flow system boundaries are either physical boundaries, caused by changes in bedrock conditions, or hydraulic boundaries, caused by potentiometric surface configurations. The upper boundary of the flow system is the water table. The lower boundary of the flow system is located at a depth where groundwater flow is dominantly horizontal and moves with such small velocities, that the volumes of water moving through the

system do not significantly impact regional flow estimates. The lateral limits of the regional flow system may be either no-flow or flow boundaries.

For the Death Valley region, the area of the region is defined by the lateral flow system boundaries (Figure 5.2-1). For these lateral boundaries, no-flow conditions exist where groundwater movement across the boundary is prevented by physical barriers or divergence of groundwater flowpaths. Flow boundaries exist where groundwater potentiometric gradients permit flow across a boundary through fractures or higher permeability zones (D'Agnese et al. 1997, p. 59). Most of the lateral boundaries are no-flow boundaries that result from the presence of low-permeability bedrock. However, flow boundaries do occur where bedrock has a high enough permeability to allow significant groundwater fluxes to enter the Death Valley regional groundwater flow system and where a hydraulic gradient exists across the regional boundary. Faulting and fracturing most frequently cause the enhanced permeability, and groundwater flow may occur at various depths through open regional fracture zones (D'Agnese et al. 1997, p. 59). Based on potentiometric and hydrogeologic data (Figures 5.2-3 and 5.2-4), areas where groundwater inflow may occur from are Pahrnagat Valley, Sand Spring Valley, Railroad Valley, Stone Cabin Valley, Ralston Valley, Fish Lake and Eureka Valleys, Saline Valley, Panamint Valley, Pilot Knob Valley, and Soda Lake Valley (Figure 5.2-5) (D'Agnese et al. 1997, p. 62).

5.2.1.2 Boundaries of Subregional Flow System

For the numerical simulation of the Death Valley region, D'Agnese et al. (1997, p. 62) modified the limits of the Death Valley region flow system and divided the region into three major subregional flow systems (Figure 5.2-6). However, not all of the Death Valley region is defined by these three subregions. The modifications made by D'Agnese et al. were based on previously defined flow system boundaries, the potentiometric surface, and the hydrogeologic framework of the Death Valley region (D'Agnese et al. 1997, p. 62). The modification and smaller size of the combined subregions was done because few data existed that would allow a precise definition of the western and southern extent and a small section of the northern extent of the Death Valley region flow system. In terms of the western boundary of the subregions, the boundary is placed to coincide with the eastern edge of Death Valley, which is interpreted as the terminal sink of the Death Valley region. For the northern and southern extent boundaries were chosen because of the sparsity of data beyond these areas. More information is given on groundwater flow across these boundaries in Subsection 5.2.5.

5.2.1.3 Hydrogeologic Units

The Death Valley region has a long and active geologic history, including intermittent marine and non-marine sedimentation, large-scale compressive deformation, plutonism, volcanism, and extensional tectonics. Consequently, diverse rock types, ages, and deformational structures are often juxtaposed to each other. As a result, subsurface conditions are variable and complex and knowledge of the geologic diversity beneath alluvial basins is indirect in most of the Death Valley region (D'Agnese et al. 1997, p. 13). A detailed discussion of the regional geology is given in

Subsection 3.2, Regional Geologic Setting, and will not be repeated here; however, the regional geology can be summarized as consisting of:

- Precambrian and Cambrian clastic and crystalline rocks
- Paleozoic clastic and carbonate rock
- Clastic and intrusive rocks of Mesozoic age
- Tertiary tuffs, lava flows, and volcanoclastic rocks
- Varied fluvial, paludal, and playa sedimentary deposits of Pliocene age
- Tertiary-Quaternary alluvial, colluvial, eolian, and volcanic deposits

Groundwater hydrology of a region can best be discussed by grouping numerous geologic formations and members into units of hydrologic significance (hydrogeologic units) (Winograd and Thordarson 1975, pp. C13, C14). A hydrogeologic unit has considerable lateral extent and has reasonably distinct hydrologic properties because of its physical (geological and structural) characteristics (Faunt et al. 1997, p. 10). Winograd and Thordarson (1975, Table 1), defined 10 hydrogeologic units in the Death Valley region. Bedinger, Langer et al. (1989b, Table 1), defined 12 hydrogeologic units in the Death Valley region.

Faunt et al. (1997, p. 1), in a study to develop a conceptual hydrogeologic framework using regional geological and hydrological data, and to develop a digital hydrogeologic map depicting the surface expressions of the hydrogeologic framework, defined 10 hydrogeologic units (Figure 5.2-4):

- Playa Deposits of Quaternary Age (Qp)
- Valley Fill of Quaternary-Tertiary Age (QTvf)
- Volcanic rocks of Quaternary-Tertiary Age (QTv)
- Volcanic Rocks of Tertiary Age (Tv)
- Volcanic and Volcanoclastic Rocks of Tertiary Age (Tvs)
- Granitic Rocks of Tertiary-Late Jurassic Age (TJg)
- Sedimentary and Metavolcanic Rocks of Mesozoic Age (Mvs)
- Carbonate Rocks of Paleozoic Age (P2)
- Clastic Rocks of Paleozoic-Precambrian Age (P1)
- Igneous and Metamorphic Rocks of Precambrian Age (pEgm)

The study area of Faunt et al. was a 100,000 km² area which included the Death Valley Regional Groundwater Flow System defined for Subsection 5.2 of this report. In defining the 10 hydrogeologic units, Faunt et al. (1997, p. 8 and table 2 p. 11) conceptualized the regional hydrogeologic system based on those of Bedinger, Langer et al. (1989b, 1989c), Winograd and Thordarson (1975), Grose (1983), and Grose and Smith (1989) (Table 5.2-1).

For the purpose of Subsection 5.2 of this report, the 10 hydrogeologic units defined by Faunt et al. (1997, pp. 12-14) will be used to define the hydrogeologic units of the Death Valley region because:

- The synthesis of the hydrogeologic units by Faunt et al. is in excellent agreement with the hydrogeologic units found in the literature and can be easily cross referenced to these previously defined hydrogeologic units.

- The hydrogeologic framework of the Death Valley Regional Groundwater Flow System defined by D'Agnese et al. (1997, p. 17), uses the 10 hydrogeologic units defined by Faunt et al. (1997, pp. 12-14).

The descriptions of the hydrogeologic units presented here are taken directly from Faunt et al. (1997, pp. 12-14). References within the hydrogeologic descriptions are those given by Faunt et al. Because Faunt et al. described an area larger than the Death Valley region defined for Subsection 5.2 of this report, some descriptions of the hydrogeologic units may pertain to areas outside the Death Valley regional flow system boundaries (Figure 5.2-4)

Playa Deposits of Quaternary Age (Qp)—The lacustrine confining beds, lake bed sediments of Quaternary age, are a relatively homogeneous deposit composed of mainly clay-sized particles. The unit includes fine-grained playa deposits, lacustrine limestone, and evaporites. Accordingly, the unit can exhibit matrix flow from the permeable unconsolidated deposits and fault and fracture-controlled flow in consolidated deposits (Downey et al. 1990). The lacustrine beds were deposited contemporaneously with the younger alluvial sediments. As a result, the deposits grade into each other. In some of the valleys, the lacustrine confining beds are several hundred meters thick.

Valley Fill of Quaternary-Tertiary Age (QTvf)—The alluvial sediments of Quaternary-Tertiary age are a heterogeneous mixture of volcanic and sedimentary rock detritus ranging from clay to boulder size. The heterogeneous mixture includes units of fine-grained playa and lake beds containing evaporites (of limited areal extent), boulder-cobble-pebble debris flow and fan deposits, and volcanic tuffs. Accordingly, they may exhibit matrix flow in the permeable unconsolidated materials, but fault- and fracture-controlled flow in more indurated materials (Downey et al. 1990). The valley fill (including fluvial deposits) accumulated largely in structural basins. As a result, the valley fill deposits range in thickness from zero at margins of valleys to several hundred meters in valley lowlands. The fill in many basins is greater than 1,300 m thick and may be as thick as 2,000 m (Bedinger, Langer et al. 1989a). The basin fill forms the major aquifer system in many of the valleys.

These basin fill aquifers constitute a regional system because of the similarities between basins and because they are the most developed source of groundwater in the region. Some basins are topographically and hydraulically closed by low-permeability bedrock, while others are part of multibasin flow systems connected by perennial streams or by flow through the basin fill or permeable bedrock (within the Death Valley regional flow system boundary, all basins are assumed to be of the multibasin flow systems). Well yields within the basin fill seem to be related to physiographic setting (Plume and Carlton 1988). The hydrologic properties of these deposits can differ greatly over short distances, both laterally and vertically, because of abrupt changes in grain size, and the degree of sorting and consolidation.

Volcanic Rocks of Quaternary-Tertiary Age (QTv)—The volcanic rocks, including lava flows and undifferentiated volcanic rocks of Tertiary and Quaternary age, underlie the valleys and crop out extensively in many of the mountains. The lava flows are primarily basalts, andesites, and rhyolites of Tertiary and Quaternary age. Columnar jointing and platy fractures are common in the flows, which vary from vesicular to dense. Secondary openings are developed along fractures and bedding

planes. Individual flows generally are less than 33 m thick; some are less than 1 m thick (Bedinger, Langer et al. 1989a). Aggregate thicknesses are as much as 1,000 m (Bedinger, Langer et al. 1989a).

Volcanic Rocks of Tertiary Age (Tv)—These volcanic rocks include tuffs and undifferentiated volcanic rocks of Tertiary and Quaternary age. They underlie the valleys and crop out extensively in northern and central portions of the Death Valley region (Figure 5.2-4), including the Yucca Mountain area, where tuffs of Tertiary age are widespread. These units have an aggregate thickness of more than 4,000 m. The composition and structure of these volcanic tablelands, and their position and mode of emplacement, drastically affect regional groundwater flow by altering flowpaths, providing numerous avenues of recharge, and altering water-table gradients.

This hydrogeologic unit includes densely welded to nonwelded, bedded, reworked, and air-fall tuffs. Welded ashflow tuffs characteristically have an interstitial porosity of about 5 percent or less (Bedinger, Langer et al. 1989a); thus, the commonly moderate to large hydraulic conductivity of welded ashflow tuffs is largely a function of secondary openings along joints, bedding planes, and partings within the flows. Where these welded tuffs are not fractured or jointed, they tend to form confining beds; thus, welded tuffs can only transmit significant quantities of water where they are fractured.

In contrast, nonwelded ashflow tuffs may have a large interstitial porosity, but low hydraulic conductivity, and can function as confining beds. Fractures and joints are virtually absent in nonwelded ashflow tuffs (D'Agnese et al. 1997). Hence, the nonwelded tuffs generally act as confining units. These nonwelded tuffs, however, have limited areal extent.

Volcanic and Volcaniclastic Rocks of Tertiary Age (Tvs)—Clastic and tuffaceous aquifers and confining beds comprise tuffs and associated sedimentary rocks. They include up to 1,500 m of a variety of nonwelded to welded ashflow tuff, ashfall tuff, tuff breccia, breccia flow deposits, tuffaceous sandstone, siltstone, mudstone, freshwater limestone, and minor amounts of densely welded tuff. Despite the widely differing origins of these rocks, this unit usually has matrices consisting of zeolite or clay minerals (Winograd and Thordarson 1975), which results in low hydraulic conductivity. Some of the limestone and densely welded tuff may not have zeolitic or clayey matrices, but are believed to have low hydraulic conductivity (Winograd and Thordarson 1975). These rocks usually separate the more permeable volcanic rocks (Tv) from the Paleozoic carbonate rocks (P2).

Granitic Rocks of Tertiary-Late Jurassic Age (TJg)—Crystalline granitic rocks of Mesozoic and Tertiary age are widespread throughout the southern portion of the region (Figure 5.2-4). They outcrop in many mountain ranges and underlie most of the southern portion of the region at depth (Bedinger, Langer et al. 1989a). Groundwater is thought to occur in these crystalline rocks only where they are fractured. Because the fractures are poorly connected, these rocks are believed to act mostly as confining units.

Sedimentary and Metavolcanic Rocks of Mesozoic Age (Mvs)—The clastic rocks of Mesozoic age are predominantly continental fluvial, lacustrine, and eolian deposits and clastic and carbonate sedimentary rocks. These rocks form extensive outcrops on the sides of the Spring Mountains where they have been thrust. The rocks have a variable thickness due to the extensive thrust faulting and

are some of the more permeable rocks in the Death Valley region; however, they are not widespread. Some of these rocks are also found in the southwestern portion of the Death Valley region (Bedinger, Langer et al. 1989a).

Carbonate Rocks of Paleozoic Age (P2)—Limestone, dolomite, and calcareous shales of Paleozoic age underlie many valleys and outcrop along the flanks of and throughout some mountains. These carbonate rocks cover an extensive portion of the area around Death Valley, extending to the north and east (Figure 5.2-4). They are often interbedded with siltstones and shales and locally interrupted by volcanic intrusions in the north. These carbonate rocks, which have an aggregate thickness of about 8,000 m, are probably the most permeable rocks in the area. Where hydraulically connected, they contribute significantly to interbasinal movement of water. This interbasinal movement includes movement of water within the groundwater basin between topographic basins, and the entrance of groundwater from basins to the northeast of the Death Valley regional flow system (Figure 5.2-5). Many of the springs in the area are associated with the carbonate rocks. Intergranular flow is not significant in these rocks; the large transmissivity is primarily due to fractures and solution channels (Winograd and Thordarson 1975). Hydraulic tests of carbonate-rock aquifers throughout Eastern and Southern Nevada indicate that faults can increase their transmissivity by factors of 25 times or more (Dettinger 1989a).

Clastic Rocks of Paleozoic-Precambrian Age (P1)—Siltstone, quartzite, shale, sandstone, and some metamorphic rocks of later Precambrian and Paleozoic age form clastic confining units. These rocks vary in aggregate thickness with a maximum thickness of about 3,500 m. These rocks have negligible interstitial groundwater movement but frequently are highly fractured and locally brecciated (Winograd and Thordarson 1975). At shallow depths, these fractures and breccias can be conduits to flow, converting these clastic rocks into locally important shallow aquifers.

Clastic rocks in the region differ hydrologically from carbonate rocks in two important ways. First, secondary porosity rarely develops along bedding planes in any of the clastic rocks because of the low solubility of their constituents including quartz, mica, and clay minerals. Second, the clastic rocks deform more plastically than the carbonates and, as a result, fractures may become sealed or isolated during deformation (Winograd and Thordarson 1975). In these rocks, the fractures may be sealed by continued deformation caused by the same process that formed them or by later plastic deformation. Open fractures in interbedded competent rocks may be sealed by plastic deformation of the less competent interbedded strata (Winograd and Thordarson 1975).

Igneous and Metamorphic Rocks of Precambrian Age (pCgm)—Crystalline metamorphic and igneous rocks of Precambrian age are widespread throughout the southern part of the region, cropping out in many mountain ranges and underlying most of the area at depth (Bedinger, Langer et al. 1989a). Hydrologically, this unit behaves similarly to the other crystalline rocks in the region (TJg). Groundwater is thought to occur only locally in these crystalline bodies where the rock is fractured. Because the fractures are poorly connected, these rocks are believed to act mostly as confining units.

Using the correlation between hydrogeologic units shown in Table 5.2-1, the stratigraphic units defined for the "Nevada Test Site and Vicinity" by Winograd and Thordarson (1975, Table 1) are related to the hydrogeologic units defined by Faunt et al. (1997, pp. 12-14) (Table 5.2-2).

A consortium of companies (IT Corporation; Tetra Tech, Inc., Geo Trans, Inc., and Daniel B. Stephens Corporation), developed a 3-D model, ("Underground Test Area Project, Phase I Data Analysis Task, Draft, March 1996," referred to here as the ITC Model) for the Department of Energy. The ITC Model was developed to provide the Department of Energy with a groundwater flow model of the Death Valley region to be used as a tool for performing preliminary transport calculations, and to provide a basis for future detailed modeling in the weapons testing area of the Nevada Test Site. The ITC Model models an area of approximately 80,650 km² defined as the Death Valley groundwater basin using boundaries defined by Waddell et al. (1984) ("Underground Test Area Project Phase I Data Analysis Task," Volume II, Draft, March 1996, pp. 1-4). The basic sets of information used as inputs to the ITC Model were: the geologic framework, the hydraulic properties of the rocks, and the locations and rates of fluxes into the system. The ITC Model did not use hydrogeologic units to define the framework of the groundwater flow system; hydrostratigraphic units were used instead, with 20 hydrostratigraphic units defined (Table 5.2-3).

Though the ITC Model is not yet approved for release and is still in draft form, the hydrostratigraphic units of the ITC Model were correlated with the hydrogeologic units of Faunt et al. (1997) (Table 5.2-4).

5.2.1.4 Hydraulic Properties of Hydrogeologic Units

While conducting a literature search of the hydraulic properties of rocks in the Death Valley region, Bedinger, Langer et al. (1989c, pp. A16-A18) noted that hydraulic properties of rocks in a region cannot be predicted without site-specific, in situ, or laboratory tests. However, at the time of the study by Bedinger et al. it was not practical to determine site-specific values of hydraulic properties. Bedinger, Langer et al. (1989c, p. A16) also noted that a considerable amount of hydraulic properties data already existed in the literature, not only for the Basin and Range province, but for rocks with similar characteristics located out of the province. These data were reviewed and synthesized by Bedinger, Langer et al. (1989c, Table 1, Figure 4), and ranges of values were compiled for hydraulic conductivity and porosity. From this information, a log-normal plot of 14 rock types in the Basin and Range province showing the generalized distribution of the hydraulic conductivity values was prepared. Bedinger, Langer et al. (1989c) also discussed the effects of lithology, depth, and degree of fracturing of the aquifer matrix on the hydraulic properties.

Faunt et al. (1997, p. 14), in summarizing the report by Bedinger, Langer et al. (1989c) stated that Bedinger et al. believed that the Death Valley Regional Groundwater Flow System is influenced by deep groundwater flowpaths. Therefore, Bedinger et al. examined the effects of depth on the hydraulic properties of the hydrogeologic framework in the region and suggested that increased jointing near the surface, caused by stress release due to erosional unloading and weathering, may yield larger hydraulic conductivity and porosity values for rocks at shallow depths. Faunt et al. (1997, p. 14) stated that Bedinger, Langer et al. (1989c) concluded the following:

- At depths below 150 to 300 m, weathering and fractures due to release of confining pressures by erosional unloading probably are not significant.

- At increased depths, overburden pressures tend to decrease the apertures of joints or fractures and the size of pores; therefore, porosity and intrinsic permeability tend to decrease.
- In some areas, solution-type voids and relict cavernous conditions may withstand overburden pressures in crystalline carbonate rocks allowing these features to remain open at depths up to 2,000 to 3,000 m.
- Surface faults and fractures are good indicators of the orientation and position of permeable zones at depth up to 1,000 m.
- Large, regional, crystal fault zones are good indicators of areas of significant increased hydraulic conductivity at great depths. The regional hydraulic conductivity as a result of fractures is dependent not only on the presence of open fractures, but also on rock type, fracture orientation, and the history of tectonic stress in the region.

Using the information from Bedinger, Langer et al. (1989c) and incorporating the effects of depth and faulting, Faunt et al. (1997, Table 3, p. 16) assigned hydraulic properties to the ten hydrogeologic units defined by Faunt et al. (Table 5.2-5).

Bedinger, Langer et al. (1989c) and Faunt et al. (1997, pp. 12-16) do a thorough job of defining the hydraulic characteristics of the Death Valley region. However, in their reports there is no mention if groundwater occurs under artesian or water-table conditions, nor is there mention of what aquifer storage properties are expected. It can be assumed that within a regional groundwater flow system, groundwater will occur under artesian and water-table conditions and a wide range of aquifer storage properties will be found. To find out what information is known on the availability and occurrence of groundwater in the Death Valley region, a literature search of reports of site specific areas within the Death Valley region was completed. In terms of hydraulic characteristics and the occurrence and availability of groundwater, these reports are summarized as follows.

Malmberg and Eakin 1962, pp. 8, 10, 13, 14, 23, 24:

In a study of Sarcobatus Flat and Oasis Valley, Malmberg and Eakin (1962, p. 8) divided the rocks of these two areas into two general groups: bedrock in the mountains and valley fill in the lowlands. The division was made based on topography and the occurrence of groundwater. The bedrock included Paleozoic limestone and dolomite and lesser amounts of shale and sandstone, and Tertiary volcanic rocks consisting principally of tuff or other pyroclastics, welded tuffs, and flows. These rocks crop out in the mountains and underlie the valley fill. The valley fill includes deposits that range in age from Tertiary to Quaternary, and include rock debris which has eroded from the surrounding mountains, and the pyroclastic deposits of tuff, welded tuff, and sedimentary deposits. Though values of transmissivity or hydraulic conductivity were not given, Malmberg and Eakin (1962, p. 10) stated that all groundwater in these two areas, that can be withdrawn economically, is in the valley fill. However, groundwater does occur in the fractures of the underlying bedrock.

In Sarcobatus Flat, Malmberg and Eakin (1962, pp. 13, 14) stated that the surface area of Sarcobatus Flat is about 380 square miles, and the saturated valley fill may have a thickness of several thousand feet, though the exact thickness is unknown. However, wells in Sarcobatus Flat are only drilled 200 to 300 feet below the water table of the valley fill.

In Oasis Valley, Malmberg and Eakin (1962, pp. 23, 24) stated that the thickness of the saturated deposits was also unknown, but was estimated to possibly be several thousand feet thick. The valley fill in Oasis Valley underlies an area of about 60 square miles. Most of the groundwater development in Oasis Valley is in the flood plain of Amargosa River, where depth to groundwater can be only a few feet below land surface. Away from the flood plain the depth to groundwater will increase. Groundwater in Oasis Valley occurs under confined and unconfined conditions, with some wells flowing. Also, in Oasis Valley, artesian groundwater may be encountered in deep wells penetrating the fractured volcanic rocks which underlie the valley fill.

Walker and Eakin 1963, pp. 14, 15, 16:

In a study of Amargosa Valley, Walker and Eakin (1963, pp. 14, 15, 16) stated that groundwater occurs in the valley fill and the underlying volcanic and Paleozoic carbonate rocks. Groundwater in Amargosa Desert was considered by Malmberg and Eakin to be part of a single large system, with elements of that system partially separated locally. This separation could be identified by variations of head or artesian pressure between some deep and shallow wells and between some wells and springs tapping alluvium and carbonate rocks. Walker and Eakin gave some estimates of specific capacity for the Amargosa Valley. In wells drilled into Tertiary and Quaternary volcanic rock which underlie the valley fill, the specific capacity of wells was estimated to be generally less than a few gallons per minute per foot of drawdown. In the valley fill deposits, of six wells tested, the specific capacity ranged from 20 to 250 gallons per minute per foot of drawdown, with four of these wells having a specific capacity ranging from 40 to 110 gallons per minute per foot of drawdown. The coarse deposits in the valley fill are the principal source of groundwater in Amargosa Valley.

Malmberg 1967, pp. 12, 22, 23, 24, 30:

In a report that describes the hydrology of the valley-fill and carbonate-rock reservoirs of Pahrump Valley, Nevada and California, Malmberg (1967, p. 12) defines the geologic units of Pahrump Valley and their water-bearing character. The rocks in Pahrump Valley were divided by Malmberg into two very generalized groups based mainly on the water-bearing character and the relative stratigraphic position of the rocks with respect to the occurrence and movement of groundwater. The rocks were divided into the consolidated rocks that form the mountain ranges and underlie the valley fill, and the unconsolidated and partially consolidated sedimentary deposits of the valley fill. Malmberg prepared a table showing principal rock units and their stratigraphic relationships, lithologic character, and water bearing properties, and prepared a map which showed the areal distribution of the lithologic units.

In the valley-fill reservoir, Malmberg (1967, p. 24) defines the principal aquifer as being the coarse-grained deposits which underlie Pahrump and Manse fans. Locally, in the southwestward part of Pahrump Valley, the coarse-grained deposits may interfinger with fine-grained deposits. Malmberg estimates the saturated thickness of the reservoir to exceed 1,000 feet, and states that groundwater occurs under confined conditions. Aquifer transmissivity of the southwestern part of Pahrump Valley was estimated by Malmberg (1967, p. 30) to range from 130 to 700 feet squared, per day. This information was estimated from well logs which showed that the valley fill in the southwest part of Pahrump Valley was dominantly clay and silt. This estimate of transmissivity was done to determine subsurface outflow out of the valley, and may not represent all of Pahrump Valley. It could be assumed for Pahrump Valley that, where coarse grain deposits occur, the aquifer transmissivity would probably be higher.

Though no wells had been drilled into the carbonate-rock reservoir, Malmberg (1967, p. 24) estimated the maximum thickness of the carbonate rock to be at least 20,000 feet locally, and was assumed to be hydraulically continuous beneath Pahrump Valley. Continuity in the carbonate-rock reservoir was thought to be achieved principally through extensive fractures and to a small degree by localized solution channels. Malmberg stated that groundwater in the reservoir was mainly unconfined in the mountainous areas where the carbonate rocks crop out and receive recharge, and confined where it underlies the fine grained deposits in Pahrump Valley. Aquifer transmissivity of the carbonate-rock reservoir was not estimated.

The general relation between the valley-fill and carbonate-rock reservoirs was shown in cross-section by Malmberg (1967, pp. 22, 23, 24). Malmberg states that if the fine grained tuff located in lower Pahrump Valley is widespread, then the hydraulic continuity between the two systems beneath the valley floor may be poor. However, Malmberg estimates that the lateral continuity may be reasonably good. Subsequently, beneath the valley floor the two groundwater reservoirs are considered to function mainly as independent flow systems, although inflow almost certainly occurs laterally along the contact between the two reservoirs.

Glancy 1968, p. 9:

Glancy (1968) defines the water-resources of the Mesquite-Ivanpah Valley area, Nevada and California. Of this area, Mesquite Valley is located in the Death Valley region. Glancy (1968, p. 9) defines the geology in terms of hydrologic characteristics, and defines two broad groups; unconsolidated and consolidated rocks. The unconsolidated rock are generally fluvial, lacustrine, and eolian deposits. The consolidated rocks were divided into non-carbonate and carbonate rocks. Groundwater occurring in the unconsolidated deposits was referred to as the valley-fill reservoir. Within Mesquite Valley, the thickness of the valley-fill reservoir was as much as 1,180 feet, with depth to groundwater ranging from about 5 to more than 130 feet below land surface. Groundwater occurring in the consolidated rock in Mesquite Valley was referred to as the carbonate-rock reservoir. Very few wells have been drilled into the carbonate-rock reservoir. However, although the water-yielding capabilities of the carbonate rocks of

the area are untested, the general hydrogeologic characteristics of carbonate rocks require that they be considered as a potential aquifer system which may facilitate interbasin groundwater flow within the region.

Winograd and Thordarson 1975, Tables 1, 3:

In defining the hydrogeologic units of the south-central great basin area, Winograd and Thordarson (1975, Table 1) discuss the water-bearing characteristics and extent of saturation of the units. Winograd and Thordarson (1975, Table 3) also discuss the results of 22 single-well aquifer tests. However, most of this information is limited to areas and wells located primarily in the Nevada Test Site. Subsequently, this information will be discussed in detail in Subsection 5.3 which discusses the hydrogeology of Yucca Mountain including most of the Nevada Test Site.

Waddell 1982, p. 1:

A 2-D, steady-state, finite-element model of the groundwater flow system of the Nevada Test Site and vicinity in Nye and Clark Counties, Nevada, and Inyo County, California, was developed by Waddell (1982, p. 1, Figure 1, Table 1) using parameter-estimation techniques. Though not defined as a regional model, this model includes much of the area defined by D'Agnese et al. (1997) as the Death Valley region, with Waddell's model extending from approximately Pahrangat Range in the northeast to Death Valley in the southwest (Figure 5.2-2). The model of Waddell simulates groundwater flow in an area underlain by clastic and carbonate rocks of Precambrian and Paleozoic age, and volcanic rocks and alluvial deposits of Tertiary and Quaternary age.

Waddell defines eight hydrologic units in the modeled area and estimates aquifer transmissivity for those units which were considered to be regionally significant (Waddell 1982, Table 1).

Czarnecki and Waddell 1984, pp. 1, 12, 16, 18:

A finite-element model of the groundwater flow system in the vicinity of Yucca Mountain was completed by Czarnecki and Waddell (1984, pp. 1, 12, 16, 18). The model simulated steady-state groundwater flow occurring in tuffaceous, volcanic, and carbonate rocks, and alluvial aquifers. Though this model was intended to be a model of the Yucca Mountain area, the model does include part of Amargosa Desert (Amargosa Valley) and Death Valley (Figure 5.2-2). Aquifer transmissivities were estimated for defined modeled zones within Amargosa Desert and Death Valley based on dominant lithology (alluvium, carbonate, tuff). Depending on location, aquifer transmissivities for the area were approximately 1.197×10^2 , 1.282×10^2 , and 1.336×10^3 m squared, per day.

Harrill 1986, pp. 6, 7:

Harrill (1986) developed and described a model of Pahrump Valley that evaluated the effects of groundwater withdrawals in the valley between 1962 and 1967. Harrill describes the valley-fill and carbonate rock reservoirs as being the two distinct groundwater units in the study area. Because the carbonate-rock reservoir had not been developed for groundwater use and was not expected to be, the carbonate-rock reservoir was only evaluated by Harrill in terms of its effect on the flow regimen of the valley-fill reservoir. However, Harrill (1986, p. 6) stated that certain types of consolidated rocks do occur in the carbonate-rock reservoir that probably transmit significant underflow out of Pahrump Valley.

As stated, no wells in the Pahrump Valley penetrated the carbonate-rock reservoir, however, Harrill inferred aquifer properties of the carbonate rocks from information on the carbonate aquifer in other areas (Harrill 1986, pp. 6, 7). The aggregate stratigraphic thickness of the sequence of rocks in the carbonate-rock reservoir of Pahrump Valley is estimated to be as much as 5,400 m; however, these rocks have been complexly faulted and folded, and the aggregate vertical thickness at any one place may be substantially more or less than this stratigraphic thickness.

Hydraulic continuity of the carbonate rock is probably achieved through extensive fractures and, to a small degree, by localized solution channels. Transmissivity is highly variable. Referencing Winograd and Thordarson (1975, p. C22) Harrill indicates that transmissivity in carbonate rock in the South-Central Great Basin can range from 130 to 120,000 feet squared per day. However, for the carbonate-rock reservoir underlying Pahrump Valley, aquifer transmissivity is estimated to range from 1,500 to 2,500 feet squared, per day.

The valley-fill reservoir is described by Harrill (1986, p. 7) as being composed of unconsolidated alluvial, colluvial, and lacustrine deposits that partly fill the structural depression underlying Pahrump Valley. Some volcanic tuff is interbedded with the valley-fill deposits. The approximate areal extent of the valley-fill reservoir is estimated to be about 650 square miles, or about two-thirds of the total area of Pahrump Valley. Thickness of the valley fill can vary depending on area, however, the maximum thickness was estimated to be about 4,800 ft.

Harrill gives estimates of areal values of vertical hydraulic conductivity and aquifer transmissivity of the valley-fill reservoir. The vertical hydraulic conductivities were estimated from geologic and hydrologic information, and then refined during calibration of the aquifer model. The source of estimates for transmissivity was not clear. Harrill states that transmissivities can be calculated from the results of aquifer tests, estimated as the product of hydraulic conductivity and thickness of aquifer, or estimated from specific capacities of wells. However, for the transmissivity values included in his report a definite source is not given.

Based on locations shown, in Figure 3 of Harrill's report the range of vertical hydraulic conductivity was:

- Less than 0.01 feet per day, with an average of 0.005 feet per day
- 0.01 to 0.02 feet per day, with an average of 0.011 feet per day
- More than 0.02 feet per day, with an average of 0.04 feet per day

Based on locations shown in Figure 4 of Harrill's report, the range of aquifer transmissivity given was:

- Less than 1,000 feet squared, per day
- 1,000 to 2,000 feet squared, per day
- 2,000 to 4,000 feet squared, per day
- Greater than 4,000 feet squared, per day

The storage coefficient of the valley-fill reservoir was defined as specific storage. With no field data to define the specific storage of Pahrump Valley, Harrill referred to nearby Las Vegas Valley, which had similar deposits and aquifer matrix. Using a relation between known aquifer head decline and land subsidence which had occurred in Las Vegas Valley, Harrill estimated the specific storage of Pahrump Valley. For the coarse grained deposits around the edge of the Valley the specific storage was estimated to range from about 0.0002 to 0.003. For the fine-grained deposits in the central part of the valley the specific storage was estimated to range from 0.001 to 0.04.

5.2.1.5 Summary of Flow System Boundaries and Hydrogeologic Units

For the purpose of this report, the area used to define the regional hydrogeology, is the Death Valley Regional Groundwater Flow System defined by D'Agnese et al. (1997). Three principal flow boundaries have been defined for the Death Valley Regional Groundwater Flow System: the upper boundary, the lower boundary, and the lateral boundaries. These flow system boundaries are either physical boundaries, caused by changes in bedrock conditions, or hydraulic boundaries, caused by potentiometric surface configurations. The upper boundary of the flow system is the water table. The lower boundary of the flow system is located at a depth where groundwater flow is dominantly horizontal and flow velocities are so small that they do not significantly impact regional flow estimates. The lateral limits of the regional flow system may be either no-flow or flow boundaries.

For the numerical simulation of the Death Valley region, D'Agnese et al. (1997, p. 62) modified the limits of the Death Valley Regional Groundwater Flow System and divided the region into three major subregional flow systems (northern, Central, and Southern Death Valley subregions). However, not all of the Death Valley region is defined by these three subregions. The modification and smaller size of the combined subregions was done because few data existed that would allow a precise definition of the western and southern extent of the Death Valley region flow system and a small section of the northern extent of the region.

The hydrogeologic units of the Death Valley region have been defined and justified by several investigators. Though each investigator's definition of the units differed somewhat, each defined the units based on similarities as follows:

- Valley or basin fill
- Volcanic or volcanoclastic rocks
- Granitic or crystalline rocks
- Carbonate rocks

A review of the literature and a logical organization of the hydrogeology of the Death Valley region defined 10 hydrogeologic units; Quaternary Playa Deposits (Qp), Quaternary-Tertiary Valley Fill (QTvf), Quaternary-Tertiary Volcanic Rocks (QTv), Tertiary Volcanic Rocks (Tv), Tertiary Volcanic and Volcanoclastic Rocks (Tvs), Tertiary-Late Jurassic Granitic Rocks (TJg), Mesozoic Sedimentary and Metavolcanic Rocks (Mvs), Paleozoic Carbonate Rocks (P2), Paleozoic-Precambrian Clastic Rocks (P1), and Precambrian Igneous and Metamorphic Rocks (pCgm). Comparisons of these 10 units were made to the units defined in the literature and each of the 10 hydrogeologic units were listed and defined based on geologic and hydraulic characteristics. Correlations were also made between the stratigraphy, major lithology, and thickness of each hydrogeologic unit.

Hydraulic properties of each hydrogeologic unit were defined primarily as a range of horizontal hydraulic conductivities. The hydraulic conductivity values came essentially from one source, the report by Bedinger, Langer et al. (1989c). The source of the information given by Bedinger was from previously published data from the Basin and Range province and from the literature which discusses rock types similar to those in the Basin and Range province. The hydraulic conductivity data of Bedinger et al. was modified by Faunt et al. (1997). The hydraulic conductivities presented by Faunt et al. is considered to be the most representative of the Death Valley region.

A summary of the literature that discusses hydraulic properties of localized areas within the Death Valley region is presented with the following conclusions:

- Groundwater is assumed to occur under artesian and water table conditions throughout the Death Valley region. However, it may be concluded that, with depth, in the valley-fill aquifer and underlying carbonate aquifers, the occurrence of groundwater under artesian conditions will dominate, and in the mountainous areas and along the flanks and recharge areas of the valley fill, groundwater will occur predominantly under water-table conditions.
- The range of aquifer transmissivity values given in these reports is in the same range as the hydraulic conductivities given by Bedinger, Langer et al. (1989c).
- Vertical hydraulic conductivity values were only given for Pahrump Valley.
- Values of aquifer storage were only given for Pahrump valley, subsequently little is known about aquifer storage values throughout the Death Valley region. For the purpose of this report, traditional aquifer storage values are suggested, with ranges of 10^{-5} to 10^{-3} for artesian aquifers and 0.1 to 0.3 for water-table aquifers (Lohman 1979, p. 8).

Though estimates of hydraulic conductivity have been made for the hydrogeologic units of the Death Valley region, much of this data is based on estimates and interpolations of data from aquifers outside of the region. Information on vertical hydraulic conductivity and aquifer storage values is available only for Pahrump Valley. For the Death Valley region, there is a tremendous lack of aquifer characteristics based on multiwell time/drawdown aquifer tests of well fields located in the region.

5.2.2 Potentiometric Levels and Hydraulic Gradients

Numerous potentiometric-surface maps have been developed for basins within the Death Valley region; several have been generalized contour maps of shallow unconfined valley-fill² aquifers; a few have included more detailed potentiometric surfaces which combined contours of the shallow valley-fill aquifers with deeper consolidated bedrock aquifers. Also, one series of map reports prepared potentiometric surfaces for the Basin and Range province in California and Nevada. In terms of defining regional potentiometric levels and hydraulic gradients, significant interpretations from these reports include the following:

- Even though groundwater occurs in valley-fill deposits and consolidated rock, few wells have been completed in the consolidated rock in comparison to the greater number of wells completed in the valley-fill.
- The yield to wells tapping consolidated rock units is due to the interception of water in fracture zones. However, in some areas in the Basin and Range province, carbonate rock is extensive in the subsurface and provides interconnection between alluvial basins through fractures and solution channels.
- Although the consolidated rock commonly has very low permeability, and very low rates of groundwater flow, the entire groundwater system, valley-fill and bedrock, should be treated as one integral system.
- Though vertical gradients exist between the valley-fill aquifers and consolidated bedrock aquifers, on a regional scale, the potentiometric levels are similar enough that all water level data, regardless of well construction, can be used to define regional potentiometric levels.

5.2.2.1 Previous Potentiometric-Surface Maps

Shallow Valley-Fill Aquifers –Numerous potentiometric-surface maps have been developed for basins within the Death Valley region (D’Agnese et al. 1998, p. 3). Several have been generalized contour maps of shallow basin-fill aquifers (Malmberg and Eakin 1962, pp. 13, 23; Walker and

² Because the source of information for this section is from many different reports that discuss potentiometric levels in alluvial fill aquifers and define these aquifers as valley-fill or basin-fill, the two terms are considered to be synonymous throughout this section and the remainder of Subsection 5.2.

Eakin 1963, pp. 16, 17; Malmberg 1967, p. 25; and Kilroy 1991, pp. 9, 11, 16). These contour maps are summarized as follows:

Malmberg and Eakin 1962, pp. 13, 23:

In a groundwater appraisal of Sarcobatus Flat and Oasis Valley, Nye and Esmeralda counties, Nevada, Malmberg and Eakin (1962, pp. 13, 23) stated that the valley fill in each area constituted the principal groundwater reservoir. Malmberg and Eakin further stated that in Sarcobatus Flat, groundwater flow is principally toward Bonnie Clare, and depending on location, the hydraulic gradient can vary from 10 feet per mile to about 2.5 feet per mile. West of Bonnie Clare, data were insufficient to determine the direction of movement with any degree of certainty. However, because virtually all groundwater discharge in Sarcobatus Flat is east of Bonnie Clare, the inferred westward sloping hydraulic gradient beneath the discharge area (Bonnie Clare Playa) suggests that some groundwater underflow moves westward from Bonnie Clare toward the gap and probably through the gap to Grapevine Canyon (Malmberg and Eakin 1962, p. 14).

The movement of groundwater in Oasis Valley can be inferred only in a general way because of the scarcity of existing groundwater data (Malmberg and Eakin 1962, p. 24). In general, groundwater moves from areas of recharge along the margins of the valley to areas of discharge. From the principal areas of recharge adjacent to Black and Timber Mountains groundwater moves southwestward toward the Amargosa River, where most of it emerges as springs or seeps or moves as groundwater underflow beneath the Amargosa River flood plain toward the Amargosa Narrows. A limited quantity of groundwater underflow also moves toward the Amargosa River from the Bullfrog Hills (Malmberg and Eakin 1962, p. 24).

Walker and Eakin 1963, pp. 16, 17:

A reconnaissance of the geology and groundwater of the Amargosa Desert, California and Nevada, was completed by Walker and Eakin (1963, pp. 16, 17). For the reconnaissance, a potentiometric map of 1962 water levels was prepared. The water-level contours revealed that groundwater in the valley fill of the Amargosa Desert is principally moving in a southeastward direction along the axis of the Desert, with some groundwater movement from east to west in some of the tributary valleys of the Amargosa Desert (Walker and Eakin 1963, p. 16). The slope of the water-level surface generally conformed to the slope of the land surface. However, the gradient of the water surface commonly was somewhat less than that of the land surface. In the southern part of the Amargosa Desert in an area north of Death Valley Junction the water-level gradient was about 12 feet per mile compared to the land-surface gradient of 13 feet per mile – a ratio of 12 to 13 (1 to 1.1); in the vicinity of Big Dune the ratio of gradients was about 1 to 1.25, and north of Lathrop Wells the ratio of gradients was about 1 to 7.5. The net effect of this general relationship was that the depth to water in wells increased northward in the Amargosa Desert (Walker and Eakin 1963, pp. 16 and 17).

Malmberg 1967, p. 25:

In a report on the hydrology of the valley-fill and carbonate-rock reservoirs of the Pahrump Valley, Malmberg (1967, plate 2) prepared a potentiometric map of Pahrump Valley, contouring 1962 water-level data of wells drilled into the valley fill. Generally, Malmberg (1967, p. 25, Figure 5), concluded that the principal direction of groundwater movement across Pahrump Valley was southwest, across the valley, indicating that the principal recharge area was in the Spring Mountains. Further, although sufficient wells were not drilled into the underlying carbonate rock, Malmberg assumed that the direction of groundwater flow in the carbonates would also be to the southwest.

Kilroy 1991, pp. 9, 11, 16:

Kilroy (1991, pp. 9, 11, 16) summarized groundwater data collected in the Amargosa Desert from 1952 to 1987, with special attention given to the 1986 to 1987 data. Potentiometric maps of predevelopment and 1986 to 1997 water levels were prepared, as well as a water-use map showing the effects of long-term pumping and the influence of subbasin structure and a regional flow system on water levels. Water-level data for the 1986-87 potentiometric map were from wells drilled primarily less than 500 feet into the basin-fill material, although some wells measured were drilled to a depth of up to 2,000 feet (Kilroy 1991, p. 9). A review of the potentiometric map contours indicates that the direction of groundwater movement was southeastward parallel to the surface gradient of the Amargosa River; however, in the Amargosa Flat area, flow is southwestward toward the main axis of the Amargosa Desert.

Vertical gradients were determined in the Amargosa Desert for 21 nested piezometer, one well cluster, and one river and well pair (Kilroy 1991, p. 11). Upward and downward gradients were found. The upward gradients in the central and southern part of Amargosa Desert were associated with freshwater limestones, carbonate-rock outcrops, and subbasin structures. The downward gradients were associated with consolidated Tertiary conglomerates, and crystalline and volcanic bedrock. The range of vertical gradient ranged from 0.001 to 1.20 (Kilroy 1991, p. 16, table 3).

Shallow Valley-Fill and Deep Consolidated Bedrock Aquifers—Only a few investigations have included more detailed potentiometric maps which combined contours of the shallow valley-fill aquifers with deeper consolidated bedrock aquifers (Rush 1970, pp. 10, 11; Winograd and Thordarson 1975, pp. C71, C72; Robison 1984, p. 8; and Waddell et al. 1984, p. 28). These potentiometric maps are discussed as follows:

Rush 1970, pp. 10, 11:

Rush (1970, pp. 10, 11) discusses three regional interbasin groundwater flow systems: the Ash Meadow system, the Pahute Mesa system and the Sarcobatus Flat system and presents a potentiometric map showing regional groundwater flow within these three systems. Though the potentiometric surface was not defined in great detail, Rush (1970, pl. 1, p. 10) indicated that local flow in the alluvium in Ash Meadows is northward,

suggesting the presence of a groundwater divide in the vicinity of the topographic divide between Penoyer Valley and Tikapoo and Groom Lake Valleys. In the Pahute Mesa flow system groundwater generally flows through interconnected faults and joints southwestward toward Oasis Valley and southward to Amargosa Desert (Rush 1970, p. 11). For the Sarcobatus Flat system, groundwater is believed to flow southwestward toward Sarcobatus Flat or southeastward toward Gold Flat (Rush 1970, p. 11).

Winograd and Thordarson 1975, pp. C71, C72:

The potentiometric map prepared by Winograd and Thordarson (1975, plate 1), describes the potentiometric surface in the Pahute Mesa, Yucca Flat, Frenchman Flat, Indian Springs, Jackass Flat, Mercury Valley, Ash Meadows, and Amargosa Desert areas. Where data was available the map defines two potentiometric surfaces; the potentiometric surface of the lower pre-Tertiary carbonate aquifers and aquitards (lower carbonate aquifer) and the upper Quaternary-Tertiary valley-fill aquifer.

For the lower carbonate aquifers, two assumptions are made for the water-level data used. The water levels used represent only head in the aquifer of interest and in the vicinity of the control wells, water flows nearly horizontally through the aquifer (p. C71). For the potentiometric surface of the upper valley-fill aquifers Winograd and Thordarson (1975, p. C71) pointed out that, in some areas, the contours probably reflect the head in the underlying lower carbonate aquifer. In drawing the contours of the lower carbonate aquifer a synthesis of hydraulic, geologic, and geophysical data were used because the contouring of water-level data without regard for geologic data led to several improbable local hydrologic conditions.

Major features shown on the potentiometric map of the lower carbonate aquifer were the trough in the potentiometric surface in Yucca Flat and the major trough that extends from Eastern Frenchman Flat to the Ash Meadows discharge area in East-Central Amargosa Desert (Winograd and Thordarson 1975, p. C71). The potentiometric surface within the lower carbonate aquifer in Yucca Flat was marked by a prominent north-northwest trending trough about 20 miles long and 2 to 8 miles wide. The apparent hydraulic gradient along the axis of the trough ranged from a fraction of a foot to 5.9 feet per mile. The apparent hydraulic gradient along the flanks of the trough was as much as 20 feet per mile.

The trough that ran from East-Central Frenchman Flat to Ash Meadows extended for a distance of about 40 miles and was about 15 miles wide at the Ash Meadows discharge area; about 5 miles wide beneath the Specter Range, and possibly as much as 20 miles wide within the Nevada Test Site, where its width was not well defined. The hydraulic gradients within this trough ranged from 0.3 to about 1.5 feet per mile. The trough indicated that groundwater within the lower carbonate aquifer beneath Yucca, Frenchman, and Eastern Jackass Flats and beneath a vast area east, northeast, and southeast of the Nevada Test Site was moving toward a prominent spring-discharge area (Ash Meadows) in the East-Central Amargosa Desert (Winograd and Thordarson 1975, p. C72).

For the upper Quaternary-Tertiary valley-fill aquifer the potentiometric map indicates that most or all of Yucca Flat, Frenchman Flat, Eastern Jackass Flats, Southern Indian Springs Valley (south of U.S. Highway 95), Mercury Valley, and the unnamed valley northeast of the springline in East-Central Amargosa Desert are tributary to the Ash Meadows discharge area (Winograd and Thordarson 1975, pl. 1, Figure 35, p. C86). Also interpreted from the valley-fill aquifer is the presence of a groundwater divide near the intersection of U.S. 95 and Nevada State Highway 52 (Winograd and Thordarson 1975, pl. 1, p. C86).

Robison 1984, p. 8:

The potentiometric map prepared by Robison (1984, p. 8) was specifically for the Yucca Mountain area. However, on a regional scale, the importance of this map is that Robison pointed out that most of the water levels used in his report were composite water levels of the volcanic rock underlying Yucca Mountain and may not have represented a single unique aquifer (Robison 1984, p. 8).

Waddell et al. 1984, p. 28:

The potentiometric map prepared by Waddell et al. (1984, pl. 3) was prepared primarily to define the potentiometric surface of the Yucca Mountain area however the map included much of the area defined as the Death Valley region with contours extending north of Cactus and Kawich Range, south to Pahrump Valley, east of Sheep Range, and west to Death Valley (Figure 5.2-2). Contour lines for the map were drawn at 100 m intervals, and composite water levels from several hydrogeologic units were used in mapping the contours (Waddell et al. 1984, p. 28). Waddell et al. stated that in Yucca Flat (Yucca Mountain area), data were available from wells completed in alluvium, tuff, and carbonate rocks, and the potentials indicated downward flow into the lower carbonate aquifer. However, even though this downward vertical potential existed, on a regional scale, the potentiometric levels were similar enough that it was unfeasible to try to contour data from different geologic units (Waddell et al. 1984, p. 28). Waddell et al. also gives a general description of groundwater gradients and flow of the Yucca Mountain area, and, depending on location, direction of flow will vary, however in terms of regional groundwater flow, the ultimate direction of flow was southwest to Death Valley, the lowermost discharge area of the region.

Potentiometric Map of the Basin and Range Province—Bedinger, Harrill et al. (1984a) and Langer et al. (1984) prepared maps of the Basin and Range province in Nevada and California which showed groundwater levels, springs, and depth to water. Bedinger, Harrill et al. (1984a, p. 2) noted that within the Basin and Range province, groundwater occurs in basin-fill deposits and consolidated rock; however, few wells exist in the consolidated rocks compared to the greater number of wells in the basin fill. The yield to wells tapping many consolidated rock units is due to interception of water in fracture zones. However, in some areas in the Basin and Range province, carbonate rock is extensive in the subsurface and provides interconnection between alluvial basins through fractures and solution channels. Bedinger, Harrill et al. concluded that although the consolidated rock commonly has very low permeability, and very low rates of groundwater flow, the entire

groundwater system, basin fill and bedrock, must be treated as one integral system. Bedinger, Harrill et al. (1984a, p. 3) also pointed out that in areas with good topographic control, the depth to groundwater can be predicted with reasonable accuracy between widely-spaced water-level data points, except where geologic discontinuities, such as faults, may alter the flow pattern.

5.2.2.2 Current Potentiometric Surface

A potentiometric-surface map was constructed by D'Agnese et al. (1998, plate 1) for the Death Valley region (Figure 5.2-3). The map was completed for conceptualization of the Death Valley Regional Groundwater Flow System and for construction of a numerical model. A Geoscientific Information System method was used by D'Agnese et al. (1998, p. 1) to incorporate available data and apply hydrogeologic rules during contour construction.

Construction of the regional potentiometric-surface map required data sets describing:

- Water levels
- Boundaries of lakes and ponds
- Topographic elevations
- Regional spring locations
- The distribution of recharge and discharge areas
- Hydrogeology

Construction of the Death Valley regional potentiometric-surface map by D'Agnese et al. (1998) was completed primarily based on the regional water-level data. However, where needed, these data were supplemented by additional comparative information derived from the hydrographic data, hydrogeologic map, and interpretations of the distribution of regional discharge and recharge to improve interpolations in areas of sparse well data.

Water-Level Data—All water-level data used by D'Agnese et al. (1998, p. 5) in the development of the Death Valley region potentiometric map originated from the USGS National Water Information System database. The National Water Information System files contain a detailed account of characteristics for regularly monitored wells and springs in an elaborate data structure. A detailed query of the National Water Information System was undertaken by D'Agnese et al. (1998, p. 5) to retrieve data that would be useful for analyzing water levels in the Death Valley region. Though regional water-level data stored in the National Water Information System were collected over several decades, most data for any given basin were gathered during short periods of time. These retrieved data were converted into a format compatible with the Geoscientific Information System database and a well-location map was generated. D'Agnese et al. (1998, p. 5) retrieved data for 2,141 wells, however, of this data, only about half of the wells were located in the Death Valley region. Because very little information was available in the database on the screened intervals of these wells, the majority of the levels were considered to be representations of the water table or composite water-level measurements of the regional potentiometric surface. Also, approximately 171 wells are completed to depths greater than 500 m below static water level and are believed to represent potentiometric levels from deeper in the system. Even though composite water levels may represent a mixing of heads within the borehole, and deeper boreholes represent a different head than shallower boreholes because of vertical gradients, on a regional scale, the difference in water level

is considered to be negligible and the water level representative of the regional potentiometric surface.

Because the potentiometric-surface map was developed primarily with water-level data, the limits of the water-level data used need to be discussed. Water resource extraction and investigation in the Death Valley region, which is a sparsely populated, arid, and mountainous region, have been mostly concentrated in alluvial basins (D'Agnese et al. 1997, p. 10). As a result, clusters of water wells, and subsequently water-level data, are concentrated in these basins. The densest concentration of water-level data in the area occurs near Las Vegas, Nevada, east of the Death Valley regional groundwater flow system. Alluvial basins within the Death Valley flow system with the densest concentration of water-level data are Amargosa and Pahrump Valleys (Figure 5.2-7), which also are the two largest agricultural communities. Additional water-level data located within the valley-fill alluvium include Oasis Valley, Sarcobatus Flat, and Yucca Flat. The only areas with extensive water-level data in consolidated bedrock are the Yucca Mountain, Pahute Mesa, and Rainier Mesa areas. Extensive drilling in the Yucca Mountain area is because of the site characterization study; the drilling in Pahute Mesa and Rainier Mesa as well as at Yucca Flat is because of atomic testing conducted in these areas.

Most wells located in the Death Valley region have been located on topographic maps that have contour intervals of 200 feet. The error in locating a well on a topographic map without the benefit of having surveyed coordinates is assumed to be one half the topographic map contour, which for wells located in the Death Valley region is 100 feet. Subsequently, with the exception of wells located in the Yucca Mountain, Pahute Mesa, Rainier Mesa, and Yucca Flat areas, all well locations and elevated water levels used in the potentiometric map are assumed to be in error by ± 100 feet. The wells located in Yucca Mountain, Pahute Mesa, Rainier Mesa, and Yucca Flat are not included in this error range because most of these wells have surveyed location coordinates.

Lakes and Ponds—The boundaries of lakes and ponds were obtained from the USGS digital line graph cartographic database (D'Agnese et al. 1998, p. 5). These products contained selected hydrographic information digitized from USGS 1:100,000-scale topographic maps. The data describe all flowing and standing water, springs, and wetlands. The information on the digital line graph maps were imported into the Geoscientific Information System database to develop a digital map describing the surface hydrography characteristics for the entire study area.

Topographic Elevations—The topographic elevation data used by D'Agnese et al. (1998, pp. 5-6) were obtained from a compilation of Defense Mapping Agency series, 1 degree by 1 degree digital elevation models. Digital elevation models are sampled arrays of ground elevations that are usually, but not always, at regularly spaced intervals. In the Death Valley region, the spacing of points on the digital elevation model's files is about 70 m east-west and 90 m north-south.

The digital elevation models required for the Death Valley region were imported into the Geoscientific Information System database, transformed to the appropriate projection, and joined to develop a rather large, raster terrain model of the region. Because of the size of terrain model, the terrain model was resampled by selecting every third cell to develop a digital elevation model that contained an elevation measurement of every 9 arc-seconds of land surface or approximately 210 m

by 270 m. This resampled digital terrain model was used in the Geoscientific Information System database.

Regional Springs—The location and elevation of all regional spring discharge points were used in development of the potentiometric-surface map (D’Agnese et al. 1998, p. 6). These springs, characterized by steady, large-volume discharges and temperatures ranging from 24°C to 35°C, typically emerge from the regional groundwater flow system by way of the valley fill and the carbonate aquifer at low altitudes along the borders or on the floor of some valleys. For interpolation of the potentiometric surface, the location of the regional springs was incorporated into the Geoscientific Information System database. More information on spring discharge can be found in Subsection 5.2.3, “Recharge and Discharge.”

Recharge and Discharge Areas—The distribution of recharge and discharge areas was also used during construction of the potentiometric-surface map (D’Agnese et al. 1998, pp. 7-8). Image classification methods were applied to multispectral satellite data to produce a vegetation map. The vegetation map was combined with ancillary data to delineate wetland, phreatophyte, and wet playas discharge areas. Recharge areas were delineated by incorporating thematic maps describing often heterogeneous complex factors affecting infiltration. These factors included: topography, slope aspect, parent material, and vegetation. These indicators were incorporated into a recharge map by ranking characteristics in order of infiltration potential. The results of the recharge and discharge studies were combined into one map describing the areal extent of groundwater recharge and discharge areas and incorporated into the Geoscientific Information System database. More information on recharge and discharge in the Death Valley region can be found in Subsection 5.2.3.

Hydrogeology—The regional hydrogeologic map developed by Faunt et al. (1997) (Figure 5.2-4) was used by D’Agnese et al. (1998, p. 8) to delineate where low permeability bedrock might influence the configuration of the water table. The regional hydrogeologic map was constructed by combining existing regional geologic maps and report data into a Geographic Information System database, creating a digital regional geologic map, and then combining the diverse geologic map units into fewer hydrogeologic units. For regional potentiometric-surface map construction, the hydrogeologic units shown on the hydrogeologic map were combined into five generalized geologic units. Rocks bearing larger permeabilities include valley-fill alluvium and carbonate rocks. Units with smaller permeabilities include clastic and crystalline rocks. The volcanic rock units occurring in the region are quite variable and were interpreted as having moderate permeabilities for potentiometric-surface map construction purposes. The results of generalizing the hydrogeologic units into five geologic units were incorporated into the Geoscientific Information System database (D’Agnese et al. 1998, p. 8).

Interpolation Concepts—The concept of a “free-surface” water table described by Domenico and Schwartz (1990) was used by D’Agnese et al. (1998, p. 8) to develop the potentiometric-surface map. Domenico and Schwartz (1990, pp. 255, 259) suggested that the regional potentiometric surface in mountainous areas, where depth to groundwater is relatively deep and the aquifer matrix is intensely fractured, can be interpreted as a series of semi-continuous, free surfaces connected between basins by large hydraulic gradients. The resulting water-table configuration, therefore, can be interpreted as plateau-like surfaces in each subbasin connected by zones of large hydraulic gradients occurring in mountain blocks of comparatively smaller permeability.

To guide interpolation of water levels in areas where data is limited, the additional previously mentioned data were used by D'Agnese et al. (1998, pp. 8-9) in accordance with five general criteria:

- During interpolation, water levels were not permitted to extend above the land surface defined by the digital evaluation model.
- The altitudes of regional springs, lakes, and ponds were used to define locations where the regional water table occurs at the land surface.
- Regional discharge areas are regional depressions in the flow system and are located at local minima in the regional potentiometric surface. The potentiometric surface at discharge areas, therefore, was interpolated to form local minima.
- Regional recharge areas develop recharge mounds (and often, groundwater divides) in the potentiometric surface. Therefore, the potentiometric surface was interpolated to form local maxima at locations of recharge areas. During revisions of the interpolated surface, D'Agnese et al. (1998), checked water levels to ensure that they did not extend far above the elevation of localized, cold-temperature springs occurring in these recharge areas.
- Lower permeability rocks typically affect the potentiometric surface by sharply refracting contours into the units with lower permeability resulting in areas with steep hydraulic gradients. The generalized geologic map developed from the hydrogeologic units data by D'Agnese et al. (1998) was used to delineate locations interpreted as having surface and subsurface units of lower permeability rock. During interactive interpolation of the potentiometric surface, gradients on the interpreted surface were steepened when necessary to reflect these hydrogeologic barriers.

Summary of Current Potentiometric Surface—The potentiometric surface map defined by D'Agnese et al. (1998, plate 1) will be used to define the potentiometric surface of the Death Valley region. Though numerous potentiometric surface maps have been developed for basins within the Death Valley region; most have been contour maps of shallow, unconfined basin-fill aquifers. The potentiometric maps that do define the potentiometric surface of the valley-fill and consolidated rock aquifers, either do not contain the same detail of contour intervals as the map by D'Agnese et al. or are not drawn for the entire Death Valley region. Data used for the potentiometric map constructed by D'Agnese et al. (1998) is considered to be the most complete and accurate data available, with all water-level data coming from the USGS National Watch Information System database. Also, documentation of the remaining data sets used in the interpolation of the potentiometric surface is considered to be good, with ample justification given for use of the data.

5.2.2.3 Gradients and Potentiometric Features

The Death Valley regional potentiometric surface may be controlled by topography, lithology, or geologic structure (D'Agnese et al. 1998, p. 10). Several dominant features of the regional potentiometric surface map that are a result of important hydrologic or geologic features include:

- Potentiometric-surface mounds and depressions
- Potentiometric-surface troughs
- Large hydraulic gradients (Figure 5.2-8)

Potentiometric Surface Mounds and Depressions—Potentiometric surface mounds are commonly associated with groundwater recharge areas where groundwater infiltration occurs. On the potentiometric surface map of the Death Valley region several recharge mounds are inferred where water-level data do not exist (D'Agnese et al. 1998, p. 10). Recharge conditions and low permeability rocks occur in these areas, however, which indicates that recharge mounds are likely to exist. Large mounds are associated with areas recharging the regional flow system, but smaller mounds are associated with recharge to subregional or local flow systems. These recharge mounds may also represent semi-perched groundwater conditions which most often occur in recharging groundwater environments. The most prominent mound, and the largest recharge area, is located at the Spring Mountains (Figure 5.2-8). Other smaller recharge mounds are present at the Sheep Range, the Groom Range, Rainier Mesa, Shoshone Mountain, Stonewall Mountain, Gold Mountain, Magruder Mountain, Grapevine Mountains, Black Mountains, and the Kingston Range.

Potentiometric surface depressions are indicators of groundwater discharge areas (D'Agnese et al. 1998, p. 11). The largest depression and the terminal discharge area of the regional groundwater flow system occurs at Death Valley (Figure 5.2-8). The depression, controlled dominantly by topography, forms the terminus of the regional groundwater flow system. Lesser depressions in the region occur at Mesquite Lake, Stonewall Flats, and Sarcobatus Flats.

Potentiometric Surface Troughs—Two prominent troughs are controlled by geologic structure (D'Agnese et al. 1998, p. 12). The trough north of the Spring Mountains is a prominent feature that has been described as the result of high-permeability, faulted and fractured rock present along the axis of the Spotted Range-Mine Mountain structural zone (Faunt 1997, plate 1, Figure 3). The trough located at Pahute Mesa is the result of a linear feature believed to be a fault. Less prominent troughs that also may be structurally controlled occur at Amargosa Valley, Grapevine Canyon, and Stonewall Pass. Troughs that may be controlled by topography and lithology are located at Yucca Flat and Emigrant Valley. A trough that may be associated with all three controls is located at Fortymile Canyon.

Large Hydraulic Gradients—Large hydraulic gradients, defined here as gradients larger than 0.1, may be controlled by recharge, lithology, topography, structure, or by a combination of any of these factors (D'Agnese et al. 1998, p. 13). A commonly discussed large hydraulic gradient in the Death Valley region occurs immediately north of Yucca Mountain (Local area 24, Figure 5.2-8). However, large hydraulic gradients are a common feature of the Death Valley regional groundwater flow system.

Two regional-scale domains of large hydraulic gradients exist in the Death Valley regional groundwater flow system. One domain separates Death Valley from adjoining areas to the northeast and east (Regional area 25, Figure 5.2-8). This abrupt drop in water-table altitude is associated with contacts between low-permeability rocks in the Amargosa Range and higher permeability rocks in Death Valley, which are associated with the Death Valley fault zone. The large hydraulic gradient may also be a result of the large topographic change between the Amargosa Valley (land-surface altitude about 700 m) and Death Valley (land-surface altitude about -80 m).

The second domain occurs along the north and western margins of the Spring Mountains (Regional area 26, Figure 5.2-8). The large hydraulic gradient in this area is associated with low-permeability, clastic confining units present north and west of the Spring Mountains. North of the Spring Mountains, the large hydraulic gradient also appears to be related to the Las Vegas Valley shear zone and may be due to low-permeability fault gouge developed in this major fault zone.

The large hydraulic gradient located in the Yucca Mountain test site extends from Yucca Mountain northeastward to Emigrant Valley (Local area 24, Figure 5.2-8). This hydraulic gradient is the result of three large-scale features:

- A largely buried contact of regional confining units and the carbonate aquifer
- A generally southward topographic decline that approximately coincides with the regional potentiometric surface declines
- Large regional recharge areas present to the north and west, in the vicinity of Pahute Mesa

The large hydraulic gradient at the Yucca Mountain test site is discussed in greater detail in Subsection 5.3.

5.2.2.4 Summary of Potentiometric Levels and Hydraulic Gradients

The potentiometric surface of the Death Valley region has been described in many publications either on a local or regional scale. An extensive review and summary of potentiometric maps in the literature was completed with the following general findings.

- Even though groundwater occurs in valley-fill deposits and consolidated rock, few wells have been completed in the consolidated rock in comparison to the greater number of wells completed in the valley-fill.
- The yield to wells tapping many consolidated rock units is due to the interception of water in fracture zones. However, in some areas in the Basin and Range province, carbonate rock is extensive in the subsurface and provides interconnection between alluvial basins through fractures and solution channels.
- Although the consolidated rock commonly has very low permeability, and very low rates of groundwater flow, the entire groundwater system, valley-fill and bedrock, must be treated as one integral system.

- Though vertical gradients exist between the valley-fill aquifers and consolidated bedrock aquifers, on a regional scale, the potentiometric levels are similar enough that all water level data, regardless of well construction, can be used to define regional potentiometric levels.
- Vertical hydraulic gradients are only available in the literature for Amargosa Desert where upward and downward gradients were found ranging from 0.001 to 1.20.
- Horizontal gradients and direction of groundwater movement were documented for several local areas. Though direction of groundwater movement is discussed briefly in this subsection, a detailed discussion of groundwater flowpaths can be found in Subsection 5.2.5.
- With the exception of groundwater occurring in the valley fill, there is little discussion of measured potentiometric levels in individual hydrogeologic units. This is because most wells in the Death Valley region are completed in the valley fill. Subsequently, in terms of hydraulic gradients between hydrogeologic units, with the exception of information given for Amargosa Desert, there is no mention of specific gradients between hydrogeologic units.
- In several reports, there is mention of wells completed solely in the valley fill, solely in the volcanic rock or carbonate rock, and wells completed in both valley fill and underlying volcanic and carbonate rocks. Though detailed discussion of hydraulic gradients across hydrogeologic units is not available, there is mention that some gradients, on a local scale, may exist. However, when discussing the potentiometric surface of the Death Valley region, it was concluded that the small differences in head between hydrogeologic units was insignificant in defining the potentiometric surface on a regional scale.
- Three areas where large hydraulic gradients occur (defined by gradients greater than 0.1) are discussed. However, no other discussion is presented of the range of hydraulic gradients throughout the Death Valley region.

5.2.3 Recharge and Discharge

Groundwater recharge can be defined as the entry into the saturated zone of water made available at the water-table surface. Groundwater discharge can be defined as the removal of water from the saturated zone across the water-table surface (Freeze and Cherry 1979, p. 211). The major source of recharge to the Death Valley region is from rainfall infiltration. The largest discharges from the Death Valley region include springs, and evapotranspiration by phreatophytes and wet playas. The ultimate discharge area for the Death Valley region is Death Valley, however intermediate discharge locations reflect topographic, geomorphic, stratigraphic, and/or structural controls.

5.2.3.1 Characterizing the Recharge Component

The major source of recharge to the Death Valley regional groundwater flow system is from precipitation on the highest mountains within the region (D'Agnese et al. 1997, p. 50). The regional flow system is also recharged by interbasinal flow. Some recharge also results from recycled irrigation and domestic waters, as well as seepage of spring discharge back into the groundwater

system (Rice 1984, p. 25). However, these recycled components are considered to be small and negligible compared to regional infiltration and interbasinal flux volumes (Waddell 1982, p. 14).

5.2.3.1.1 Previous Methods of Characterizing Recharge from Precipitation

Empirical, water-balance, and distributed-parameter methods have been used to characterize the location and amount of recharge in the Death Valley region. Each method attempts to characterize the complex array of factors controlling recharge; each has limitations (D'Agnese et al. 1997, pp. 50-51).

Empirical Methods—D'Agnese et al. (1997, p. 51) summarizes an empirical precipitation-recharge relation developed by Maxey and Eakin (1949) from water mass-balance estimates for basins in Southern and Eastern Nevada. D'Agnese states that in the Maxey-Eakin report, it is suggested that the annual precipitation amount and the percentage of precipitation that becomes groundwater recharge increases with increasing altitude. Depending on the valley, Maxey and Eakin assumed that no recharge occurs where mean annual precipitation is less than about 200 mm, or altitude is lower than 1,524 m. Above 1,524 m in altitude, based on a series of 305 m altitude intervals, Maxey and Eakin assigned an increasing percentage of precipitation that was assumed to become recharge (Table 5.2-6).

This empirical method of estimating recharge from annual precipitation developed by Maxey and Eakin (1949) became dominate in its use in the Basin and Range province. A later report by Eakin et al. (1951) uses the same method for determining recharge and is often cited in the literature. Other investigators working in the Great Basin who used the Maxey-Eakin method to develop similar area-altitude relations for their studies are (Malmberg and Eakin 1962, pp. 13, 15, 16, 23, 24; Walker and Eakin 1963, pp. 17, 19, 20, 21; Miller 1977, pp. 20, 21; Malmberg 1967, pp. 26, 27; Winograd and Thordarson 1975, pp. C92, C93; and Harrill 1986, p. 22). In terms of groundwater recharge, these reports are summarized as follows:

Malmberg and Eakin 1962, pp. 13, 15, 16, 23, 24:

Malmberg and Eakin (1962, pp. 13, 15, 16, 23, 24) discuss the groundwater resources of Sarcobatus Flat and Oasis Valley, Nevada. In the Sarcobatus Flat area, precipitation at the higher altitudes is one of the main sources of groundwater recharge. Additional sources of recharge may occur from precipitation on the valley floor, seepage from bedrock, underflow from Stonewall Flat, and underflow from Gold Flat northeast of Pahute Mesa (Malmberg and Eakin 1962, p. 13).

In Oasis Valley, the average annual recharge was derived principally from precipitation on the slopes of Black and Timber Mountains in the north and east parts of the valley, respectively. Some recharge also occurs in other topographically high areas, such as the Bullfrog Hills. Underflow through bedrock from areas beyond the drainage divide to the north and northeast of Oasis Valley apparently contributes a considerable proportion of the groundwater recharge to the valley (Malmberg and Eakin 1962, p. 23)

Part of the recharge occurring within the Sarcobatus Flat and Oasis Valley areas could be estimated as a percentage of the average annual precipitation. In determining this recharge, the average annual precipitation was estimated from a generalized precipitation map of Nevada. This map was divided into precipitation zones, based largely upon records of precipitation, altitude, and types of vegetation. In general, Malmberg and Eakin (1962, p. 15) indicated that precipitation increases with altitude, and subsequently recharge would also increase with altitude. The precipitation zones used by Malmberg and Eakin were adapted from a method developed by Eakin et al. (1951, pp. 79-81, page numbers cited by Malmberg and Eakin). These precipitation zones were less than 8 inches (203 mm) of precipitation for elevations of 0 to 5,000 feet (0 to 1,524 m), 8 to 12 inches (203 to 305 mm) of precipitation for elevations of 5,000 to 6,000 feet (1,524 to 1,829 m), and 12 to 15 inches (305 to 381 mm) of precipitation for elevations of 6,000 to 7,000 feet (1,829 to 2,134 m). The recharge was estimated as a percentage of the precipitation zones greater than 5,000 feet. For the precipitation zone of 0 to 5,000 feet, no recharge was expected. Though a high degree of reliability could not be guaranteed, this method was considered a reasonable approximation of average recharge. Estimated average annual recharge from precipitation based on precipitation zones, were 1,200 acre-feet (1.48 million m³) for Sarcobatus Flat, and 250 acre-feet (0.31 million m³) for Oasis Valley Malmberg and Eakin (1962, pp. 15, 24)

Interbasin flow was also estimated by Malmberg and Eakin (1962, pp. 16, 24). Because there had been little groundwater development in Sarcobatus Flat or Oasis Valley, the aquifers were considered to be in equilibrium (steady-state conditions), with the average annual recharge to the aquifers equal to the average annual discharge from the aquifers. A comparison of the estimated average annual recharge computed from precipitation and the estimated average annual discharge indicated that discharge from the aquifers was considerably more than the computed recharge. Malmberg and Eakin stated that if the reconnaissance estimates of discharge and recharge were reasonably good, then it could be concluded that interbasin underflow accounted for approximately 2,300 acre-feet (2.84 million m³) of groundwater recharge into Sarcobatus Flat and 1,800 acre-feet (2.22 million m³) of groundwater recharge into Oasis Valley. The source of the underflow into Sarcobatus Flat was from Stonewall Flat and Gold Flat. The source of underflow into Oasis Valley was from Gold Flat.

Walker and Eakin 1963, pp. 17, 19, 20, 21:

Walker and Eakin (1963, p. 17) stated that, in the Amargosa Desert, recharge is derived from precipitation within a specified drainage area of the Amargosa Desert and from groundwater underflow through bedrock from the east and northeast beyond the drainage area. As in Malmberg and Eakin (1962, p. 15), Walker and Eakin (1963, p. 19) use precipitation zones to estimate recharge due to precipitation. Using this method, average annual recharge from precipitation for the Amargosa Desert was estimated at 1,500 acre-feet (1.85 million m³), with most of the recharge derived from precipitation in Oasis Valley and Fortymile Canyon, which are tributaries to Amargosa Desert. Walker and Eakin (1963, p. 20) also discussed groundwater recharge from precipitation for the northern and western slopes of the Spring Mountains, an area which they thought may

contribute recharge to Amargosa Desert. Annual recharge from precipitation from the slopes of the Spring Mountains was estimated to be 3,500 acre-feet (4.32 million m³), which could give a combined recharge due to precipitation to the Amargosa Desert of 5,000 acre-feet (6.17 million m³).

Walker and Eakin (1963, p. 21) also discuss groundwater recharge to the Ash Meadows spring system in terms of interbasin underflow. Underflow from Spring Mountain was estimated to be 13,000 acre-feet (16.04 million m³) a year. Groundwater underflow from Paleozoic carbonate rocks located to the northeast of Ash Meadows was estimated to be 4,000 acre-feet (4.93 million m³) per year.

Miller 1977, pp. 20, 21:

Miller (1977, p. 20) stated that, in the Death Valley National Monument area, interbasin flow of groundwater and seepage from stream channels during floods was the most dominant source of recharge in the Death Valley. He also indicated that direct infiltration of precipitation was a rare event in the alluvial part of the valley, however, infiltration probably occurs in fractured rocks in the mountains surrounding Death Valley. In deriving recharge rates from precipitation for the Death Valley area, Miller references the reports by Eakin et al. (1951) and Walker and Eakin (1963), and discusses the concept that precipitation increases with increasing altitude, and that some percentage of this precipitation becomes groundwater recharge. Using this method of estimating recharge from annual precipitation, Miller (1977, p. 21) estimates recharge to Death Valley from precipitation to be about 8,000 acre-feet (9.87 million m³) per year.

Although Miller states that interbasin flow and seepage from stream channels was the most dominant source of recharge to Death Valley, he offers that a detailed estimate of the total recharge was beyond the scope of his report. However, he does discuss seepage from underflow beneath the Amargosa river channel in the south end of Death Valley, indicating that about 900 acre-feet (1.11 million m³) per year of groundwater recharge occurs in this area.

Miller gives a lengthy discussion of the uncertainties of estimating recharge in the Death Valley area which was reviewed by D'Agnesse et al. (1997, p. 52). This summary of uncertainties is discussed later in this report.

Pahrump valley with references to Maxey and Jameson (1948, p. 117, page number cited by Malmberg) and Eakin et al. (1951, pp. 26, 27, page numbers cited by Malmberg). Malmberg 1967, pp. 26, 27:

Malmberg (1967, pp. 26, 27) discusses groundwater recharge from precipitation in the Malmberg (1967, pp. 26, 27) uses the method described by Eakin et al. (1951) to reappraise the estimated recharge to Pahrump Valley. Malmberg (1967, pp. 26, 27) indicated this method was similar to the method described by Maxey and Jameson (1948) in that it was based on the assumption that a fixed percentage of a given average annual rate of precipitation ultimately recharges the groundwater reservoirs. However,

Malmberg (1967, pp. 26, 27) uses more altitude zones to correspond more closely to the amounts of precipitation. These altitude zones are the same as the precipitation zones discussed by Malmberg and Eakin (1962, p. 19); however, Malmberg (1967, pp. 26, 27) includes additional precipitation zones of 7,000 to 8,000 feet (2,134 to 2,438 m) and above 8,000 feet (2,438 m). Using this method, Malmberg (1967) estimates the average annual recharge to Pahrump Valley to be 22,000 acre-feet (27.14 million m³) and states that recharge estimated by this method may occur in three ways:

- By direct, infiltration of rainfall in areas that are generally higher than 5,000 feet
- By seepage loss from streams in the mountains and in the valley
- By lateral movement from the carbonate-rock reservoir, as well as from fractures in the other consolidated rocks to the valley-fill reservoir

Because there were many unknown factors in the spatial distribution both of recharge to and of underflow between groundwater reservoirs, Malmberg (1967, pp. 26, 27) did not make direct estimates of recharge to each of the two reservoirs (valley-fill reservoir or carbonate-rock reservoir). However, when discussing groundwater discharge of Pahrump Valley, an indirect "probable" division was made that computes annual recharge of 12,000 acre-feet (14.80 million m³) to the valley-fill reservoir and 10,000 acre-feet (12.33 million m³) to the carbonate-rock reservoir.

Winograd and Thordarson 1975, pp. C92, C93:

Winograd and Thordarson (1975, pp. C92, C93) give a detailed account of sources of recharge to the lower carbonate aquifer underlying the Ash Meadows groundwater basin. Within this basin the lower carbonate aquifer is recharged principally by precipitation in areas of high precipitation and favorable rock type, by underflow, and by downward leakage of water from the overlying hydrogeologic units (Winograd and Thordarson 1975, p. C92). Recharge from precipitation is probably beneath and immediately adjacent to the highly fractured Paleozoic carbonate rocks of Sheep Range, Northwestern Spring Mountains, Southern Pahrangat Range, and, to a lesser extent, beneath the Pintwater Desert and Spotted Ranges. Using a method which involved a relation between land surface elevation and the amount of precipitation, an estimated recharge of 60,000 acre-feet (74.01 million m³) of year of recharge from precipitation occurs in areas receiving 8 inches (203 mm) or more of precipitation. Underflow into the Ash Meadows groundwater basin, which is suspected of coming into the basin from the northeast, was estimated to be 6,000 acre-feet (7.40 million m³) a year. This flux was estimated by Winograd and Thordarson based on a comparison of the deuterium content of the groundwater. Minor recharge is estimated by Winograd and Thordarson (1975, p. C93) to come from downward leakage from semi-perched groundwater in the overlying hydrogeologic units. In Yucca Flat, the magnitude of downward leakage was estimated to be in the range of 25 to 65 acre-feet (0.03 to 0.08 million m³) per year. Downward leakage of similar magnitude is probable also in Frenchman Flat, Desert

Valley, Eastern Emigrant Valley, the northern two-thirds of Three Lakes Valley, and the northern two-thirds of Indian Springs Valley.

Winograd and Thordarson (1975, p. C93) also discuss recharge due to underflow from the northwest side of the Ash Meadows groundwater basin; however the amount of flow is considered to be small. It was estimated that less than 600 acre-feet (0.74 million m³) a year of recharge due to underflow from the northwest occurs.

Harrill 1986, p. 22:

Harrill (1986, p. 22) refers to the recharge estimates made by Malmberg (1967, p. 36 page number cited by Harrill) for Pahrump Valley (22,000 acre-feet [27.14 million m³] per year) which were based on a fixed percentage of a given average annual rate of precipitation. Harrill points out that recent techniques of estimating the percentage of precipitation recharge incorporated higher precipitation rates on the side of mountains facing a prevailing storm track and also used different percentage rates of precipitation recharge where there were significant areas of higher altitude. Applying these new techniques, Harrill estimated recharge from precipitation in Pahrump valley to about 26,000 acre-feet (32.07 million m³) per year. However, because there were insufficient data to determine which set of precipitation recharge was best, a range of recharge from 22,000 to 26,000 acre-feet (27.14 to 32.07 million m³) per year was incorporated into Harrill's model.

Water Balance Method. In a summary of a report by Rice (1984), D'Agnese et al. (1997, p. 51) indicates that Rice developed a relatively detailed recharge calculation as part of a regional modeling study. Rice employed a water-balance method that used average annual precipitation distributions derived from a report by Quiring (1965). These computations showed that recharge occurs if the altitude is greater than 1,675 m and the annual precipitation is greater than 254 mm. Because these two criteria meet the plant requirements of Pinyon Pine and Juniper, Rice placed the area of recharge to extend below that plant zone. D'Agnese et al. (1997, p. 51) stated that more recent investigations by West (1989) have placed the lower altitude limits of regional recharge at the Mixed Shrub-Transition Zone where Blackbrush flourishes. West noted that these communities represent the altitudinal zone at which winter recharge of soil moisture is normally balanced by summer evapotranspiration loss. Therefore, in wet years some regional recharge may occur in these areas.

Rice's water-balance method has several significant limitations (D'Agnese et al. 1997, p. 51). Rice (1984) suggested that:

- The recharge calculations are too gross a scale to compute small amounts of recharge, such as the amount that probably occurs at Yucca Mountain.
- The method depends only on temperature and an empirical crop coefficient to calculate evapotranspiration rates that are influenced by numerous climatic conditions.

- This method averages rainfall events into monthly distributions and does not account for high-intensity storms and runoff events which are common to the area and may significantly contribute to recharge.

D'Agnese et al. (1997, p. 51) concluded that because the error associated with each component of the water-balance equation may be larger than the net total recharge calculated for many arid basins, water-balance methods are of limited usefulness.

Distributed-Parameter Method—D'Agnese et al. (1997, p. 51) discusses reports by Lichty and McKinley (1995) and Leavesley et al. (1983), who have attempted to use distributed-parameter precipitation-runoff models to estimate groundwater recharge in several hydrographic basins of the Death Valley region. These models attempt to simulate the processes in the soil-plant-atmosphere system through a series of integrated modules. For basins that contain both a surface-water and groundwater component, monthly or storm-based water-balance simulations may be modeled. D'Agnese et al. (1997, p. 51) reports that although successful simulations have been conducted using these models for various regions of the United States, the use of such models in extremely arid environments where little surface-water exists has proven to be difficult.

Maxey-Eakin Method—Comparing empirical (Maxey-Eakin) water balance, and distributed-parameter methods for estimating rainfall recharge, the Maxey-Eakin method is considered the best method for use in an arid environment. Most water resource investigations in the Death Valley region have used a version of the Maxey-Eakin method. Because of its acceptance for determining rainfall recharge in the Great Basin province, D'Agnese et al. (1997, p. 52) used the Maxey-Eakin method to develop a preliminary map of potential recharge areas in the Death Valley region. However, even though the Maxey-Eakin method is the most widely used in the Death Valley region, the method as previously used has limitations.

5.2.3.1.2 Limitations of the Empirical Maxey-Eakin Method

Despite the empirical nature of the Maxey-Eakin method, it still remains the most widely-used means of estimating regional groundwater recharge in the Great Basin (D'Agnese et al. 1997, p. 52). Subsequently, the Maxey-Eakin method was used by D'Agnese et al. to develop a preliminary map of potential recharge areas for the 3-D flow model of the Death Valley region using digital altitude data and a digital representation of average annual precipitation data. To assess the accuracy of the predicted recharge areas, this map was compared by D'Agnese et al. to maps showing low-temperature (local) spring locations and vegetation classes. The local springs are believed to represent discharges of locally recharged groundwater. The selected vegetation classes reflect moisture at shallow depths. Careful comparison by D'Agnese et al. (1997, p. 52) of these three maps showed that the preliminary map of potential recharge areas using the Maxey-Eakin method failed to identify some lower altitude areas where long-term recharge appeared likely from the pattern of spring locations and vegetation, and also included some higher altitude areas where long-term recharge may not occur. Because the Death Valley regional groundwater flow system is compartmentalized, any under- or over-estimation of recharge volumes may result in discrepancies in interbasinal transfers.

In a review of the report by Miller (1977), D'Agnese et al. (1997, p. 52) stated that Miller had experienced similar problems when using the Maxey-Eakin method for a study of the groundwater resources of Death Valley National Park. D'Agnese et al. stated that Miller attributed the discrepancies to many factors that were summarized as follows:

- The method was originally developed for basins that were believed to be unaffected by interbasinal flow.
- Drainage of mountain slopes are influenced by aspect controls that affect evapotranspiration rates and soil moisture that ultimately control recharge. North and east facing slopes are typically cooler and wetter, while south and west facing slopes are warmer and drier. Therefore, more recharge will probably occur in north and east facing slopes, and less will occur on south and west facing slopes. However, the Maxey-Eakin method does not take this phenomenon into account.
- Uncertainties in the estimates of discharge rates, which are used to calculate recharge rates, may contribute to volumetric discrepancies.
- High altitudes (in excess of 3,000 m) may contribute significantly more recharge than the 25 percent of precipitation predicted by the Maxey-Eakin method.
- Altitude-percentage constants used in the Maxey-Eakin method may need to be adjusted on a basin-by-basin basis to account for factors such as lithology, aspect, and vegetation.
- The Maxey-Eakin method assumes that recharge does not occur below 1,524 m, but the presence of dense vegetation and cold springs at lower altitudes indicate that significant infiltration occurs in these areas at steady-state.
- The Maxey-Eakin method is extremely dependent on the prediction of average annual precipitation which is poorly understood and quantified; therefore, a more accurate characterization of precipitation may lead to more accurate recharge estimates if the recharge coefficients are likewise revised.
- The Maxey-Eakin method and its variants are simplistic and should be modified to consider critical factors such as rock type, permeability of weathered rock and soil, permeability of stream channel deposits, and soil moisture at the time of precipitation and slope.

5.2.3.1.3 Modifying the Maxey-Eakin Method

The Maxey-Eakin method was modified by D'Agnese et al. (1997, p. 52) to make it more sensitive to the critical factors affecting recharge by using four potential recharge indicators existing within the Geoscientific Information System database. The four potential recharge indicators used by D'Agnese were:

- Altitude
- Slope-aspect

- Relative rock and soil permeability
- Vegetation

Appropriate map categories were reclassified to represent these four potential recharge indicators on a six-point scale; a value of zero indicated no recharge potential, a value of one represented a low recharge potential, and a value of five represented a high recharge potential. The recharge values for each of the indicators are as follows:

- Potential recharge classifications for altitude zones:

Altitude significantly affects recharge. As altitude increases precipitation increases along with the potential for recharge. The digital terrain model was reclassified by D'Agnese et al. (1997, p. 52) according to the following ratings to produce a map describing recharge potential based on altitude.

Altitude Zone	Recharge Rating
greater than 2,743 m	5
2,438 to 2,743 m	4
2,134 to 2,438 m	3
1,829 to 2,134 m	2
1,524 to 1,829 m	1
less than 1,524 m	0

- Potential recharge classification for vegetation zones:

The vegetation landform map was reclassified by D'Agnese et al. (1997, p. 53) in a similar manner as the altitude zones. Because the mixed shrub-transition zone is believed by D'Agnese et al. to be the lowest vegetation zone to experience any long-term recharge flux, those vegetation classes that reflect these soil moisture conditions and wetter conditions were ranked by D'Agnese et al. into the following ratings and a vegetation-based recharge potential map was developed.

Vegetation Zone	Recharge Rating
Coniferous forests	5
Pinyon-Juniper	3
Mixed shrub	1
All others	0

- Potential recharge classification for slope-aspect zones:

Slope-aspect determines the amount of direct solar radiation received on a hillslope and the amount of drying activity that occurs during the day. Therefore, a slope-aspect based recharge potential map was developed by D'Agnese et al. (1997, p. 53) by assigning north

and east facing slopes higher recharge potential ratings and south and west slopes lesser recharge potential ratings. The recharge classification for slope-aspect zones are as follows.

Slope-Aspect Zone	Recharge Rating
Northeast	5
Northwest	4
Flat	3
Southeast	2
Southwest	1

- Potential recharge classification for parent material types:

The bedrock material through which water will infiltrate during a recharge event affects recharge potential. Therefore, the relative permeability of bedrock materials and the soils developing on them can be used to develop a permeability-based recharge potential map.

For example, parent materials that develop high-permeability soils, such as alluvium, carbonate, granite, sandstone, and gneiss, may be assigned higher ratings, while rocks that develop low-permeability soils, such as tuffs, siltstone, and shale, may be assigned lesser ratings (D'Agnese et al. 1997, p. 53). D'Agnese et al. also pointed out that, locally, low-permeability soils may lead to runoff and recharge in an adjacent area. Using the hydrogeologic unit map (Figure 5.2-4) D'Agnese et al. developed a recharge classification for parent rock types, however, the effects of rainfall runoff to potentially recharge adjacent areas was not factored into the recharge classification. The recharge classification for parent material (rock) type is as follows.

Hydrogeologic Unit (See Figure 5.2-4)	Recharge Rating
QTvf	5
TJg, Mvs, pEgm	4
P2	3
Qp, QTv, Tv, P1	2
Tvs	1

The four recharge potential maps created from the recharge indicators of altitude, slope-aspect, relative rock and soil permeability, and vegetation were overlain to produce a map that combined the ratings from each map (Figure 5.2-9). The recharge ratings of the four maps were then reclassified into six recharge potential classes (class numbers) (Table 5.2-7).

The most significant factor which influenced the new classification was altitude. This factor was explicitly included in the altitude-based recharge potential map, and was also implicitly included in the vegetation-based recharge potential map. Vegetation distributions are dominantly controlled by altitude and moisture availability.

The areas most likely to have high recharge potential were those that possessed all four favorable factors. For example, high recharge potential would most likely occur on northeast facing slopes, at altitudes higher than 2,743 m, where coniferous trees are growing on alluvial soils. Low recharge potential would exist on southwest facing slopes, at altitudes lower between 1,524 and 1,829 m, where mixed shrub communities are growing on clayey soils derived from argillaceous volcanic rocks.

Areas in the region that are lower than 1,524 m (5,000 ft) are assigned a zero recharge potential in regional analysis and modeling. However, at some localities, particularly those close to this minimum altitude, some net infiltration, and thus recharge, undoubtedly occur. In Subsection 5.3.4.1.3, for example, net infiltration at the potential repository site, where altitudes range from about 1,300 m to 1,500 m, is discussed principally in relation to topographic position and surficial lithology. The ridge tops and steep side slopes of the washes at Yucca Mountain have little if any soil cover over a well fractured welded tuff allowing rapid and deep infiltration, though of relatively small volumes. In contrast to its role in less arid uplands, the thick alluvium that occupies the central and lower reaches of the major channels at Yucca Mountain is assigned a low recharge potential. This assignment reflects the capability of the alluvium to capture and store the relatively small infiltration volumes within the deep root zone, where it can subsequently be transpired to the atmosphere by plants that grow in the washes.

5.2.3.1.4 Accuracy of the Modified Maxey-Eakin Method

The accuracy and appropriateness of the modified Maxey-Eakin method were evaluated by D'Agnese et al. (1997, p. 55) by comparing a map of the new recharge areas with the maps showing locations of low-temperature springs and vegetation types. D'Agnese et al. indicated that upon inspection, areas uphill from low-temperature springs, regardless of altitude, were found to be coincident with predicted regional recharge areas. Because vegetation constraints were incorporated in the rating criteria, all predicted recharge areas were restricted to vegetation zones classified as either Coniferous Forests, Pinyon-Juniper Woodlands, or Mixed Transition Shrublands. As a result, the refined recharge areas map was considered an improvement to the map based on the traditional Maxey-Eakin method and an acceptable indicator of areas in the region where long-term, regional groundwater recharge may occur. While the modified recharge areas may not exactly describe recharge locations on a local scale, they appear to be appropriate for delineating large-scale zones of recharge that is consistent with previous investigations (Prudic et al. 1993, pp. 23, 24 page numbers cited by D'Agnese et al.). However, it should be noted that even with better defined potential recharge areas, recharge rates are still based on empirical estimates rather than actual measured rates and reflect a significant unknown flux in modeling this region (D'Agnese et al. 1997, p. 55).

5.2.3.1.5 Evaluation of Current Recharge Estimate

To evaluate the suitability of recharge rates for conceptualization and numerical simulation, the total volume of recharge in each of the hydrographic areas of the Death Valley region (Figure 5.2-10) was calculated by D'Agnese et al. (1997, p. 55). These recharge volumes were compared by D'Agnese et al. to previous Maxey-Eakin estimates (Table 5.2-8)

In general, the values of recharge computed by the refined Maxey-Eakin method developed by D'Agnese et al. (1997, p. 55) were higher than those computed by previous investigations. The total amount of refined Maxey-Eakin estimates of recharge was 30 percent greater than the original Maxey-Eakin recharge estimates for the Death Valley flow system. D'Agnese et al. attributed these differences to the following:

- The recharge rates were computed using percentages of recently estimated average annual precipitation. These rates may reflect slightly higher region-wide precipitation rates.
- Hydrographic areas in the northern and eastern parts of the Death Valley region are estimated to have larger rates of recharge than by the Maxey-Eakin method. These basins are located at higher altitudes than the remainder of the study area. They typically possess highly permeable soils (alluvium and carbonate derived), and support vegetation that require high precipitation rates to survive. These conditions are believed to result in high-recharge potential in these basins.
- Hydrographic areas in the central and southern parts of the Death Valley region are generally estimated to have smaller rates of recharge than by the Maxey-Eakin method. The lower estimates are attributed to the low-recharge potential characteristics of these basins. These lower estimates suggest that the Maxey-Eakin elevation-precipitation-recharge relations, which were developed in the Northern Great Basin, may not be good recharge estimation techniques in the Transition Desert and Mojave Desert.
- Some previous investigators (Malmberg and Eakin 1962; Walker and Eakin 1963; Malmberg 1967) adjusted the Maxey-Eakin recharge percentages in basins to reflect the large discharge volumes observed. Many of these large discharge volumes probably reflect inter-basinal fluxes and not infiltration of locally recharged waters.

5.2.3.1.6 Summary Characterizing the Recharge Component

The major source of recharge to the Death Valley regional groundwater flow system is from precipitation on the highest mountains. The regional system is also recharged by interbasinal flow. Some recharge also results from recycled irrigation and domestic waters as well as seepage of spring discharge back into the groundwater system, however, these recharge volumes are considered to be negligible.

Of three methods for estimating rainfall recharge (Empirical Maxey-Eakin method, water-balance method, and distributed-parameter method) the Maxey-Eakin method is considered to be the best method for determining rainfall recharge in an arid environment. Historically, most estimates of rainfall recharge have used a form of the Maxey-Eakin method. However, though factors other than the basic relation of altitude and percentage of rainfall recharge were sometimes incorporated, none combined the four key factors introduced by D'Agnese et al. These factors of altitude, slope-aspect, relative rock and soil permeability, and vegetation combined to develop a modified version of the Maxey-Eakin that gave a better areal distribution of rainfall recharge than the original Maxey-Eakin method. Subsequently, because of the detailed documentation of the modified Maxey-Eakin method

presented by D'Agnese et al., the modified Maxey-Eakin method is considered to be the most current and accurate method of estimating rainfall recharge for the Death Valley region.

In terms of interbasin recharge to the Death Valley region, most rates of interbasin flow are the difference between rainfall recharge and evapotranspiration when balancing localized basin water budgets. Because groundwater inflow and outflow volumes are not well defined in the Death Valley region, specific groundwater fluxes are not discussed in this report. To discuss these volumes, estimates will need to be derived from the groundwater flow models currently being developed for the Death Valley region.

5.2.3.2 Characterizing the Discharge Component

Death Valley has long been recognized as the ultimate discharge area for the Death Valley regional groundwater flow system (D'Agnese et al. 1997, p. 43). Intermediate discharge locations reflect topographic, geomorphic, stratigraphic, or structural controls; many involve combinations of these controls. The largest discharges from the regional groundwater flow system include evapotranspiration by phreatophytes and wet playas, springs, and groundwater pumpage.

5.2.3.2.1 Evapotranspiration by Phreatophytes and Wet Playas

Most water-resource investigations of localized areas within the Death Valley region have estimated evapotranspiration by delineating areas of phreatophytes on areal photos. Outside of these site specific areas, estimates of evapotranspiration for the remainder of the Death Valley region has never been done. To estimate evapotranspiration rates for the Death Valley region, D'Agnese et al. (1997, p. 43) used six evapotranspiration classes: wetlands, hardwood phreatophytes, herbaceous phreatophytes, saltbush flats, wet playas, and mixed phreatophytes, and developed a detailed map of potential evapotranspiration areas of the Death Valley region.

Historical Estimates of Evapotranspiration—D'Agnese et al. (1997, p. 43) stated that most studies of groundwater resources in the Death Valley region have estimated groundwater discharge from evapotranspiration by delineating areas of phreatophytes on areal photos and applying empirically derived mean consumptive-use rates for those species of phreatophytes at the discharge sites (Malmberg and Eakin 1962, pp. 16, 17, 18, 25, 26; Walker and Eakin 1963, pp. 21, 22; Malmberg 1967, pp. 27 - 33; and Glancy 1968, pp. 25-34). In terms of groundwater discharge, these reports are summarized as follows:

Malmberg and Eakin 1962, pp. 16, 17, 18, 25, 26:

In their study of Sarcobatus Flat and Oasis Valley, Malmberg and Eakin (1962, pp. 16, 17, 18, 25, 26), stated that groundwater is discharged by transpiration, evaporation, underflow, and well pumpage. In Sarcobatus Flat groundwater discharge occurs principally through transpiration. Based on studies of the consumptive use of phreatophytes in the Great Basin, Malmberg and Eakin estimated the transpiration of Sarcobatus Flat to be 2,800 acre-feet (3.45 million m³) per year. Evaporation from a 9,000-acre playa located in Sarcobatus Flat was estimated to be 200 acre-feet (0.25 million m³) per year. Based on hydrologic and geologic conditions at the head of

Grapevine Canyon and adjacent areas, underflow from Sarcobatus Flat through Grapevine Canyon was estimated to be 500 acre-feet (0.62 million m³) per year. For groundwater discharge due to well pumpage, it was estimated that within Sarcobatus Flat, there was a potential for the aquifer to yield 3,500 acre-feet (4.32 million m³) per year. However, at the time of Malmberg and Eakin's report the system was not being pumped at that rate.

In Oasis Valley Malmberg and Eakin (1962, pp. 25, 26), reported that groundwater discharge occurred principally through transpiration, evaporation, and underflow. Historical groundwater discharge data were not available for Oasis Valley. Transpiration and evaporation accounted for most of the groundwater discharge with a combined discharge estimated at 2,000 acre-feet (2.47 million m³) per year. Groundwater underflow, which was thought to flow from Oasis Valley through the Amargosa Narrows, was estimated to be 400 acre-feet (0.49 million m³) per year.

Walker and Eakin 1963, pp. 21, 22:

In their study of Amargosa Desert, Walker and Eakin (1963, pp. 21, 22), stated that groundwater is discharged from Amargosa Desert by the natural processes of transpiration of vegetation, evaporation from the soil and free-water surfaces, and to a lesser extent by stream flow and underflow from the Alkali Flat southeast of Death Valley Junction. A transpiration rate of 11,500 acre-feet (14.19 million m³) per year was estimated by Walker and Eakin based on published transpiration rates of certain phreatophytes. Groundwater discharge due to evaporation was estimated to be 12,000 acre-feet (14.80 million m³) per year. Groundwater discharge out of Amargosa Desert by underflow and surface flow through the valley (gap) at Eagle Mountain was estimated to be 500 acre-feet (0.62 million m³) per year. In all, the total average annual groundwater discharge from Amargosa Desert was estimated to be about 24,000 acre-feet (29.60 million m³).

Malmberg 1967, pp. 27 - 33:

In his study of Pahrump Valley, Malmberg (1967, pp. 27 - 33), discusses groundwater discharge from the upper valley-fill reservoir and deeper carbonate rock reservoir. For the valley-fill reservoir, groundwater discharge occurs by well pumpage, evapotranspiration, spring flow, and subsurface outflow. As of 1962 it was estimated that well pumpage dominated groundwater discharge, with 29,000 acre-feet (35.77 million m³) of groundwater pumped during 1962, representing about 60 percent of the total discharge from Pahrump Valley. The increase in well pumpage in Pahrump Valley caused a considerable drop in the potentiometric surface, which caused a decline in spring discharge. For 1962, spring discharge was estimated to be 1,400 acre-feet (1.73 million m³) per year. Spring discharge was estimated to be the volume of spring flow that actually left Pahrump Valley through evapotranspiration, and may not represent the total spring outflow, since some spring discharge percolated back into the aquifer as groundwater recharge. Evapotranspiration for 1962 was estimated to be 10,000 acre-feet (12.33 million m³) per year. This amount was estimated from the type of phreatophytes,

acreage, and rate of groundwater used for each type in Pahrump Valley. Subsurface outflow was estimated based on a form of Darcy's law, with 2,000 acre-feet (2.47 million m³) a year estimated for 1962 as underflow out of the valley-fill reservoir. The groundwater discharge from the valley-fill reservoir moves southwestward in Pahrump Valley, into the carbonate-rock reservoir.

Malmberg, stated that virtually all groundwater discharge from the carbonate-rock reservoir is by subsurface outflow beneath topographic divides to Chicago and California Valleys and possibly to Ash Meadows. A minor amount of discharge may occur in the vicinity of Sixmile Spring. It was estimated that subsurface outflow from the carbonate-rock reservoir was about 12,000 acre-feet (14.80 million m³) per year.

Glancy 1968, pp. 25-34:

In his study of the Mesquite and Ivanpah Valley area, Glancy (1968, pp. 25-34), states that groundwater discharge in Mesquite Valley occurs principally by evapotranspiration and well pumpage. Evapotranspiration occurs only in Mesquite Valley because the depth to groundwater in Ivanpah Valley is too deep for evapotranspiration to occur. Estimates of evapotranspiration were determined by Glancy based on phreatophyte type and area (acres) covered by the phreatophytes. Groundwater discharge due to transpiration was estimated to be 1,600 acre-feet (1.97 million m³) per year. Bare soil evaporation was estimated to be 600 acre-feet (0.74 million m³) per year. Groundwater pumpage for 1966-67 for an estimated 60 wells located in Mesquite Valley was 1,400 acre-feet (1.73 million m³) per year.

Current Estimation of Evapotranspiration Volumes—In reviewing the reports of Malmberg and Eakin (1962), Walker and Eakin (1963), Malmberg (1967), and Glancy (1968), D'Agnese et al. (1997, p. 43) reported that, though evapotranspiration rates have been estimated locally within the Death Valley region, estimates of evapotranspiration have not been precisely determined for plant communities and bare soil conditions throughout the Death Valley region. Therefore, for his report, detailed maps of potential evapotranspiration areas were developed.

Areas where groundwater is found at shallow depths are potentially significant discharge zones. Such zones can be identified by shallow water depths, the presence of moist soil conditions, and certain vegetative communities. Four data sets were combined by D'Agnese et al. (1997, p. 43) to identify such areas: vegetation types, vegetation density, soil classes, and locations of springs. A map of potential evapotranspiration was developed by D'Agnese et al. (1997, p. 43) by combining the high-density phreatophytes, salt bush, bare soil, and unclassified regions of the vegetation map with locations of regional spring discharges and high-salinity soil areas. Where bare soils are coincident with high salinity areas, evaporation occurs through discharging or wet playas. Unclassified areas on the vegetation map included additional phreatophyte or saltpan areas that could not be grouped into the other classes.

The potential evapotranspiration map represents conditions as of the mid-1980s, and includes all areas in the Death Valley region where significant evapotranspiration volumes may occur from phreatophyte vegetation or moist bare soil. Field verification of each delineated potential discharge

zone resulted in a refined final evapotranspiration map containing six evapotranspiration classes: wetlands, hardwood phreatophytes, herbaceous phreatophytes, saltbush flats, wet playas, and mixed phreatophytes areas (Figure 5.2-11).

- **Wetlands** occur near discharging springs and include areas of standing water, reeds, rushes, sedges, and other wetland grasses.
- **Hardwood phreatophytes** dominate where low-salinity groundwater occurs at shallow depths or where fresh water is present in large quantities as a result of regional spring discharge.
- **Herbaceous phreatophytes** include high-salinity species such as pickleweed, saltgrass, and rabbitbrush.
- **Saltbush flats** occur on alluvial flats surrounding wet playas and are dominated by greasewood and saltbush. Because species of the saltbush possess root systems capable of growth to depths of 15 m, their presence may indicate evapotranspiration of relatively deep groundwater.
- **Wet playas** and alkali flats are included within the bare soil areas class. In these areas, the capillary fringe extends to within a few inches of the land surface and the soil texture becomes fluffy. These large pore spaces disrupt capillary action. A fluffy texture may indicate that water has moved upward through the playa deposits and precipitated dissolved salt during evaporation.
- **Mixed phreatophytes** include areas containing such heterogenous mixtures of the above classes that classification into any one class is difficult.

Water consumption rates for each of the six evapotranspiration classes were required to estimate evapotranspiration fluxes by D'Agnese et al. (1997, p. 44). However, precise data for each class were unavailable, so estimated annual rates of water consumption were obtained from the results of previous investigations of areas within the Death Valley region by: Robinson, T.W. (1958); Malmberg and Eakin (1962); Walker and Eakin (1963); Malmberg (1967); Rush (1970); Czarnecki (1990); and Duell (1991). The rates reported in these reports were taken by D'Agnese et al. (1997, p. 44) and multiplied by the area of each evapotranspiration class to obtain estimated volumes of groundwater discharge due to evapotranspiration (Table 5.2-9).

Generally, the evapotranspiration discharge estimates developed by D'Agnese et al. (1997, p. 44) are slightly larger than those used in previous investigations. The reasons for these differences are:

- Some of the discharge areas included were never before defined as regional evapotranspiration areas.
- Some areas included have previously been considered to contribute negligible amounts of discharge.

- Some areas identified include areas of phreatophytes that had not been identified and mapped by previous studies.

5.2.3.2.2 Spring Discharge Accounting

Numerous springs in the Death Valley region occur as small discharges in many of the mountain ranges (D'Agnesse et al. 1997, p. 44). This spring water is from nearby "local" groundwater sources, and the locations of these springs are controlled by permeability variations in the rocks and water levels related to land-surface altitude, which cause the water to discharge at the surface. These springs, which have small (less than 25 m³/day) to moderate yields (25 to more than 2,200 m³/day), commonly represent perched or semiperched, local groundwater flow systems associated with regional recharge areas. These springs commonly emerge from consolidated rock within the mountains or ridges flanking valleys and are characterized by highly variable discharge rates and by variable temperature, usually less than 21°C (Winograd and Thordarson 1975, p. C50).

Springs that discharge from the regional groundwater flow system are not included in the group of "local" springs. Regional springs typically emerge from the valley fill and the carbonate aquifer at low altitudes along the borders or on the floor of some valleys (Winograd and Thordarson 1975, p. C50) (Figure 5.2-12). The locations of the regional springs are a result of:

- An intersection of the land surface and the water table
- Large permeability faults or fractures which act as conduits, directing regional groundwater to the surface
- A stratigraphic contact of large permeability material with small permeability material, which forces flowpaths to arc toward the land surface
- A structural contact caused by the juxtaposition of large permeability material with small permeability material causing an abrupt change in groundwater flowpaths (D'Agnesse et al. 1997, p. 44)

These valley-level springs, defined by D'Agnesse et al. (1997) as regional springs, represent discharge points for a regional saturated zone; they are characterized by high and uniform discharge and uniform temperatures that range from 24°C to 35°C (Winograd and Thordarson 1975, p. C50).

Based on these criteria, the regional spring data set was modified and attributed by D'Agnesse et al. (1997, p. 47) using the most recently measured regional spring discharge rates and temperature data collected from several sources (Pistrang and Kunkel 1964; Miller 1977; Bedinger, Harrill et al. 1984a; Langer et al. 1984; Bedinger, Langer et al. 1989a, 1989b). Once completed, a summation of total spring discharge was developed (Table 5.2-10).

Regional spring discharge totals differ from spring discharge values given in Table 5.2-9. This difference is due to rounding of values from Table 5.2-10, and because flow of minor springs in the Death Valley region was estimated in Table 5.2-9 and are not included in Table 5.2-10.

5.2.3.2.3 Groundwater Pumpage

To characterize the amount of human-induced water use in the basin, a data set of water-producing wells was developed by D'Agnese et al. (1997, p. 47). D'Agnese et al. stated that estimates of water use for the Death Valley region have been reported on a somewhat discontinuous basis. These estimates are reported by use (commercial, irrigation, mining, or domestic) for each hydrographic area by the state of Nevada, however, such records do not exist for all of the hydrographic areas in the Death Valley region. D'Agnese et al. (1997, p. 47) stated that Bedinger, Harrill et al. (1984b) and Bedinger, Langer et al. (1984) attempted to develop complete water-use estimates for the entire region by averaging empirical rates of use based on well data contained in the USGS National Water Information System database. Harrill (1986) also presented groundwater use information. Data from the reports by Bedinger and Harrill and from the Nevada State Engineer's Office were compiled and evaluated by D'Agnese. Average annual consumptive water-use (total pumpage) values for each hydrographic area were estimated and reported (Table 5.2-11).

5.2.3.2.4 Summary Discharge in the Death Valley Region

Death Valley has long been recognized as the ultimate discharge area for the Death Valley regional groundwater flow system. The largest discharges from the regional groundwater flow system include evapotranspiration by phreatophytes and wet playas, springs, and groundwater pumpage.

Using the six evapotranspiration classes of wetlands, hardwood phreatophytes, herbaceous phreatophytes, saltbush flats, wet playas, and mixed phreatophytes, D'Agnese et al. developed a detailed evapotranspiration map of the Death Valley region. D'Agnese et al. give sufficient documentation of the development of the evapotranspiration map for it to be considered the most current and accurate method for estimating evapotranspiration for the Death Valley region.

Groundwater discharge from springs and well pumpage were documented by D'Agnese et al. (1997). For spring discharge, D'Agnese makes a distinction between local spring discharge, which is due to local groundwater flow systems, and regional springs that discharge due to the regional groundwater flow system. For the Death Valley region flow system, local spring flow was considered to be negligible and only regional spring discharge was used. Groundwater pumpage was estimated from data retrieved from the Nevada State Engineer's Office and from reports by Bedinger and Harrill. Though estimates of groundwater pumpage are given for each hydrogeographic area in the Death Valley region, more detailed information of groundwater use is given in Subsection 5.2.7.

5.2.4 Chemistry of Regional Groundwater

5.2.4.1 Major Ion Composition of Regional Groundwater

There is a large database for chemistry and isotopic composition of groundwater for Southern Nevada and adjacent California. Recent compilations of chemical data include McKinley et al. (1991), Perfect et al. (1995), Rose, T.P. et al. (1997), and Oliver and Root (1997). The latter two adds some isotopic data to the compilation and the last uses data screens to eliminate analyses of questionable quality such as those with a poor charge balance. For purposes of the following

discussion, the data will be treated as representing two regionally important aquifers: the carbonate aquifer and the valley-fill aquifer which includes the volcanic rocks.

Discussions of the groundwater chemistry can be found in Blankennagel and Weir (1973), Winograd and Thordarson (1975), Dudley and Larson (1976), White (1979), and Claassen (1985). Water recharged into the carbonate aquifer acquires a calcium-magnesium bicarbonate character. Water recharged into the volcanic rocks or into sediments derived from volcanic rocks acquires a sodium-potassium character. Where the volcanic rocks have been zeolitized, the dominance of sodium becomes more pronounced because of the removal of calcium. In places where clays occur as alteration products, the abundance of potassium relative to sodium may decrease as a result of ion exchange. Within the valley-fill aquifer, sodium and chlorine appear to behave conservatively (White 1979).

Figure 5.2-13 is taken from Winograd and Thordarson (1975) and summarizes the chemical character of groundwater at various locations at and near the Nevada Test Site. Type I waters represent the calcium-magnesium bicarbonate waters typical of the regional carbonate aquifer. The letters designate localities:

- A is within the Spring Mountains (4 samples).
- B is within Indian Springs Valley, Northwestern Las Vegas Valley, and Southern Three Lakes Valley (10 samples).
- C is within Pahrump Valley (26 samples).
- D is within Pahranaagat Valley (3 samples).

Water samples from multiple zones in three deep wells into the carbonate aquifer suggest that the chemical composition is fairly uniform with depth (Winograd and Thordarson 1975).

Figure 5.2-13 is a Piper diagram showing types of chemical compositions found at and near the Nevada Test Site (from Winograd and Thordarson 1975). Type I waters characterize the regional carbonate aquifer; Type II waters characterize waters from the tuff aquifer (or waters in tuff-derived alluvial aquifers). Type III and VI waters are believed to be derived from a mixture of Types I and II either by mixing of waters or by flow through a mixed source. Circles with crosses represent perched waters (near here).

Type II waters represent the sodium-potassium bicarbonate waters typical of the valley-fill aquifer. The letters designate the following localities:

- A is at Rainer Mesa (24 samples), the hills west of Yucca and Frenchman Flats (9 samples), and the hills west of Oasis Valley (5 samples).
- B is within Emigrant Valley (northwest of the Nevada Test Site, 3 samples).
- C is within Yucca Flat (5 samples).

- D is within Frenchman Flat (3 samples).
- E is within Jackass Flat (3 samples).
- F is at Pahute Mesa (10 samples).
- G is within Oasis Valley (17 samples).

Limited sampling from packed-off zones within the valley-fill aquifer show no more variability than is noted among closely spaced wells.

Type III waters are calcium-magnesium-sodium bicarbonate that have originated by a mixed source. The letters correspond to localities:

- A is Ash Meadows (6 samples), which is the principal discharge area of the carbonate aquifer.
- B is the East-Central Amargosa Desert (3 samples) where water from the carbonate aquifer leaks up into a valley-fill aquifer dominated by volcanic detritus.
- C is the Eastern Nevada Test Site (6 samples) where waters in the carbonate aquifer have infiltrated through volcanic materials.

These waters are thought to make up a component of flow at Ash Meadows.

The final water type shown in Figure 5.2-13, designated as Type VI, is a sodium-sulfate bicarbonate composition represented by 3 samples from the Furnace Creek Wash-Navares Springs area. This water may originate as a Type III which subsequently reacts with sulfide minerals in the core of the Funeral Range, or with evaporites within the Paleozoic strata, or possibly with evaporites within the basal Tertiary section. Of the three possibilities, the last seems least likely in that there is very little Tertiary section between the Amargosa drainage and the springs. A source within the Precambrian core of the range is supported by isotopic data, discussed below.

5.2.4.2 Isotopic Composition of Regional Groundwater

The isotopic database for groundwater from Southern Nevada and adjacent California is not quite as extensive as that for major ion compositions. Furthermore, most studies have focussed on a particular isotope or group of isotopes such that compositions of a particular well or spring have not been determined for a single sample, but rather several samples usually collected on different dates. None-the-less, the database provides good coverage for δD , $\delta^{13}C$, ^{14}C , $\delta^{18}O$, $\delta^{87}Sr$, and $^{234}U/^{238}U$. Major sources of information include:

- Winograd and Friedman (1972) for δD , and $\delta^{18}O$ in the carbonate aquifer
- Winograd and Pearson (1976) for δD , $\delta^{13}C$, ^{14}C , and $\delta^{18}O$ in the carbonate aquifer

- Peterman, Stuckless et al. (1992) for $\delta^{87}\text{Sr}$ in the carbonate aquifer
- Benson and McKinley (1985) for δD , $\delta^{13}\text{C}$, ^{14}C , $\delta^{18}\text{O}$ in groundwater in the Yucca Mountain vicinity
- White and Chuma (1987) for δD , $\delta^{13}\text{C}$, ^{14}C , $\delta^{18}\text{O}$ in the volcanic and alluvial aquifer in Oasis Valley, Pahute Mesa, Fortymile Wash, and Northern Amargosa Desert
- Claassen (1985) for δD , $\delta^{13}\text{C}$, ^{14}C , $\delta^{18}\text{O}$ in Crater Flat and the Amargosa Desert
- Peterman and Stuckless (1993) and Paces, Forester et al. (1996) for $\delta^{87}\text{Sr}$ in the Yucca Mountain area, Oasis Valley, Crater Flat, and the Amargosa Desert
- Ludwig, Peterman et al. (1993) for $^{234}\text{U}/^{238}\text{U}$
- Rose et al. (1997) for δD , $\delta^{13}\text{C}$, ^{14}C , $\delta^{18}\text{O}$, $^{36}\text{Cl}/\text{Cl}$, $\delta^{87}\text{Sr}$, and $^{234}\text{U}/^{238}\text{U}$ for much of the groundwater basin

In addition, there is an excellent record of isotopic compositions as a function of time recorded in calcites deposited at Devils Hole. Data are available for $\delta^{18}\text{O}$ (Winograd, Coplen et al. 1992), $\delta^{13}\text{C}$ (Coplen et al. 1994), $\delta^{87}\text{Sr}$ (Marshall, Peterman et al. 1990, 1991, 1993) and $^{234}\text{U}/^{238}\text{U}$ (Ludwig, Simmons et al. 1992).

Early work on stable isotopes (Winograd and Friedman 1972) showed that water in the carbonate aquifer was lightest in the north (Pahranagant Valley), heavier to the south (Spring Mountains), and intermediate at discharge along the spring line (Figure 5.2-14). This observation led to a simple model which suggested that 35 percent of the discharge at the spring line originated as underflow from the Pahranagant Valley. Limited uranium isotope data (Osmond and Cowart 1982) tended to support this conclusion. However, carbon isotope data (Figure 5.2-15) show that discharging waters are heavier than either of the recharge sources, although this could be the result of reaction with the Paleozoic carbonate which have a value close to zero. The uranium data also argue against a simple mixing of two recharge areas. Figure 5.2-16 shows reciprocal of concentration of uranium versus isotopic composition. A simple mixing relationship will produce a straight line. No such relationship exists, and in fact, the two proposed end-members plot toward the same side of the diagram. A stronger argument against simple mixing of two recharge sources in the combined strontium and uranium data is shown in Figure 5.2-17. Although neither element is truly conservative in groundwater, the data suggest a minimum of three end-members.

The $\delta^{87}\text{Sr}$ values along much of the spring line are fairly uniform (Figure 5.2-18) and significantly more radiogenic than the host carbonate rock, which has a $\delta^{87}\text{Sr}$ near zero. The lack of equilibration between strontium in the carbonate and in the water may indicate that the heavy carbon in water discharging along the spring line is not due to reaction with the carbonate rocks. The southern three springs are anomalously radiogenic, suggesting recharge and flow through Precambrian rocks in the Northwestern Spring Mountains.

Values for $\delta^{18}\text{O}$ within the valley-fill aquifer generally become heavier from north to south (Figure 5.2-19). This can be interpreted as southern waters being older and recharged in a warmer climate, being recharged at a lower elevation, or being a mixture of waters from different sources with one component being recharge like that at Pahute Mesa and the other being moderately heavy. The first alternative is inconsistent with the paleoclimate date, but not impossible. The second is favored by Claassen (1985). The third alternative is currently untestable.

Values for $\delta^{13}\text{C}$ also become heavier from north to south (Figure 5.2-20). The isotopic composition of carbon in groundwater is controlled by input from the atmosphere, biological activity, and available inorganic carbon. Except for recharge directly through bedrock, the latter two sources dominate the isotopic composition of carbon, and values of about -12 percent would be reasonable for recharge at Pahute Mesa. As with oxygen and deuterium, the isotopic composition of carbon becomes heavier to the south. White and Chuma (1987) propose an open system reaction between soil gas and shallow groundwater to explain the heavy carbon in groundwater in Oasis Valley. Alternatively, Stuckless, Whelan et al. (1991) propose that upward leakage from the carbonate aquifer would introduce heavy carbon as well as increase the temperature of groundwater, and both features are observed in Oasis Valley. Furthermore, the isotopic composition of carbon beneath Yucca Mountain becomes heavier from north to south, and at this locality, the groundwater table is deep (up to 700 m, Robison 1984) and the hydraulic head in the carbonate aquifer is about 20 m greater than that in the basal Tertiary units (Craig and Robison 1984).

The isotopic composition of strontium becomes more radiogenic from north to south, but there are fine structures in the data that reflect the geologic framework. For example, well water in the Eastern Amargosa Desert is more radiogenic than that near the center of the drainage basin (Figure 5.2-18) and thus reflects input of more radiogenic strontium from the Precambrian core of the Funeral Mountains. The input can represent either water recharged into the mountains, or interaction of groundwater with detritus derived from the Precambrian. Wells VH-1 and VH-2 are separated by less than 2 km, but the western-most well has $\delta^{87}\text{Sr}$, nearly twice that of the nearby well. The altered carbonates in Bare Mountain with $\delta^{87}\text{Sr}$ values as high as 23, or detritus derived from them, provide a probable source for the radiogenic strontium (Peterman, Widmann et al. 1994). In contrast, the unaltered carbonates have $\delta^{87}\text{Sr}$ values of about 1 and could provide a source for the unradiogenic strontium noted in Oasis Valley, thereby agreeing with interpretations of upward leakage of water as proposed on the basis of temperatures and carbon isotopic data.

Uranium isotopic compositions, in contrast to other systems, do not show a discernable north-south pattern (Figure 5.2-21). Many values, particularly beneath Yucca Mountain, are anomalously large. There is a trend of decreasing $^{234}\text{U}/^{238}\text{U}$ from Franklin Lake to Stove Pipe Wells. This trend would be consistent with a flow, analyzed spring discharge from approximately 10 springs located along a 16-km-long fault-controlled spring line at Ash Meadows. The ^{14}C content of the spring discharge at the center of the spring line was 5 times greater than that in discharge water from other major springs along the lineament. This represents a ^{14}C range of 2.3 to 11.1 percent, which is an approximate unadjusted time span of 18,000 to 30,000 years. The difference in ^{14}C stood in contrast to the similarity of alkalinity, pH, ^{13}C , O^{18} , deuterium, tritium, and other major and trace ions of all the spring waters sampled. Winograd and Pearson (1976, pp. 1131, 1132) offered ten possible explanations of the ^{14}C anomaly. The four most plausible hypothesis required the presence of a major longitudinal heterogeneity in the distal portion of the groundwater basin to explain the

anomaly. Flow channeling with an amplitude of at least 11 km was indicated. The simplifying assumption commonly used in simulation ^{238}U (Ludwig, Simmons et al. 1992) and $\delta^{87}\text{Sr}$ (Marshall, Peterman et al. 1990) have varied only small amounts over the last 500,000 years.

5.2.4.3 Age of Regional Groundwater

Groundwater cannot be dated directly except in the case where the water is young enough to contain tritium. The only dating method in common use within the Death Valley groundwater basin is that of ^{14}C , which provides a date for the water assuming the bicarbonate ion travels at the same velocity as water (NUREG/CR-4912, NRC 1987). Unfortunately, the initial activity of ^{14}C must be known, and if the system is not closed because of either gain or exchange of carbon, corrections to the apparent age must be made.

Benson and McKinley (1985) present ^{14}C data for wells at and near Yucca Mountain. The range of apparent ages is approximately 3,900 to 18,500 years for water in the valley-fill aquifer. Groundwater from well UE-25 p#1, which is drilled into the underlying carbonate aquifer, had an age of about 30,300 years, but this sample almost certainly contained "dead carbon" dissolved from the Paleozoic rock. Claassen (1985) reported data for groundwater in the valley-fill aquifer of the East-Central Amargosa Desert, and determined apparent ages ranging from 7,000 to 20,000 years.

White and Chuma (1987) reported apparent ages for water from the valley-fill aquifer in Oasis Valley ranging from 8,700 to 22,100 years. They applied a correction to the apparent ages by using a chemical-correction method based on closed system CO_2 consumption silicate hydrolysis, calcite dissolution, and secondary mineral precipitation. Their corrected ages for groundwater in Oasis Valley range from approximately 3,900 to 17,000 years. They also corrected ages for four wells in Fortymile Wash that had been reported by Benson and McKinley (1985) as 3,900 to 10,200 years. Ages by their correction range from 2,000 to 8,100 years.

Winograd and Pearson (1976) report ^{14}C data for water from the carbonate aquifer. Apparent ages range from about 1,500 to 35,000 years. The youngest ages occur in Cold Creek Spring which is in the Spring Mountains and closest to the source of recharge. Apparent ages rapidly become older such that, by Indian Springs, one sample yielded an age of 3,030 years and two others yielded ages of 20,086 years. Much farther along the flow system, a sample from Army Well 1 yielded an apparent age of 29,550 years. With the exception of Crystal Pool Spring, apparent ages along the spring line ranged from 26,800 to 37,300 years, but were generally about 30,000 years. Two samples from Crystal Pool Spring were much younger with apparent ages of 17,800 and 28,500 years. All of the samples were chemically indistinguishable. The authors concluded that the young ages represented channelized flow. Thomas, J.M. et al. (1996) averaged the data for 11 samples from the Ash Meadow springs and applied four different model corrections to the ^{14}C data. The resulting ages ranged from modern to 10,100 years with a preferred model age of 2,300 years.

Thomas, J.M. et al. (1996) tried dating groundwater by separating the dissolved organic carbon. The results for Crystal Pool Spring and Big Spring (two of the springs in the spring line at Ash Meadows) yielded ages of 2,500 and 4,600 years, respectively. This new method strives to overcome the problem of "dead carbon" acquired from the aquifer, but even snails living in a discharge spring that contains abundant "dead carbon" yield apparent ages for their shells as old as 27,000 years

(Riggs 1984). The younger ^{14}C ages for the dissolved organic carbon report by Thomas, J.M. et al. (1996) are consistent with the well-defined $\delta^{18}\text{O}$ record in travertine at Devils Hole which closely matches the marine record of climate change. This agreement is inconsistent with groundwater travel times of tens of thousands of years and also with multiple flowpaths with drastically different travel times which would blur the isotopic record.

5.2.5 Groundwater Flowpaths

The Death Valley region is divided into three subregions: Northern, Central, and Southern Death Valley. These subregions are further divided into groundwater basins and sections using generalized topographic controls. Groundwater flowpaths are discussed using these subdivisions within the subregions. Groundwater movement throughout the Death Valley region is generally controlled by structural and topographic controls.

Historically, water budgets have been completed for local areas within the Death Valley region; however, because inflow and outflow volumes are not well defined for all of the Death Valley region, the water budget for the groundwater flow system is difficult to compute. Subsequently, for the Death Valley region, only generalized regional flux in and flux out quantities are estimated.

5.2.5.1 Source and Movement of Groundwater

The Death Valley regional flow system consists of groundwater moving through a 3-D body of consolidated and unconsolidated materials. D'Agnese et al. (1997, p. 62) divided the Death Valley regional groundwater flow system into three major subregional flow systems (Northern, Central, and Southern Death Valley subregions) (Figure 5.2-6, and Figures 5.2-22, -23, and -24). The description of the source and movement of groundwater in the Death Valley regional groundwater flow system is most easily undertaken according to these three flow systems. For convenience, the subregions were subdivided by D'Agnese et al. (1997, p. 62) into basins and sections (Table 5.2-12) (Figure 5.2-25). Although the groundwater basins and sections were located using some generalized topographic controls, they are used for descriptive purposes only and do not define discrete independent flow systems.

5.2.5.1.1 Northern Death Valley Subregion

Groundwater in the Northern Death Valley subregion is derived from precipitation on high altitudes of the Montezuma Range and the Palmetto, Gold, and Stonewall Mountains (Figure 5.2-22). An unknown volume of groundwater may also be entering the subregion across the subregion boundary from Ralston Valley (D'Agnese et al. 1997, p. 65).

Groundwater recharged on the mountains in the northwest part of this subregion moves toward the central axis of adjacent valleys. In this subregion, the potentiometric surface indicates that much of the groundwater flow appears to be controlled by the northeast/southwest trending structural zones described by Carr, W.J. (1984, p. 30). Deep regional interbasinal flow is unlikely because the subregion is mostly underlain by relatively impermeable shallow Tertiary intrusive granites and crystalline Precambrian rocks. The regional aquifer is believed to be extensive and continuous only in the southeastern part of the subregion (D'Agnese et al. 1997, p. 65), near Eastern Pahute Mesa and

Southern Sarcobatus Flats. Four dominant groundwater sections, associated with four discharge areas, contain the majority of flow in the basin: Lida-Stonewall, Sarcobatus Flats, Grapevine Canyon, and Oriental Wash (Figure 5.2-22).

The Lida-Stonewall section contains discharge areas at east and East Stonewall Flat, and the playa near Lida Junction. Groundwater evapotranspired in these areas is believed to be derived mostly from within the Northern Death Valley subregion; however, some water may travel at great depths along buried northeast/southwest trending linear features near Ralston Valley, north of the subregion boundary, to these discharge areas (Figure 5.2-22).

The Sarcobatus Flats section contains discharge areas at Sarcobatus Flats and Coyote Holes playas. These areas are believed to evapotranspire groundwater that has moved along north/south subregional flowpaths. At Coyote Holes playas, restriction of groundwater flow by bedrock at shallow depths immediately south of the playas results in evapotranspiration of groundwater that may originate on Eastern Pahute Mesa. As with the Lida-Stonewall section, a northeast/southwest trending linear feature may affect regional groundwater flow patterns. For example, groundwater originating from Cactus and Gold Flats northeast of the subregion boundary may be forced to the surface and discharged at Bonnie Claire and Sarcobatus Flats.

The Grapevine Canyon section contains a major discharge area at Grapevine and Straininger Springs. Discharge at these sites appears to originate as groundwater that flowed from the northeast to the southwest past Stonewall and Sarcobatus Flats. The springs also may result from structural and topographic controls. The intersection of the low-permeability, northwest/southeast trending Death Valley fault, with an apparently large-permeability northeast/southwest trending structural zone (D'Agnese et al. 1997, p. 65), may result in the truncation of the large-permeability zone causing groundwater to discharge.

The Oriental Wash section includes a small discharge area at Sand Springs in Northern Death Valley. These comparatively low-temperature and small-volume springs appear to be discharging locally-derived groundwater recharged on the dominantly granitic mountains to the north. Groundwater flow apparently is directed toward the springs along the axis of Oriental Wash, which is associated with a northeast/southwest trending structural zone (D'Agnese et al. 1997, p. 65) and the discharges occur along the northern terminus of the Death Valley fault.

5.2.5.1.2 Central Death Valley Subregion

In the Central Valley subregion, the dominant flowpaths have historically been associated with major regional or subregional discharge areas (Figure 5.2-23). In this subregion, flowpaths have traditionally been grouped into three groundwater basins, each containing several sections: Pahute Mesa-Oasis Valley, Ash Meadows, and Alkali Flat-Furnace Creek (D'Agnese et al. 1997, p. 65).

Pahute Mesa-Oasis Valley Groundwater Basin—Groundwater in the Pahute Mesa-Oasis Valley basin is derived from infiltration in the Kawich and Belted Ranges and Pahute Mesa. Additional recharge may occur as regional groundwater flows across system boundaries from Railroad Valley and Stone Cabin Valley north of the subregion boundary (Figure 5.2-23). Because the western boundary of this basin is poorly defined, groundwater in the western part of the basin (parts of

Cactus and Gold Flats), may flow toward the eastern part of Sarcobatus Flats. This groundwater basin has two dominant sections: Kawich Valley and Oasis Valley (D'Agnese et al. 1997, p. 65).

In general, groundwater recharged on the nearby mountains moves toward the central axis of Kawich and Oasis Valleys. Groundwater in the Kawich Valley section may flow toward a potentiometric surface trough located under Eastern Pahute Mesa (Figure 5.2-8, area 17) (D'Agnese et al. 1997, p. 68). A possible regional fault or fracture zone has been described at this location. Water flowing along this trough toward Oasis Valley comprises the Oasis Valley section of this basin. At Oasis Valley groundwater is discharged by evapotranspiration and spring flow. Groundwater that does not discharge within Oasis Valley flows through the subsurface at the Amargosa Narrows south of Beatty and into the Alkali Flat-Furnace Creek groundwater basin (D'Agnese et al. 1997, p. 68). Small amounts of groundwater in Oasis Valley also may flow toward Crater Flat under Bare Mountain.

Ash Meadows Groundwater Basin—The Ash Meadows groundwater basin is the largest basin in the Central Death Valley subregion. Much of the groundwater in the basin is derived from infiltration on the mountain ranges that surround the basin. Additional recharge may occur as regional groundwater flows across subregion boundaries from Sand Spring Valley north of the subregion and Pahranaagat Valley northeast of the subregion (D'Agnese et al. 1997, p. 68). This basin is subdivided into six sections: Pahranaagat Valley, Tikaboo Valley, Indian Springs Valley, Emigrant Valley, Yucca-Frenchman Flat, and Spector Range (Figure 5.2-23) (D'Agnese et al. 1997, p. 68).

Groundwater recharged on the surrounding mountains moves toward the anomalously large potentiometric surface trough within the basin (Figure 5.2-8, area 16). Groundwater in Tikaboo Valley, Emigrant Valley, and Yucca and Frenchman Flat is interpreted as flowing toward the trough.

Regional and subregional groundwater recharged on the Sheep and Spring Mountains also flows into this trough from the east and south, thereby contributing to groundwater flow past Indian Springs Valley.

The potentiometric surface trough (Figure 5.2-8, area 16) may be a zone of high permeability associated with the Spotted Range-Mine Mountain structural zone and is believed to include numerous regional faults and fractures (D'Agnese et al. 1997, p. 68). The trough is bounded on the south and southeast by the Las Vegas Valley shear zone. The shear zone may contain low-permeability material, possibly fault gouge, causing discharge at Indian and Cactus Springs. The flowpaths along the trough are directed through the Spector Range area until they encounter a northwest/southeast trending fault at Ash Meadows. This fault causes much of the groundwater to be discharged as spring flows and evapotranspiration (D'Agnese et al. 1997, p. 68). Groundwater that does not discharge at Ash Meadows flows into the Alkali Flat-Furnace Creek groundwater basin where it mixes with groundwater moving along regional and subregional flowpaths.

Alkali Flat-Furnace Creek Groundwater Basin—In this basin, groundwater is derived from infiltration on Pahute Mesa, Timber Mountain, Shoshone Mountain, and the Grapevine and Funeral Mountains. Additional recharge to this basin occurs as interbasinal groundwater flows across boundaries from Oasis Valley and Ash Meadows. The Alkali Flat-Furnace Creek groundwater basin

is divided into four sections: Fortymile Canyon, Amargosa River, Crater Flat, and Funeral Mountains (Figure 5.2-23) (D'Agnese et al. 1997, p. 68).

Locally recharged groundwater moves toward discharge areas in the southern parts of the basin. Dominant groundwater flowpaths appear to mimic surface-water flow. The surface-water flow seems to be structurally controlled along the Amargosa River and Fortymile Wash and in Crater Flat. In the northwestern portions of the basin, subregional groundwater movement is dominantly lateral and downward toward regional flowpaths. Near Yucca Mountain, however, gradients are dominantly upward into the volcanic units (D'Agnese et al. 1997, p. 68). In the south-central portions of the basin, near the Nevada-California border, regional groundwater movement is dominantly upward from carbonate units into the subregional system and toward discharge areas along the Amargosa River, Carson Slough, and Alkali Flat.

In the Southern Amargosa Valley, regional groundwater movements are toward the southwest and south. This groundwater may either flow through fractures in the southeastern end of the Funeral Mountains and discharge at Furnace Creek, or flow southward and discharge at Alkali Flat (D'Agnese et al. 1997, pp. 68-69). Once past the springs at Furnace Creek, the groundwater flows toward Death Valley and is discharged either by stands of mesquite on the lower part of the Furnace Creek fan or by evaporation from the Death Valley.

Groundwater that moves along shallow flowpaths, but does not discharge at the Amargosa River, Carson Slough, or Ash Meadows, moves southward toward Alkali Flat where it discharges as spring flow and evapotranspiration.

5.2.5.1.3 Southern Death Valley Subregion

In general, groundwater in the Southern Death Valley subregion is derived primarily from infiltration on the Spring Mountains and small inputs from the Kingston and Greenwater Ranges (Figure 5.2-24). Additional minor groundwater volumes may flow into this subregion across the boundary from Alkali Flat-Furnace Creek basin south of Alkali Flat (Figure 5.2-23), and across the subregion boundary from areas south of Salt Spring Hills, Valjean and Shadow Valleys. The subregion contains four sections: Pahrump Valley, Shoshone-Tecopa, California Valley, and Ibex Hills (Figure 5.2-24) (D'Agnese et al. 1997, p. 69).

Groundwater recharged on the Spring Mountains moves toward Pahrump Valley. Historically, springs discharged at Manse and Bennett Springs along the base of the broad alluvial fans at the foot of the Spring Mountains. Pumping of groundwater in the valley has caused these springs to cease to flow. Groundwater in the Pahrump Valley section flows along subregional flowpaths either to the west toward Stewart Valley and the northern end of Chicago Valley, or to the southwest toward California Valley. Because the Nopah Range is composed of low-permeability quartzite rocks in the subsurface, it is believed to cause a bifurcation in groundwater flow. Some of the groundwater flowing toward the north and west is discharged at Stewart and Pahrump Valley playas. Some of this groundwater may also discharge at the southern end of Ash Meadows at Big, Bole, and Last Chance springs (Winogard and Thordarson 1975, p. 91; Peterman, Stuckless et al. 1992, pp. 70 and 712, page numbers cited by D'Agnese et al. 1997, p. 69). Groundwater flow that continues toward Chicago Valley, within the Shoshone-Tecopa section, mixes with groundwater flowing from south

of Alkali Flat, and ultimately discharges as spring flows and evapotranspiration in an area between the towns of Shoshone and Tecopa. In the California Valley section, groundwater that flows south from Pahrump Valley discharges south of Tecopa at springs along the Amargosa River canyon in the Sperry Hills and at China Ranch.

Groundwater that does not discharge at the Shoshone-Tecopa section may continue flowing to the southwest into the Ibex Hills section and discharged as spring flow and evapotranspiration in the Saratoga Springs area, which includes adjacent areas of shallow groundwater along the floodplain of the Amargosa River. Some additional groundwater may enter the basin from Valjean and Shadow Valleys into California Valley and discharge at Saratoga Springs. Small volumes of groundwater may continue north past Saratoga Springs to discharge at the Badwater Basin.

5.2.5.2 Regional Flow System Water Budget

Historically, water budgets have been completed for local areas (Malmberg and Eakin 1962; Walker and Eakin 1963; Miller 1977; Malmberg 1967; Winograd and Thordarson 1975; and Harrill 1986). These budgets were based on estimates of recharge and discharge using the:

- Maxey-Eakin method
- Evapotranspiration and spring discharge
- Estimated interbasin underflow, which was calculated from the difference between rainfall recharge and evapotranspiration

D'Agnese et al. (1997, p. 69) stated that because inflow and outflow volumes are not well defined for most areas modeled in the Death Valley region, the water budget for the groundwater flow system is difficult to compute in detail. D'Agnese et al. felt that the large size of the regional system precludes the comprehensive and accurate assessment of all inflows to and outflows from the system. Subsequently, specific groundwater fluxes within the Death Valley region were not determined in the modeling report; only generalized region wide flux in and flux out quantities were estimated for the Death Valley region.

A lumped value water budget of the Death Valley regional groundwater flow system was produced by D'Agnese et al. (1997, p. 69) for the 3-D groundwater flow model. Each component of the water budget (Flux In, rainfall recharge and groundwater inflow; Flux Out, evapotranspiration, spring discharge, groundwater outflow and groundwater pumpage) were generally defined as a lumped value, instead of discrete regional, subregional, or groundwater basin values (Table 5.2-13).

D'Agnese et al. (1997, p. 71) stated that Hollett et al. (1991) noted that using a lumped-budget approach to estimate groundwater flux permits an overview of any groundwater flow system; however, potential interpretation errors may result from slight differences in total inflow or outflow. These slight differences in the regional budget may represent large errors within small areas of a groundwater basin. Because the model computes separate groundwater budgets for small areas of the system, these potential errors frequently become obvious when using a groundwater flow model to analyze a groundwater flow system (D'Agnese et al. 1997, p. 71).

Although individual recharge and discharge component values, including human-induced changes, were determined, errors are inevitable in such estimates. The estimates of inflows to the system that result from interbasinal flows across boundaries are especially problematic. The imbalance between defined inflows and outflows is assigned to net interbasinal flux. The major limitation of this approach is the assumption of steady-state conditions. This assumption requires that the significant historical groundwater withdrawals in the Death Valley region must be offset by reductions in natural discharge or by increased induced inflow from outside the basin (D'Agnese et al. 1997, p. 71).

The lumped water budget from the Death Valley region 3-D groundwater model estimated an outflow of 374,000 m³/day, which exceeded the estimated inflow of 344,200 m³/day by approximately 29,800 m³/day. This water budget balances within 10 percent of the estimated flux volumes, and appears reasonable given the many uncertainties surrounding the estimates of most components. The difference may be due to uncertainties surrounding the estimation or assignment of volumes for groundwater pumpage and evapotranspiration from Death Valley (D'Agnese et al. 1997, p. 71).

Considerable uncertainty surrounds the significance of the 89,000 m³/day volume of water estimated to be withdrawn by pumpage. If non-equilibrium conditions exist and pumping causes groundwater to be withdrawn from storage, then the estimated withdrawal should be counted as a change in storage rather than a component of outflow. Changes in groundwater storage within the basin, however, can only be determined after further evaluation of the Death Valley region boundary conditions and aquifer properties (D'Agnese et al. 1997, p. 71).

5.2.5.3 Summary of Groundwater Flowpaths

For the numerical simulation of the Death Valley region flow model developed by D'Agnese et al. (1997, p. 62), the Death Valley region groundwater flow system was subdivided into three subregions (northern, central, and southern) that represent the principal areas where regional groundwater flow moves from recharge areas toward Death Valley, the ultimate terminus of the flow system.

For convenience, the subregions were subdivided into basins and sections. Although the groundwater basins and sections were located using some generalized topographic controls, they were defined primarily for descriptive purposes, and do not define discrete independent flow systems.

The discussion of regional flowpaths was adapted exclusively from D'Agnese et al. (1997).

Although only D'Agnese et al. was cited for this section, the source of information used to define the flowpaths by D'Agnese et al. was geologic information (Carr, W.J. 1984; Grose 1983; and Faunt et al. 1997), flow lines based on the potentiometric surface map (Figure 5.2-3), and hydrochemistry data (Winograd and Thordarson 1975). Other sources cited by D'Agnese include Waddell (1982), Waddell et al. (1984), Blankennagel and Weir (1973), Czarnecki and Waddell (1984), Sinton (1987), Kilroy (1991), Luckey, Tucci et al. (1996), Czarnecki (1990), Czarnecki and Wilson (1991), and Walker and Eakin (1963).

Because the inflow and outflow volumes are not well defined for most areas in the Death Valley region, a detailed water budget for the groundwater flow system cannot be completed. Subsequently, the water budget developed for the Death Valley region was a lumped value water budget for the whole region. Discrete water budgets for individual basins within the Death Valley region need to be completed using the groundwater flow models currently being developed for the Death Valley region.

5.2.6 Regional Paleohydrology

5.2.6.1 Paleo Groundwater Levels

There is abundant geologic evidence of previous high levels of the water table in the South-Central Great Basin (Figure 5.2-26) during the Quaternary period. The evidence consists of tufas, spring orifices, calcitic veins, and cylindrical calcite-lined tubes that mark the routes of former groundwater flow to springs; former water levels marked by calcite cave deposits on the walls of Brown's Room within Devils Hole (a fault-controlled solution feature in Ash Meadows); and widespread marsh deposits (composed of silty marls, diatomaceous earth and authigenic clays) formed from former groundwater discharge. Most of these features have been described in reports by Winograd and Thordarson (1975), Dudley and Larson (1976), Mifflin and Wheat (1979), Winograd and Doty (1980), Khoury et al. (1982), Pexton (1984), Winograd, Szabo et al. (1985), Hay et al. (1986), and Swadley and Carr (1987). The paleohydrologic significance of these deposits is the subject of papers by Winograd and Doty (1980), Pexton (1984), Winograd and Szabo (1988), Quade and Pratt (1989), Marshall, Peterman et al. (1991), Paces, Taylor et al. (1993), Forester and Smith (1994), Quade, Mifflin et al. (1995), and Paces, Forester et al. (1996).

The oldest dated groundwater deposits, which range from 2 to 4 Ma (Hay et al. 1986), are located in the Eastern Amargosa Desert. These have been interpreted as widespread marsh and lacustrine deposits which resulted from discharge from the Paleozoic aquifer. The deposits are described by Walker and Eakin (1963), Denny and Drewes (1965), Khoury et al. (1982), Swadley (1983), and Pexton (1984). Hay et al. (1986) present evidence based on stratigraphy, mineral composition, fossil assemblages, and lithofacies relationships that these sediments were deposited in marshes or small ponds, flood plains, and playas fed by groundwater rather than developing in a lake environment. These deposits occur at altitudes as high as 790 m (Winograd and Doty 1980) in Amargosa Flat in the east-central portion of the Amargosa Desert. Given the very small gradient for the Paleozoic aquifer in this region, the deposits are about 70 m above the highest modern water level in Devils Hole (altitude 719 m).

Winograd and Doty (1980) mapped tufa and vein calcite in the Ash Meadows area of the Amargosa Desert, south of Highway 95 and east of Highway 29. They concluded that the potentiometric surface in the lower carbonate aquifer was once apparently as much as 50 m higher than the highest modern water levels in the Ash Meadows discharge as recorded at Devils Hole (altitude 719 m). Uranium disequilibrium dating of a few of these calcite veins provides the records of higher water levels during middle Pleistocene time, 750 to 500 ka (Winograd, Szabo et al. 1985; Winograd and Szabo 1988). Szabo and Winograd (1995) report that deposits in Brown's Room at Devils Hole record water levels of 5 to 9 m above current levels for the time period of 20 to 120 ka.

There are well-exposed spring deposits along Furnace Creek at Travertine Point (Winograd, Szabo et al. 1985; Winograd and Szabo 1988). The relationship of these deposits to the Paleozoic (or Cenozoic) aquifer is equivocal, but the veins are dated at 750 ka to more than 2.4 Ma. Here, feeder veins and travertine out-flow deposits are tens to hundreds of meters above the modern potentiometric surface; however, much of this elevation difference may be due to tectonic uplift of Funeral Mountain block which contains the spring deposits (Hunt and Mabey 1966). Szabo and Winograd (1995) calculate an uplift rate of 0.26 m/ka, assuming that the elevation above the water table is due to uplift of the veins. This rate agrees well with the 0.3 m/ka reported by Carr, W.J. (1984) for uplift of the Artist's Drive Formation in the Black Mountains immediately south of Furnace Creek. Similar rates of uplift have been reported for the Panamint Range (0.3 m/ka) during the last 40 ka (Smith, R.S.U. 1975) and for the Sierra Nevada Mountains (0.35 m/ka) during the Quaternary period (Huber 1981).

The fact that the Pliocene discharge deposits of the carbonate aquifer have not been buried by subsequent discharge events suggests there may have been a general lowering of the potentiometric surface in this flow system as a function of time. Winograd and Szabo (1988) infer that, regionally, the water table in the lower carbonate aquifer is likely to have lowered during the Quaternary period. The following evidence is cited in support of their hypothesis:

- The several-thousand-meter topographic relief in Death Valley dates largely from Pliocene and Pleistocene time (Hunt and Mabey 1966; USGS 1984), and the movement of the floor of Death Valley probably has been downward relative to sea level and to bordering areas (Hunt and Mabey 1966).
- Interbasin flow of groundwater through Paleozoic carbonate rock and Tertiary welded-tuff aquifers toward Ash Meadows and Death Valley occurs today (Winograd and Thordarson 1975). Interbasin flow of groundwater toward Death Valley likely also occurred during the Quaternary period in response to the lowering of groundwater discharge outlets; as a result, Death Valley gradually evolved during the Quaternary period into a regional sump for groundwater.
- An increase in aridity due to uplift of the Sierra Nevada and Transverse Ranges would have resulted in a reduction of groundwater recharge east of the uplifts. The uplift and its subsequent rain-shadow effect have been cited as the reason for deuterium depletion in groundwaters of the Southern Great Basin during the last 2 million years (Winograd, Szabo et al. 1985).

Another climate-associated feature that can be related to a decline of the regional water table may have been the level of Lake Manly, a Pleistocene lake that filled Death Valley to about 120 m above sea level (Hunt and Mabey 1966). With the drying of the lake, groundwater base level in Death Valley would have declined. The exact age of Lake Manly and its duration are not well known. Hunt and Mabey (1966) considered the lake to be no older than Wisconsin time. Hale (1985) suggests that it is much older, perhaps of early- to mid-Pleistocene age. That the lake is either very old, had a short duration, or both, is suggested by the paucity of geomorphic and sedimentologic evidence for its existence (Hunt and Mabey 1966).

Winograd and Szabo (1988) also suggest that the regional water table decline postulated for the lower carbonate aquifer during the Quaternary period was accompanied by a water-level decline in the overlying Cenozoic welded-tuff and valley-fill aquifers. Thus far, no geologic evidence has been found to prove this hypothesis, and as discussed below, the fairly young discharge deposits in Crater Flat and the Amargosa Desert seem to argue against a long-term water table decline. The authors also note that, "The suggested progressive lowering of the regional water table throughout the Quaternary does not preclude superimposed and relatively rapid cyclical fluctuations in water level in response to the glacial (i.e., pluvial) and interglacial climates of the Pleistocene." As noted below, the prediction of subsequent higher elevations for groundwater has been verified.

Evidence for increased aridity in the South-Central Great Basin is discussed here because it may relate to the above-cited inference of water table lowering throughout the Quaternary period. Also, if the increased aridity has resulted from the rise of the Sierra Nevada Mountains, future climates would not be expected to be wetter than those that have existed since the rise of the Mountains. Huber (1981) demonstrated that the Central Sierra Nevada has been rising since early Miocene time (23.7 million years ago) and that the rate of uplift has been increasing from approximately 0.03 m/1,000 year during early Miocene to 0.35 m/1,000 year at present. In the past 3 million years the Sierra Nevada has risen about 1,000 m.

Because the major source of cool season (November to May) precipitation for the Great Basin is the Pacific Ocean, this major uplift is likely to have significantly reduced precipitation in the region. Under today's climate conditions, warm-season precipitation, which is derived largely from the Gulf of California and the Gulf of Mexico, is not considered important because this moisture is unlikely to contribute much to groundwater recharge (Winograd and Riggs 1984). Smith, G.I. et al. (1983) suggest that when the Sierra Nevada was about 1,000 m lower (3 million years ago), about 50 percent more moisture might have moved into the Great Basin. Based on paleobotanical records, Raven and Axelrod (1978) and Axelrod (1979) believe that aridity increased in the Great Basin, Mojave Desert, and Sonoran Desert during the late Tertiary and the Quaternary periods. They attributed this to uplift of the Sierra Nevada, Transverse Ranges, Peninsular Ranges, and the Mexican Plateau. On the basis of sediment depositional environments, Pexton (1984) believes that the Ash Meadows-Amargosa Desert area became more arid during the Quaternary period. Winograd, Szabo et al. (1985) describe what appears to be a progressive depletion in the deuterium content of groundwater during the Quaternary period, and the most likely explanation for this is a decrease in Pacific moisture due to uplift of the Sierra Nevada and Transverse Ranges.

Lowering of the water table within the Paleozoic aquifer might have occurred during the Quaternary period, even in the absence of down-dropping of Death Valley or increased aridity. Winograd and Szabo (1988) cite Winograd and Doty (1980), noting that "the major springs at the Ash Meadows oasis (Figure 5.2-26) differ in altitude by as much as 35 m and are as much as 50 m lower than the water level in Devil's Hole. Thus, periodic initiation of discharge from new spring orifices (or an increase in existing discharge) in the lower portions of this oasis due to faulting and extensional fracturing would have resulted in new and lower base levels for groundwater discharge." Implicit in this hypothesis is the belief that the faulting would be extensional opening new (or widening old) avenues of discharge from the buried Paleozoic carbonate rock aquifer that underlies Eastern Ash Meadows and that feeds all the modern springs (Winograd and Thordarson 1975). In support of this hypothesis, Winograd and Szabo (1988) note that most of the calcitic veins in Pliocene and younger

rocks at Ash Meadows strike N. $40^\circ \pm 10^\circ$ E. This is nearly at right angles to Carr's, W.J. (1974) estimate of the direction of active extension in the region, namely N. 50° W. to S. 50° E. This mechanism may also have periodically lowered the water table in East-Central Death Valley where the difference in altitude between the highest (Nevarés) and lowest (Texas) major springs discharging from the regional carbonate aquifer is about 170 m (Winograd and Thordarson 1975).

In summary, available data from calcitic veins and marsh deposits indicate a 50 to 70 m apparent lowering of the water table in the East-Central Amargosa Desert since the middle Pleistocene and, in the Furnace Creek area, an apparent lowering of perhaps as much as 130 m since the end of the Pliocene. A strong inference can be made that the water-table altitude in the Paleozoic aquifer actually declined regionally throughout Plio-Pleistocene time due to increasing aridity coupled with an absolute lowering of groundwater base level in Death Valley. This postulated general lowering does not preclude superimposed water table fluctuations in response to climate changes.

There are also several discharge deposits from the valley-fill aquifer. A sample from the south end of Crater Flat (Figure 5.2-26) described as nodular tufa spring deposits was dated by the uranium-series method as approximately 30,000 year B.P. (Szabo et al. 1981). The authors questioned the age because the sample was suspected of representing an open system. Paces, Taylor et al. (1993) reported uranium-series ages (obtained by mass spectrometry) for similar material, of 18 ± 1 , 30 ± 3 , and >70 ka. The site is thought to be 100 to 120 m above the current potentiometric surface (Paces, Forester et al. 1996). The data suggest strong fluctuations in the elevation of the water table during Wisconsin time. More recently, rhizoliths from the deposit have yielded U-series ages of 10 ± 1.3 and 12.9 ± 0.6 ka (Paces, Forester et al. 1996). Four ^{14}C ages for rhizoliths, ranging from 6.02 ± 0.7 to 16.05 ± 0.32 ka, confirm the young (and possibly Holocene) age for groundwater discharge in Crater Flat. The initial $^{234}\text{U}/^{238}\text{U}$ values calculated from the U-series ages and the initial $^{87}\text{Sr}/^{86}\text{Sr}$ values (Marshall, Peterman et al. 1991) agree with the values obtained for samples from the valley-fill aquifer in Crater Flat (Ludwig, Peterman et al. 1993; Peterman and Stuckless 1993), thereby confirming the origin of the deposit as groundwater discharge from the regional aquifer.

There is another groundwater discharge site about 5 km southwest of the Crater Flat locality (Figure 5.2-26). The site, known variously as the horse-tooth locality and the Lathrop Wells diatomite deposit, is thought to be 98 to 116 m above the current potentiometric surface (Paces, Taylor et al. 1993). Here, too, the strontium isotopic composition of carbonate (Marshall, Peterman et al. 1991) agrees with that of the regional valley-fill aquifer (Peterman and Stuckless 1993). Previous workers thought that this deposit was lacustrine and represented the Pliocene or early Pleistocene Lake Amargosa (Swadley and Carr 1987). They note that the Horse Tooth deposit contains vertebrate remains including *Mammuthus sp.*, *Equus sp.* and a camelid; as well as noting abundant different diatoms and that some of the beds are highly tuffaceous. The vertebrate fossils indicated an age of less than 2 Ma. Hoover (1989) classified these deposits as the "waterlaid sediments of Amargosa marsh" and the boundaries of the Amargosa marsh correspond roughly to the boundaries of Swadley and Carr's (1987) Lake Amargosa. He described these as diatomaceous marl overlain by tufa and, based on the vertebrate fossil evidence, concluded that they represented "deposition of the waterlaid sediments of the Amargosa marsh [that] probably ended in early Pleistocene times" (Hoover 1989).

The stratigraphic top of the Lathrop Wells deposit includes a capping marl. A single rhizolith was dated by ^{14}C with a resulting age of 6.51 ± 0.16 ka (Paces, Forester et al. 1996). Five terrestrial snails, one aquatic snail, and one aquatic bivalve from a capping marl unit yielded ^{14}C ages of 16.2 to 16.9 ka. Fifteen samples of rhizoliths and nodular calcite yielded U-series ages with essentially the same range of ages (Paces, Forester et al. 1996). These yielded initial $^{234}\text{U}/^{238}\text{U}$ values of about 3.5 to 4.0, consistent with formation from water discharged from the regional aquifer.

A diatomite underlies the capping marl. Thermoluminescence ages within this unit are somewhat older (around 30 ka) and in agreement with the stratigraphic relationship. Two rhizoliths at the base of the unit yield still older ages of 42 and 56 ka, with initial $^{234}\text{U}/^{238}\text{U}$ values of about 3.8 and 4.7 (Paces, Forester et al. 1996).

The deepest unit is a green sand. U-series ages for this unit range from about 115 ka near the top of the unit to 186 ka near the bottom (Paces, Forester et al. 1996). Initial $^{234}\text{U}/^{238}\text{U}$ values were variable but elevated and consistent with formation from the regional aquifer. Aquatic bivalves and a terrestrial snail from a green sandy unit yielded ^{14}C ages of about 35 to 42 ka, but these appear to be contaminated with small amounts of secondary calcite overgrowth (Paces, Forester et al. 1996). Thermoluminescence ages also appear to be anomalously young, and Paces, Forester et al. (1996) postulate that this may be due to the presence of diatoms, which may behave differently from forms of crystalline silica with respect to thermoluminescence.

About 3 km to the east-southeast of the Lathrop Wells deposit is a small flat area of white beds (Figure 5.2-26) that have yielded uranium-series ages of 19.9 ± 0.6 and 15.2 ± 0.2 ka (Paces, Forester et al. 1996). Again, the initial $^{234}\text{U}/^{238}\text{U}$ values are elevated and consistent with an origin involving the regional valley-fill aquifer.

The largest and most extensive paleodischarge site for the valley-fill aquifer is located near Stateline, Nevada (Figure 5.2-26). This site is particularly significant in that it occurs where discharge is predicted by the regional groundwater flow model under conditions of nearly a 15-fold increase in recharge and a water table rise of about 100 m beneath Yucca Mountain (Czarnecki 1985). Eight uranium-series ages on five different samples from this locality range from 11.0 ± 2.3 to 107.4 ± 5.7 ka. Three ^{14}C ages for snails from this locality range for 9.01 ± 0.25 to 10.76 ± 0.24 ka, but the older age is for an aquatic snail. Such snails living in the discharge of the Paleozoic aquifer today have inherited large amounts of dead carbon and, therefore, yield anomalously old ages (Riggs 1984).

Large fluctuations in past groundwater levels occurred over a broader region of the Southern Great Basin than is represented by the Amargosa Desert. Quade and Pratt (1989) have described extensive deposits in the vicinity of Cactus Springs and Indian Springs (Figure 5.2-26), which represent past discharge of groundwater during late Wisconsin time. Humate material from the younger part of the section yield Holocene ages (9.68 ± 0.10 and 9.46 ± 0.70 ka). The deposits are now 60 to 70 m above the groundwater table (Quade, Mifflin et al. 1995). These authors also note that one or more spring discharge events of Wisconsin age, have been recorded by deposits in Chicago, Piute, and Pahrump Valleys; at Tule, Corn Creek, and Coyote Springs; and at Valley Wells.

5.2.6.2 Groundwater Flowpaths During the Quaternary Period

The distribution of calcitic veins, tufas, and marsh deposits suggest that flowpaths during Quaternary time were approximately the same as they are today. Marsh and other discharge deposits kilometers to tens of kilometers up-gradient from areas of modern groundwater discharge, indicate that flow to points of groundwater discharge were shorter in the past. Tectonic tilting of the land surface, tectonic lowering of the base level, and increasing aridity due to a rain-shadow effect of the Sierra Nevada Mountains have all been suggested to explain the apparent lengthening of the flowpath. The relative youthfulness of the deposits argues against major importance of such long-term, slow rate processes. Likewise, the fact that the model for the current flow system accurately predicts past discharge points under times of greater recharge argues against a major importance for land tilting or rain shadow effects. Discharge deposits closer to Yucca Mountain have been diligently looked for but have not been found. The flow model does not suggest that such close-in discharge should exist. Furthermore, there is abundant evidence, discussed below in Subsection 5.3.7, that the water table in the site area has never been more than about 100 m higher than it is today. All available lines of evidence indicate that the only changes in flowpath for the valley-fill aquifer during the Quaternary occurred in response to climate change, and that change was reflected only by a shortening of the distance to discharge by a few tens of kilometers (from Franklin Lake Playa to the Stateline deposits).

5.2.7 Regional-Scale Flow Modeling

The Death Valley regional groundwater flow system was conceptualized and analyzed using a 3-D, steady-state model that incorporates a nonlinear least squares regression technique to estimate aquifer variables (or parameters). Output from the regional model was used to provide input for site-scale flow-model boundary conditions. A summary of model geometry, boundary conditions, model calibration for present-climate conditions, and alternate-climate simulations are given in the following sections. A detailed description of the regional flow model for present-climate conditions is provided by D'Agnese et al. (1997), and by D'Agnese et al. (D'Agnese, F.A. et al., *Simulated Effects of Climate Change on the Death Valley Regional Ground-Water Flow System, Nevada and California*, Milestone Report SP23OM3, DTN GS970708312144.003 (TBV), Water Resources Investigations Report 98-4041, unpublished) for alternate-climate conditions.

5.2.7.1 Model Construction

Calibration of the saturated-zone flow models by strictly trial-and-error methods was judged to be both ineffective and inefficient; therefore, nonlinear regression methods were used to estimate parameter values that produce the best fit to observed heads and flows. Related methods were used to evaluate model results.

The numerical code used for the regional flow model was MODFLOWP (Hill, M.C. 1992). MODFLOWP is an adaptation of the USGS 3-D, finite-difference modular groundwater flow model (MODFLOW) (McDonald and Harbaugh 1988; Hill, M.C. 1992) in which nonlinear regression is used to estimate flow-model parameters that result in the best fit to measured hydraulic heads and flows. MODFLOWP is a block-centered finite-difference code that views a 3-D flow system as a sequence of layers of porous material organized in a horizontal grid or array. The grid is generated

by specifying array dimensions in the x, y, and z directions, based on a separate hydrogeologic framework model for the region. Flow between cells in each model layer is controlled by user-supplied transmissivity values. Flow between model layers is controlled by user-supplied values of a vertical transmission or leakage term, known as VCONT (McDonald and Harbaugh 1988, pp. 5-39).

The remainder of the model inputs describing boundary conditions, recharge, evapotranspiration, spring flow, and well discharge are specified using arrays or lists of row-column cell location. The model calculates the heads from inputs to, outputs from, and flow between nodes. With the preconditioned conjugate-gradient iterative solver used (Hill, M.C. 1992), the model recalculates the head distribution in each node of each layer until head changes between solver iterations and cell-by-cell budget errors drop below a user-specified value.

5.2.7.2 Model Geometry

The regional model consists of a finite-difference grid of 163 rows, 153 columns, and 3 layers. The grid cells are oriented north-south and are of uniform size, with side dimensions of 1,500 m (Figure 5.2-27). The layers represent conditions at 0 to 500 m, 500 to 1,250 m, and 1,250 to 2,750 m below the estimated water table. The first and second layers are designed to simulate local and subregional flowpaths mostly within valley-fill alluvium, volcanic rocks, and shallow carbonate rocks. The third (lowest) layer simulates deep regional flowpaths in the volcanic, carbonate, and clastic rocks. The required regional model parameter values were supplied by discretization of a 3-D hydrogeologic framework model (D'Agnese et al. 1997, pp. 33-43) and by digital representations of the remaining conceptual model components. The framework model is shown by means of a fence diagram in Figure 5.2-28.

5.2.7.3 Boundary Conditions

Similar model boundary locations occur in all three layers (Figure 5.2-27). All boundaries in the top layer were designated as no-flow except along the western side of the model in Death Valley where constant-head values were selected. No groundwater is believed to enter or exit the Death Valley system at intermediate depths, so all the boundaries in the middle layer were set to no-flow conditions. In layer three, the boundaries were set to no-flow conditions except at four locations along the northern and eastern limits of the model, where the conceptual model suggests interconnections with adjacent systems along buried zones of higher permeability. The upper boundary of the flow model is the water table, and the lower boundary is set at a depth of 2,750 m below the water table, where few fractures are believed to be open to allow significant amounts of groundwater flow. Flow conditions between layers were not explicitly defined, because MODFLOWP is capable of defining such interactions by internally computed vertical-conductance arrays to simulate this flow.

The hydrogeologic conditions represented in the 3-D framework model vary considerably within the volumes represented by each of the three layers in the numerical simulation model. MODFLOWP zone arrays were used to simplify this complexity. Initially, eight rock-conductivity units were defined to reflect dominant conditions within the layer, including hydrogeologic unit, depth, and presence or absence of significant faulting. Subsequently, to further reduce the number of

parameters subjected to estimation by the model, these eight rock-conductivity units were reclassified to form four K (hydraulic conductivity) zones. These K zones are not contiguous; each includes cells distributed throughout the model. Transmissivity values for the layers were calculated by multiplying the applicable K zone by layer thickness.

Model source and sink parameters defining recharge, evapotranspiration, spring-flow discharge, and groundwater pumpage were obtained from a digital geographic information systems database. Evapotranspiration estimates were developed from land-surface altitudes, extinction depth values, and maximum evapotranspiration rate maps created within the geographic information systems. A recharge-potential map was reclassified to produce a recharge array that contained four zones (zero, low, medium, and high) of recharge potential. For each zone a parameter could be assigned to represent the percentage of precipitation that infiltrates, and a second array was used to define the variation expected in the recharge rates. Spring discharge rates were obtained from historical records. Springs were specified using the general-head boundary package (McDonald and Harbaugh 1988); this required information defining the altitude of the spring orifice and conductance. Because the conductance values were poorly known, springs were grouped by geographic location and a single conductance value was assigned to each group. Pumping was simulated using the well package (McDonald and Harbaugh 1988), and all pumping wells were assigned to the first (uppermost) layer. Return flows were accounted for by specifying percentages of pumped water that is permanently removed from the system.

5.2.7.4 Model Calibration

Calibration of the regional model using the techniques available in MODFLOWP allowed for estimation of a series of parameters that provide a best fit to observed hydraulic heads (500 observations) and flows (63 observations). Numerous conceptual models were evaluated during calibration to test the validity of various interpretations about the flow system. Conceptual model evaluations focused on testing hypotheses concerning the location and type of flow system boundaries, the extent and location of recharge areas, and the configuration of hydrogeologic framework features. For each hypothesis tested, a new set of parameters was estimated using MODFLOWP and the resulting new simulated heads and flows were compared to observed values. Only those conceptual model changes contributing to a significant improvement in model fit, as indicated by a reduction in the sum of squared errors, were retained in the final optimized model.

The final model was evaluated to assess the likely accuracy of simulated results by comparing measured and expected quantities with simulated values. The quantities included in these comparisons are: hydraulic heads and spring flows, which were matched by regression; hydraulic conductivities, which were represented by parameters that were estimated in the regression; and water budgets. During calibration, five additional K zones were added to better simulate various regional structural features and low-permeability rocks, such as the Eleana Formation. Initial estimates of the percentage of precipitation represented by each of the four recharge zones were also modified as a result of calibration. Residuals for hydraulic heads show a good model match with observed conditions in flat hydraulic gradient areas (generally within 50 m), and a relatively good match in large hydraulic gradient areas (Figure 5.2-29). Residuals for spring flows show somewhat of a bias in that simulated spring flows are generally lower than observed (Figure 5.2-30). The difficulty in simulating these spring flows in previous models of this area, without imposing

discharge by using a specified flux, suggests that even the somewhat lower simulated discharges are an improved match over previous models with observed conditions. Estimated parameters were evaluated to determine if reasonable values were estimated for values of hydraulic conductivity, vertical anisotropy, and recharge rates. All estimated parameter values are within expected ranges. The calculated linear confidence intervals also were well within the range of expected values (Figure 5.2-31). Water budgets were evaluated to determine if they were within the range of expected values. Model results suggest that even with the limited understanding of fluxes in and out of the regional groundwater flow system, overall budgets are within the expected ranges for the flow system (Table 5.2-14).

Problems with the regional model are indicated by weighted residuals that are not entirely random, indicating some model error (D'Agnese et al. 1997, pp. 95-109). This is related to the occurrence of large positive-weighted residuals for hydraulic heads, where simulated hydraulic heads are distinctly lower than the observed values, and large negative-weighted residuals for spring flows, where simulated flows are distinctly less than observed flows. The problem is also related to nonnormally distributed, less extreme, weighted residuals. These results, combined with the observation that every model update considered thus far significantly improved model fit, suggests that an additional calibration effort may significantly improve model accuracy. This analysis suggests that the model is a reasonable representation of the physical system, but evidence of important model error exists.

5.2.7.5 Alternate-Climate Simulations

To assess the effects of climate change, two simulations were made with the regional groundwater flow model, which are documented in detail by D'Agnese et al. (D'Agnese, F.A. et al., *Simulated Effects of Climate Change on the Death Valley Regional Ground-Water Flow System, Nevada and California*, Milestone Report SP23OM3, DTN GS970708312144.003 (TBV), Water Resources Investigations Report 98-4041, unpublished). As a reasonableness check on future-climate conditions, a simulation based on past-climatic conditions (21,000 years ago, under full glacial conditions) was evaluated by comparing the results of the simulation to observations of paleodischarge. A possible, future groundwater flow system representing global-warming conditions (a doubling of atmospheric CO₂) was also simulated. Climate changes were simulated with the regional groundwater flow model primarily by changing the distribution and rates of groundwater recharge.

Average annual precipitation maps for both past- and future-climate scenarios were resampled to the model grid resolution. A polynomial function representing the Maxey-Eakin area-altitude relationship was then used to estimate recharge rates and distributions from precipitation for these two conditions. Results of climate-change simulations were evaluated through analyses of simulated discharge areas, water-level changes, potentiometric surface configurations, and water budgets.

During past-climate conditions, recharge increased in most areas to produce a significantly different regional groundwater flow system. Wetter past-climate conditions provided enough groundwater in the system to maintain paleolake levels in the northern parts of the model domain and at Lake Manley in Death Valley. Groundwater discharge occurred at most of the observed paleodischarge sites, which indicated that the recharge distribution used in the simulation generally was valid. Large

hydraulic gradients in the region were preserved and enhanced under simulated past-climate conditions. Simulated recharge over the region increased by factor of about five relative to present-day recharge. Under these extremely wet conditions, simulated water levels in the vicinity of Yucca Mountain rise between 60 and 150 m (Figure 5.2-32).

Under simulated future-climate conditions, recharge both increased and decreased throughout the model domain. The configuration of the simulated potentiometric surface changed only slightly relative to simulated present-day conditions to indicate depressions at discharging playas. Simulated discharge to these playas, however, was not as great as during the full-glacial (past) climate and perennial lakes probably were not supported at these locations. Simulated discharge under global-warming conditions increased over present-day discharge at Ash Meadows, Oasis Valley, and Death Valley. Under future-climate conditions, large hydraulic gradients were maintained and enhanced in some areas. Simulated recharge throughout the model increased by a factor of about 1.5 relative to simulated present-day recharge. Under these climatic conditions, simulated water levels in the vicinity of Yucca Mountain rise less than 50 m (Figure 5.2-33).

The limitations to evaluating the effects of climate change on a regional groundwater flow system using numerical modeling are substantial, and these limitations are described in detail by D'Agnesse et al. (D'Agnesse, F.A. et al., *Simulated Effects of Climate Change on the Death Valley Regional Ground-Water Flow System, Nevada and California*, Milestone Report SP23OM3, DTN GS970708312144.003 (TBV), Water Resources Investigations Report 98-4041, unpublished). Therefore, the simulated effects of climate change should be considered conceptual in nature and should be used only to describe potential impacts to the regional groundwater flow system relative to the present-day conditions.